Behaviour of Continuous Concrete Beams Reinforced with FRP Bars

by

MOSTAFA ABDELHAMEED TAHER EL-MOGY

A Thesis submitted to the Faculty of Graduate Studies of

The University of Manitoba

in partial fulfillment of the requirements of the degree of

DOCTOR OF PHILOSOPHY

Department of Civil Engineering

University of Manitoba

Winnipeg, Manitoba, Canada

ABSTRACT

The non-corrodible nature of FRP bars along with their high strength, light weight and ease of installation made it attractive as reinforcement especially for structures exposed to aggressive environment. In addition, the transparency of FRP bars to magnetic and electrical fields makes them an ideal alternative to traditional steel reinforcement in applications sensitive to electromagnetic fields such as magnetic resonance imaging (MRI) units.

Continuous concrete beams are commonly-used elements in structures such as parking garages and overpasses, which might be exposed to extreme weather conditions and the application of de-icing salts. In such structures, using the non-corrodible FRP bars is a viable alternative to avoid steel-corrosion problems. However, the linear-elastic behaviour of FRP materials makes the ability of continuous beams to redistribute loads and moments questionable. The objective of this research project is to investigate the flexural behaviour of continuous concrete beams reinforced with FRP and their capability of moment redistribution. An experimental program was conducted at the University of Manitoba to realize the research objectives. Ten full-scale continuous concrete beams were constructed and tested to failure in the laboratory. The specimens had a rectangular cross-section of 200×300 mm and continuous over two spans of 2,800 mm each. The main investigated parameters were the amount and material of longitudinal reinforcement, the amount and material of transverse reinforcement and the spacing of used stirrups. The experimental results showed that moment redistribution in FRP-reinforced continuous concrete beams is possible if the reinforcement configuration is chosen properly, and is improved by increasing the amount of transverse reinforcement.

A finite element investigation was conducted using ANSYS-software. A 3-D model was created to simulate the behaviour of continuous beams reinforced with FRP. The model was verified against the experimental results obtained from the present study. This verified model was used to investigate the effect of the concrete compressive strength, longitudinal reinforcement ratio, midspan-to-middle support reinforcement ratio and the amount of transverse reinforcement on the behaviour of FRP-reinforced beams. The analytical results of this parametric investigation along with the experimental results were used to propose an allowable limit for moment redistribution in FRP-reinforced continuous concrete beams.

ACKNOWLEDGEMENT

I would like to express my deepest and sincere gratitude to my supervisor Dr. Ehab El-Salakawy Ph.D., P.Eng., Canada Research Chair in Durability and Modernization of Civil Structures in the Department of Civil Engineering at the University of Manitoba, for his guidance, continuous encouragement and unlimited support throughout the course of this research program. The assistance of Dr. Amr El-Ragaby is also tremendously appreciated.

I would like to express my gratitude and sincere appreciation for the financial support received from the Natural Science and Engineering Research Council of Canada (NSERC), through Canada Research Chairs program. The equipment funds received from Canada Foundation for Innovation (CFI) is greatly appreciated. The help received from the technical staff of the McQuade Heavy Structural Laboratory in the Department of Civil Engineering at the University of Manitoba is also acknowledged.

I would like to thank Mr. Mohamed Mady, Mr. Felipe Tabet, Mr. Steven Foubert, Ms. Juliana Alves and Ms. Lydia Schoeppner for their support and encouragement.

Finally, I would like to express my deepest gratitude to my parents and my two sisters for their invaluable support throughout my academic career.

Mostafa El-Mogy

TABLE OF CONTENTS

LIST OF TABLES

LIST OF FIGURES

CHAPTER 1: INTRODUCTION

1.1. General

In the last few decades, advanced composite materials such as fibre reinforced polymers (FRP) were widely used in civil engineering applications. Being originally used in aerospace industry, automobile industry and defence, FRPs proved high efficiency performance. This is due to their favourable properties such as high tensile strength, fatigue and corrosion resistance, and high strength-to-weight ratio. FRPs are introduced to civil engineering as potential solution for one of the main problems facing reinforced concrete structures, which is the ageing and deterioration of civil infrastructures. The main reason behind this problem is corrosion of steel reinforcement. There are many techniques and methods that could be used to protect steel reinforcement, such as the use of galvanized or stainless steel bars, epoxy coating and cathodic protection. None of these methods, however, provided a radical solution for steel corrosion problem. The non-corrodible nature of FRP along with other outstanding characteristics suggests that these materials could be a promising solution for this problem. In addition, the transparency of FRP bars to magnetic and electrical fields makes them a viable alternative to traditional steel reinforcement in applications sensitive to electromagnetic fields such as magnetic resonance imaging (MRI) unites.

Intensive research has been done in the last decade on the use of FRP as internal reinforcement in new structures as well as strengthening and retrofitting of existing ones. Previous work investigating the replacement of steel reinforcement with FRP bars focused mainly on simple structures, usually simply-supported structural elements. Very limited research has been done on statically indeterminate structures such as continuous beams.

1.2. Problem Definition

FRP bars have been used as reinforcement in structures exposed to harsh environments such as marine structures, bridges and other civil infrastructures. This is mainly due to the non-corrodible and durable nature of FRP. However, the wide spread of using FRP reinforcement in statically indeterminate concrete structures is limited. This might be attributed to the lack of design guidelines and incomplete understanding of the behaviour of FRP-reinforced statically indeterminate concrete structures. Statically indeterminate reinforced concrete elements such as continuous beams are very common in structures like parking garages and overpasses, which might be exposed to harsh weathering and de-icing salts. Replacing the traditional steel with FRP reinforcement in such structures is quite beneficial in terms of the life span of the structure and the regular maintenance cost. However, the analysis procedures developed for steel-reinforced structures are usually not applicable to FRP-reinforced structures. This is due to the difference in physical and mechanical characteristics between steel and FRP bars in terms of modulus of elasticity, stress-strain relationship, bond properties, ductility, etc. Hence, the behaviour of such FRP-reinforced elements should be investigated independently.

Generally, continuous beams have the ability to redistribute bending moment between critical sections. This permits portion of undesirable hogging bending moment peaks that form over the middle support to be shed over sagging bending moment at mid-span. This redistribution gives the structure more favourable ductile behaviour, with ample warnings before failure. The moment redistribution in steel-reinforced structures is well established and permitted in design codes. It depends on the rotational capacity provided by the yielding of the steel bars in the cross section. However, the linear-elastic behaviour of FRP materials up to failure raises concerns about the ability of such materials to redistribute loads and moments in continuous beams.

Therefore and due to the lack of research, design codes and guidelines do not allow for moment redistribution in FRP-reinforced continuous beams. Most of the FRP design codes and guidelines (ACI 2006; CSA 2002; ISIS Canada 2007; CSA 2006) give very limited recommendations for continuous beams. Thus, more research is still required for better understanding the behaviour of such beams.

Moreover, little research investigated experimentally the feasibility of using FRP bent bars as transverse reinforcement (stirrups). During the manufacturing process and due to stress concentration as well as the unidirectional fibre layout, the tensile strength of the stirrup is typically reduced at the bend location. This reduced strength, as a percentage of the tensile capacity of the straight bar, could be in the proximity of 40% as recommended by Shehata (1999). Also, previous investigations on FRP-bent bars found that there are two main factors affecting their behaviour. These factors are the radius of the bend and the tail length (ISIS Canada 2007). The presence of stirrups in a reinforced concrete section is known to increase the confinement around the compression zone and enhance the ductility of concrete (Park and Paulay, 1975). To date, there are no experimental results that investigate the effect of transverse reinforcement on the behaviour of continuous concrete beams reinforced with FRP bars.

1.3 Research Significance

The behaviour of steel-reinforced continuous concrete beams is well established and thoroughly investigated. Previous research found that moment redistribution in continuous beams reinforced with steel can be identified in two stages (Carmo and Lopes 2006). The first stage is due to the difference in stiffness of critical sections after cracking. The second stage is due to the formation of plastic hinges after steel-yielding. Due to the lack of research, current design codes and

guidelines for structures reinforced with FRP do not allow for moment redistribution in FRP-reinforced continuous beams. However, in lieu of having a yielding plateau in the used reinforcement material, there are several factors that could be utilized to redistribute bending moments between critical sections. The main factors are the large deformations and wide cracks that forms in FRP-reinforced beams which is typically higher that their steel-reinforced counterparts. In addition, the inelasticity of concrete and the different bond characteristics of FRP bars are also among these factors. This study investigates the effect of these factors on availability of moment redistribution.

The last few years witnessed great advance in polymer science, which resulted in improved FRP produced with better physical and mechanical properties (bond, tensile strength and modulus of elasticity). Among all the common fibres used in the FRP composites, glass FRP (GFRP) received the most attention in development and improvement due to the economical aspects of its production. There is an urgent need for more updated research utilizing the advanced new products to keep up with the industry.

Furthermore, very limited research studied the combined effect of longitudinal and transverse FRP reinforcement on the behaviour of continuous beams. To the best of the author's knowledge, this is the first study to investigate experimentally the behaviour of continuous concrete beams reinforced with GFRP bent bars as transverse reinforcement (stirrups). This provides valuable information on the feasibility of using GFRP stirrups as shear reinforcement.

1.3. Objectives and Scope

FRP bars are increasingly used as internal reinforcement for concrete structures. Through the last ten years, simply-supported concrete beams reinforced with FRP were intensely studied. These

efforts make it possible to take FRP reinforcement further towards statically indeterminate structures. Very limited work has been done to study the behaviour of continuous concrete beams reinforced with FRP bars. The main objectives of this research are:

- Experimentally investigate the structural behaviour of continuous FRP-reinforced concrete beams;
- Studying the possibility and the extent of moment-redistribution in continuous concrete beams reinforced with FRP;
- Determining the effectiveness of GFRP shear reinforcement and its effect on moment-redistribution;
- Construct a numerical model based on finite element method (FEM) that simulates the behaviour of FRP-reinforced continuous concrete beams;
- Conduct a parametric study using the developed FEM model to extend the investigated parameters affecting the behaviour of FRP-reinforced continuous concrete beams.

These main objectives can be achieved through a set of more specific ones including the effect of different reinforcing ratios of flexural reinforcement and transverse reinforcement, spacing and material of the used transverse reinforcement (stirrups). In addition, following the verification against the experimental results, the FEM model is used in a parametric study to investigate the effect of compressive strength of the used concrete, the longitudinal reinforcement ratio, the ratio between longitudinal reinforcement at critical sections and the spacing of stirrups.

The scope of this study is restricted to two-span continuous concrete beams reinforced for flexure with GFRP or carbon FRP (CFRP) bars, and for shear with steel or GFRP reinforcement.

However, to provide a basis for comparison a part of this study is dedicated to two-span continuous beams longitudinally reinforced with conventional steel bars. The comparison is based on deflection, cracking pattern, ultimate capacity, mode of failure, reinforcement and concrete strain, and load distribution.

1.4. Methodology

To achieve the above mentioned objectives, an experimental program is conducted. The program consists of testing ten large-scale concrete beams continuous over two spans. The test beams have rectangular cross sections and reinforced with GFRP or CFRP bars as longitudinal reinforcement. Both steel and GFRP stirrups are utilized as transverse reinforcement.

The test parameters are:

1. Flexural reinforcement ratio in both mid-span and middle support sections (to allow for moment redistribution of 0% or 20%);
2. Material of longitudinal reinforcement (steel, GFRP and CFRP);
3. Shear reinforcement material (steel and GFRP);
4. Steel or GFRP shear reinforcement spacing (120 and 80 mm);
5. Steel or GFRP shear reinforcement ratio (0.40% and 0.63%).

A finite element method (FEM) modeling was conducted using ANSYS software, release 13 (ANSYS, 2010). The produced model is used in a parametric study involving some new parameters, such as the effect of concrete compressive strength and the ratio between reinforcement at critical sections, along with more extensive study of the experimentally studied parameters, such as stirrups spacing and longitudinal reinforcement ratio.

CHAPTER 2: LITERATURE REVIEW

2.1. General

During the past four decades, the behaviour of steel-reinforced concrete beams has been investigated in a significant amount of research. Due to their critical influence on the general behaviour of continuous beams, moment redistribution and rotation capacity were the main investigated parameters in previous studies. The behaviour of continuous concrete beams reinforced with steel is now well established as adequate knowledge is available on how they perform and what parameters affect their behaviour. Nonetheless, there is a lack of research on continuous concrete beams reinforced with FRP bars. This is reflected on the available FRP codes and guidelines, which provide no recommendations on continues beams and moment redistribution.

In fact, more research is needed for better understanding the behaviour of FRP-reinforced continuous beams in order to be utilized in buildings. This would solve corrosion related problems in structures exposed to corrosive environment, an issue that costs billions of dollars worth of repair in North America as well as other parts of the world. The difference in the mechanical properties between steel and FRP bars is the main reason behind the difference in the structural behaviour of concrete elements reinforced with either of them. This makes the design formulas and guideline for steel-reinforced structures inapplicable to those reinforced with FRP.

In this chapter, a brief summary of the material properties and the main characteristics of FRP products are presented. This is followed by a demonstration of the main studies that investigated the behaviour of continuous concrete beams reinforced with traditional steel bars. The following section illustrates the structural behaviour of FRP-reinforced concrete simply-supported beams and the main parameters affecting their performance. Moreover, previous experimental and

analytical studies investigating the behaviour of continuous concrete beams reinforced with FRP are also presented.

2.2. FRP Materials

2.2.1. Historical development

The development of FRP as reinforcement can be traced back to the expand use of composites after the Second World War. The advantages of the light weight and high strength of composite materials had been long recognised by the aerospace industry. Pultrusion offered an economic and fast manufacturing method to produce constant profile parts for commercial use. However, it was not until the 1960s that composite materials were seriously considered for use as reinforcement in concrete. The expansion of infrastructure projects and highway systems in the 1950s increased the need to provide year-round maintenance. Appling de-icing salts on highway bridges resulted in extensive corrosion in steel reinforcement in these structures and those subjected to marine environment. It was in the late 1970s when the FRP reinforcing bar became commercially available as an alternative to steel rebar to overcome corrosion problems. In the 1980s, the market demanded non-metallic reinforcement for specific advanced technology such as facilities for MRI medical equipment. FRP became the standard reinforcement used in this type of construction. Recently, FRP reinforcement began to be considered as a common solution for corrosion problems in bridges especially after detection of corrosion in the commonly used epoxy-coated bars.

2.2.2. Constituent materials

Fibre reinforced polymers are composite materials essentially made of two basic components, reinforcing fibres and a matrix (resin). The fibres, which are responsible for carrying the load and providing strength, are ideally elastic, brittle and have high strength. The resin basically

provides a cohesive environment to transfer stresses between fibres, keep the fibres together, and provide lateral support for the fibres against buckling. In addition, the resin plays an important role in protecting the fibres from mechanical and environmental damage. The fibres are significantly stronger than the resin material and control the elastic modulus and final strength of the composite. In order for fibres to provide a reinforcing function, the fibre-volume ratio should not be less than 55% of FRP bars and rods and 35% of FRP grids (ISIS Canada 2007). The mechanical properties of the final FRP product depend on a number of parameters. This includes fibre type, quality, volumetric ratio, adhesion resin and most importantly the manufacturing forces. Figure (2.1) shows the relationship between stress and strain for fibres, resin and the FRP composite.

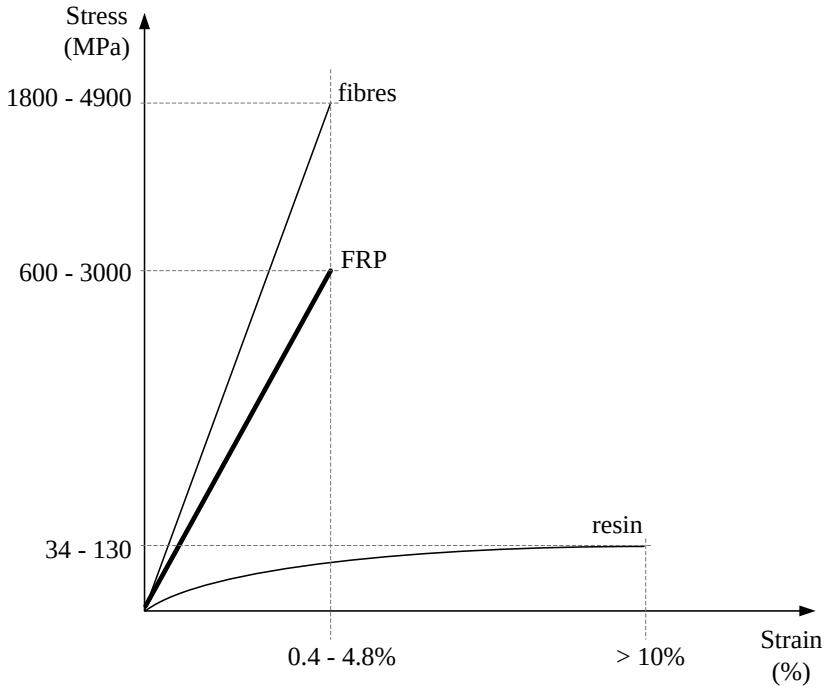

Figure (2.1): stress-strain relationship of fibres and resin for FRP composites (reproduced from ISIS Canada 2007)

2.2.2.1. Fibres

The most commonly used fibres are carbon, glass and aramid fibres. The performance of the fibres is affected by a number of factors such as length, cross-sectional shape and chemical composition.

Glass fibres are the most commonly used fibres in the FRP composites products. This is due to the economical aspect of the production process of glass fibres which is relatively cheaper than other types of fibres. There are a number of glass fibres commercially available. Some of these types are identified as follows (GangaRao and Vijay 2007).

1. E-glass: has low alkali content and is considered the most common type of glass fibre in high-volume commercial use. It has low susceptibility to moisture and high mechanical properties;
2. Z-glass: is a high alkali-resistant, typically used in cement mortars and concrete as reinforcing fibres;
3. A-glass: has high alkali content;
4. C-glass: common in chemical applications that require great corrosion resistance to acids;
5. S- or R-glass: is produced for applications that require extra-high strength and high modulus;

The advantages of glass fibres are low cost, high tensile strength, high chemical resistance and excellent insulating properties. On the other hand, the disadvantages are, low tensile modulus, relatively high specific gravity and relatively low fatigue resistance.

Carbon fibres can be classified into two main categories, chemically known as polyacrylonitrile fibres (PAN) and Pitch-based fibres. PAN fibres are synthetic fibres with very high strength (up

to 40000 MPa), and typically expensive. There are two types of PAN fibres, high strength PAN and high modulus PAN fibres. Table (2.1) shows the mechanical properties of these types. Pitch-based fibres are originally obtained from distillation of coal. They are cheaper than PAN fibres, however, with lower strength and modulus. There are two types of Pitch fibres, ordinary and high modulus. The mechanical properties are also demonstrated in Table (2.1). Carbon fibres have excellent resistance to alkaline and acid environments with superior mechanical properties, however they are expensive and sensitive to the processing conditions such as tension and temperature during manufacturing.

Aramid fibres is the abbreviated name given to aromatic ployamide fibres. These are manufactured fibres that were first introduced in the early 1970's by DuPont in Germany under the name of Kevlar. There are four types of Kevlar fibres, among these types Kevlar 49 has been designed for reinforcement applications. The mechanical properties are shown in Table (2.1). The main advantages of aramid fibres are excellent resistance to damage against impact and other dynamic loading, low thermal conductivity and high damping coefficient. However, there are also certain advantages. Aramid fibres are susceptible to moisture absorption up to 10% of fibre weight. This would lead the fibres to crack internally at high moisture content. Moreover, aramid fibres exhibit mechanical property deterioration under elevated temperature. The fibres also are sensitive to Ultra Violet lights.

Table (2.1): Mechanical properties of fibres (reproduced from ISIS Canada 2007)

Fibre type		**Tensile strength (MPa)**	**Modulus of Elasticity (GPa)**	**Elongation %**	**Poisson's Ratio**
Carbon					
PAN	High Strength	3500	200-240	1.3-1.8	0.2
	High Modulus	2500-4000	350-650	0.4-0.8	
Pitch	Ordinary	780-1000	38-40	2.1-2.5	N/A
	High Modulus	3000-3500	400-800	0.4-1.5	
Aramid					
Kevlar 29		3620	82.7	4.4	0.35
Kevlar 49		2800	130	2.3	
Kevlar 129		4210	110	N/A	
Kevlar 149		3450	172-179	1.9	
Glass					
E-GLASS		3500-3600	74-75	4.8	0.2
S-glass		4900	87	5.6	0.22
Z-glass		1800-3500	70-76	2.0-3.0	N/A

2.2.2.2. Resins

The selection of the proper resin is an important issue in the manufacturing of FRP composites as the physical and thermal properties of the resin has a significant influence on the mechanical properties as well as the manufacturing process of the product. The resin could be a thermosetting or thermoplastic compound. Thermosetting resins will harden under elevated temperature and cannot be returned to the liquid state. The thermoplastic resins, on the other hand, can be liquefied by heat and solidified by cooling. Polyesters, vinyl esters and epoxies are the common types of thermosetting resins, while polyvinyl chloride (PVC), polyethylene and polypropylene are thermoplastic resins (GangaRao and Vijay 2007).

2.2.3. Manufacturing process

There are three main manufacturing processes for FRP composites; pultrusion, braiding, and filament winding (ISIS Canada 2007).

1. Pultrusion: This process makes a constant cross-section part of unlimited length which is constrained only by building and shipping limitations. The pultrusion process uses continuous fibres from a series of creel positions. All the fibre rovings are drawn to a wet-out bath that contains the resin matrix, catalyst, and other additives. The rovings are impregnated in the bath. Excess liquid resin is removed and returned to the bath, while the wet-out roving enters the pultrusion die. Polyester resin and vinyl esters are the major matrix materials used in the pultrusion process. Reinforcement rebar and variety of standard sections are made by this process. Figure (2.2) shows a schematic representation of the process.
2. Braiding: is a process in which two or more systems of yarns are interwined diagonally to form an integrated structure. The fibres are impregnated with resin and cured to form the final product. FRP sheets and laminates can be made by this process.
3. Filament winding: This process takes continuous fibres in the form of parallel strands (rovings), impregnates them with matrix resin and winds them on a rotating cylinder. The resin-impregnated rovings are made to traverse back and forth along the length of the cylinder. A controlled thickness, wind angle, and fibre volume fraction laminate is thereby created. The material is cured on the cylinder and then removed. Pipes, storage tanks, and the like are made by this process.

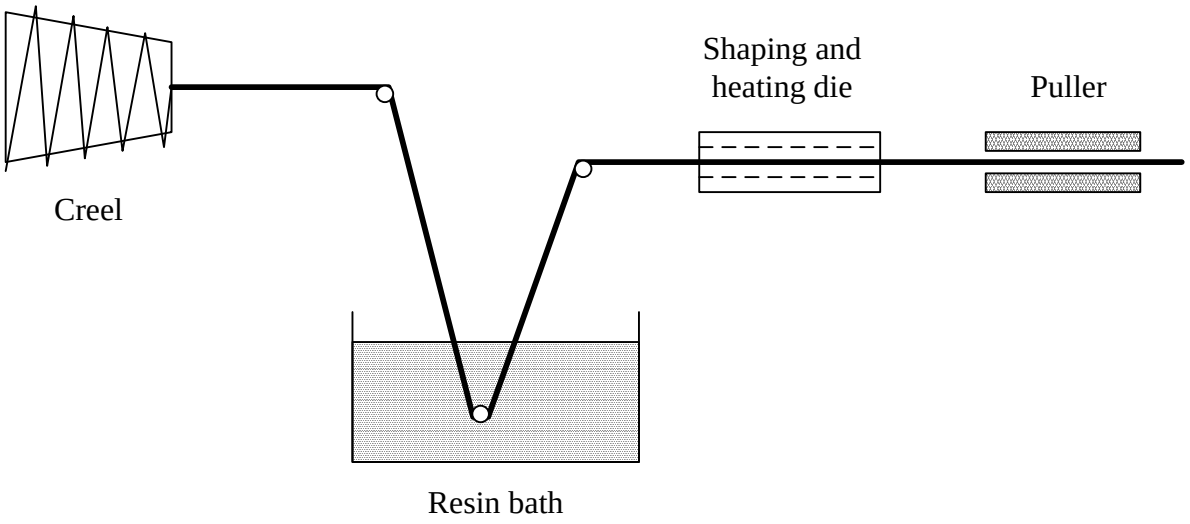

Figure (2.2): Pultrusion process (reproduced from ISIS Canada 2007)

2.2.4. FRP products for internal reinforcement

FRP bars can be produced in different diameters and different shapes, straight, bent, circular and spiral. The surface of the bars can be sand-coated, ribbed, helically wrapped and braided. The bond performance of FRP bars embedded in concrete is mainly dependent on surface conditions. The manufacturing process changes significantly to process different shapes or different surface conditions of FRP bars. The mechanical properties of some commercially available FRP bars are shown in Table (2.2). The FRP industry is an evolving field and new products are constantly being introduced to the market.

Table (2.2): Typical mechanical properties of FRP bars (reproduced from ISIS Canada 2007)

Trade Name	**Tensile strength (MPa)**	**Modulus of Elasticity (GPa)**	**Ultimate tensile strain**
CFRP			
V-ROD	1596	120	0.013
Aslan	2068	124	0.017
Leadline	2250	147	0.015
NEFMAC	1200	100	0.012
GFRP			
V-ROD	710	46.4	0.015
Aslan	690	40.8	0.017
NEFMAC	600	30	0.012

2.3. Continuous Beams Reinforced with Conventional Steel Reinforcement

2.3.1. Introduction

Considering the behaviour of steel-reinforced concrete beams near the ultimate load, it is important to determine the possible redistribution in bending moments that could be used in design. If sufficient ductility is available at critical sections, it is possible to use a distribution of moments and forces different from that given by elastic linear analysis. The amount of this redistribution mainly depends on the moment-curvature relation of critical cross sections (Park and Paulay 1975). Figure (2.3) shows a typical moment-curvature relationship for steel under-reinforced concrete section.

Several parameters affect the moment-curvature relation of a steel-reinforced section. Some of these parameters are: mode of failure, tension reinforcement ratio, compression reinforcement ratio, concrete compressive strength and confinement.

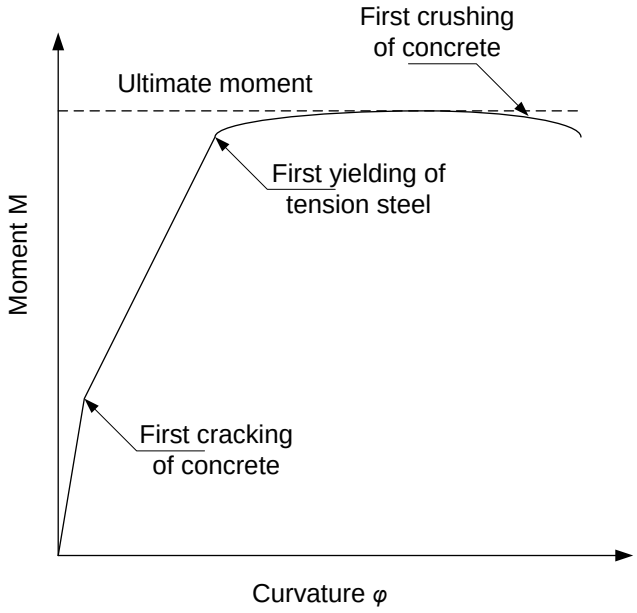

Figure (2.3): Typical moment-curvature relationship for under-reinforced section (reproduced from Park and Paulay 1975)

2.3.2. Parameters affecting the behaviour of continuous steel-reinforced beams

Several experimental and analytical studies have been conducted to investigate the parameters affecting the behaviour of continuous steel-reinforced beams. The literature discussed the effect of different parameters on moment-curvature relationship, ductility and rotation capacity of steel-reinforced concrete beams.

2.3.2.1. Tension and compression reinforcement ratio

Park and Paulay (1975) discussed the parameters affecting the moment-curvature relationship for singly-reinforced sections in both tension and compression failure modes. It was concluded that maximum curvature achieved in a section failing in compression is dramatically reduced compared to tension failure. This is due to the loss of ductility provided by yielding of steel reinforcement. As for the effect of different tension and compression reinforcement ratios on the moment-curvature behaviour, increasing the tension reinforcement decreases section ductility and maximum curvature is reduced consequently. Increasing the compression reinforcement

counters portion of internal tensile force developed in tension reinforcement. Hence, section ductility is improved and consequently maximum curvature.

Due to the non-linear nature of moment-curvature relationship of steel-reinforced sections, it is evident that this will cause some adjustment to the values of bending moments when loaded beyond service range. Because of plastic rotation at critical section, bending moments may assume a different pattern from those calculated by linear-elastic analysis.

Lin and Chien (2000) studied the effect of section ductility considering moment redistributions in reinforced concrete continuous beams. The main parameters studied were amount of transverse reinforcement, tensile reinforcement, compression reinforcement and concrete strength. The significance of this research was in proposing new reasonable formulas for moment redistribution. This research implemented both experimental and analytical methods. It was found that increasing the compression reinforcement and decreasing the tension reinforcement improved section ductility and caused more moment redistribution.

2.3.2.2. Shear reinforcement ratio and spacing

Increasing the confinement in steel-reinforced sections by providing more stirrups gives the concrete in the compression zone more ductile behaviour. This could have a significant positive effect on maximum achieved curvature only in case of compression failure mode. As in this mode of failure, concrete has a more effective role in section behaviour compared to its role in tension failure mode (Park and Paulay 1975).

Rodriguez et al. (1959) studied experimentally the effect of percentage and spacing of web reinforcement on the shear behaviour of reinforced concrete continuous beams. The research aimed to study the effect of continuity on shear strength. Research significance lies in the need to

verify the applicability of design formulas and equations developed using simply supported beams to design continuous beams, hence study whether the continuity has any effect on shear behaviour.

Predicted values using available expression developed from simply-supported and restrained beams were in good agreement with obtained experimental results. The author indicated that factors like longitudinal reinforcement and span to effective depth ratio have major effect on shear behaviour. Tested specimens demonstrated four main types of failure: diagonal tension, flexural, shear-compression, and splitting failure. Ultimate loads of specimens that experienced the first three types of failure were in good agreement with analysis used for simple beams. Studying stirrups spacing, it was found that using the required amount of transverse reinforcement by ACI code is important to prevent shear failure. It was also found that the analysis for diagonal tension cracking used for simple beams is applicable for continuous beams.

The shear span length was found to have an influence on the load capacity of beams after formation of diagonal tension cracks. The load capacity of shorter spans is less affected by the formation of initial diagonal tension crack. Regarding the effect of continuity, this investigation showed that continuity has a marked effect on redistribution of stresses, as yielding of longitudinal reinforcement in a continuous beam does not mean that failure has been reached.

Results of tested beams also showed that it is possible to have a shear failure even after yielding of longitudinal reinforcement.

Corley (1966) studied experimentally the effect of confinement of the concrete in compression on the rotational capacity of reinforced concrete beams. This work, following the work of Mattock (1965), studied more factors in an attempt to evolve a precise method to predict inelastic

rotations. All beams were simply-supported with rectangular cross-section loaded with one concentrated load at mid-span. Using large number of stirrups closely spaced demonstrated considerable rotational capacity more than beams with fewer stirrups. This may be attributed to the increase of maximum useful strain in concrete by binding of reinforcement in compression zone. In addition it was found that the spread of inelastic deformations beyond a distance d/z from section with maximum moment depends mainly on the geometry (where d is the effective depth and z is the distance from maximum to zero moment along the span). Finally, the author also concluded that equations derived from principals of compatibility of strains and equilibrium of forces can be used to arrive at a reasonable estimate of curvatures and rotations, provided that reinforcement strain hardening and maximum concrete compressive strain are considered.

Lin and Chien (2000) indicated that proper confinement using transverse reinforcement results in significant increase in moment redistribution. The authors indicated that the amount of transverse reinforcement plays an effective role in member ductility, consequently affects the moment distribution.

2.3.2.3. Concrete strength

Lopes and Bernardo (2003) carried out an experimental investigation to study the plastic rotation capacity of high strength concrete beams. The main objective of this work was to clarify doubts about whether high strength concrete can demonstrate adequate behaviour to satisfy the required structural ductility. It was found that increasing the concrete compressive strength increase the plastic tendency of the beam. In addition, it was found that the longitudinal reinforcement ratio has the most influence on the beam ductility.

2.3.2.4. Size of specimen

Corley (1966) also studied the effect of specimen size on rotational capacity. The significance of studying the size of specimens came from the fact that experimental tests usually use small size specimens than those used in prototypes. Thus laboratory studies validity should be examined with large-scale specimens. The size effect was studied by comparing specimens with the same amount of stirrups. The average concrete strain values indicate that there is a trend toward slight more strain with smaller size. However, considering the scatter in strain values, it appears that no significant direct effect of size on rotational capacity.

2.3.3. Moment redistribution

After cracking of critical sections in a continuous steel-reinforced concrete beam, the difference between actual and predicted linear-elastic moment distribution in such beams can be identified in two stages. The first stage is caused by difference in concrete cracking in critical regions, and the second stage is caused by plastic deformation of steel reinforcement. Also, for beams with constant cross-section, flexural stiffness after cracking was found to be approximately proportional to tensile reinforcement ratio. Consequently, the distribution of bending moment after cracking will change according to the provided reinforcement as demonstrated in Figure (2.4) (Carmo and Lopes 2006).

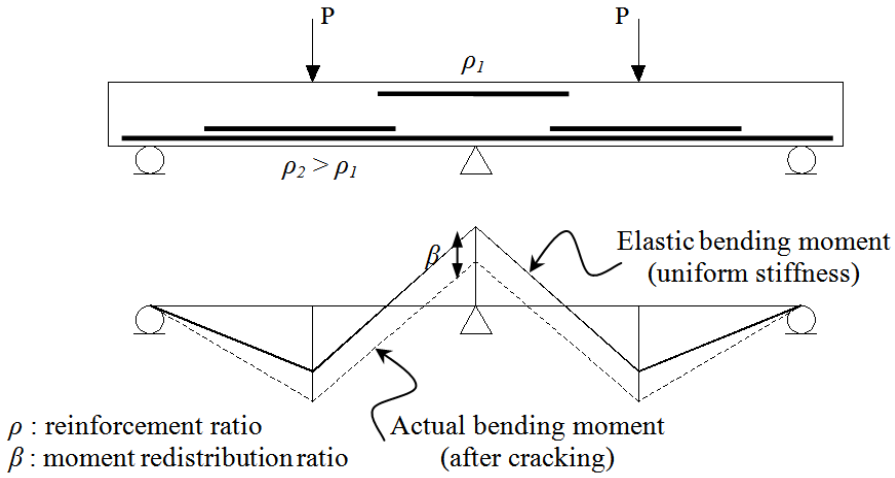

Figure (2.4): Elastic and actual bending moment in a continuous beam (El-Mogy et al. 2010)

Ernst (1958) conducted an experimental study on two-span continuous concrete beams. The main objective of the study was to investigate degree of moment and shear distribution after yielding of reinforcement at the first critical section. Studied variables in this work were reinforcement ratio, reinforcement layout, loading pattern and different support settlement conditions. The authors indicated that the same behaviour of moment and shear redistribution was observed for all beams, regardless of differences in length of top bars and reinforcement ratio. In addition, calculated failure load based upon crushing moment at all critical sections was less than the experimental failure load. Moreover, the provided shear stirrups designed to take all shear at plastic collapse prevented diagonal tension failure, except for the case when the cut-off of top bars ended near a high hogging bending moment zone.

Mattock (1959) studied experimentally the redistribution of design bending moments in reinforced concrete continuous beams. The main objective of the research was to investigate the influence of arbitrary redistribution of design bending moments on continuous reinforced concrete beams performance at design load. It was mentioned that earlier research has been directed to show that any assumed redistribution of bending moments will occur before failure,

and so an adequate factor of safety is achieved. The main parameters evaluated in this study were moment redistribution ratio and type of reinforcing steel bars.

Four two-span continuous concrete beams were tested up to failure. Beams were designed to achieve the same design load assuming different percentage of moment redistribution. The first specimen in this series was designed for the bending moment distribution given by the elastic theory (0% redistribution), the succeeding three beams were designed assuming 9.4%, 17.2%, and 30.4% redistribution.

Test results showed that moment redistribution was already taking place in the working load range, even though the steel stresses were below yielding stress. The author indicated that a redistribution of slightly more than one quarter of the assumed redistribution used in design was observed at service load. This redistribution was attributed to the non-linear moment/rotation relationship of reinforced-concrete section under low loads. Redistribution automatically occurs when sections with reduced design bending moments gets overstressed, and have reduced stiffness. Sections with lower stresses will be stiffer, thus, attracting bending moment in more stiff regions and pushing it away from regions with lower stiffness.

Calculating failure load assuming complete moment redistribution at failure was found to be a safe estimate of the failure load measured experimentally. It was also confirmed that redistribution of design bending moments does not have a significant influence on the ultimate load-bearing capacity of continuous reinforced concrete beams.

The research concluded that redistribution of design bending moments up to 25% does not affect the performance of continuous reinforced concrete beams in both working and failure stages.

Deflection and cracking of beams with redistributed bending moment is not more severe than beams designed using bending moments predicted by the elastic theory.

Macchi (1965) studied experimentally the behaviour of continuous beams in an attempt to evaluate theory of moment distribution in continuous concrete beams. The theory states that moment redistributions starts with the first crack, and reach a considerable amount at service load level. The author indicated that this could result in overestimation of carrying capacity of structures. This danger is more significant when a higher percentage of reinforcement is used or in the presence of axial load, which considerably reduce section rotation capacity.

Experimental results demonstrated that an elastic distribution assumption of moments can lead to an overestimation of the ultimate capacity of the structure. Moreover, the authors concluded that considerable moments redistributions are produced by small inelastic deformations due to cracks of width usually permitted at service loads. In addition, they indicated that separate adaptation of limit analysis of individual sections without controlling inelastic moment distributions can lead to overestimation of structures' carrying capacity, especially for brittle sections.

Scholz (1993) carried out a theoretical investigation to re-examine the definitions and limitations for continuous reinforced concrete beams. The study evaluated the effect of variation in beams stiffness and slenderness. In addition, the author proposed a new definition of moment redistribution.

Equating the ductility demand and the ductility capacity both using equations driven by the author resulted in a relation between possible redistribution β and neutral axis depth at ultimate to effective depth ratio c/d. This relation is not as simple as suggested by the Canadian code

(CSA 2002), other independent variables are involved such as plastic hinge length L_p, elastic moment at support, reinforcement yield stress f_y, and concrete crushing strain ε_c.

Limiting the maximum allowable moment redistribution is important. For large moment redistribution percentage it is possible that stress in tension reinforcement reaches yield at service load level. Nonetheless, experimental work on beams with large moment distribution percentage done by Mattock (1959) did not illustrate any unfavourable cracking behaviour.

The stiffness variation in continuous reinforced concrete was also discussed. The author indicated that after cracking, a uniform stiffness along the beams using gross moment of inertia can no longer be assumed. Hence, a different stiffness at interior support regions could apply compared to the span. A variation in stiffness along the beam would change the elastic moment diagram and affects the plastic rotation in addition to curvature at first yield.

The author commented on previous experimental work on ductility capacity carried out by Mattock (1959) and Cohn (1964). Their work indicated that the formula proposed by the American concrete specification (ACI 2005) to calculate the ductility capacity was conservative. Further experimental results reported by previous research demonstrated a large scatter of experimental measurements. This could be attributed to pattern and level of secondary stresses (due to creep and shrinkage), material and geometric imperfection, workmanship, strain-hardening behaviour and loading aspects.

Kodur and Campbell (1996) investigated the percentage of moment distribution in continuous prestressed concrete beams using results from non-linear finite element analysis of large number of beams. An approach was proposed to determine the percentage of redistribution based on two

parameters, redistribution ratio β and moment ratio *MR*. The study was based on the overall structural behaviour rather than on cross-sectional behaviour.

The authors mentioned that failure of continuous prestressed concrete beams depends on the extent of moment redistribution at failure. Depending on different parameters the redistribution can be full, partial or nil. Stiffness of the span and presence of secondary moment are among the parameters affecting the extent of moment redistribution.

Using a symmetric two-span prestressed beam loaded with concentrated load, a formula driven by the authors was reached by equating the total available rotation at the central support region with the inelastic rotation required for a redistribution percentage. From the reached formula, the authors concluded the following points: 1) Moment redistribution increases as the span stiffness and plastic hinge length increase; 2) Moment redistribution decreases by increasing stiffness at support section (higher c/d ratio at support section); 3) Increasing the span to depth ratio ℓ/d decreases moment redistribution; 4) Percentage of redistribution is affected by the type of loading.

On the analytical side, a number of studies investigated analytically the factors affecting moment redistribution by developing a model that could simulate the behaviour of continuous beams.

Gravina and Warner (2003) studied analytically moment redistribution and plastic rotation in steel-reinforced continuous concrete beams. The authors presented a local deformation model that can predict accurately the flexural deformations in reinforced concrete beams. The model predicts the progressive development of flexural cracks and local strains in tensile reinforcement, in addition to the slip between tensile reinforcement and surrounding concrete. The authors developed a computer program using the model to predict the overall behaviour of determinate

as well as indeterminate beams. It was indicated that the standard method of analysis which assumes perfect bond between tensile reinforcement and surrounding concrete, and planner strain distribution in cross-section does not represent accurately the real behaviour in a flexural member. The authors used a bond-slip relation based on model proposed by Eligehausen et al (1983) with quantitative data given in CEB-FIP Model code (CEB-FIP 1990). The relation accounts for different degrees of confinement, the reduction in bond near transverse crack, and the effect of steel yielding. The model was applied in a continuous beam to hogging and sagging moment regions to study moment redistribution and over load behaviour up till failure.

The analytical model was verified by comparing experimental results reported in previous studies to the predicted results. Reasonable accuracy was found with predicted results.

The authors concluded that the proposed local deformation model was reasonably accurate in predicting the full-range of flexural behaviour of statically indeterminate beams. The model takes into consideration the progressive formation of flexural cracks, bond slip behaviour between tensile reinforcement and surrounding concrete, and stress-strain relationships for the reinforcing steel.

Carmo and Lopes (2006) studied analytically factors affecting moment redistribution in reinforced concrete structures which are ignored in design codes. The studied parameters are structural type, load type, concrete strength, and beam slenderness. The main objective of the study was to understand better the capacity of forces redistribution in reinforced concrete beams.

In this work the authors made use of the available new calculation tools and the technological development that has occurred in recent years to reanalyse the process of moment redistribution.

The ductility demands in code and guide lines are usually represented by either the maximum limit of the neutral axis to effective depth ratio *c*/*d* or a minimum value for plastic rotation. There are limits for the maximum degree of redistribution for beams with high or low reinforcement ratio. Beams with high reinforcement ratio exhibit reduced plastic rotation capacity, while beams with low reinforcement ratio may experience wide crack and the risk of shear failure.

For a member properly designed for moment redistribution, the required plastic rotation should be smaller or equal to that available. The required plastic rotation should be determined by ensuring the deformations compatibility conditions, thus it is affected by structural type, load type, and behaviour of the reinforcing material and its distribution through the structure. The authors pointed out that redistribution cannot be analysed based on section behaviour, it should be analysed based on overall member behaviour instead. The relative stiffness between critical sections along several stages of the loading and their moment-rotation relationships also have to be considered. The difficulty in determining the right flexural stiffness is due to the contribution of concrete between cracks (tension stiffening) which may increase the flexural stiffness. The authors indicated that determining the plastic rotation capacity is complex problem as it depends on a number of indeterminate factors. These factors are concrete compressive strength, size and shape of cross-section, transverse reinforcement ratio, slenderness of member, shear force, and longitudinal reinforcement ratio, which is the most important factor.

The authors developed an analytical model to simulate the behaviour of indeterminate reinforced concrete element to calculate the strength and deformability of critical section. The model was used to study the effect of concrete compressive strength on the required plastic rotation. It was found that the higher the compressive strength the higher the required rotation. The model was also used to compare different types of loading. It was found that the required plastic rotation for

continuous beam loaded with concentrated load at mid-span is lower than that required in case of a uniformly-distributed load. It was also found that the required plastic rotation equals zero when the assumed moment redistribution equals to one.

Moreover, the model was also used to study the structure type. Two-span continuous beam was compared to beam with infinite number of span both uniformly loaded. It was found that the beam with two spans needs smaller plastic rotation for the same degree of moment redistribution. Beams slenderness was also studied. It was found that as the span to depth ℓ/h ratio increases the required plastic rotation also increases.

2.3.4. Rotational capacity

The flexural behaviour of reinforced concrete continuous beams is very sensitive to the rotational capacity of the critical sections (middle support and mid-span sections). Several experimental and analytical studies investigated the rotational capacity of steel-reinforced concrete sections.

Ernst (1957) conducted an experimental investigation to determine the amount of concentrated plastic rotation developed at reinforced concrete beam-to-column connections. The observed plastic rotations at steel yielding and at concrete crushing were not large, and were not a major portion of the rotation available at the maximum load. It was found that concentrated plastic rotation is markedly reduced when the steel reinforcement ratio exceeds 0.01. It is reduced even more when using fast rate loading. Hence, it was concluded that whenever a redistribution of moment, produced by concentrated plastic rotation, is used to determine the ultimate capacity of the structure, the effect of the steel reinforcement ratio and rate of loading should be considered.

Mattock (1965) investigated experimentally the rotational capacity of hinging regions in reinforced concrete beams at the middle support in a continuous beam. The author proposed a

method whereby the rotational capacity for such regions could be calculated with reasonable precession. After analysing the experimental results, the author indicated that the ultimate curvature was found to be inversely proportional with the depth of neutral axis, *c*. It was also found that curvature is inversely proportional with the amount of tension reinforcement and directly proportional with the amount of compression reinforcement index. In addition, the author concluded that the inelastic rotation occurring in hinging regions maybe considerably greater than expected. This was based on the fact that the maximum compressive strain in concrete at section of maximum bending moment can be very much in excess of the usually assumed strain value of 0.003 (ACI 2005). Consequently, the curvature at ultimate strength maybe much greater than the value calculated based on this assumption.

Baker and Amarakone (1965) experimentally studied the rotational capacity of steel reinforced concrete sections. The study was intended to investigate the moment-curvature characteristics regarding the influence of the following parameters: grade of concrete and steel, reinforcement steel ratio, single and double loads, axial force, shear, transverse binding, and ratio of compression steel. Experimental results have shown that the main parameters influencing the ultimate strain in concrete are: the degree of binding, depth of neutral axis and the concrete grade obtained using cylindrical strength. It was found that the equivalent plastic hinge length on one side of critical section have a nearly linear relationship with the ratio of neutral axis depth to effective depth. The importance of binding was also observed in preventing brittle failure. Experimental results also demonstrated that the influence of type of tension steel and grade of concrete have a small effect of the rotation at plastic hinge, however they have more influence on the concrete strain.

2.3.5. Code provisions for steel-reinforced concrete sections

Nowadays the behaviour of steel-reinforced concrete beams is well established. All the formulas and recommendations regarding the design and detailing of such elements are available in the current design codes and guidelines. The following section presents the code provisions regarding steel-reinforced continuous concrete beams. More details can be found in Appendix B.

2.3.5.1. According to CAN/CSA-A23.3-04

For continuous beams, the hogging moments at supports calculated by elastic analysis may be reduced by a percentage equals to (30-50 *c/d*) %, but not more than 20%, (Clause 9.2.4).

2.3.5.2. According to ACI 318-08

For continuous beams, the bending moments calculated by elastic theory is permitted to be decreased by a percentage not more than the smallest of $1000\varepsilon_t$ or 20 percent, (Clause 8.4.1). Redistribution is only permitted if ε_t equals to or greater than 0.0075, where ε_t is the net tensile strain in longitudinal reinforcement.

2.4. FRP as Internal Reinforcement

Glass fibre reinforced polymers (GFRP) and carbon fibre reinforced polymers (CFRP) can be used as internal reinforcement for concrete structures. Such reinforcement can be in the shape of bars, stirrups, tendons, anchors, etc. Using FRP reinforcing bars provides a viable alternative to steel reinforcement, due to their non-corrodible nature and favourable characteristics for durability. FRP bars are commonly used in aggressive environments such as water treatment plants, costal environments, sea walls, tanks, box-culverts, facades and retaining walls. In recent years, FRP bars have been used in Canada in bridge decks and roads due to the use of de-icing salts, which damage traditional steel reinforcement. On the other hand, some special structures

may require being devoid of metal such as Magnetic Resonance Imaging (MRI) rooms in hospitals and research laboratories (Gravina 2008).

2.4.1. Flexural behaviour of FRP reinforced concrete beams

The behaviour of FRP-reinforced sections is different compared to sections reinforced with traditional steel reinforcement. This is due to the different mechanical behaviour between the two types of reinforcements. FRP bars exhibit linear stress-strain behaviour up to failure without any yielding. Therefore, tension failure in FRP-reinforced section is sudden and catastrophic; hence, it should be avoided. On the other hand, compression failure of FRP-reinforced sections offers more favourable response, as concrete ductility is utilized in giving ample warnings before failure. Most of current codes and guide lines require FRP-reinforced section to be design for compression failure

2.4.2. Moment capacity, modes of failure

Vijay and GangaRao (2001) studied the bending behaviour of sand-coated GFRP-reinforced concrete simply supported beams with rectangular sections. The research was a contribution towards better understanding of the flexural behaviour of such beams. The authors used experimental results reported by different researches in an attempt to recognise the different failure modes of GFRP-reinforced concrete beams and to calculate bending capacity corresponding to each mode of failure.

The authors pointed out that reinforced concrete beams can theoretically be designed for tension, compression or balanced failure. For traditional steel-reinforced beams, tension failure is the most favourable mode of failure to take advantage of the plastic behaviour of steel bars after yielding. However, GFRP has linear stress-strain behaviour up to failure; therefore important

factors should be taken into consideration such as mode of failure and energy absorption. Balanced failure for GFRP-reinforced concrete beams takes place when strains in both GFRP reinforcement and concrete in compression zone reach their ultimate values simultaneously. This condition is very difficult to achieve in reality. However, balanced failure condition is considered as a limiting value between tension failure and compression failure. Tension failure in GFRP-reinforced concrete beams is catastrophic failure due to the sudden rupture of GFRP bars. Nonetheless, compression failure is less catastrophic and more favourable for GFRP-reinforced beams due to obvious ample warnings prior to complete failure. These warnings are in the form of large deflection, very wide cracks, and the crushing and spalling of concrete. Compression failure could be achieved by providing longitudinal reinforcement more than the balancing reinforcement ratio.

After analysing the experimental results, the authors found that increasing the reinforcement ratio is not proportional to the increase in ultimate moment capacity, unlike other failure modes such as bond or shear-compression failure. Moreover, it was found that the use of GFRP bars as compression reinforcement does not have a significant effect on increasing the section moment resistance. In fact, to increase the moment resistance with a small value will need to provide a higher amount of compression reinforcement. This is due to the low modulus of elasticity of GFRP bars which will not allow significant compression force to be developed in the bars. In addition, the research also indicated that using high-strength concrete above 41.3 MPa is very effective with GFRP reinforcement. This gives the chance for the better use of the high stress-strain properties and improves the stiffness of cracked concrete section.

2.4.3. Transverse reinforcement and shear capacity

Placed perpendicular to the longitudinal flexural reinforcement, transverse reinforcement is designed mainly to resist shear forces in a reinforced concrete element. However, it is well established that providing more confinement to concrete in compression results in a more ductile behaviour and higher concrete strength. This increase in ductility usually enhances the available rotation capacity at any given cross-section. On the other hand, moment redistribution in continuous beams is mainly dependent on the available rotation capacity at critical sections. Hence, transverse reinforcement is considered to have a positive effect on the available moment redistribution. This phenomenon was found to be more pronounced in over-reinforced sections designed for compression failure, which is the common case for the FRP-reinforced concrete sections. In the last ten years, several studies investigated the feasibility of using FRP bent bars or grids as transverse reinforcement in simply-supported concrete beams, which introduced the possibility of constructing totally steel-free structures.

In the shear design process, both concrete and stirrups contribution in shear resistance should be determined. Compared to steel-reinforced sections with the same reinforcement ratio, a cross-section reinforced with FRP for flexure after cracking has a smaller depth to the neutral axis. Thus, the compression area of the cross section is reduced and the cracks are wider. Consequently, the shear resistance provided by the concrete in the form of aggregate interlock and compressed concrete is smaller.

Ashour (2006) reported test results of 12 simply-supported rectangular-section concrete beams reinforced for flexure with GFRP bars and without shear reinforcement. Beams were tested under four-point bending system. The main investigated parameters were beams depth and GFRP reinforcement ratio. Two modes of failure were observed, namely flexure and shear

failure. The flexural failure was mainly due to the rupture of GFRP bars. Shear failure was initiated by a major diagonal crack within the beam shear span. This diagonal crack extended horizontally at the level of longitudinal bars indicating bond failure. The study presented a simplified method to estimate the shear capacity of a concrete section provided by the concrete without shear reinforcement.

Another experimental study was conducted by El-Sayed et al. (2006) to evaluate the effect of shear strength of FRP-reinforced concrete beams without transverse reinforcement. The main investigated parameters were the reinforcement ratio and the modulus of elasticity of the longitudinal reinforcement bars. Nine large-scale simply supported concrete beams were tested in four-point bending. The study indicated that the relatively low modulus of elasticity of FRP resulted in reduced shear strength compared to control beams reinforced with steel. In addition, the study concluded that the higher the reinforcement ratio or the modulus of elasticity of the reinforcement, the higher the obtained shear strength.

FRP can be moulded into different stirrup shapes similar to traditional steel stirrups. However, due to the difference in properties, FRP cannot be directly substituted for steel stirrups in design. Compared to steel, several issues need to be taken into consideration in design of members reinforced with FRP for flexure and shear including:

- Bars have a lower dowel resistance;
- Lower modulus of elasticity;
- Tensile strength is decreased in bent bars.

Ahmed et al. (2010) presented experimental results on shear strength of concrete beams reinforced GFRP stirrups. Four large scale simply supported concrete beams with a T-shaped cross-section were tested under four-point bending till failure. The main investigated parameters were type and ratio of shear reinforcement. The study indicated that the presence of GFRP stirrups in the tested specimens, similar to steel stirrups, enhanced the concrete contribution after the formation of the first shear crack. It was observed that as the spacing was decreased, the shear resistance was enhanced due to the confinement, which improves the aggregates interlocking. Moreover, the study suggested that using FRP stirrups with strength of bend-to-straight portion ≥ 0.6 enables using the full capacity of the straight portion of the FRP stirrups, while lower ratios will cause the bend strength to govern the tensile strength of the stirrup.

2.4.4. Deflection and cracking

Due to the relatively low modulus of elasticity of FRP bars compared to traditional steel reinforcement, the serviceability requirements such as deflection and crack width are the main concern of in their behaviour. A significant number of experimental studied were conducted to investigate the behaviour of FRP-reinforced element under service conditions. Moreover, a number of formulas and equations were proposed to predict the response of concrete elements reinforced with FRP at service loading conditions with reasonable accuracy.

Benmokrane et al. (1996) studied the flexural response of FRP-reinforced concrete beams. An experimental and theoretical comparison was carried out between conventionally reinforced concrete beams and their counterparts reinforced with FRP bars. The conducted comparison was based on cracking behaviour, modes of failure, load capacity, load deflection behaviour, rigidity and strain distribution. The authors concluded that there was perfect bond between FRP bars and surrounding concrete, which was demonstrated by the experimental strain distribution results.

Moreover, it was observed that cracking patterns and spacing in FRP-reinforced concrete beams at low load were very similar to those of steel reinforced beams. However, at service loads more and wider cracks were experienced by FRP-reinforced beams.

Toutanji and Saafi (2000) studied the flexural behaviour of concrete beams reinforced with GFRP bars. The research aimed to provided design equations to predict deflection and crack width in-lieu of ACI 318-95 provisions. The main studied parameters were the reinforcement ratio and mode of failure. The study indicated that GFRP-reinforced beams exhibit large deflection and crack width compared to their counterparts reinforced with steel. This was attributed to the lower modulus of elasticity for GFRP bars. Consequently, the authors assumed that current design methods developed for steel-reinforced structures for prediction of deflection and crack width may not be applicable for GFRP reinforced beams. The researchers proposed a modified equation based on Branson's equation for predicting deflection taking into account FRP modulus of elasticity and reinforcement ratio. Obtained experimental results were in good agreement with proposed analytical models.

Yost et al. (2003) investigated the deflection behaviour of GFRP-reinforced concrete beams. The main objective of the study was to evaluate the effective moment of inertia (I_e) experimentally by comparing the results with available formulas given in design codes and previous research. The study evaluated the deflection behaviour of simply-supported beams with normal-strength and high strength concrete, deferent reinforcement ratios, and shear span-to-depth ratios.

The obtained results were compared with deflection models in ACI committee 440's report (ACI 1996). It was found that the ACI 440R model is over estimating the effective moment of inertia. The authors proposed an appropriate modification to this formula for more precise prediction of

effective moment of inertia. The authors concluded that, due to the almost sudden transition from gross to cracked section properties for GFRP-reinforced concrete beams, the effective moment of inertia, I_e, approaches cracked moment of inertia I_{cr} much faster than similar steel-reinforced beams. Moreover, it was found that the ratio I_g/I_{cr} for GFRP reinforcement beams is within four to eight times higher than that for steel-reinforced beams, were I_g is the gross moment of inertia of the un-cracked cross-section.

Another experimental study was carried out by El-Salakawy and Benmokrane (2004) to investigate the flexural behaviour and serviceability performance of concrete deck slabs reinforced with different types of FRP bars. The study presented the results of 10 full-size simply-supported one-way concrete slabs tested under four-point bending. These results were reported in terms of deflection, crack width, strains in concrete, ultimate capacity and mode of failure. The tested parameters were the type and size of FRP reinforcement bars and the reinforcement ratio. The study concluded that the carrying capacity of concrete slabs reinforced with FRP bars was much higher than the steel-reinforced counterparts. In addition, the flexure stiffness of FRP reinforced specimens was found to be higher when the reinforcement ratio was increased. Moreover, no significant effect was found of using different bar diameters on deflection or ultimate capacity.

Furthermore, extensive studies were dedicated to provide formulas to predict the load-deflection response of FRP-reinforced concrete beams. Most of the available formulas were based on Branson's equation to calculate the effective moment of inertia (I_e). As this equation was developed for steel-reinforced beams, modification factors were applied for the equation to be applicable with FRP-reinforced beams. ACI Committee 440 (2006) provides a modification

factor β_d to the gross moment of inertia (I_g) in Branson's equation as in Eq. (2.1), where β_d = 1/5 (ρ/ρ_b).

$$I_e = \left(\frac{M_{cr}}{M_a}\right)^3 \beta_d * I_g + \left[1 - \left(\frac{M_{cr}}{M_a}\right)^3\right] * I_{cr} \leq I_g \qquad (2.1)$$

ISIS Canada (2007) recommends Eq. (2.2) for I_e based on the work of Mota et al. (2006) as it provides consistently conservative results.

$$I_e = \frac{I_g * I_{cr}}{I_{cr} + \left(1 - 0.5\left(\frac{M_{cr}}{M_a}\right)^2\right) * (I_g - I_{cr})} \qquad (2.2)$$

CSA S806-02 (CSA 2002) recommends a different formula based on the integration of curvature along the span to determine deflections as in Eq. (2.3).

$$I_e = \frac{I_{cr}}{1 - \eta * \left(\frac{M_{cr}}{M_a}\right)^3} \quad where\ \eta = 1 - \left(I_{cr}/I_g\right) \qquad (2.3)$$

Bischoff (2007) proposed Eq. (2.4) with a rational correction factor (β_d) to Branson's equation that reduces tension stiffening to reasonable levels by setting $\beta_d\, I_g / I_{cr} \approx 3.3$.

$$I_e = \left[1 + 2.3 * \left(\frac{M_{cr}}{M_a}\right)^3\right] * I_{cr} \qquad (2.4)$$

Habeeb and Ashour (2008) investigated the load-deflection response in their experimental study on continuous concrete beams reinforced with GFRP bars. The authors proposed a modification factor to the equation proposed by ACI 440 (2006) to calculate the effective moment of inertia (I_e). A modification factor γ_G =0.6 as shown in Eq. (2.5) was found to be an effective tuning parameter for the deflection prediction of the tested beams.

$$I_e = \left(\frac{M_{cr}}{M_a}\right)^3 \beta_d * I_g + \left[1 - \left(\frac{M_{cr}}{M_a}\right)^3\right] * I_{cr} * \gamma_G \qquad (2.5)$$

2.4.5. Ductility and deformability

For reinforced concrete in general, ductility is mainly a measure of the capacity of energy absorption through plastic deformation. The ductility of traditional steel-reinforced concrete beams is defined as a ratio of deflection or curvature or rotation values at ultimate loading to those at the steel yielding. This definition mainly depends on the yielding plateau typically illustrated by steel bars. Moreover, the steel-reinforced section has to be under-reinforced to be able to develop yielding stress in the bars and avoid compression crushing of concrete. Interpretation of ductility of concrete beams reinforced with FRP bars on the basis of conventional definitions is misleading due to the linear stress-strain relationship of FRP up to failure. Therefore, a new way to describe ductility in FRP-reinforced beams was introduced

(Theriault and Benmokrane 1998). The new definition has been introduced under the name of *J* factor (Jaeger et al. 1995; Mufti et al. 1996; Vijay et al. 1996). This factor takes into consideration the increase in moment as well as the increase of curvature or deflection.

J-factor = Strength factor × Deformation factor (curvature or deflection) (2.6)

$$\text{Strength factor} = \frac{\text{Moment at ultimate}}{\text{Moment at concrete compressive strain of } 0.001}$$

$$\text{Curvature factor} = \frac{\text{Curvature at ultimate}}{\text{Curvature at concrete compressive strain of } 0.001}$$

$$\text{Deflection factor} = \frac{\text{Deflection at ultimate}}{\text{Deflection at concrete compressive strain of } 0.001}$$

The American Concrete Institute (ACI) Committee 440 (2006) is also considering the influence of FRP properties on the deformability of members. To compensate for the lack of ductility in FRP-reinforced elements, compared to steel, the committee suggests that a higher factor of safety should be used in design. Moreover, it is proposed that a smaller strength reduction factor be used when the failure is controlled by rupture of the FRP. Furthermore, The Canadian Highway Bridge Design Code (CSA 2006) assess the deformability of sections reinforced with FRP by a ‘‘performance factor’’ very similar to *J*-factor described above. This code requires that the performance factor be greater than 4 or 6 for rectangular and T-sections, respectively.

Vijay and GanaRao (2001) discussed the effect of failure mode on ductility/deformability of FRP-reinforced beams. The study found that deformability of a GFRP-reinforced beam depends on the following: (1) uniform elongation of FRP bars compared to localize yielding of steel bars;

(2) effect of confinement; (3) the bond between concrete and bars; (4) uniform crack location and spacing in FRP reinforced concrete; (5) the formation of plastic hinge in concrete.

The study concluded that compression failure of FRP reinforced beams achieved higher deformability compared to tension failure. This was attributed to plastic hinge formation, confinement, and significant concrete cracking in compression zone. The authors also compared the achieved deformability with compression failure of GFRP-reinforced and steel-reinforced concrete beams. The values were found to be similar.

Newhook et al. (2002) conducted a parametric study to provide a procedure for flexural design of sections reinforced with FRP that satisfies the deformability requirement by limiting the tensile strain in FRP bars at service. The study recommended that the design of cross-sectional area should be based on a permissible value of tensile strain in FRP bars at service not greater than $2{,}000 \times (10)^{-6}$. The study showed that this permissible value of strain commonly results in a deformability factor (DF) greater than 4; thus, there is no need to check the deformability.

2.4.6. Ductility improvement

Wu (2006) presented a novel technique to achieve ductility in reinforced concrete members through compressive yielding instead of tensile yielding. This technique is quite useful when the tensile straining of reinforcement is limited or when the tensile reinforcement does not yield. This work addressed the problem of reduced ductility from an innovative and novel point of view. The proposed technique involved the concept of compression yielding using a ductile compressive material or mechanism at the compression zone of a plastic hinge in a reinforced concrete member. According to the proposed idea, ductility could be improved by replacing concrete in the compression zone of a plastic hinge with a block with good elasto-plastic

material. This configuration of ductile compression zone will act as a fuse in the structural system that will be triggered when excessive loading conditions occurs. Once it is triggered, the structure will be forced to behave in a more plastic manner to avoid sudden failure.

The author concluded that, there is no limit on the achievable ductility in a flexural member using compression yielding as long as the compression zone exhibit sufficient ductility. In addition, while the common and most popular method of confining concrete improves ductility as well as concrete strength which increase the risk of tension bars rupture, the proposed new technique ensures a ductile rather than sudden failure mode.

2.5. Continuous Beams Reinforced with FRP Materials

2.5.1. Introduction

Statically indeterminate beams usually have the potential to redistribute stresses between critical sections. This redistribution results in a more favourable behaviour providing higher load capacity and more efficient utilization of the used material. As indicated earlier in the literature, a successful redistribution between critical sections in continuous beams depends on satisfying required plastic rotation by the available rotation. Due to the linear stress-strain behaviour of FRP bars up to failure, it appears at first glance that moment redistribution in FRP-reinforced continuous beams is not possible. This is reflected on the current available design recommendations and guidelines, which do not permit moment redistribution in such beams. However, it is evident as discussed earlier in the previous section for steel-reinforced beams that a significant amount of redistribution occurs well before yielding of steel. Similar behaviour was observed in continuous beams reinforced with low-ductility reinforcement. This can be attributed to the relative moment of inertia between critical sections which is influenced by the degree of cracking according to the provided reinforcement.

Moreover, as illustrated in the following section, recent experimental studies on FRP-reinforced continuous beams reported observation of moment redistribution in such beams. Further theoretical investigations were conducted in an attempt to predict the response up to failure of FRP-reinforced continuous beams. In these investigations, factors usually not considered in simplified calculations such as concrete tension stiffening and bond-slip response of reinforcement are taken into account. These factors were used to calculate redistribution of bending moment between critical sections in continuous beams reinforced with FRP bars. It was also indicated that the response of such beams is more member-dependent rather than being section-dependent. Thus, the relation between the critical sections controls the beam response rather than the properties of one section.

To date, to the best of the author's knowledge, little to no research on the available moment redistribution of continuous FRP-reinforced beams on a quantitative level; a fairly accurate prediction of their response up to failure, is still required. It is clear that through a better understanding of the full range of behaviour of continuous beams reinforced with FRP is required to provide reliable guidelines that represent the actual structural response.

2.5.2. Experimental studies on FRP-reinforced continuous beams

Tezuka et al. (1995) conducted an experimental investigation on two-span continuous beams either reinforced or pretensioned with FRP bars or conventional steel wires. The main objective of the study was to investigate the moment distribution behaviour in case of continuous beams designed for compressive failure at internal support prior to FRP tension failure at loading points. The studied variables were reinforcement material (Aramid FRP, Carbon FRP and steel prestressing wires), and prestressing level of reinforcement (with or without prestressing).

The authors conducted a very simple non-linear analysis to predict moment-curvature relationship taking into consideration the non-linearity of the used materials. The analysis was based on the assumption that 1) plane section remains plan after loading; 2) tension stiffening of concrete between cracks is ignored; 3) concrete cracks at tension strain of 0.0001. Comparing experimental with calculated moment-curvature relationship, it was found that the computed curvature tends to be higher than the experimental one at the same moment. This was attributed to the under estimation of the section rigidity at the middle support. Moreover, the difference between experimental and computed results of specimens reinforced with non-prestressed CFRP and AFRP were found to become larger as moment increased. Experimental results of moment-curvature relationship obtained at the middle support indicated that the slope of the curve hardly change up to failure. Reported moment distribution percentages measured experimentally at the middle support section of beams reinforced with AFRP and CFRP were found to be 14.1% and 29.7%, respectively. A software package based on non-linear finite element method was used to study the relationship between the applied load and the percentage of moment redistribution with different reinforcement ratios. For the beam reinforced with non-prestressed AFRP, it was found that moment distribution converges to a smaller value as the load increases. This was attributed to the reduction in section rigidity which is approximately the same at middle support and loading point.

Grace et al. (1998) studied experimentally the behaviour and ductility of simple and continuous beams reinforced with different types of FRP. Used reinforcement types were steel, carbon and glass FRP bars. Test results showed that using GFRP stirrups increases shear deformation then deflection increases consequently. Moreover, using GFRP stirrups changed the mode of failure from flexural failure to shear or flexural shear failure depending on the used longitudinal

reinforced. Continuous beams reinforced by FRP experienced higher deflection compared to their counterparts reinforced with steel. In addition, the dowel effect had an influence on FRP continuous beams load carrying capacity.

Razaqpur and Mostofinejad (1999) studied experimentally the shear behaviour of continuous beams reinforced with CFRP. The main objective of the research was to investigate the feasibility of using FRP grid as shear reinforcement. The main variables studied in this experimental work were shear reinforcement material (steel stirrups or CFRP grid), and reinforcement ratio (over or under-reinforced). The experimental results indicated that CFRP grid as shear reinforcement performed as well as conventional steel stirrups. It was observed that tested beams did not collapse when the load corresponding to the flexural capacity of middle support section was reached. The beams, however, retained 80% of their strength despite the failure of hogging moment section. This gave an indication that over-reinforced members with FRP bars exhibit a semi-ductile behaviour.

The authors concluded that despite the lower modulus of elasticity of CFRP grid tested beams failed at a higher load than beams reinforced with steel stirrups with higher shear reinforcement ratio. Thus, it is possible to use CFRP grids as shear reinforcement.

Habeeb and Ashour (2008) studied experimentally the flexural behaviour of continuously concrete beams reinforced with GFRP longitudinal bars and steel stirrups. For comparison purposes another continuous concrete beam reinforced with steel bars was also tested. The main parameter investigated in this research was the amount of GRFP reinforcement. The research also compared between the deflections obtained experimentally and those predicted from

simplified methods proposed by the ACI 440 committee (ACI 2006). Good agreement was found between obtained results and perdition equations.

Throughout the experimental tests four different modes of failure were observed. These four modes of failure were: bar rupture, concrete crushing, concrete crushing combined with shear failure and conventional ductile flexure failure.

Bar rupture failure mode was observed in beams with GFRP under-reinforcement section at mid-span. Concrete crushing failure mode, however, was experienced by beams with over-reinforced section at mid-span. Wide cracks were observed over the middle support before concrete crushing at the mid span section.

In concrete crushing combined with shear failure mode, the diagonal shear cracks were emerged and propagated simultaneously with the flexure cracks, leading to the sudden collapse of the beam. This mode was experienced with beam having over reinforcement ratio in both bottom and top layers.

The last type of failure was demonstrated by the steel reinforced concrete beam. The failure occurred due to yielding of tensile steel followed by concrete crushing at both middle support and mid span sections.

Reactions were recorded at middle and end supports to assess the load distribution of each beam. The elastic reactions using uniform flexure stiffness throughout the beam were calculated to be compared with measured reactions. In beams with bottom reinforcement ratio at mid-span higher than or equal to the top reinforcement ratio at middle support, signs of moment redistribution were observed as the recorded end reactions were higher than the elastic reaction at the same load level.

The study concluded that GFRP reinforced continuous concrete beams develop earlier and wider cracks than similar steel reinforced concrete beams. Moreover, it was indicated that ACI 318-05 (ACI 2005) proposition regarding the spacing of steel stirrups has to be reconsidered when used with GFRP reinforcement to avoid shear failure. In addition, increasing the top reinforcement ratio over the middle support does not contribute significantly in increasing the load capacity, on the other hand over reinforcing the bottom layer in continuous beams is the key factor in improving the load capacity and controlling deflection in addition to delaying of crack propagation.

2.5.3. Analytical studies on FRP-reinforced continuous beams

Gravina and Smith (2008) conducted a theoretical study on the flexural behaviour of statically indeterminate concrete beams with FRP bars. The study was performed using a local deformation model which was presented by Gravina and Warner (2003). The research objective was to apply the theoretical model to continuous beams reinforced with FRP to predict the bending moment distribution, flexural cracks, crack spacing and crack width.

The significance of this research lays in the need for a better understanding of the full range of behaviour of FRP reinforced concrete members in both service and ultimate loading levels. This required a more rigorous method that can be used to evaluate the flexure behaviour of this type of members. The authors modified the method presented in Gravina and Warner (2003) which was developed for steel reinforcing bars to be used for FRP reinforcing bars.

The bond-slip relation between FRP bars and surrounding concrete was taken into consideration. However, the authors pointed out that very little work has been done to develop a general analytic bond-slip formula for FRP reinforcement. The analytical model presented by the authors

was verified with experimental results for both simply supported and continuous FRP-reinforced beams. It was not possible to check some features of the model such as crack width, crack spacing and stress levels in FRP and concrete due to shortage in high-enough quality of the reported experimental data. Moreover, the quantity of bond-slip relation has not been reported there for it was assumed. The results were found to be very sensitive to the assumed relation.

After being verified by experimental results, the analytical model was used in a numerical study for better understanding of flexural behaviour, moment distribution and ductility of indeterminate FRP-reinforced concrete beams. The behaviour of steel-reinforced concrete beams was also calculated for comparison. The studied parameters were steel reinforcement ductility type (normal ductility or low ductility), carbon or glass FRP bars, and surface condition of FRP bars (ribbed or grain covered). Ribbed and grain coated FRP bars demonstrated very little difference in the overall structural response, which may indicate that tension stiffening and load-deflection response are independent of bond. Considering the crack width, the grain coated bars exhibit better bond characteristics compared to ribbed bars, hence developed smaller cracks.

As the modeling approach used in the study is capable of simulating different stages of stress redistribution in indeterminate beams, moment redistribution was calculated for different reinforcing material types and bond characteristics. All beams had the same amount of reinforcement in both hogging and sagging regions. First crack appeared at the middle support. To maintain system equilibrium stresses were redistributed to the span region. With further load increase, the span section cracks and the ratio M_{sup}/M_{sp} slightly increases then remains constant (where M_{sup} is the moment at middle support and M_{sp} is the moment in the span). Only for ductile steel-reinforced beams that further moment redistribution occurred when the steel yielded.

Moreover, the authors discussed the strain localisation concept. It is defined as localised high strains in reinforcement near crack being much larger than strains away from cracks. As the used analytical model is capable of calculating the stress in reinforcement along the member length at different loading stages, the ratio $\varepsilon_{peak}/\varepsilon_{avg}$ could be determined, where ε_{peak} is peak tensile strain in reinforcement at the crack location and ε_{avg} is the average strain between cracks. For FRP bars, strain localisation was found to be insignificant since high levels of slip are able to develop prior to failure. In addition, the tension stiffening ratio $\varepsilon_{peak}/\varepsilon_{avg}$ for FRP bars was found to be small compared to steel bars. Hence FRP-reinforced members exhibit more deformation prior to failure which can result in more rotational capacity and ample warnings before failure. As some factor were not taken into consideration, the authors indicated that more work is needed to investigate the effect of other factors such as concrete strength, confinement, bar diameter and embedment length on the bond performance of FRP bars.

The authors presented in this work some recommendations for future design. There are concerns as to whether continuous FRP-reinforced concrete will demonstrate enough ductility to sustain deformation at overloading prior to collapse. Thus quantifying the ductility aspects is of high importance if FRP bars are to be accepted in reinforcing statically indeterminate structures. The presented analytical model is capable of predicting the ductility and moment redistribution characteristics of continuous FRP-reinforced beams. A design guide line can be provided by comparing the available rotation capacity in critical regions with the required by the assumed moment redistribution. However, the definition of available rotation capacity has to be redefined since FRP bars have no yield points.

2.5.4. Code provisions for FRP-reinforced sections

The design formulas and provisions for FRP-reinforced structures can be found in the Canadian standards CSA-S806-02 (2002), CSA-S6-09 (2009) and ACI committee 440.1R-06 (2006). Due to the lake of research, the current design codes do not have sufficient provisions and do not allow for moment redistribution in continuous concrete beams reinforced with FRP. In this current research concerning moment redistribution in continuous beams, the Canadian standard CAN/CSA-A23.3-04 (CSA 2004) for steel reinforced structures was used as a guide in selecting the moment redistribution ratio.

More details regarding code provisions for design of FRP-reinforced structures can be found in Appendix B.

CHAPTER 3: EXPERIMENTAL PROGRAM

3.1. General

Based on the literature discussed in the previous chapter, an experimental investigation was conducted to study the behaviour of FRP-reinforced continuous beams considering key factors affecting their behaviour and dealing with current research needs in this area. The main objective of the experimental program was to investigate the structural behaviour of FRP-reinforced concrete continuous beams compared to their counterparts reinforced with steel. In addition, the experimental program specifically aimed to investigate the effect of the material type of longitudinal bars and their arrangement, and also the material type, spacing and the reinforcement ratio of the transverse reinforcement. Moreover, the study included testing a specimen to evaluate the serviceability performance of continuous concrete beams reinforced with GFRP. In the following section, details on the tested specimens and the investigated parameters are provided.

3.2. Test Specimens

Ten large-scale continuous concrete beams were experimentally tested. All beams had a rectangular cross-section of 200 × 300 mm with overall length of 6000 mm. The beams were continuous over two equal spans of 2800 mm and 200 mm overhang, each. The dimensions and geometry of the test specimens are shown in Figure (3.1).

The tested parameters in this experimental investigation were flexural reinforcement ratio in both sagging and hogging bending moment sections, material of longitudinal reinforcement as well as transverse reinforcement material, spacing, and reinforcement ratio. In addition, the target design load was also an investigated variable to evaluate the serviceability performance of continuous

beams reinforced with FRP. Table (3.1) shows all ten tested specimens and the corresponding tested parameter.

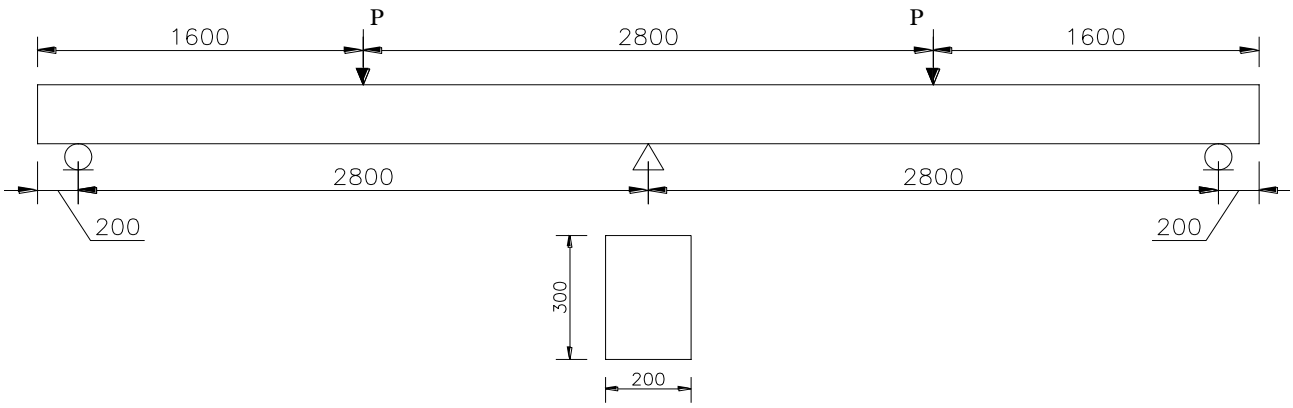

Figure (3.1): Dimensions of test specimens

Table (3.1): Tested variables

Studied parameter	SSc-8*d*/2*p*	GSu-8*d*/2*p*	GSu-8*d*/2*e*	GSu-8*d*/3*p*	GSu-10*d*/2*p*	GSs-10*d*/2*p*	GGu-10*d*/2*p*	GGu-10*d*/3*p*	CSu-8*d*/2*p*	CSu-8*d*/2*e*
Assumed moment redistribution	20%		0%	20%						0%
Material of flexural reinforcement	Steel	GFRP							CFRP	
Material of Stirrups	Steel						GFRP		Steel	
Spacing of stirrups (mm)	120			80	120			80	120	
Diameter of stirrups (mm)	8				10		9.5		8	
Target design load	Control	Ultimate load				Service	Ultimate load			

The test beams were named based on the material of longitudinal reinforcement as well as the material, diameter and spacing of stirrups. The first and second capital letters in the beam name represent the materials of longitudinal and transverse reinforcement, respectively; "G" for GFRP and "S" for steel bars. The third lowercase letter represents the design load criteria; "u" for beams designed to achieve the targeted ultimate load, "s" for the beam designed to meet the targeted service load and "c" for the control beam intended to serve as reference for comparison. The fourth number represents the roundup diameter of the used stirrups in millimetres; "8" mm or "10" mm. The second-last character represents the spacing of the stirrups; "*d*/2" for 120 mm spacing between stirrups or "*d*/3" for 80 mm spacing, where *d* is the beam effective depth. The last letter "e" for beams provided with reinforcement configuration to satisfy the elastic moment distribution along the beam or "p" for beams allowed for plastic redistribution. For example, GSu-8*d*/2p denotes for a beam reinforced with GFRP in the longitudinal direction, designed to reach a specific ultimate load, with steel stirrups of 8-mm diameter spaced at 120 mm along the beam length and provided with reinforcement ratio at mid-span higher than that at the middle support to allow for plastic moment redistribution.

Beam SSc-8*d*/2*p* was reinforced in both the longitudinal and the transverse direction with traditional steel reinforcement to be considered as a reference beam. Four beams, GSu-8*d*/2*p*, GSu-8*d*/2*e*, GSu-8*d*/3*p* and GSu-10*d*/2*p*, reinforced with GFRP longitudinal bars and steel stirrups were tested to investigate the effect of different configurations of longitudinal reinforcement in addition to the effect of the amount of transverse reinforcement and stirrups spacing. The flexural reinforcement ratios in critical sections were changed to allow for either 0% or 20% moment redistribution. Moreover, the spacing of stirrups was changed while the

same transverse reinforcement ratio was kept the same to isolate the effect of stirrup spacing. Finally, two different bar diameters were used for stirrups (8 and 10 mm) to study the effect of increasing the amount of transverse reinforcement diameter.

Two beams, CSu-8*d*/2*p* and CSu-8*d*/2*e*, were reinforced with CFRP longitudinal bars and steel stirrups to investigate the effect of changing the material type of the longitudinal reinforcement. Three different materials for longitudinal reinforcement were used in this study, namely steel, GFRP and CFRP bars. Another two beams, GGu-10*d*/2*p* and GGu-10*d*/3*p*, were reinforced with GFRP longitudinal bars and stirrups. Testing these two beams aimed to study the effect of changing the material type of the transverse reinforcement and the validity of using GFRP bent bars as transverse reinforcement. Two materials for transverse reinforcement were used in this studied, either steel or GFRP stirrups. The last beam, GSs-10*d*/2*p*, reinforced with GFRP longitudinal bars and steel stirrups was designed to have the same service load as the control specimen.

3.3. Design Concept

The proposed specimens are designed according to the applicable design codes to satisfy both flexural and shear strength requirement. The Canadian standard CSA S806-02 (2002) was used for the FRP-reinforced specimen while CSA A23.3-04 (2004) was used to design the steel-reinforced specimen. It should be noted that, due to different design concepts of FRP and steel RC elements, there are two approaches to design the specimens to be comparable. The first is to have similar ultimate capacity, while the second is to have similar service load (satisfy serviceability requirements). First approach was selected for nine of the ten tested beams. This is because moment redistribution is expected to be more profound at high loading stages close to failure when large deformations develop. This design approach led to different service loads for

the test specimens. The second approach, however, was applied in the design of one beam to evaluate the performance of FRP-reinforced continuous beams under service loading conditions. All beams were designed to have a similar ultimate load carrying capacity of approximately P = 125 kN, except for one beam designed to have similar service load compared to the steel-reinforced control beam, where P is the applied load at the middle of each span. Table (3.2) shows the design loads as well as expected ultimate and service loads for all tested beams.

Table (3.2): Design loads of tested beams

Beam	Design load approach	Ultimate load (kN)[a]	Service Load (kN)[c]	Assumed redistribution
SSc-8*d*/2*p*	Control specimen	129[b]	60	20%
GSu-8*d*/2*p*	Ultimate load (≈125 kN)	126	33	20%
GSu-8*d*/2*e*		118	40	0%
GSu-8*d*/3*p*		126	33	20%
GSu-10*d*/2*p*		126	33	20%
GGu-10*d*/2*p*		126	33	20%
GGu-10*d*/3*p*		126	33	20%
CSu-8*d*/2*p*		124	59	20%
CSu-8*d*/2*e*		129	94	0%
GSs-10*d*/2*p*	Service load (60 kN)	165	60	20%

[a] Based on the target concrete strength (30 MPa).
[b] Assuming failure is reached at yielding stress of 400 MPa
[c] The load corresponding to allowable stresses in bars as specified by the applicable code.

The reinforcement for both flexure and shear were selected to lead the specimens to the desired mode of failure. Transverse reinforcement was provided to ensure that the shear strength is higher than flexure strength to avoid premature shear failure. A summary of design calculations of all tested beams can be found in Appendix A.

3.3.1. Flexural design

The steel-reinforced control beam was designed to fail due to steel yielding at both mid-span and middle support sections. This was achieved by providing both sections with reinforcement ratio less than the balanced reinforcement ratio (ρ_b). On the other hand, the FRP-reinforced continuous beams were designed to have compression failure (concrete crushing) at both critical sections as recommended by the CSA S806-02 code (CSA 2002). Therefore, both mid-span and middle support sections were provided with reinforcement ratios ranging between 1.2 and 2.5 ρ_b

3.3.2. Shear design

Currently, there are several design codes and guidelines available to design FRP-reinforced concrete structures (CSA 2002, ACI 2006, CSA 2009). The shear capacity of the tested FRP-reinforced beams was designed according to the CSA S806-02 code (CSA 2002) to satisfy the shear force corresponding to the targeted design load. The provided spacing of the stirrups respected the maximum and minimum code limits. The amount of transverse reinforcement was one of the tested parameters in this study. Two beams, GSu-8*d*/3*p* and GSu-10*d*/2*p*, were provided with transverse reinforcement ratio ($\rho_v = A_v / b\ s$) approximately 1.6 higher than beam GSu-8*d*/2*p*. For the same purpose, beam GGu-10*d*/3*p* had ρ_v approximately 1.5 higher than GGu-10*d*/2*p*.

3.3.3. Predicted failure load

The beams were loaded symmetrically by applying a concentrated load at the middle of each span. The loading and the corresponding elastic bending moment and shear diagrams are shown in Figure (3.2). Based on elastic analysis, the connecting moment over the middle support ($0.188P\ell$) is higher than that at the mid-span section ($0.156P\ell$), where ℓ is the clear span. However, when a 20% moment redistribution is assumed to occur at the middle support section, this results in changing the moment distribution to be $0.15P\ell$ and $0.175P\ell$ for the sections at middle support and mid-span, respectively. The calculated failure load is considered to be the load at which one of the critical sections develops the maximum flexural capacity expected by the used code formulas.

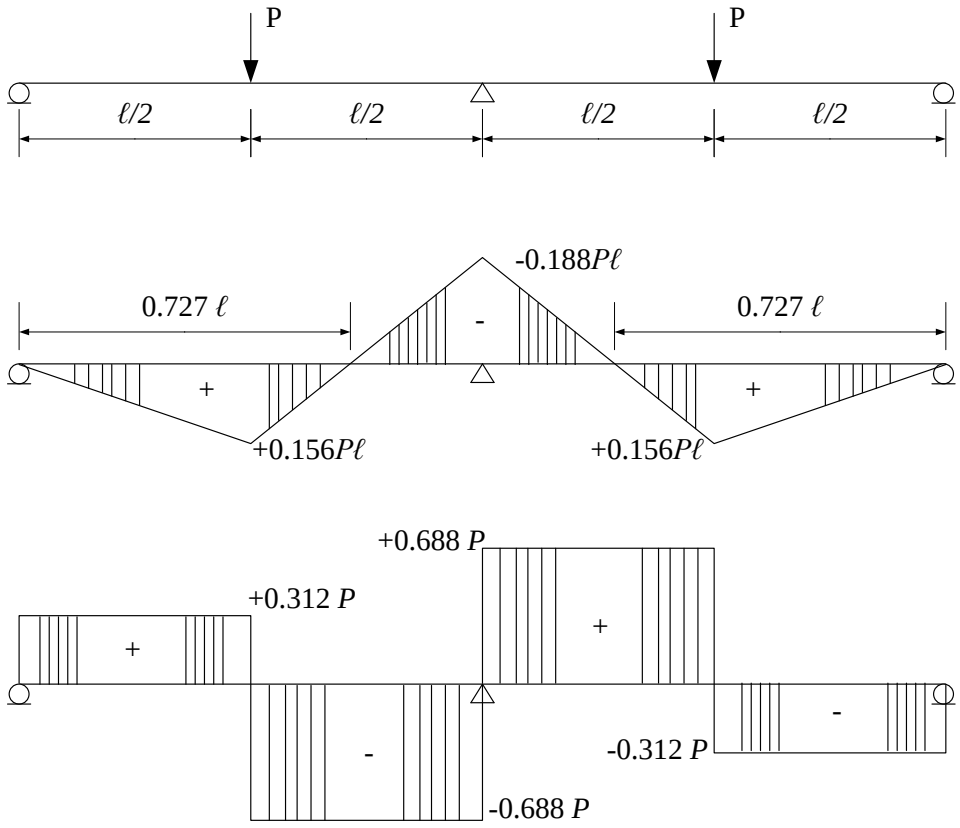

Figure (3.2): Elastic bending moment and shear force diagrams of the applied loads

3.4. Materials

All test specimens were constructed using normal weight, ready-mix concrete with target compressive strength of 30 MPa at 28 days. The concrete was ordered from a local concrete plant with maximum aggregate size of 20 mm and 100 mm slump. The actual compressive strength of the concrete is determined by testing five standard cylinder specimens on the day of testing as shown in Table (3.4). Three different types of longitudinal reinforcement were used. The CFRP and GFRP bars used in this study had a sand-coated surface to enhance bond and force transfer between bars and concrete. The bars were made of continuous longitudinal fibres impregnated in a thermosetting vinyl-ester resin with a fibre content of 73% by weight (Pultrall Inc. 2009). Deformed steel bars, No. 15M, were used in the flexural reinforcement of the control beam. The mechanical properties of these bars were obtained from standard tests carried out according to ASTM A370-05 (ASTM 2005). The obtained yield strength and yield strain of the used steel bars are shown in Table (3.3). The used GFRP stirrups have an overall height of 245 mm, width of 155 mm, and bend radius, r_b, of 38 mm ($4d_b$, where d_b is the bar diameter). The tensile capacity and modulus of elasticity of the straight portions of the GFRP stirrups are shown in Table (3.3)**.** The tensile strength of the straight portion in the bent bar was 512 MPa, which represents 70% of the tensile strength of the pultruded bar. Table (3.3) also lists the mechanical properties of the reinforcing bars as determined by tensile tests on representative specimens in accordance with ACI 440.3R-04 (ACI Committee 440 2004). Figure (3.3) shows a photograph of the used FRP bars and GFRP stirrups.

Table (3.3): Mechanical properties of the used reinforcing bars

Bar Type	Bar Diameter (mm)	Bar Area (mm2)	Modulus of Elasticity (GPa)	Tensile Strength (MPa)	Ultimate Strain %
Longitudinal steel bars	15.9	200	200	f_y = 485*	ε_y = 0.0024*
Steel stirrups	8	49.4	190	f_y = 300*	ε_y = 0.0016*
GFRP No. 16	15.9	198	46 ± 1	731 ± 9	0.016 ± 0.0005
CFRP No. 10	9.5	71	116 ± 2	1388 ± 62	0.012 ± 0.0007
GFRP stirrups	9.5	71	45 ± 1	512 ± 9**	0.016 ± 0.0005

* f_y and ε_y is the yield stresses and yield strain of steel, respectively.
** Strength of the straight portion in the bent bar, taken as 70% of the strength of the pultruded bar.

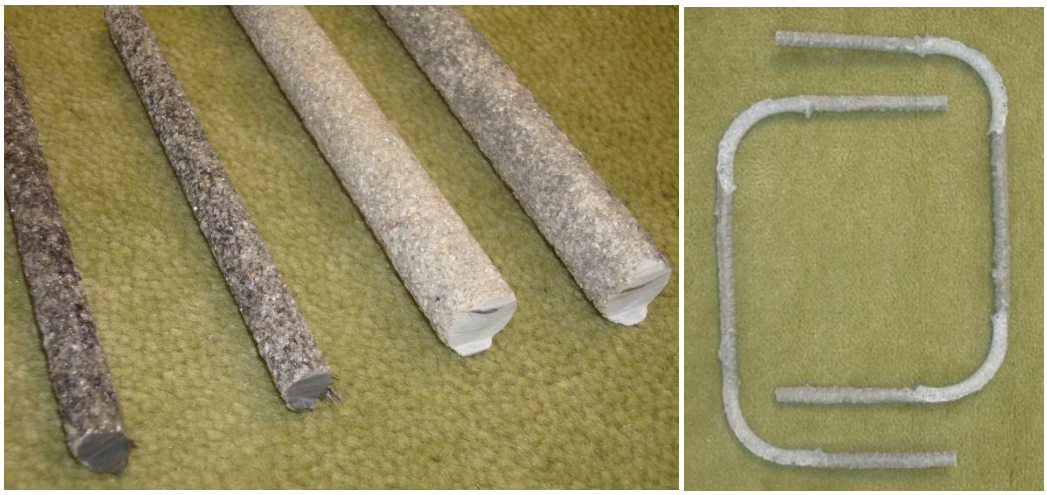

Figure (3.3): Glass and carbon FRP sand-coated bars and GFRP stirrups

3.5. Details of Tested Beams

The followed design concepts resulted in the following reinforcement configurations of the tested beams. The steel reinforced control beam, SSc-8*d*/2*p*, was reinforced with three No.15M steel bars as top reinforcement at the middle support section and four No.15M steel bars as bottom reinforcement. The used transverse reinforcement was 8 mm steel stirrups spaced at 120 mm all over the beam length. Beams GSu-8*d*/2*p* , GSu-8*d*/3*p* , GSu-10*d*/2*p* , GGu-10*d*/2*p* , and GGu-10*d*/3*p* were reinforced with two No.16 GFRP bars at the top and three No.16 GFRP bars at the bottom of the beam. This reinforcement configuration was designed to allow for 20% moment redistribution. In contrary, beam GSu-8*d*/2*e* was reinforced with two No.16 GFRP bars at the bottom and three No.16 GFRP bars at the top of the beam. This configuration follows the elastic moment distribution along the beam, which does not allow for moment redistribution. Beam CSu-8*d*/2*p* was conceptually designed similar to beam GSu-8*d*/2*p* but using No.10 CFRP bars as longitudinal reinforcement. Beam CSu-8*d*/2*e* also was reinforced with CFRP bars, however, with an opposite arrangement of bars including two No.10 CFRP bars at the bottom and three No.10 CFRP bars at the top of the beam. Beam GSs-10*d*/2*p* was reinforced with seven No. 16 GFRP bars at the bottom and four similar bars at the top of the beam. This beam was designed to have similar service load to the control steel-reinforced beam SSc-8*d*/2*p*. Therefore, beam GSs-10*d*/2*p* was provided with higher reinforcement ratio than beam SSc-8*d*/2*p* to satisfy serviceability requirements. Beam GSs-10*d*/2*p* was provided with enough longitudinal reinforcement to keep mid-span deflection, crack width and tensile stress in reinforcement below the allowable limits specified by the code. The allowable serviceability limits for FRP reinforced structures are known to be different from those reinforced with steel. Therefore, the behaviour of beam GSs-10*d*/2*p* and SSc-8*d*/2*p* at service load is not expected to be identical. Deflection of

beam GSs-10*d*/2*p* at mid-span and the allowable limit were predicted according to the CSA S806-02 code (CSA 2002). The provisions that specify the tensile stress in FRP reinforcement and crack width at service load according to the CSA S6-06 code (CSA 2006) were also taken into consideration. This design approach resulted in beam GSs-10*d*/2*p* with ultimate failure capacity higher than beam SSc-8*d*/2.

Beams GSu-8*d*/2*p*, GSu-8*d*/2*e*, CSu-8*d*/2*p* and CSu-8*d*/2*e* were provided with transverse reinforcement similar to the steel-reinforced control specimen. These beams had 8 mm steel stirrups spaced at 120 mm all over the length of the beam. Beams GSu-8*d*/3*p*, GSu-10*d*/2*p*, and GSs-10*d*/2*p*, were also reinforced with steel stirrups. The first had 8 mm stirrups spaced at 80 mm, while the other two were provided with 10 mm stirrups each 120 mm. Beams GGu-10*d*/2*p* and GGu-10*d*/3*p* had GFRP stirrups spaced at 120 and 80 mm, respectively. The reinforcement details of all tested beams are shown in Table (3.4) and Figure (3.4).

Table (3.4): Reinforcement configuration and concrete strength of tested beams

Beam	Bar material	Flexural bars		Transverse stirrups ($\rho_v = A_v/bs$)	Concrete characteristics (MPa)	Studied parameter
		Top	Bottom			
SSc-8*d*/2*p*	Steel	3No.15M	4No.15M	8-mm@120 (steel) ρ_v =0.4%	f_c` = 28 ± 3.5 f_t = 2.7± 0.4	Control specimen
GSu-8*d*/2*p*	GFRP	2No.16	3No.16		f_c` = 28 ± 3.5 f_t = 2.7± 0.4	Flexural bars material
GSu-8*d*/2*e*		3No.16	2No.16		f_c` = 26 ± 1.4 f_t = 2.4± 0.3	Flexural strength ratio
GSu-8*d*/3*p*		2No.16	3No.16	8-mm@80 (steel) ρ_v=0.63%	f_c` = 32 ± 1.5 f_t = 3.1± 0.4	Spacing of stirrups
GSu-10*d*/2*p*				10-mm@120 (steel) ρ_v=0.65%	f_c` = 33 ± 1.4 f_t = 3.0± 0.3	Diameter of stirrup
GSs-10*d*/2*p*		4No.16	7No.16		f_c` = 33 ± 1.4 f_t = 3.0± 0.3	Target design load
GGu-10*d*/2*p*		2No.16	3No.16	No.10 @120 (GFRP) ρ_v=0.6%	f_c` = 27 ± 1.0 f_t = 2.3± 0.2	Material of stirrups
GGu-10*d*/3*p*				No.10 @80 (GFRP) ρ_v=0.9%	f_c` = 32 ± 1.5 f_t = 3.1± 0.4	Spacing of stirrups
CSu-8*d*/2*p*	CFRP	2 No.10	3 No.10	8-mm@120 (steel) ρ_v=0.4%	f_c` = 26 ± 1.4 f_t = 2.4± 0.3	Flexural bars material
CSu-8*d*/2*e*		4 No.10	3 No.10	8-mm@120 (steel) ρ_v=0.4%	f_c` = 27 ± 1.0 f_t = 2.3± 0.2	Flexural strength ratio

* f_c` and f_t are the concrete compressive and tensile strength, respectively.

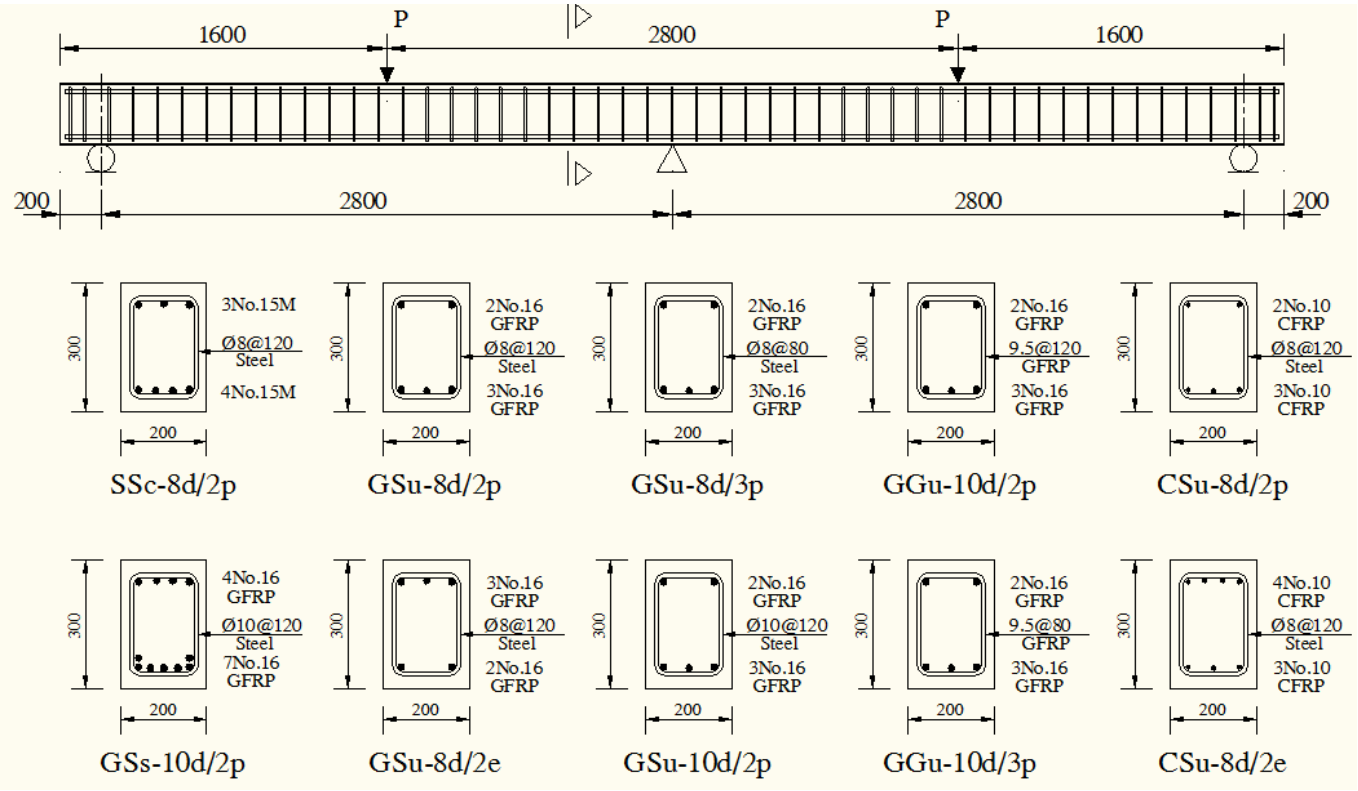

Figure (3.4): Reinforcement details of tested beams

3.6. Construction of Tested Beams

The construction of the tested beams started with building formworks made of plywood. This was followed by preparation of reinforcement cage stage. This process was started by marking the strain gauge locations on the longitudinal bars. Afterwards, the surface of the bars were prepared and cleaned to receive the strain gauges. This was achieved by removing the sand coating layer of the FRP bars or grinding off the ribs of the deformed steel bars. After that, strain gauges were attached to the bars at the designated locations. These strain gauges were bonded with special glue specifically designed for this purpose, then covered with a thin layer of silicone coating throughout the gauge length. This layer was applied to protect the strain gauges against moisture, impact or damage during casting

The reinforcement cage was assembled and placed with extreme care in the plywood forms after brushing the insides with oil to facilitate their removal after casting and curing of the concrete. The reinforcement cage rested on plastic chairs to maintain a 40-mm clear concrete cover.

The concrete was poured in the forms while properly vibrated using electrical vibrator. The reinforcement cage was carefully maintained in the center of the forms to keep the side-cover uniform and equal, while extreme care was dedicated to the strain gauges and the attached wires not to be damaged in the process. The surface of the concrete was finished later to a smooth surface and then covered with a plastic sheet. Enough concrete samples were prepared by casting concrete in plastic cylindrical forms with the standard dimensions of 300 mm height and 150 mm diameter. The cylinders where filled with concrete over three layers while tamping each layer with a steel rod for 25 times. The curing process for the constructed beams as well as the concrete cylinders was started the next day and the concrete surface was kept wet for seven days.

Beams were lifted and stored away after testing enough concrete cylinders samples to make sure that the concrete tensile strength can support the own weight of the specimen without cracking. After 28 days, all beams were prepared for testing by painting them in white and marking the surface with a grid in order to trace the crack pattern during the test. Figure (3.5) shows some of the construction stages of the tested beams.

a) Reinforcement cage before casting

b) During curing

c) After construction

Figure (3.5): Construction stages of test specimens

3.7. Test Setup and Instrumentation

The tested continuous beams consisted of two equal spans supported on two roller supports at both ends and one hinged support at the middle. A 1000-kN hydraulic actuator bolted to an independent loading frame was used to apply monotonic concentrated loading on the mid-point of a rigid steel spreader beam. This spreader beam was used to deliver two equal concentrated

loads to the mid-point of each span. Two load cells were used to measure the reactions at the two end-supports. It worth mentioning that, the reactions readings were set to zero right before loading to exclude the effect of the specimen self weight. Applied loads and reactions were transmitted to the tested beams by means of 250 × 75 × 25 mm steel plates to prevent premature crushing or bearing failure at these locations. To ensure uniform contact between loading or supporting plates and concrete surface of the specimen, a thin layer of neoprene strips was used.

Moreover, deflection was measured, using linear variable differential transformers (LVDTs), at three different locations in each span, at mid-point, one-quarter and three-quarters of the span length. To be able to measure the actual strains at critical locations, a number of strain gauges are installed on the reinforcement and on the concrete surface to monitor their strain during loading. Twelve electrical strain gauges with 6-mm gauge length were attached to the top and bottom longitudinal reinforcement at both sagging and hogging moment regions. Moreover, three strain gauges were attached to the concrete side surface in the compression zone of critical sections at 10 mm from the beam top and bottom surface, as appropriate, to measure the corresponding compressive strains in concrete. In addition, 200-mm long PI gauges were also attached to the concrete side surface at the tensile reinforcement level; centered with the critical sections. The readings from these PI gauges give the average tensile strains in concrete in the critical section zone. The applied load, displacements, crack widths, and strain readings were electronically recorded during the test using a data acquisition system monitored by a computer. Figure (3.6) shows the details of the used test setup and the external instrumentation while Figure (3.7) shows the internal instrumentation.

The test procedure for all beams starts with pre-cracking the test specimen by loading until approximately $1.5P_{cr}$ followed by unloading to zero, where P_{cr} is the expected cracking load

(approximately P = 25 kN). This was conducted to determine the cracking loads, assess the stiffness of specimens in pre-cracking and post-cracking stages, and attach crack-width measuring sensors (high-accuracy LVDTs with ±0.001 mm) on major cracks. The load was applied to the beam monotonically till failure with a load-controlled rate of 10 kN/min. Figure (3.8) shows a specimen during testing.

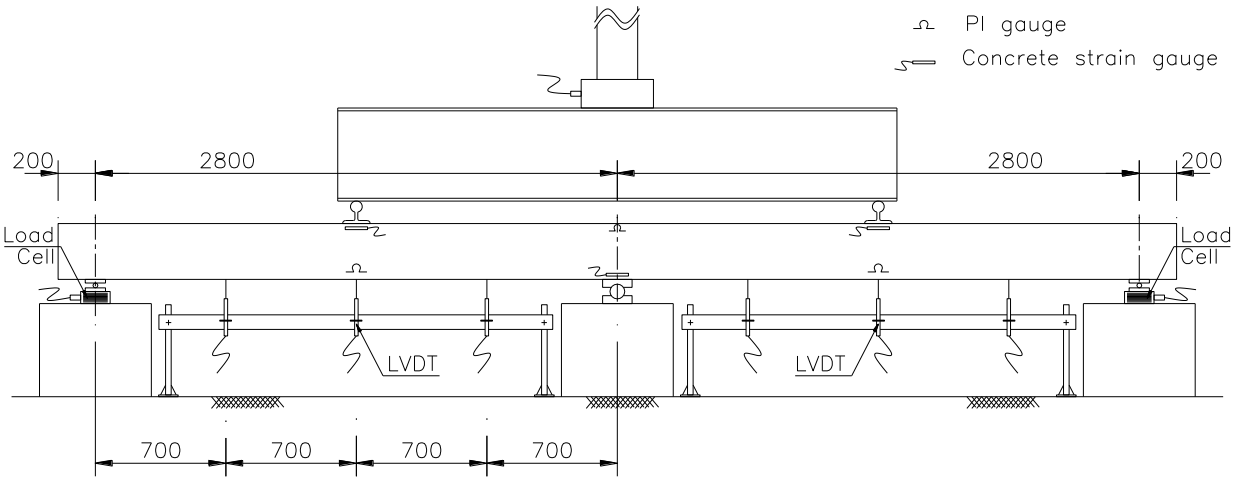

Figure (3.6): Test setup and external instrumentation of test specimens

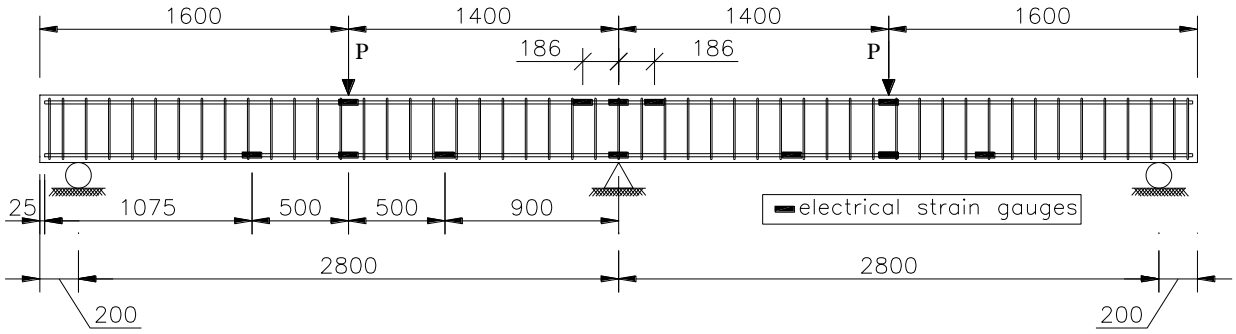

Figure (3.7): Internal instrumentation of test specimens

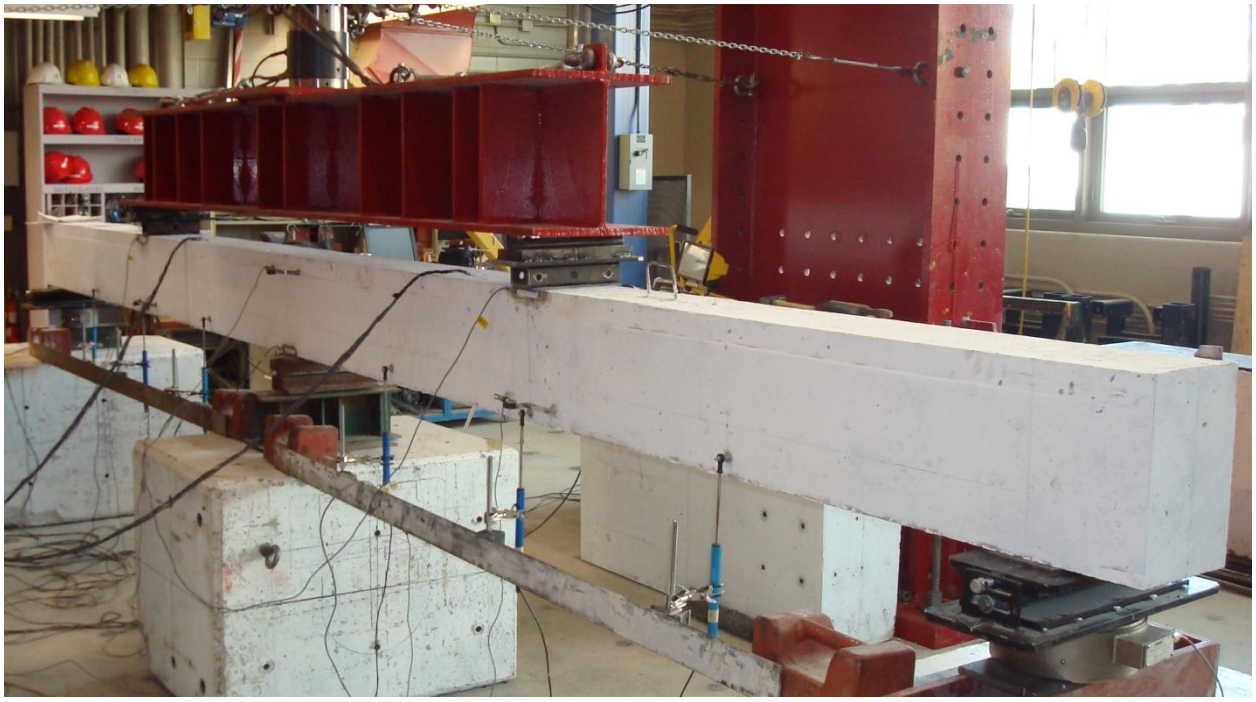

Figure (3.8): A specimen during testing

CHAPTER 4: RESULTS AND DISCUSSIONS

4.1. General

In this chapter, the experimental results of the tested specimens are presented. As previously described, ten reinforced concrete beams continuous over two equal spans were tested. Beams were tested under one point loading at each mid-span using monotonic loading. The behaviour of the tested beams during the test was carefully observed. The displacement at different locations, the strains of reinforcement and concrete surface, the reactions at the end supports, and crack width at middle support were recorded using an automatic data acquisition system.

The complete behaviour of the tested beams is described in this chapter. Moreover, cracking patterns, load-deflection curves, and strain variations on the reinforcement bars and concrete surface are shown. In addition, moment redistribution calculated using measured end-supports reactions at critical sections are also discussed. Furthermore, a comparison between the load-deflection response for the tested beams and some of the deflection-prediction formulas available in literature is also presented in this chapter.

For the sake of clarity of the reported results, the tested beams are divided into two series. Series I is related to beams investigating the effect of changing the longitudinal reinforcement ratio and material type, while Series II investigates the spacing, amount and material type of transverse reinforcement. Series I consists of six beams, SSc-8*d*/2*p*, GSu-8*d*/2*p*, GSu-8*d*/2*e*, CSu-8*d*/2*p*, CSu-8*d*/2*e*, and GSs-10*d*/2*p*. Series II consists of four beams, GSu-8*d*/3*p*, GSu-10*d*/2*p*, GGu-10*d*/2*p* and GGu-10*d*/3*p*, in addition to beam GSu-8*d*/2*p* from the previous group for comparison purposes.

4.2. Results and Discussion of Beam of Series I

4.2.1. Effect of longitudinal reinforcement ratio and material type

This section presents the experimental results of six tested beams that mainly investigated the effect of longitudinal reinforcement on the behaviour of FRP-reinforced continuous beams. The main investigated parameters in this section were the reinforcement ratio and the material type of the longitudinal reinforcement.

4.2.2. General behaviour and modes of failure

During testing of all beams, it was observed that first cracks were always vertical flexural cracks at the middle support section followed by similar vertical cracks at mid-span. New cracks continued to form while existing ones propagated vertically toward the compression zone up to approximately 50% of the maximum load, then the rate of formation of new cracks significantly decreased at higher loading stages. At this stage, existing cracks grow wider and deeper, then became inclined following compression stresses trajectories, and finally failed in shear.

Beam SSc-8*d*/2*p* was the first beam to test. The beam was reinforced in the longitudinal direction using traditional steel bars. It was designed to fail due to steel yielding at both mid-span and middle support sections. This was achieved by providing both sections with reinforcement ratio less than the balanced reinforcement ratio (ρ_b). The ratio between provided and balanced reinforcement ratios (ρ/ρ_b) at middle support section was 0.4 and at mid-span section was 0.5. This beam demonstrated the conventional ductile behaviour of steel-reinforced continuous concrete beams. The tensile steel reinforcement at the middle support yielded first followed by the tensile reinforcement at the mid-span section, as illustrated in reinforcement strains discussion later on. As the load was increased, shear stresses became influential. Tensile flexure cracks near the mid-span diagonally propagated towards the compressive side at the loading

location. The failure started in a flexural mode by yielding of longitudinal reinforced followed by shear-tension failure at mid-span.

Beam GSu-8*d*/2*p* was designed as GFRP over-reinforced concrete beam. This was achieved by providing both critical sections with reinforcement ratio greater than ρ_b. At the middle support section, the ratio ρ/ρ_b = 1.6, while at mid-span section the ratio ρ/ρ_b = 2.4. This means that the longitudinal reinforcement ratio in the mid-span section was 1.5 times that at the middle support section to allow for 20% plastic moment redistribution. The failure of beam GSu-8*d*/2*p* was initiated by concrete crushing in both middle support and mid-span sections, with wide cracks near the middle support. As both critical sections were over-reinforced, concrete in compression crushed before the ultimate strain of the GFRP bars was reached. As the load was increased, wide cracks near the middle support propagated diagonally towards the support, which led to the rupture of bottom GFRP bars in dowel action at this section.

Beam GSu-8*d*/2*e* was provided with longitudinal reinforcement configuration that satisfies the elastic moment diagram without any moment redistribution. This beam, opposite to beam GSu-8*d*/2*p*, had less reinforcement at the mid-span section than that at middle support. The ratio ρ/ρ_b at hogging and sagging bending regions was 2.5 and 1.7, respectively. As the load increased, diagonal cracks between middle support and mid-span propagated towards the loading point. Beam GSu-8*d*/2*e* failed by concrete crushing at mid-span but with less cracking at the middle support region compared to beam GSu-8*d*/2*p* and the final shear failure occurred close to the mid-span section. This is because the mid-span section of beam GSu-8*d*/2*e* had a flexural capacity less than middle support section.

Beam CSu-8*d*/2*p* was designed with similar concept of over-reinforced sections and was provided with CFRP reinforcement ratio at the mid-span section higher that at the middle support to allow for 20 % moment redistribution. The provided CFRP reinforcement at mid-span to the balanced reinforcement ratio was 1.9, while this ratio was 1.3 at middle support. At high loading stages, the vertical flexural cracks in the sagging moment region propagated towards the loading point. At the same time, diagonal cracks close to the middle support became much wider. The failure mode of beam CSu-8*d*/2*p* was compression failure at both middle support and mid-span immediately followed by bar rupture of CFRP bars at middle support.

Beam CSu-8*d*/2*e* was provided with CFRP longitudinal reinforcement configuration opposite to that used in CSu-8*d*/2*p*. This beam had less reinforcement at the mid-span section (ρ/ρ_b = 1.2) than the middle support section (ρ/ρ_b = 1.6) to satisfy the elastic moment diagram without any moment redistribution. Close to the failure load, the vertical flexural cracks in the vicinity of critical sections propagated diagonally towards the loading points. The failure mode of beam CSu-8*d*/2*e* was concrete crushing at middle support section. This process was gradual and gave ample warning before deflection at the mid-span section rapidly increased along with significant widening of the diagonal cracks. The final failure occurred close to the mid-span section. This was expected as the mid-span section of beam CSu-8*d*/2*e* had a flexural capacity less than middle support section.

Beam GSs-10*d*/2*p* was designed to satisfy the serviceability requirements at the same service load of the steel-reinforced beam SSc-8*d*/2*p*. In addition, the behaviour of beam GSs-10*d*/2*p* was very similar to the steel-reinforced control beam. The failure of beam GSs-10*d*/2*p* was initiated by compression failure at both middle support and mid-span as concrete exceeded crushing strain. As the beam continued to support more load, diagonal flexural-shear cracks extended

from the compression zone at the middle support all the way to the load-application zone at the mid-span section. This behaviour indicated enhanced shear resistance of the beam compared to the failure shape of the rest of the tested beams. The longitudinal reinforcement ratio, which was the highest in this beam, is believed to be the reason behind increasing the shear capacity especially through the increased dowel capacity. This observation is supported by the obtained mode of failure since the longitudinal bars in this beam did not rupture in dowel action.

The failure shapes of all tested beams are shown in Figure (4.1) to Figure (4.6).

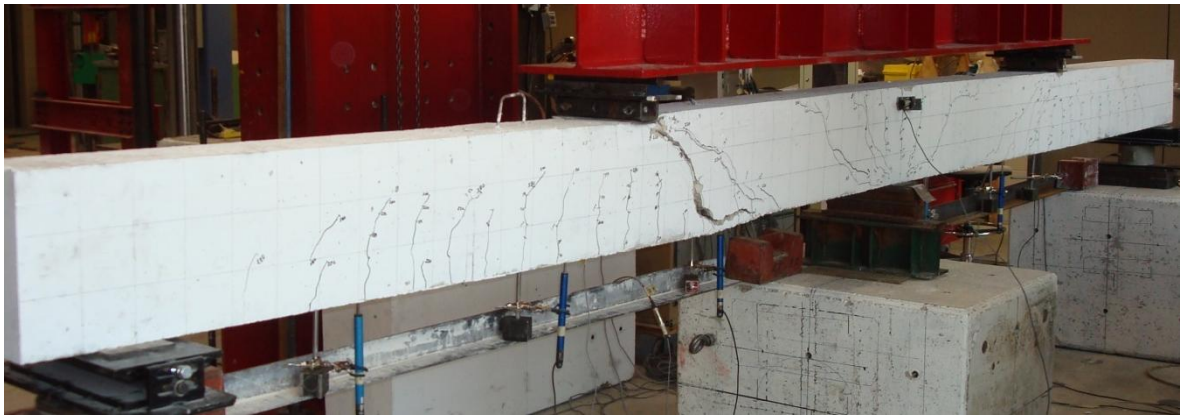

Figure (4.1): Beam SSc-8*d*/2*p* at failure

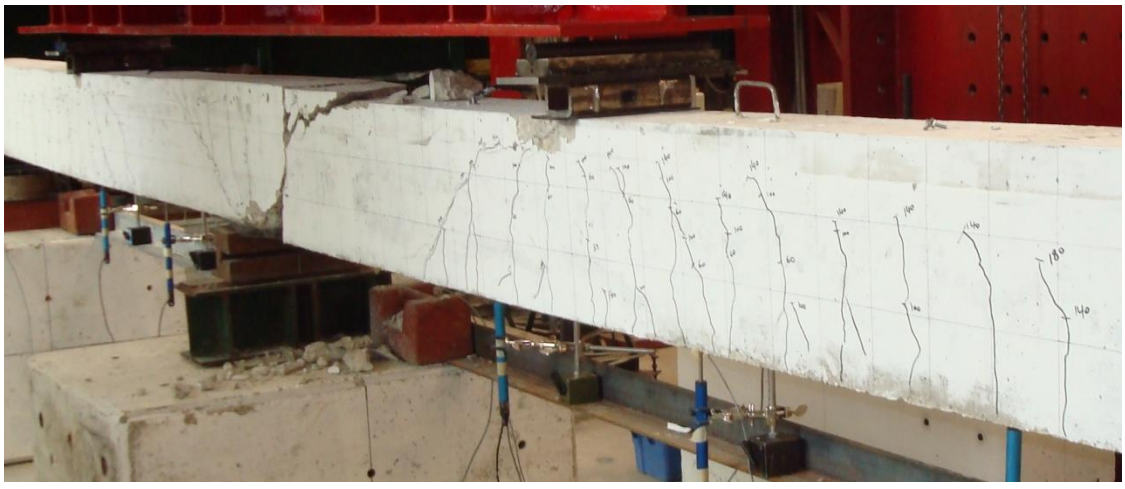

Figure (4.2): Beam GSu-8*d*/2*p* at failure

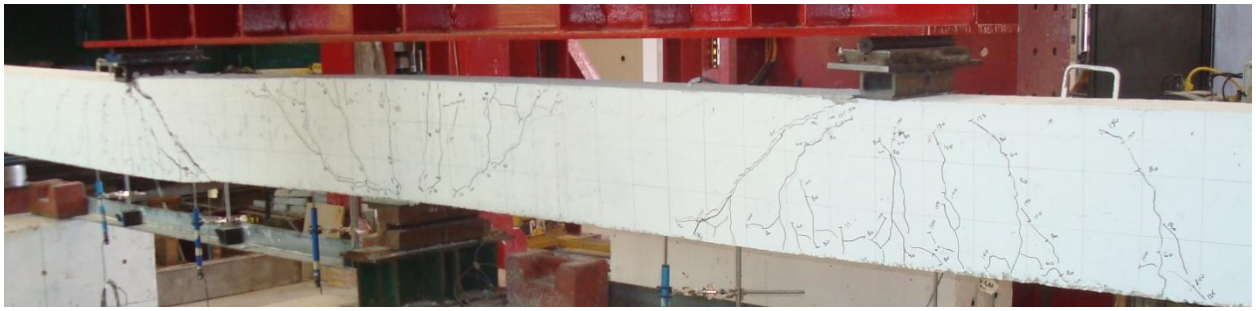

Figure (4.3): Beam GSu-8*d*/2*e* at failure

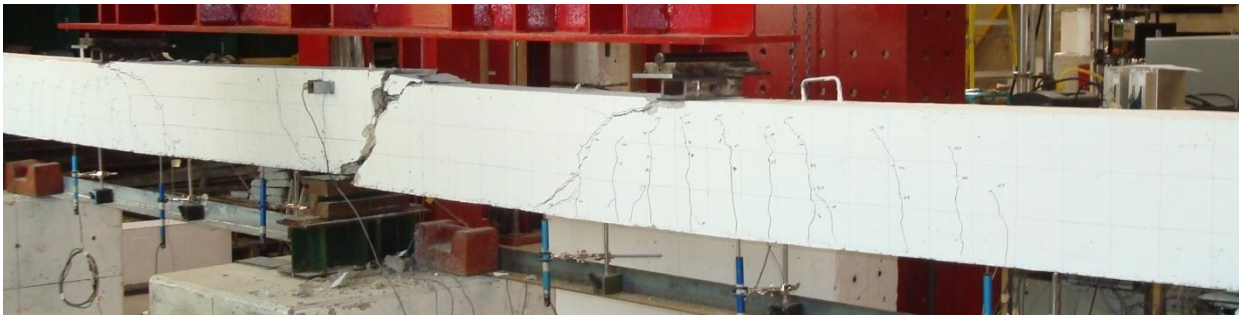

Figure (4.4): Beam CSu-8*d*/2*p* at failure

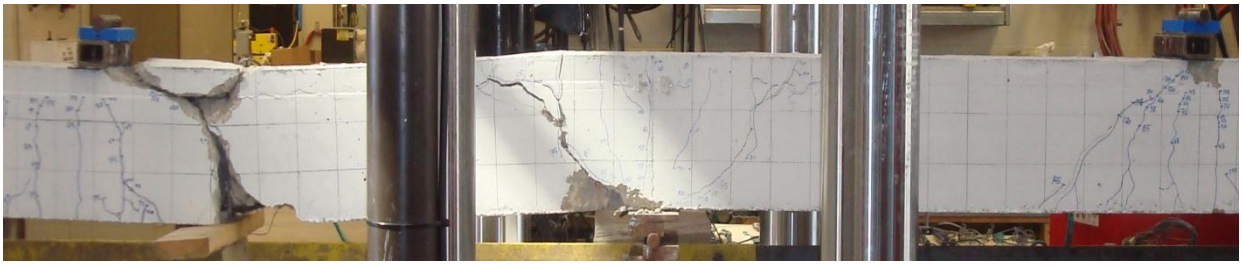

Figure (4.5): Beam CSu-8*d*/2*e* at failure

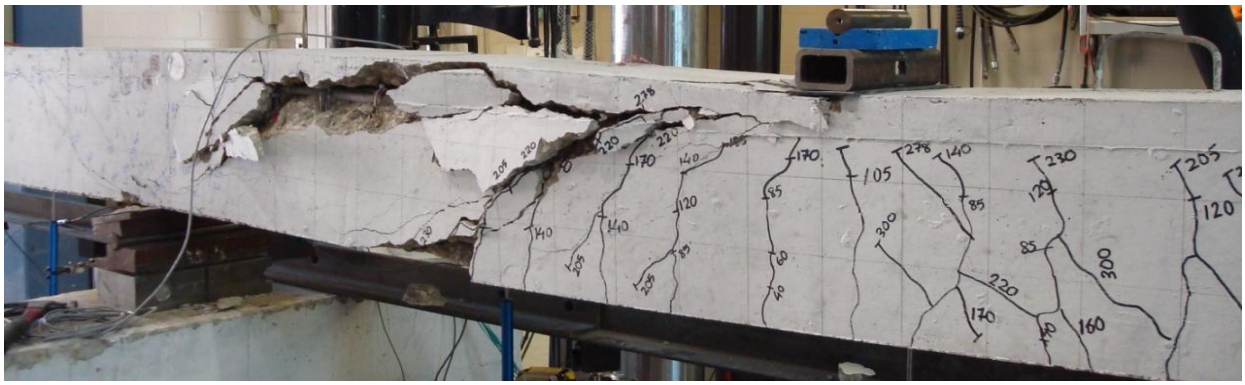

Figure (4.6): Beam GSs-10*d*/2*p*at failure

4.2.3. Cracking pattern and crack width

The first crack in beam SSc-8*d*/2*p* was observed in the hogging moment region at the middle support at a load of P = 20 kN. With the increasing load, another crack was noticed in the sagging moment region at one of the mid-spans at about 23 kN. As the load was further increased, vertical flexural cracks are noted in the sagging moment regions of both spans. The spacing of these cracks ranged between 110 and 130 mm, which is very close to the spacing of the used shear stirrups (120 mm). The number of cracks in the hogging moment region at the middle support also increased as the load increased and propagated towards the supporting point.

For beam GSu-8*d*/2*p*, the cracking behaviour was similar to beam SSc-8*d*/2*p*. The first crack was observed at the middle support at a load of 16 kN, followed by another crack at the mid-span at a load of 18 kN. The number and spacing of cracks in beam GSu-8*d*/2*p* was similar to those of beam SSc-8*d*/2*p*, however, cracks were wider and deeper.

The first crack in beam GSu-8*d*/2*e* was observed at the middle support at a load of 13 kN, followed by a crack at mid-span at 20 kN. The number of cracks in sagging and hogging moment regions increased as the load increased and the spacing of these cracks ranged between 130 and 260 mm. At high loading stages close to failure, diagonal cracks between middle support and mid-span propagated towards the loading point.

The first crack in beam CSu-8*d*/2*p* was observed in the vicinity of the middle support at a load of 20 kN followed immediately by a crack at the mid-span. Very few and wider cracks were observed at the middle support section indicating poor bond strength between the used No.10 CFRP bars and surrounding concrete. Beam CSu-8*d*/2*e* illustrated different behaviour, especially at the middle support region. While the cracking load and the spacing between cracks were

similar to beam CSu-8*d*/2*p*, the cracking pattern at middle support was significantly different. Beam CSu-8*d*/2*e* experienced more cracks with less width at the area of middle support than beam CSu-8*d*/2*p*, which indicates proper transfer of stresses from the bars to the surrounding concrete without exceeding the bond strength. This might be due to the fact that beam CSu-8*d*/2*e* had double the amount of reinforcement at middle support section compared to beam CSu-8*d*/2*p* which provided more surface area to transfer stresses through bond.

The first crack in beam GSs-10*d*/2*p* was observed in the vicinity of the middle support at a load of 33 kN followed by a crack at the mid-span at a load of approximately 39 kN. These cracking loads were about 30% higher than those of the other FRP-reinforced beams due to the fact that this beam had higher flexural reinforcement ratio. This increased the transformed inertia at both critical cross-sections, which led to higher cracking loads. The cracking pattern and behaviour of this beam was very similar to the steel-reinforced reference beam SSc-8*d*/2*p*. However, beam GSs-10*d*/2*p* experienced a larger number of cracks with closer spacing than the steel-reinforcement control specimen, despite the fact that both had the same stirrup spacing. This behaviour might be attributed to the difference between GFRP and steel bars in bond-stress transfer mechanism to the surrounding concrete. Because their bond resistance is dependent on friction more than on mechanical interlock, the increasing slip in GFRP relative to steel bars resulted in bigger number of cracks.

Schematic drawings of the cracking patterns of the tested beams at failure are shown in Figure (4.7). In this figure, the following were observed.

- Steel-reinforced concrete beam (SSc-8*d*/2*p*) demonstrated uniform crack distribution in both sagging and hogging moment regions with spacing close to the provided shear

reinforcement spacing;

- GFRP-reinforced beam with flexural reinforcement at mid-span greater than middle support (GSu-8*d*/2*p*) exhibited similar cracking pattern to beam SSc-8*d*/2*p* with more cracks within the span and less cracks at the middle support. Although the critical sections of both beams were designed to achieve the same flexural strength, the axial stiffness (*EA*) of steel reinforcement was much higher than that of GFRP. The ratio EA_{steel}/EA_{frp} at middle support and mid-span was 6.6 and 5.9, respectively;
- Beam CSu-8*d*/2*p* had fewer and wider cracks at the middle support compared to beam CSu-8*d*/2*e*. This might be attributed to inadequate bond strength of CFRP bars at the middle support section of beam CSu-8*d*/2*p* due to high stresses in the CFRP bar with smaller surface area;
- Beam GSu-8*d*/2*e* demonstrated larger cracking spacing in the sagging moment region compared to beam GSu-8*d*/2*p*, in addition to significant number of horizontal crack at the reinforcement level. This can be attributed to the high deflections and deformation experienced by beam GSu-8*d*/2*e*, which has led to slippage between reinforcement bars and surrounding concrete (i.e. bond failure).

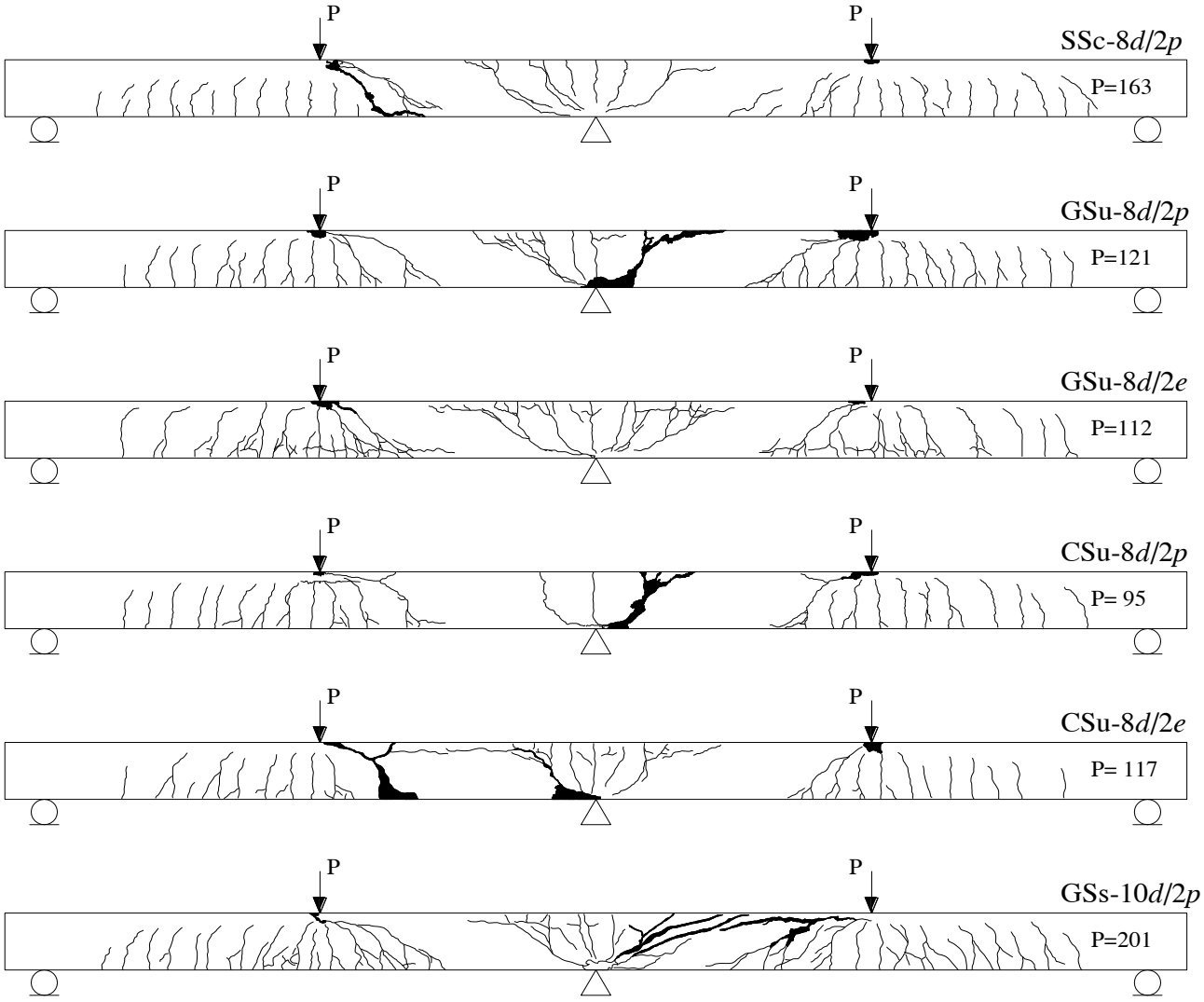

Figure (4.7): Cracking pattern of tested beams

Figure (4.8) shows the maximum measured crack width for the tested beams over the middle support at the top reinforcement level. It can be seen that at the same loading level between cracking and failure, steel-reinforced beam SSc-8*d*/2*p* showed 65 % smaller crack width compared to specimens GSu-8*d*/2*p* and CSu-8*d*/2*p* reinforced with GFRP and CFRP, respectively. This was expected due to the higher axial stiffness of steel reinforcement (5.8 to 6.8 times higher) compared to the FRP reinforcement for beams GSu-8*d*/2*p* and CSu-8*d*/2*p*. It can also be seen that the crack width increased significantly in beam SSc-8*d*/2*p* after steel yielding,

which signals the formation of plastic hinges. Compared to specimens GSu-8*d*/2*p* and CSu-8*d*/2*p*, beams GSu-8*d*/2*e* and CSu-8*d*/2*e* exhibited approximately 50% smaller crack width at the middle support. This is due to the provided reinforcement configuration in this specimen, which enabled the higher reinforcement ratio at middle support to develop cracks with smaller width. Moreover, the provided reinforcement in beams GSu-8*d*/2*e* and CSu-8*d*/2*e* at mid-span was less than at middle support, which nominally increased the flexural stiffness at the middle support section. In addition, the axial stiffness (*EA*) of the provided reinforcement at mid-span section in beams GSu-8*d*/2*e* (18,000 kN) and CSu-8*d*/2*e* (24,000 kN) was smaller compared to beams SSc-8*d*/2*p*, GSu-8*d*/2*p* and CSu-8*d*/2*p* (160,000, 27,000 and 26,000 kN, respectively).

Furthermore, serviceability requirements, mainly crack width and deflection, are based on the service loads. The Canadian code CSA-A23.3-04 (CSA 2004) for steel-reinforced structures consider stresses in steel reinforcement to be 60% of yield stress at service load. While, CSA-S6-06 (CSA 2006) assumes stresses in GFRP and CFRP reinforcement, at service load, not to exceed 25 and 65% of the ultimate strength of bars, respectively. This leads to different design service loads for the tested beams. Based on the CSA codes, the calculated design service loads for beams SSc-8*d*/2*p*, GSu-8*d*/2*p*, GSu-8*d*/2*e*, CSu-8*d*/2*p* and CSu-8*d*/2*e* are P = 60, 33, 40, 57 and 80 kN, respectively. At these service loads, the measured crack width was 0.3, 0.5, 0.4, 1.2 and 0.9 mm for beams SSc-8*d*/2*p*, GSu-8*d*/2*p*, GSu-8*d*/2*e*, CSu-8*d*/2*p* and CSu-8*d*/2*e*, respectively. It can be seen that CFRP-reinforced beams did not satisfy the allowable crack width of 0.5 mm for exterior exposure (CSA 2006).

For beam GSs-10*d*/2*p*, designed to carry similar service load to the steel-reinforced beam SSc-8*d*/2*p* (60 kN), the measured crack width was 0.48 mm, which satisfies the CSA code limit of 0.5 mm. It worth mentioning that beam GSs-10*d*/2*p* illustrated approximately 50% wider cracks than

the steel-reinforced control beam for the loading range between cracking load and steel yielding. This observation is in good agreement with the FRP design code concepts.

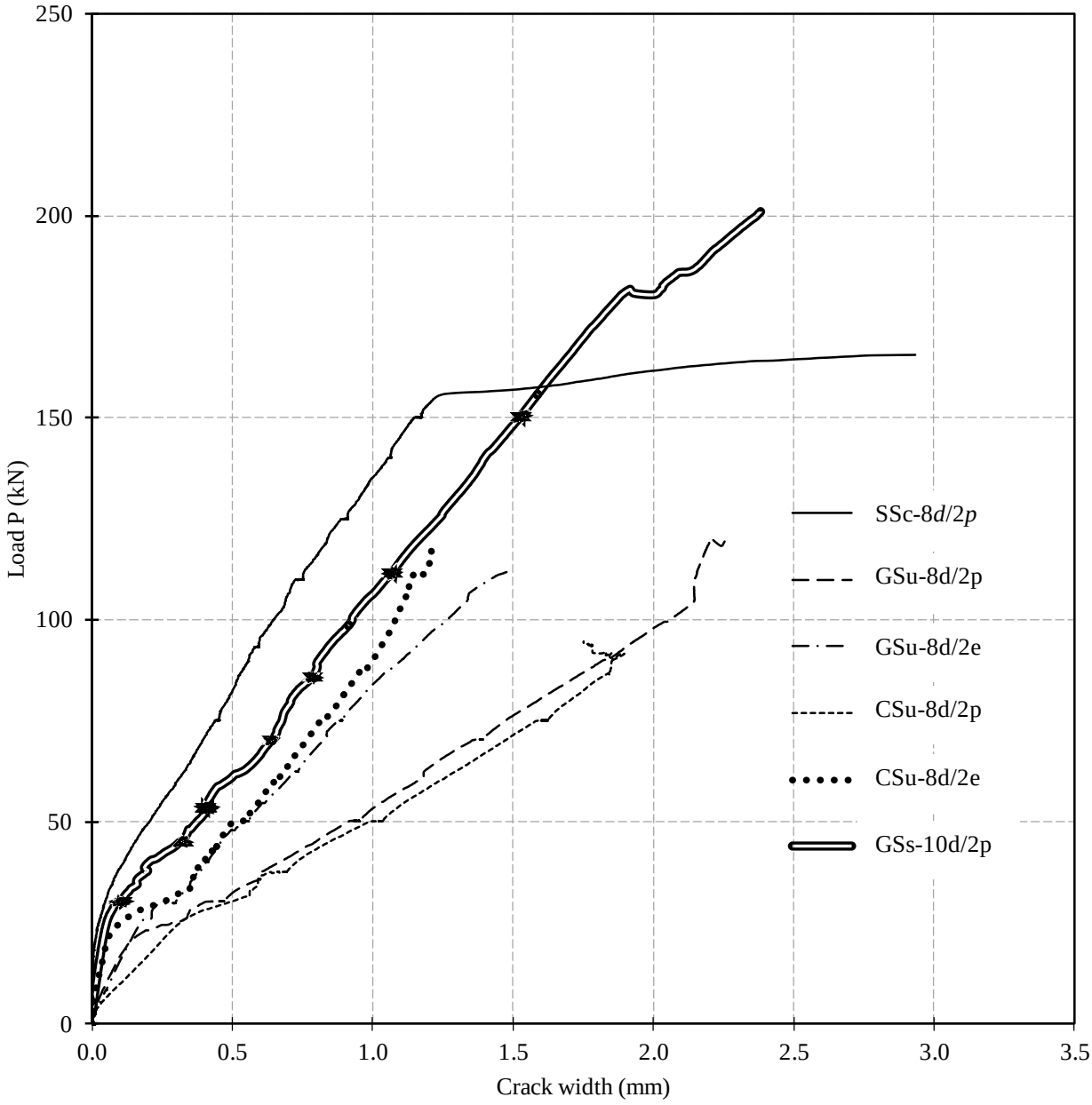

Figure (4.8): Load-crack width relation measured at middle support

4.2.4. Load-strain variation in reinforcement and concrete

As discussed in the previous chapter, several strain gauges were installed on the reinforcement and on the concrete surface at critical locations to monitor strain during loading. Figure (4.9) and Figure (4.10) show the measured tensile strains at the mid-span section (in the bottom reinforcement) and at the middle support section (in the top reinforcement) against the applied load for the tested beams. The same figures also show the compressive strains in concrete at the same sections but bottom at the middle support and top at mid-span. These figures show that compressive strains in concrete at sections where compression failure was expected reached or exceeded the maximum compressive strain of 0.0035 specified in the CSA standards (CSA 2002 and 2004). Regarding tensile strains, the figures show that the strains in FRP bars increased suddenly after concrete cracking. The measured strains indicate that the section at middle support, in all tested beams, cracked before the mid-span section. This is due to the higher elastic moment at the middle support section. The tensile strains in FRP bottom bars were 3.5 to 4.5 times that in the steel bottom bars at the maximum load, while the strains in top FRP bars were 1 to 1.5 times that of steel at middle support at the same load level. This was expected due to the low axial stiffness of FRP reinforcement compared to steel. In beam SSc-8*d*/2*p*, top steel reinforcement at the middle support yielded at 90% (P = 149 kN) of the ultimate load, while the bottom reinforcement at mid-span yielded at 95% (P = 157 kN) of the ultimate load.

Furthermore, the measured strain in the top reinforcement over the middle support was 1.4, 1.2 and 1.5 times that in the bottom reinforcement at mid-span in beams SSc-8*d*/2*p*, GSu-8*d*/2*p* and CSu-8*d*/2*p*, respectively, through the entire loading after cracking till failure. However, after steel yielding in beam SSc-8*d*/2*p*, top tensile strains became 3.5 times higher. Unlike the other beams, the tensile strain in beams GSu-8*d*/2*e* and CSu-8*d*/2*e* measured at the mid-span section

was higher than those measured at the middle support section. During loading between cracking and failure, tensile strain at mid-span section was around 1.3 times that at middle support. It can also be noted that the maximum tensile strains in GFRP bars did not reach the ultimate value as these beams were designed as over-reinforced to have concrete crushing failure. On the other hand, it can be seen that CFRP bars in tension at middle support section in beam CSu-8*d*/2*p* and at mid-span section in beam CSu-8*d*/2*e* reached the ultimate strain value (12,000 micro-strain). This is due to the excessive mid-span deflection experienced by these beams after concrete crushing.

For beam GSs-10*d*/2 at the service load of 60 kN, the tensile stress in top bars in the hogging moment zone (middle support) and bottom bars in the sagging moment zone (mid-span) bars was 106 and 75 MPa, respectively, which is less than 183 MPa; 25% of the bars ultimate strength as specified by the code (CSA 2006).

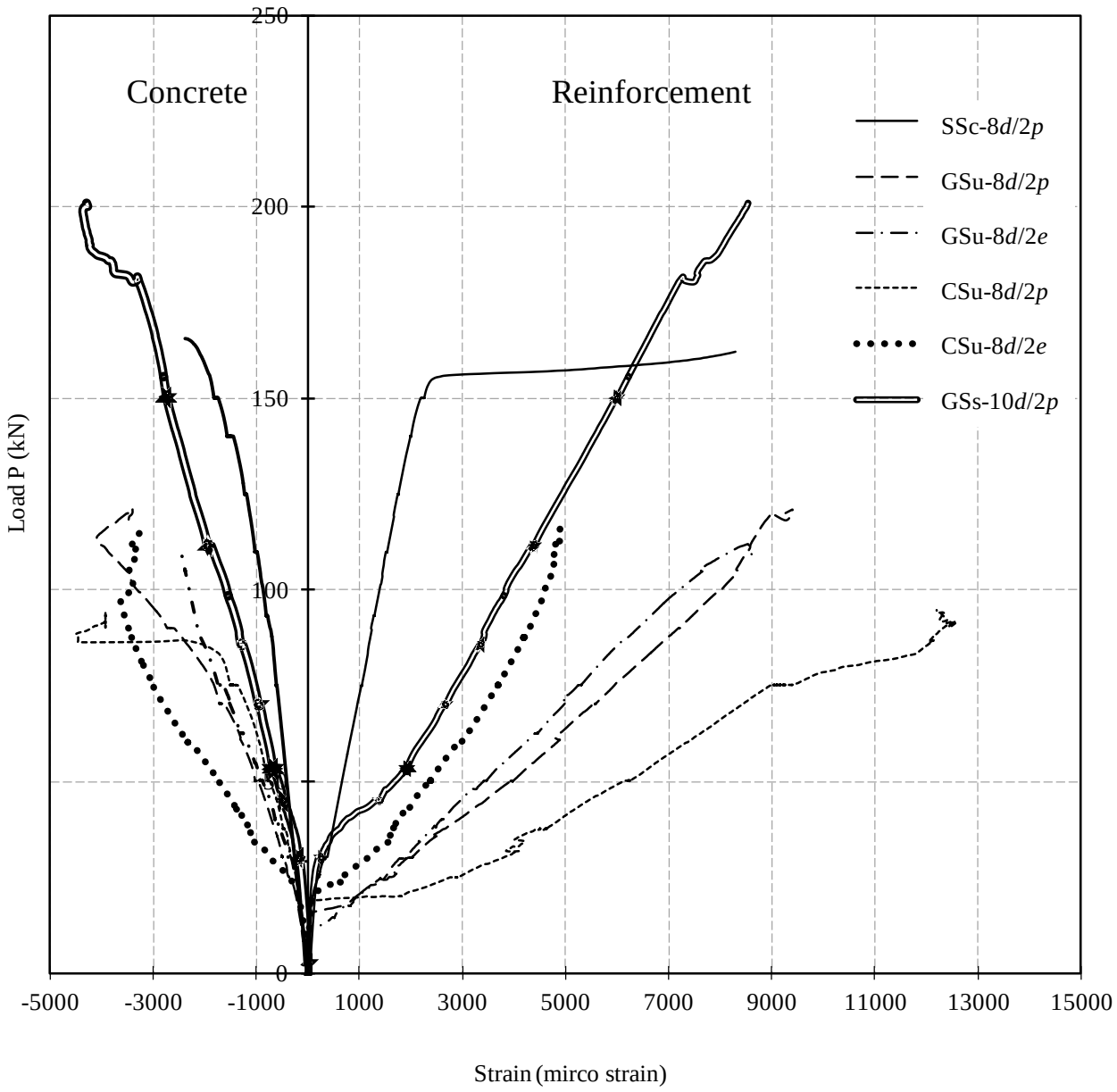

Figure (4.9): Variation of strain with load at middle support section

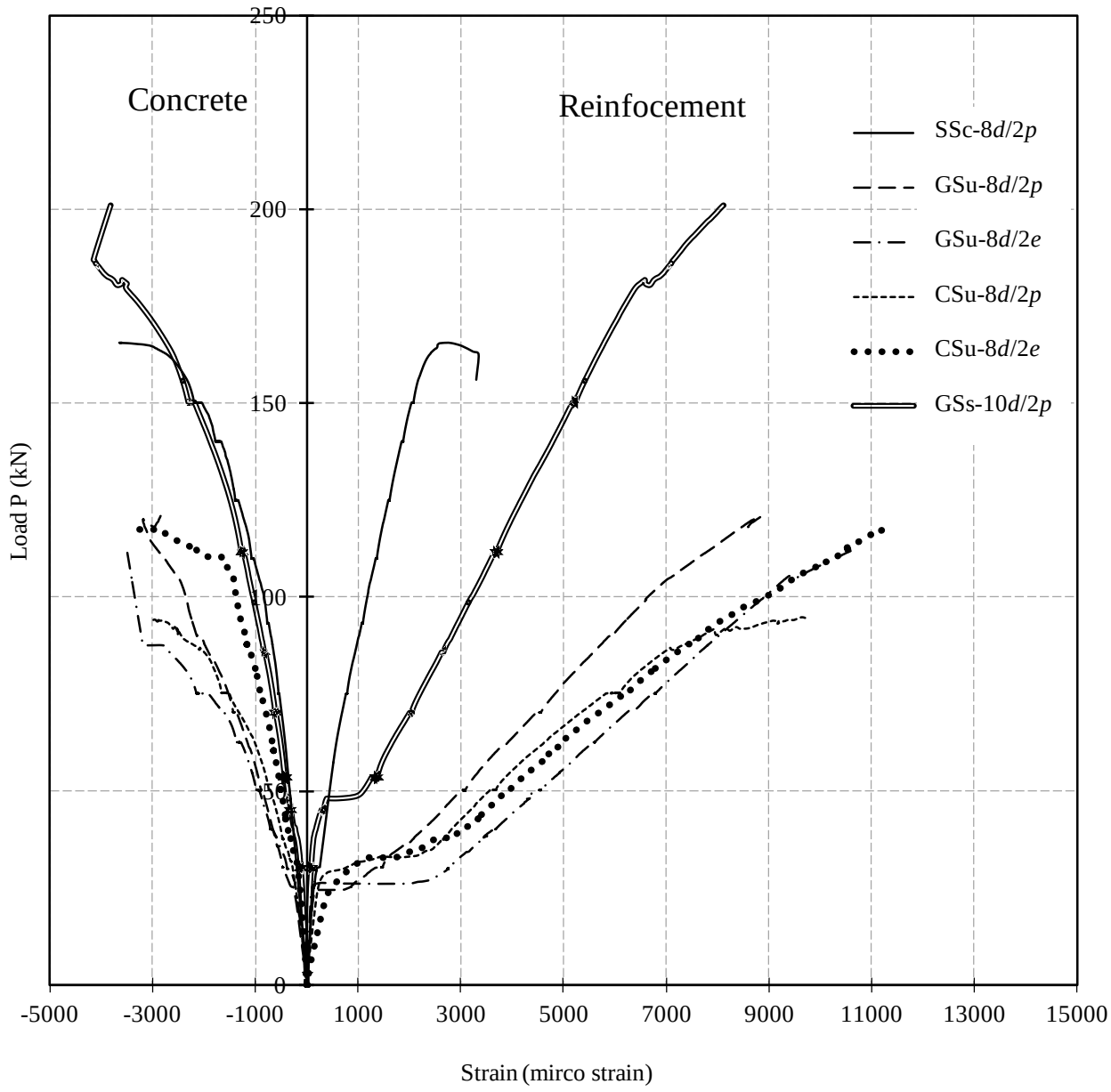

Figure (4.10): Variation of strain with load at mid-span section

Comparing measured stains in internal reinforcement with strains on the concrete surface is useful for evaluating the compatibility of strains between the bars and the surrounding concrete. In general, there was good agreement between measured tensile strains on the concrete surface and internal reinforcement at different critical section, since the difference was within 8% in average. This indicates good bond strength between reinforcement and concrete. However, for beams CSu-8*d*/2*p*, the measured tensile strains on concrete surface after cracking where about 30% less than those measured in the internal reinforcement, and this difference significantly increased close to failure. This difference indicates significant stress concentration at the location of the strain gauge on the tension reinforcement compared to the average tensile strain on the concrete surface measured over 200 mm length (PI gauge length). This reflects the sharp change in tensile stresses and consequently the distribution of bond stresses at the middle support section. The limited number of wide cracks at this section also supports this observation as it indicates poor bond strength.

4.2.5. Load-deflection response

The relationship between the applied load, *P*, and the recorded deflection at mid-span is shown in Figure (4.11). Since the measured deflections in the two spans of each beam were similar, one side mid-span deflections are reported. This indicates that loads were very similar at both spans as intended. The tested beams demonstrated linear load-deflection behaviour before cracking. Upon cracking, stiffness was reduced as the load increased. Once again, as expected, due to the low axial stiffness of the FRP bars, beams GSu-8*d*/2*p*, GSu-8*d*/2*e*, CSu-8*d*/2*p* and CSu-8*d*/2*e* demonstrated wider cracks compared to beam SSc-8*d*/2*p* and consequently exhibited higher mid-span deflection. It can also be observed that beam GSu-8*d*/2*e* demonstrated higher deflections compared to GSu-8*d*/2*p*. This is because beam GSu-8*d*/2*p* was provided with higher sagging and

less hogging GFRP reinforcement compared to GSu-8*d*/2*e*.

Considering serviceability, the maximum deflection should be compared to the allowable permitted deflections in codes and design guidelines. The allowable deflection permitted by CSA-S806-02, Clause 8.3.2.1 (CSA 2002) ranges from $\ell/180$ to $\ell/480$ depending on the type and function of the structure. The allowable deflection for the tested beams according to CSA (2002) should be within the range of 6 to 15 mm (2800/480 to 2800/180) based on the type of structural application. It can be observed that the maximum deflections corresponding to the calculated service loads for beams SSc-8*d*/2*p*, GSu-8*d*/2*p*, GSu-8*d*/2*e*, CSu-8*d*/2*p* and CSu-8*d*/2*e* were 0.9, 3.0, 5.0, 9.0 and 14 mm, respectively. It can be seen that the CFRP-reinforced beams did not satisfy serviceability limits for certain applications.

Beam GSs-10*d*/2*p*, as expected, had higher ultimate load capacity than SSc-8*d*/2*p* as both were designed to have similar design service load rather than same ultimate capacity.

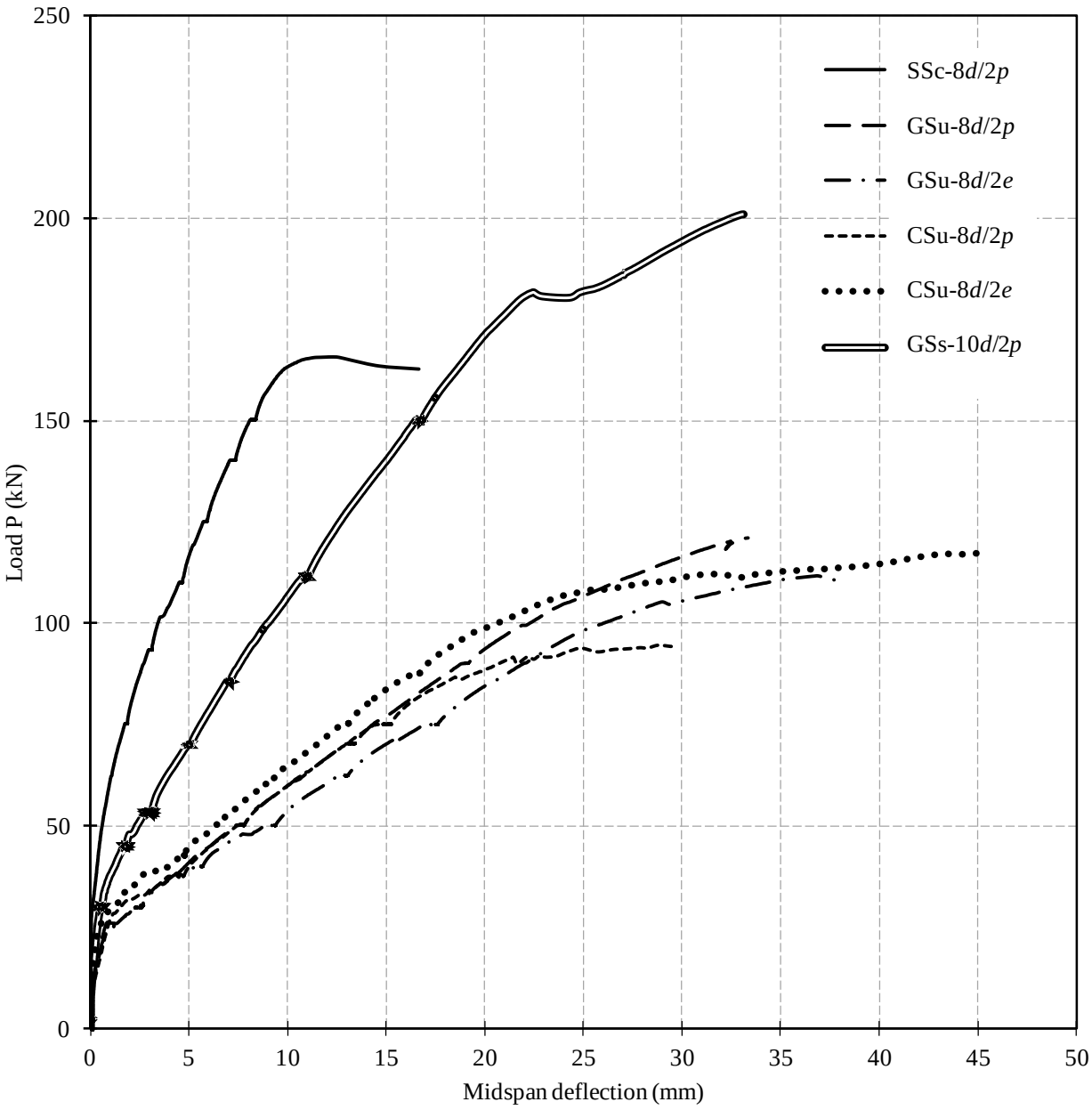

Figure (4.11): Load-deflection relations for tested beams

4.2.6. Reactions and moment-redistribution

Two load cells were used at the end supports to measure the reactions. As the beams were statically indeterminate, the measured end support reactions, *R*, were used to calculate the actual internal forces, mainly bending moments, at any location along the length of the specimens. Figure (4.12) shows the variation of end reactions versus the applied load for all tested beams. The elastic end reaction with the value of $R = 0.312\ P$ was also plotted to evaluate the amount of load redistribution.

The amount of moment redistribution can be obtained by comparing the actual and elastic bending moments. Generally, in steel–reinforced continuous concrete beams significant load redistribution is expected after yielding of tensile reinforcement at the middle support. In beam SSc-8*d*/2*p*, however, it was observed that redistribution started before reaching the load corresponding to steel yielding at middle support section (P = 149 kN). This might be attributed to the difference in stiffness between mid-span and middle support sections. As the reinforcement ratio in mid-span section is higher than that in middle support section, stiffness of the beam cross-section at mid-span is higher. Beam GSu-8*d*/2*p* was similarly designed as beam SSc-8*d*/2*p* with higher reinforcement ratio in mid-span compared to section at middle-support. Similar load redistribution behaviour was observed for beam GSu-8*d*/2*p*. In fact, this beam utilized all the available load redistribution provided by the existing reinforcement configuration. As can be seen in Figure (4.12), the maximum measured reaction at the end-support corresponding to a failure load of P = 121 kN was around 43 kN. Based on the elastic analysis, the end support reaction was calculated to be 37.8 kN. Therefore, the actual bending moment at the middle support, calculated from the measured end reaction, was 49.0 kN.m, which represents 77% of the calculated elastic moment of 63.7 kN.m at the failure load (P = 121 kN). In other

words, it was found that about 23% of the elastic bending moment at middle support was redistributed to the mid-span at failure load as demonstrated in Figure (4.13).

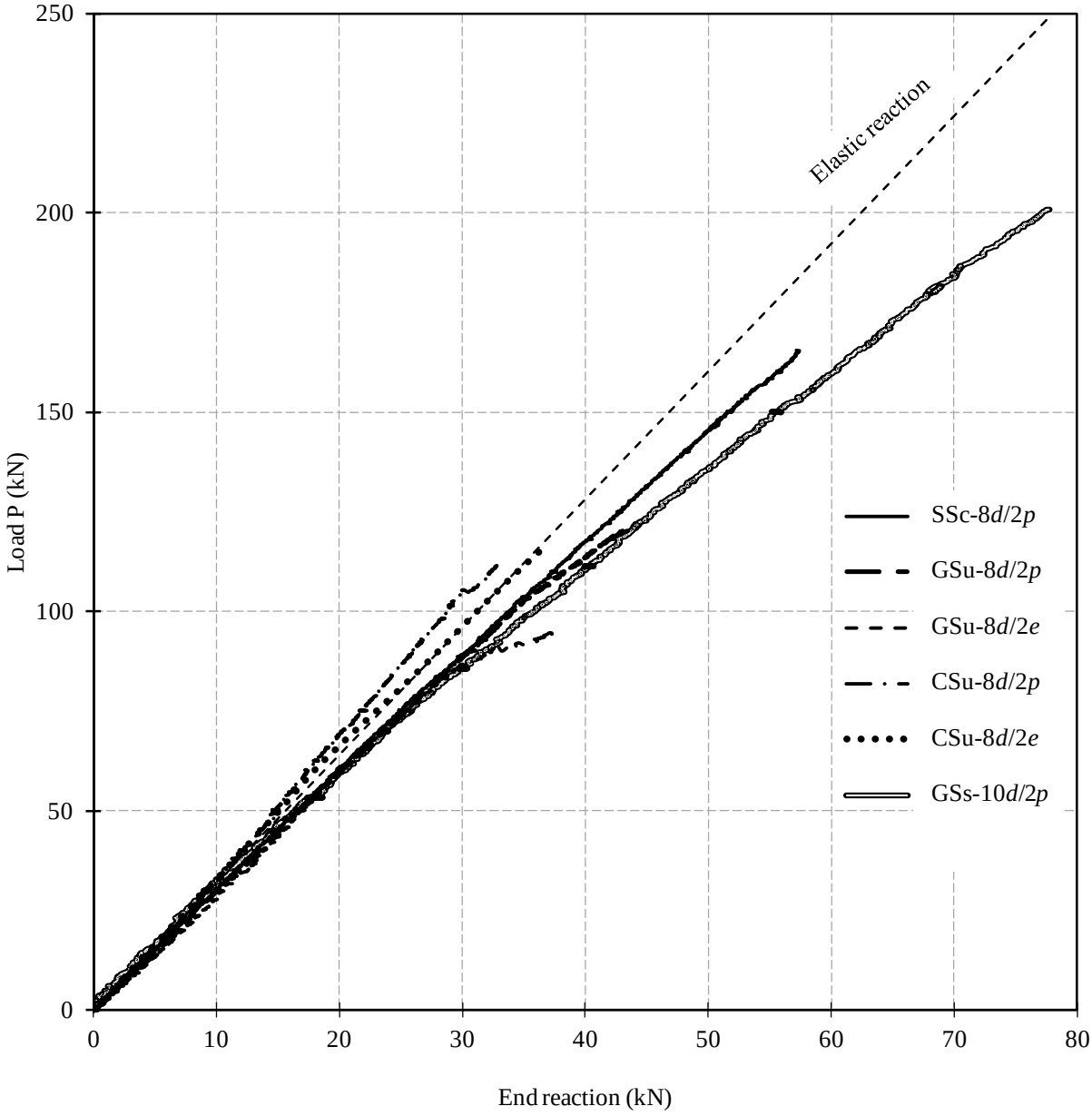

Figure (4.12): Load versus end support reactions of the tested beams

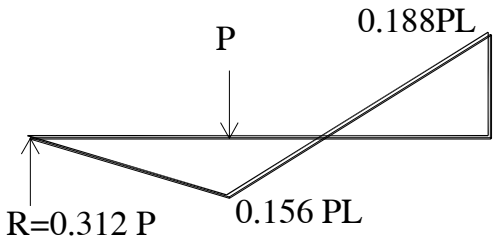

Elastic moment distribution

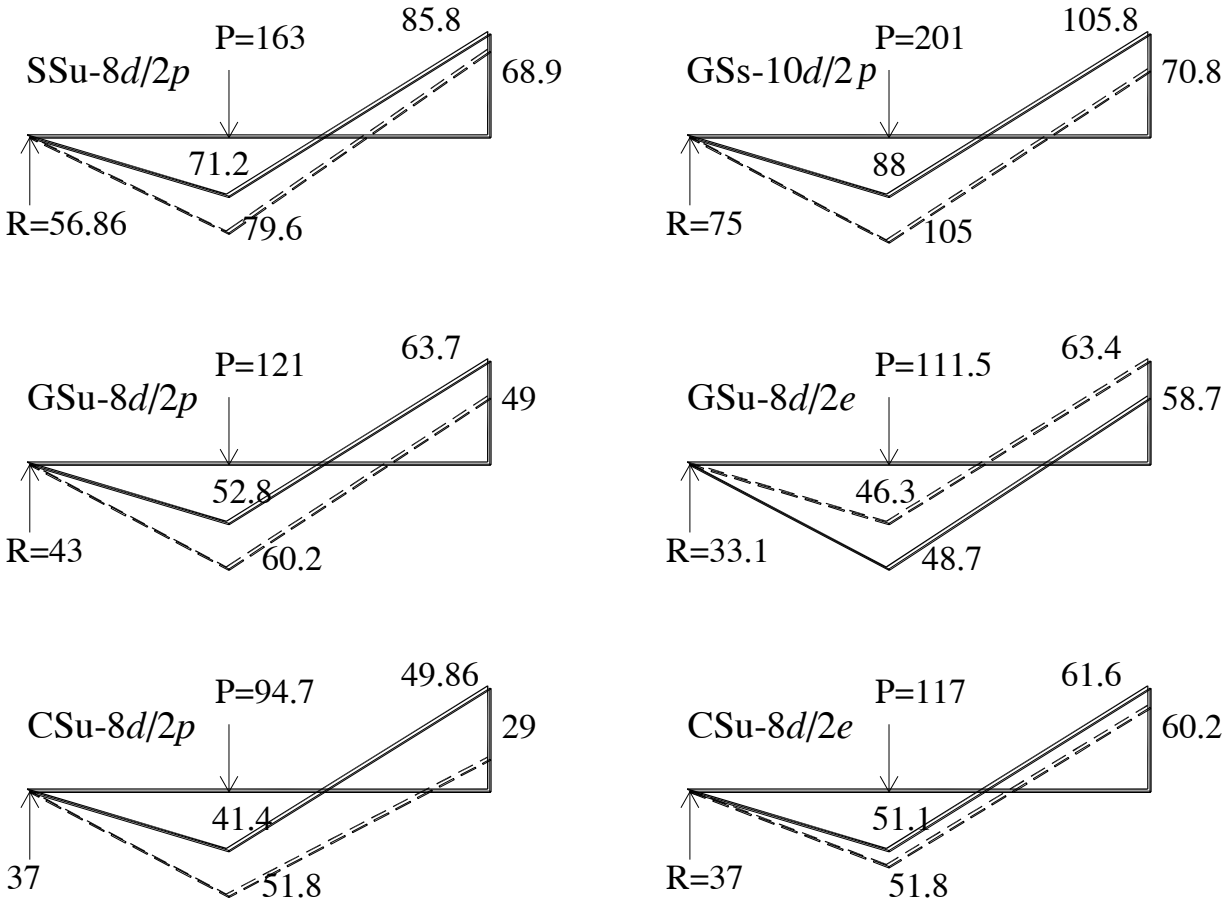

Legend

- - -	Experimental bending moment (kN.m)	P	Load at failure (kN)
———	Elastic bending moment (kN.m)	R	Reaction at failure (kN)

Figure (4.13): Actual versus elastic bending moment at failure

Moreover, Figure (4.14) shows the relationship between the applied load and the percentage of moment redistribution at middle support hogging moment. Beams SSc-8*d*/2*p*, GSu-8*d*/2*p* and CSu-8*d*/2*p* where designed assuming 20% redistribution of the elastic bending moment from middle support to mid-span. It was observed that these beams experienced an actual redistribution of bending moments at their service load level of about 13%, which represents 65% of the assumed design value. At failure load, beam SSc-8*d*/2*p* exhibited about 20% moment redistribution while beam GSu-8*d*/2*p* showed about 23% moment redistribution as discusses in the previous paragraph. Beam CSu-8*d*/2*p* was able to distribute about 42% of the elastic bending moment from middle support to the mid-span section. This is due to the significant slippage between the tension reinforcement and surrounding concrete at the middle support section of this beam as a result of inadequate bond strength as described earlier.

Beams GSu-8*d*/2*e* and CSu-8*d*/2*e* were designed to satisfy the elastic bending moment (no moment redistribution is assumed) by providing reinforcement at middle support higher than that at mid-span section. This reinforcement arrangement caused "opposite" 8% moment redistribution from mid-span to middle support section unlike the rest of the tested beams.

Due to the high reinforcement ratio provided in beam GSs-10*d*/2*p*, and the adequate transverse reinforcement, this beam illustrated significant moment redistribution. Close to failure, beam GSs-10*d*/2*p* achieved 33% moment redistribution. The longitudinal reinforcement ratio is believed to have an effect on the amount of moment redistribution achieved. This parameter was closely investigated in the FEM study presented in the following chapter.

A continuous concrete beam reinforced with GFRP, similar to beam GSu-8*d*/2*p* in this study, was tested by Habeeb and Ashour (2008). Similar load re-distribution behaviour between the

under-reinforced section at middle support and the over-reinforced section at mid-span was observed in their beam. This similarity strengthens the theory that GFRP-reinforced continuous beams can re-distribute bending moments between critical sections. For beam CSu-8*d*/2*p*, although part of the load was redistributed from the middle support section to the mid-span section, the beam could not develop the expected ultimate flexural capacity at the hogging moment region. This may be attributed to significant slippage between the top CFRP bars and the surrounding concrete. This slippage was observed in the difference between tensile strain reading on the internal bars and on the external surface of concrete at that section. Beams GSu-8*d*/2*e* and CSu-8*d*/2*e* demonstrated load redistribution from the mid-span to the middle support section. This is due to the higher stiffness at the middle support section provided by the higher reinforcement ratio, which is 1.5 and 1.3 times the mid-span section of beam GSu-8*d*/2*e* and CSu-8*d*/2*e*, respectively.

The observed results discussed above demonstrate that FRP-reinforced continuous beams are capable of redistributing bending moments due to a number of factors in lieu of yielding in steel-reinforced beams. The two main components are the high elastic deformation provided by FRP and the material non-linearity represented by concrete crushing/cracking and bond slippage. The moment redistribution achieved in the stage where stresses in concrete are still linear is mainly cause by the high elastic deformations of FRP reinforcement. At loads close to ultimate failure, the nonlinearity of concrete along with reinforcement slippage add up to the elastic moment redistribution. More in-depth study of the mechanics of redistribution is required to identify the contribution of each component.

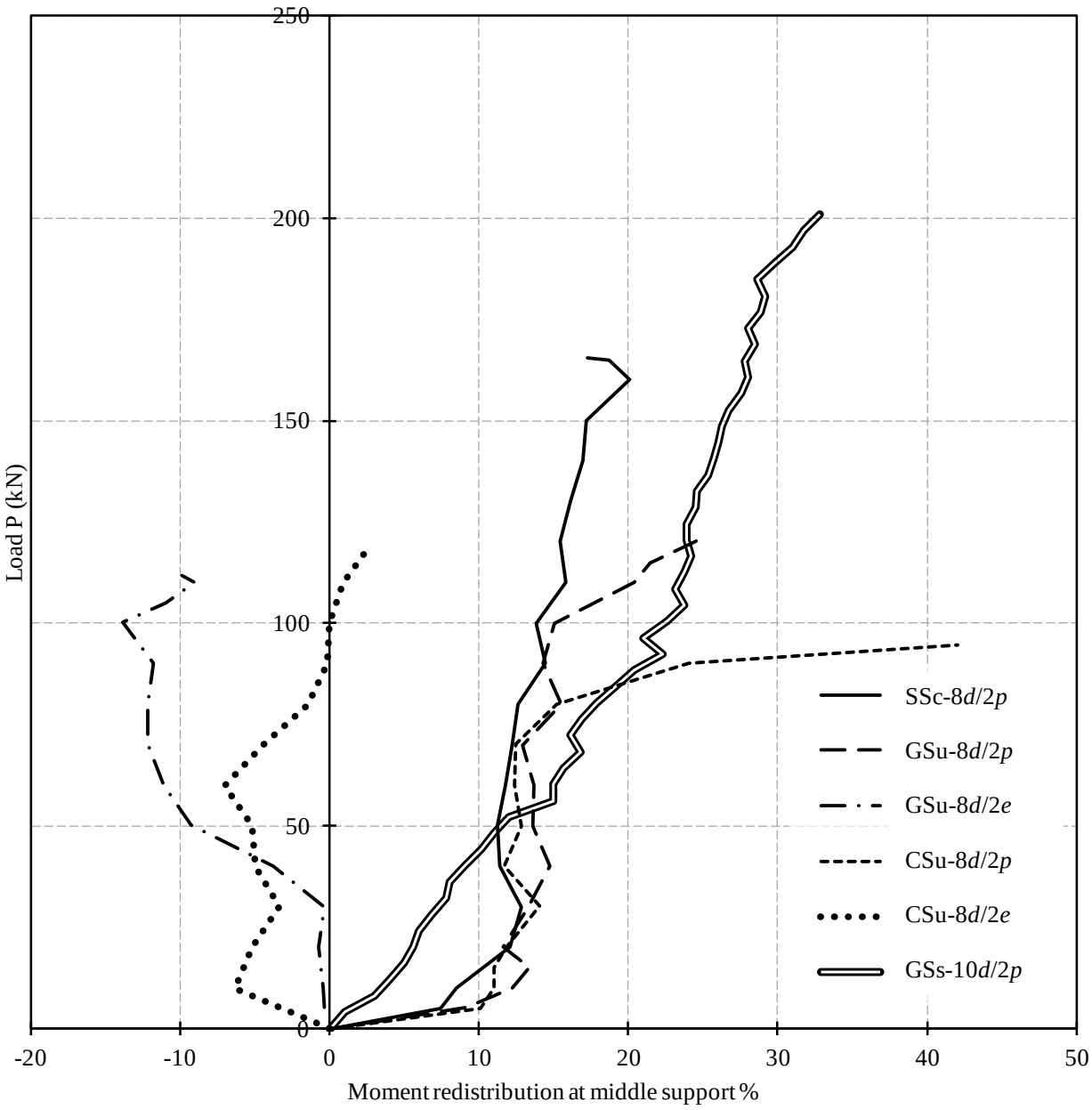

Figure (4.14): Load versus percentage of moment redistribution

4.3. Results and Discussion of Beam of Series II

4.3.1. Effect of transverse reinforcement

This series investigates three main parameters; spacing, material type and the amount of transverse reinforcement. There are four beams reported in this series in addition to one beam from the previous series (beam GSu-8*d*/2*p*) for comparison purposes.

4.3.2. General behaviour and modes of failure

All beams presented in this series had similar longitudinal reinforcement configuration similar to beam GSu-8*d*/2*p*. Therefore, the general behaviour was very similar. The failure of beams GSu-8*d*/3*p*, GSu-10*d*/2*p*, GGu-10*d*/2*p* and GGu-10*d*/3*p* was similar as these beams had the same flexural reinforcement. The failure was initiated by concrete crushing in both middle support and mid-span sections, with wide cracks at the middle support section. Both critical sections were over-reinforced, which was the reason for concrete crushing before the ultimate strain of the GFRP bars was reached. As the load was increased, the wide cracks near the middle support propagated diagonally towards the support. After concrete started crushing at the compression zone, all GFRP bars were ruptured in dowel action at this section. Ample warnings were observed prior to failure such as concrete crushing and obvious wide cracks. This is attributed to the compression failure mode illustrated by the tested beams, which is relatively more ductile than the FRP-rupture failure mode. The failure shapes of tested beams are shown in Figure (4.15) to Figure (4.19).

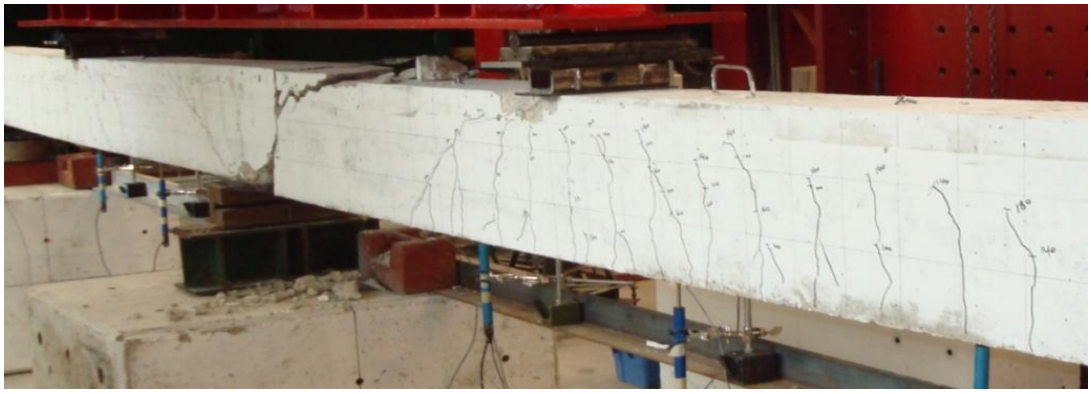

Figure (4.15): Failure shape of beam SGu-8*d*/2*p*

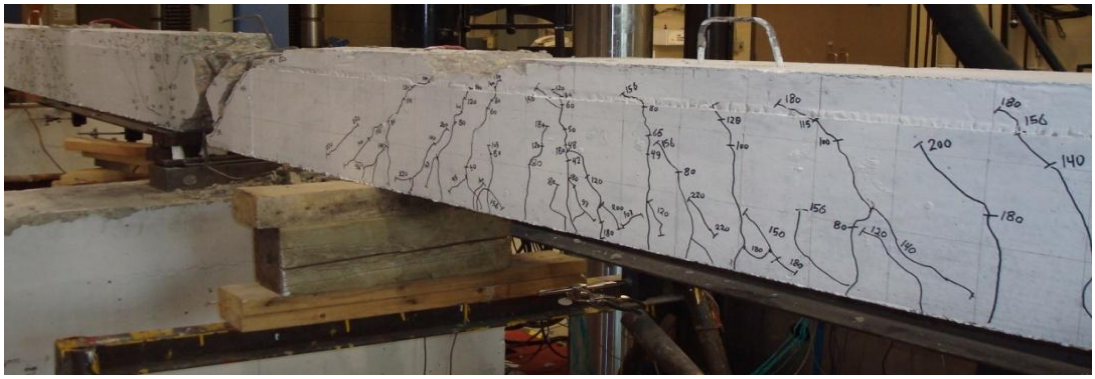

Figure (4.16): Failure shape of beam SGu-8*d*/3*p*

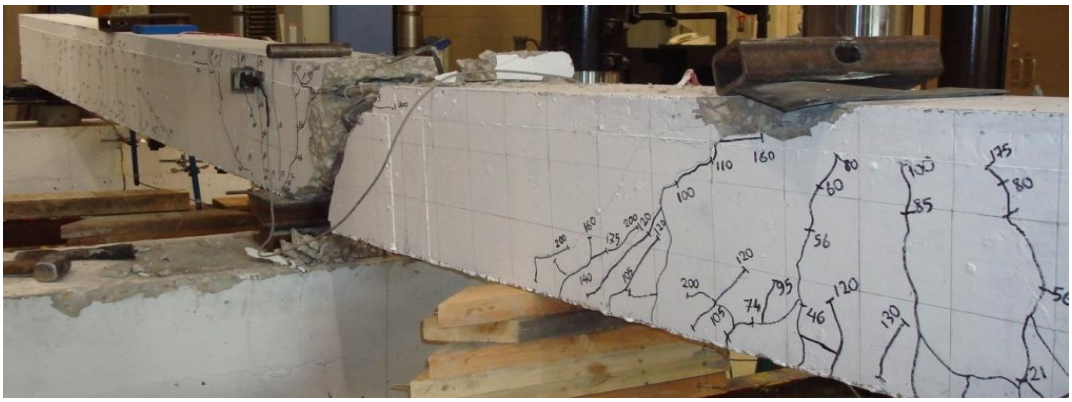

Figure (4.17): Failure shape of beam GSu-10*d*/2*p*

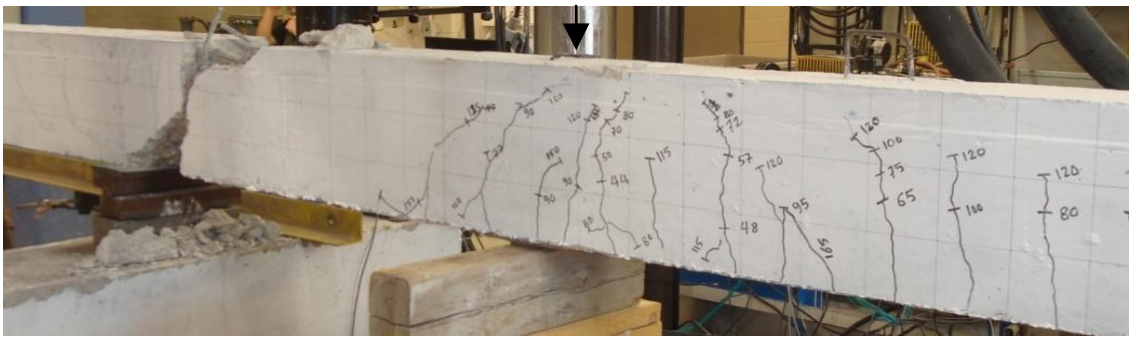

Figure (4.18): Failure shape of beam GGu-10*d*/2*p*

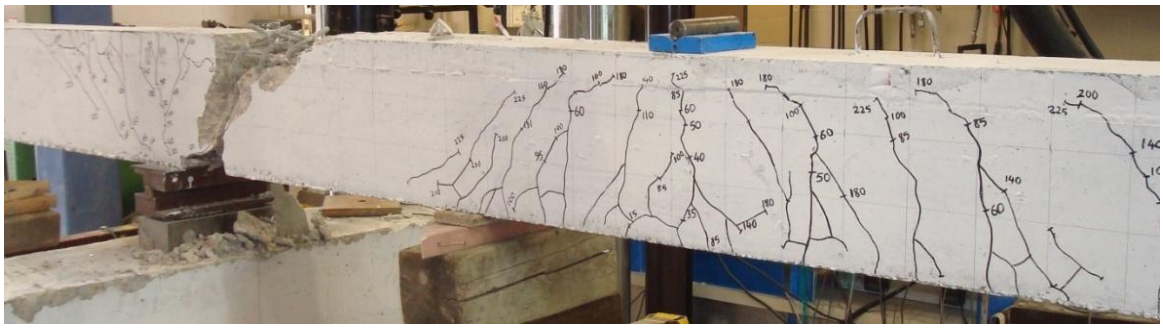

Figure (4.19): Failure shape of beam GGu-10*d*/3*p*

4.3.3. Cracking pattern and crack width

Generally, the cracking pattern of beams GSu-8*d*/3*p*, GSu-10*d*/2*p*, GGu-10*d*/2*p* and GGu-10*d*/3*p* was similar. The first crack in these beams was observed in the hogging moment region at the middle support at approximately P = 16 kN. With the increasing load, another crack was noticed in the sagging moment region at the middle of one span at approximately 23 kN. As the load was further increased, vertical flexural cracks were noted in the sagging moment regions of both spans. The spacing of these cracks ranged between 90 and 130 mm, which is very close to the spacing of the used stirrups in each beam. The number of cracks in the hogging moment region at the middle support also increased as the load increased and propagated towards the middle support zone. The number of cracks at the middle support in beams with smaller stirrup spacing (*d*/3) was larger than beams with wider spacing (*d*/2). The reason for this behaviour is that stirrups often act as crack initiator and consequently affect the flexural crack spacing as indicated by Rizkalla *et al.* (1983). Therefore, closer stirrup spacing was expected to result in smaller flexural crack spacing. Moreover, these beams were provided with the same longitudinal reinforcement ratio at critical sections, which is the main factor that controls the width of flexural cracks as indicated by Zakaria et al. (2009). Hence, the flexural crack width of the tested beams with the same longitudinal reinforcement ratio should be similar. This was confirmed by the measured crack width readings of these beams at middle support section, which were within a comparable range up to approximately 45 kN as illustrated in the following section discussing crack width. This observation of more cracks with comparable width in addition to the increased confinement and enhanced ductility of concrete, suggest that closer spacing increased the rotation capability of the beam and allowed for more rotation at middle support.

The cracking patterns of all tested beams at failure are shown in Figure (4.20).

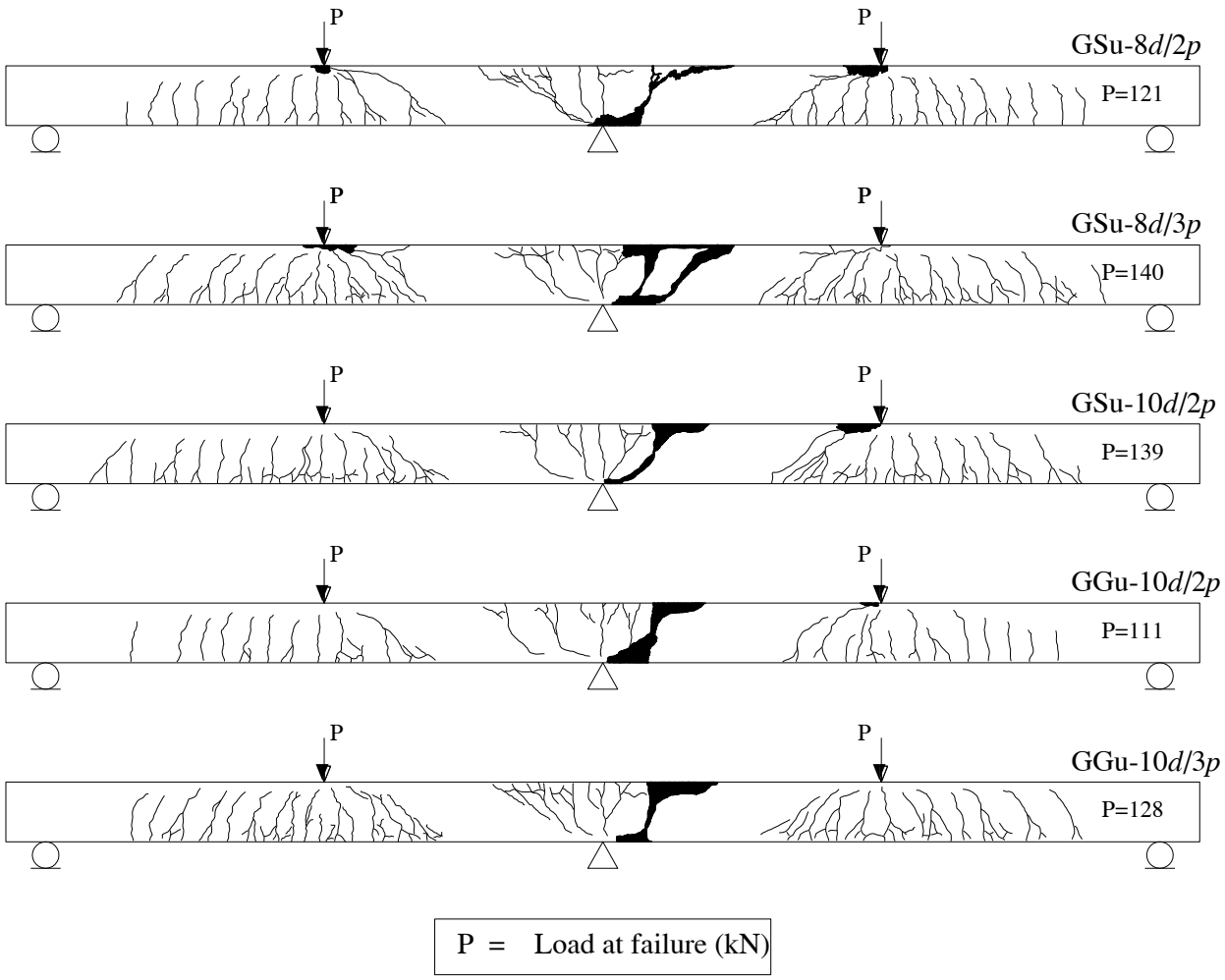

Figure (4.20): Cracking pattern of tested beams

Figure (4.21) shows the maximum measured crack width for the tested beams over the middle support at the top reinforcement level. These GFRP-reinforced beams, designed with the same flexural reinforcement, had close crack width readings at the same load up to approximately 45 kN. For higher loads, beam GGu-10*d*/2*p* with GFRP stirrups and the same spacing as GSu-8*d*/2*p* had about 9.5% higher crack width which might be attributed to the lower modulus of elasticity of GFRP stirrups. The load-crack width response of these two beams was again similar up to failure, which demonstrates the similar performance of GFRP stirrups and their steel counterparts. Nonetheless, beams GGu-10*d*/3*p* with closer GFRP-stirrups spacing, showed

significant reduction in crack width measurements compared to GSu-8*d*/2*p*. This reduction was approximately 22% close to the failure load of GSu-8*d*/2*p* (121 kN). Moreover, comparing beams GGu-10*d*/2*p* and GGu-10*d*/3*p*, it can be seen that increasing the transverse reinforcement ratio by 48% resulted in approximately 30% reduction in crack width close to failure. This indicates that higher GFRP transverse reinforcement has positive effect on reducing the crack width. Beams GSu-8*d*/3*p* and GSu-10*d*/2*p* had approximately the same transverse reinforcement ratio (0.64%) with two different spacing of 120 and 80 mm, respectively. These two beams had similar crack width up to 50% for their failure load. However, beam GSu-8*d*/3*p* with closer stirrups spacing demonstrated smaller crack width compared to GSu-10*d*/2*p* at higher loads. This might be attributed to the fact that the middle support section of beam GSu-8*d*/3*p* had lower tensile strain in longitudinal reinforcement than GSu-10*d*/2*p*, as discussed in the following section, which resulted in a smaller width of the measured crack. Another possible reason for this behaviour is the smaller crack width of shear cracks, which are more dominant at higher loading stage, due to closer spacing of transverse reinforcement as proven by Zakariya et al. (2009).

Furthermore, the Canadian standards CSA-S6-06 (CSA 2006) limit the allowable crack width, at service, to 0.5 mm for exterior exposure. At the service load level of 33 kN, beams GSu-8*d*/3*p*, GSu-10*d*/2*p*, GGu-10*d*/2*p* and GGu-10*d*/3*p* satisfied that limit with recorded crack width of about 0.4 mm.

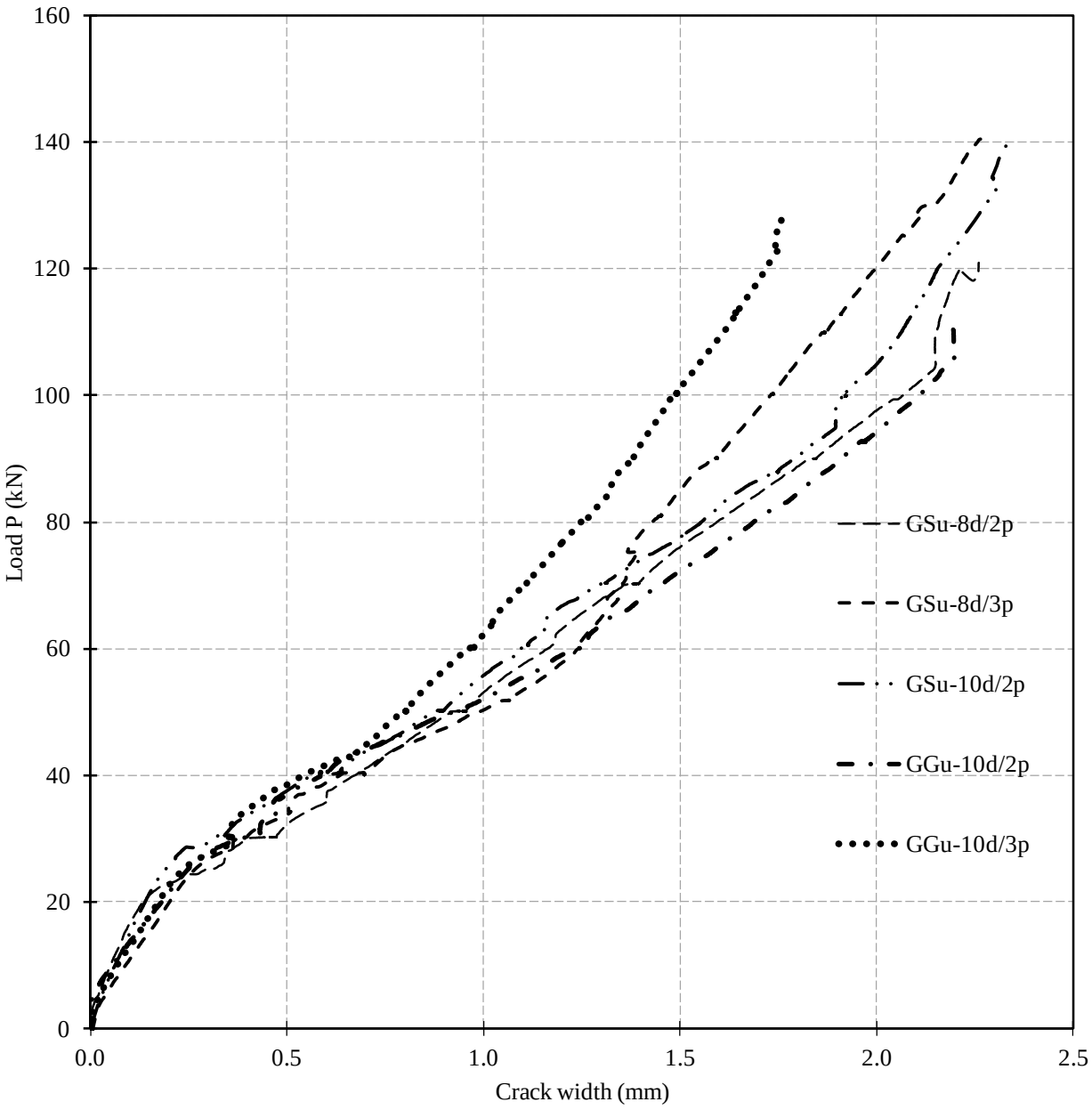

Figure (4.21): Load-crack width relationship measured at middle support

4.3.4. Load-strain variation in reinforcement and concrete

Figure (4.22) and Figure (4.23) show the maximum measured strains in reinforcement and concrete at the critical sections (mid-span and middle support) against the applied load for the tested beams. These figures show that compressive strains in concrete at failure reached or exceeded the maximum compressive strain of 0.0035 specified in CSA standards (CSA 2002 and 2004). Nonetheless, the middle support section of beam GGu-10*d*/2*p* is the only section where concrete did not reach the crushing strain. This resulted in approximately 18% loss of the section expected flexural capacity due to the premature failure of concrete which can be seen in Table (4.1) from the difference between expected and achieved flexural capacity. This could be attributed to the lower modulus of elasticity of the GFRP stirrups, compared to steel in its counterpart beam GSu-8*d*/2*p*, which could not maintain enough confinement in the compression zone to support the high stresses at this location. Regarding tensile strains, the figures show that the strains in FRP bars increased suddenly after concrete cracking. The measured strains indicate that the section at middle support, in all tested beams, cracked before the mid-span section. This was expected due to the higher elastic moment at the middle support section.

The measured strain in the top reinforcement over the middle support was about 1.2 times that in the bottom reinforcement at mid-span in all FRP-reinforced beams. It can also be noted that maximum tensile strains in GFRP bars did not reach the ultimate value as these beams were designed as over-reinforced to have concrete crushing failure.

The measured strains in internal reinforcement were compared to the strains measured on the concrete surface to investigate the compatibility of strains between the bars and the surrounding concrete. All GFRP-reinforced beams showed approximately 10% difference between measured tensile strains in the internal reinforcement and the concrete surface before cracking and up to

30% of failure load. Following that stage, significant difference in the measured strains was observed when several transverse cracks formed at the critical sections. This difference increased at higher load levels, which is believed to be due to increasing slippage of GFRP bars as their bond strength was reached. This belief is supported by observing a number of horizontal cracks at the tensile reinforcement level prior to failure of GFRP-reinforced beams. The strain difference at the middle support section was found to be typically higher than that at the mid-span section. The reason behind this behaviour is the higher strains developed at the middle support section compared to the mid-span section.

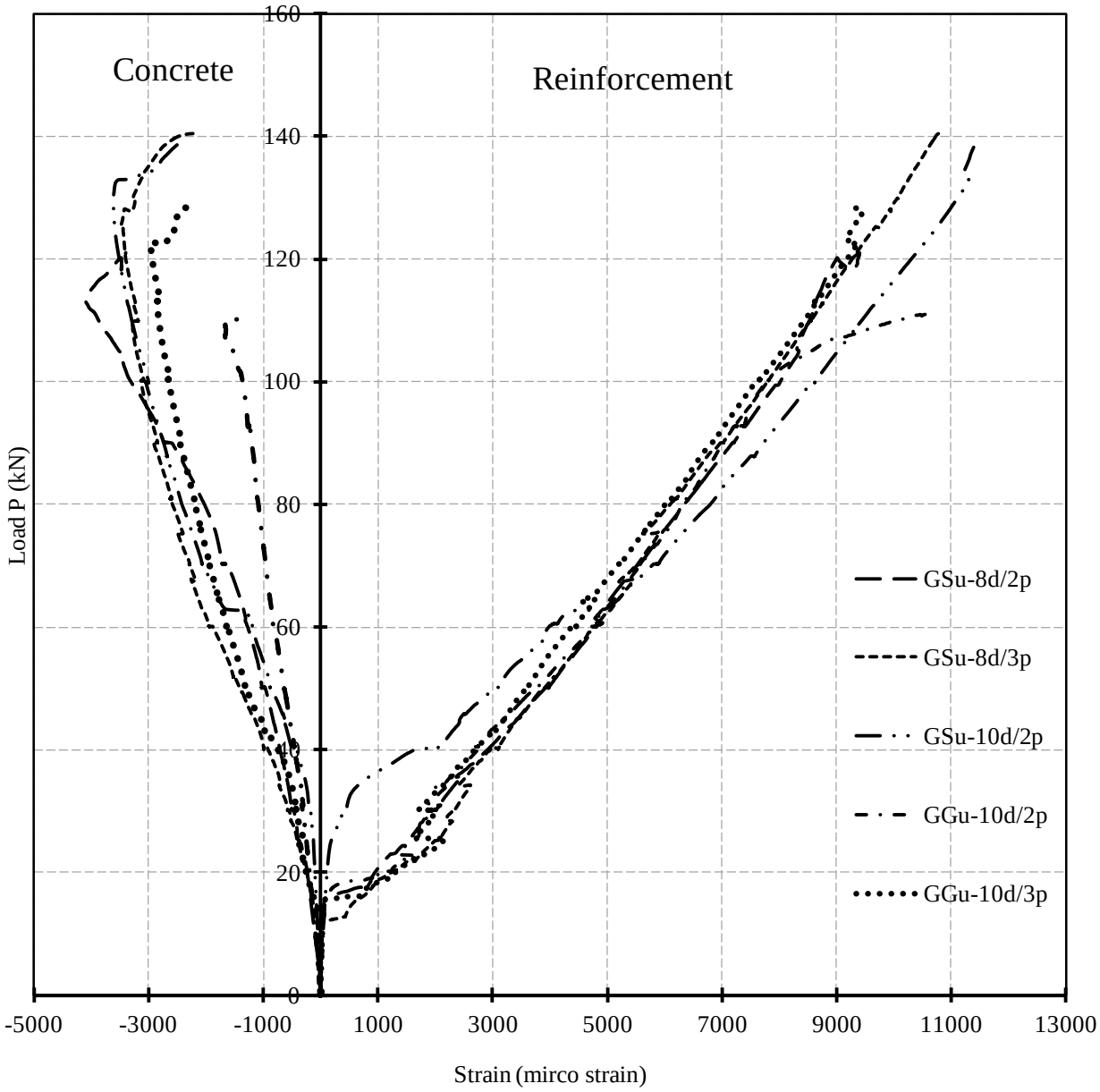

Figure (4.22): Variation of strain with load at middle support section

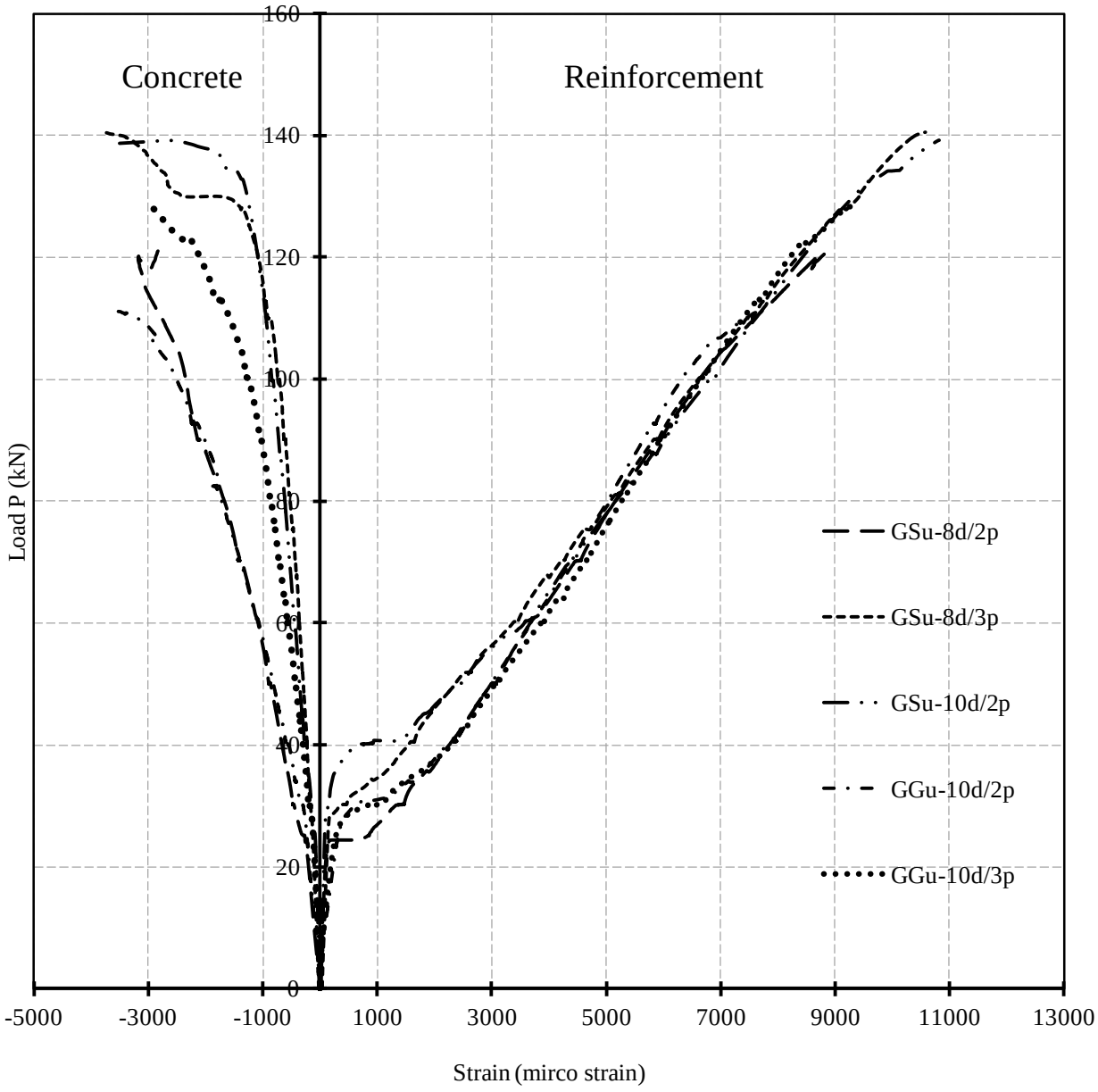

Figure (4.23): Variation of strain with load at mid-span section

4.3.5. Load-deflection response

The relationship between the applied load at each span and the measured deflection at mid-span is shown in Figure (4.24). The tested beams demonstrated linear load-deflection behaviour before cracking. Upon cracking, stiffness was reduced as the load increased. Up to approximately 95% of its failure load, beam GGu-10*d*/2*p* with GFRP stirrups had similar load-deflection behaviour as beam GSu-8*d*/2*p*, which had identical flexural reinforcement and same spacing of stirrups made of steel. Using GFRP stirrups did not change beam performance during loading, however, beam GGu-10*d*/2*p* could not achieve the same failure load of beam GSu-8*d*/2*p* (with steel stirrups) due to the lower modulus of elasticity of GFRP stirrups compared to steel.

Increasing the transverse reinforcement whether made of steel or GFRP as in beams GSu-8*d*/3*p*, GSu-10*d*/2*p* and GGu-10*d*/3*p* compared to GSu-8*d*/2*p* resulted in improvement in the ultimate load capacity and less deflection at any particular applied load. Beam GSu-8*d*/3*p* and GSu-10*d*/2*p* had approximately the same transverse reinforcement ratio (ρ_v) equals to 0.64% which is 60% more than beam GSu-8*d*/2*p* (ρ_v = 0.4%). This increase in transverse reinforcement resulted in 15% increase in the ultimate failure load. Comparing GSu-8*d*/3*p* to GSu-10*d*/2*p*, it can be seen that using closer stirrups spacing as in GSu-8*d*/3*p* without changing ρ_v allowed for more deflections at mid-span without affecting the ultimate failure load. Beam GSu-8*d*/3*p* with 33% smaller spacing compared to GSu-10*d*/2*p* had about 8.5% more deflection at the same applied load level after cracking and prior to failure. This had a positive effect on available rotation capacity and moment redistribution at critical sections. In beams GGu-10*d*/2*p* and GGu-10*d*/3*p* with GFRP stirrups, again the same behaviour was observed as increasing the transverse reinforcement ratio with smaller spacing resulted in improvement in the ultimate load capacity and reduction in the mid-span deflection. Beam GGu-10*d*/3*p* with 48% increase in reinforcement

ratio and 33% smaller stirrups spacing compared to GGu-10*d*/2*p* had 15% higher failure load and approximately 8% reduction in mid-span deflection.

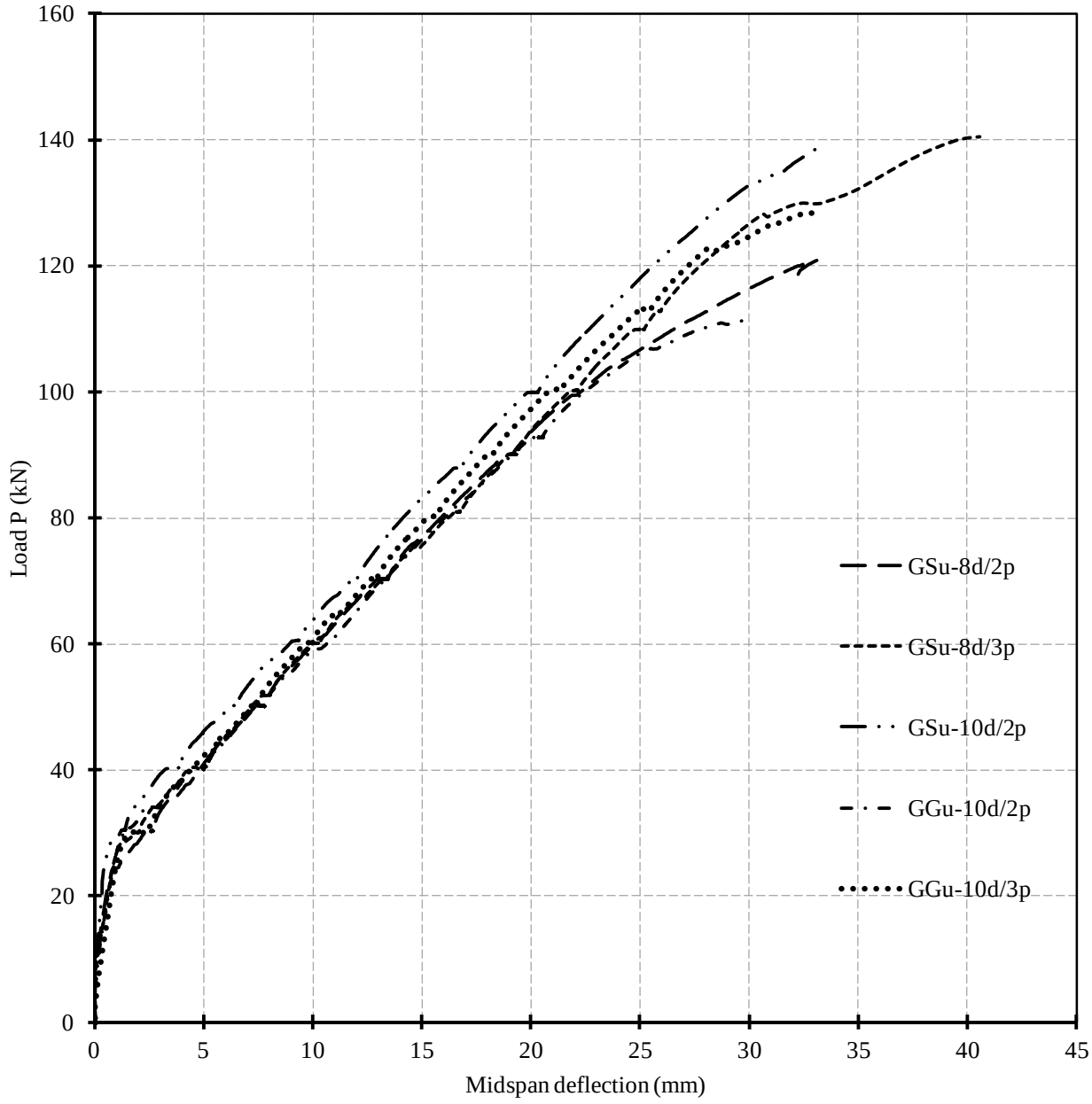

Figure (4.24): Load-deflection relations for tested beams

4.3.6. Reactions and moment-redistribution

Figure (4.25) shows the variation of end reactions versus the applied load for the tested beams. Using the measured reactions, the experimental bending moments at both middle support and mid-span was calculated and the amount of moment redistribution was obtained. The tested beams in this series were provided with reinforcement configuration that allows for 20% moment redistribution. These beams succeeded in redistributing more than 20% of the connecting bending moment at the middle support into the mid-span while achieving the expected failure load. Beam GGu-10*d*/2*p* is the only beam that achieved only 90% of the expected failure load (*P* =125 kN) as the middle support section did not reach the designed flexural capacity. However, this beam experienced a rapid increase in moment redistribution, approximately 30%, from the middle support to the mid-span prior to failure.

Figure (4.26) illustrates the actual and elastic moment distribution at the critical section of tested beams with FRP reinforcement. Comparing the actual and elastic bending moment in each beam at failure, it can be seen that beams GSu-8*d*/2, GSu-8*d*/3, GSu-10*d*/2, GGu-10*d*/2 and GGu-10*d*/3 redistributed up to 23%, 37%, 32%, 30% and 32% of hogging bending moment, respectively.

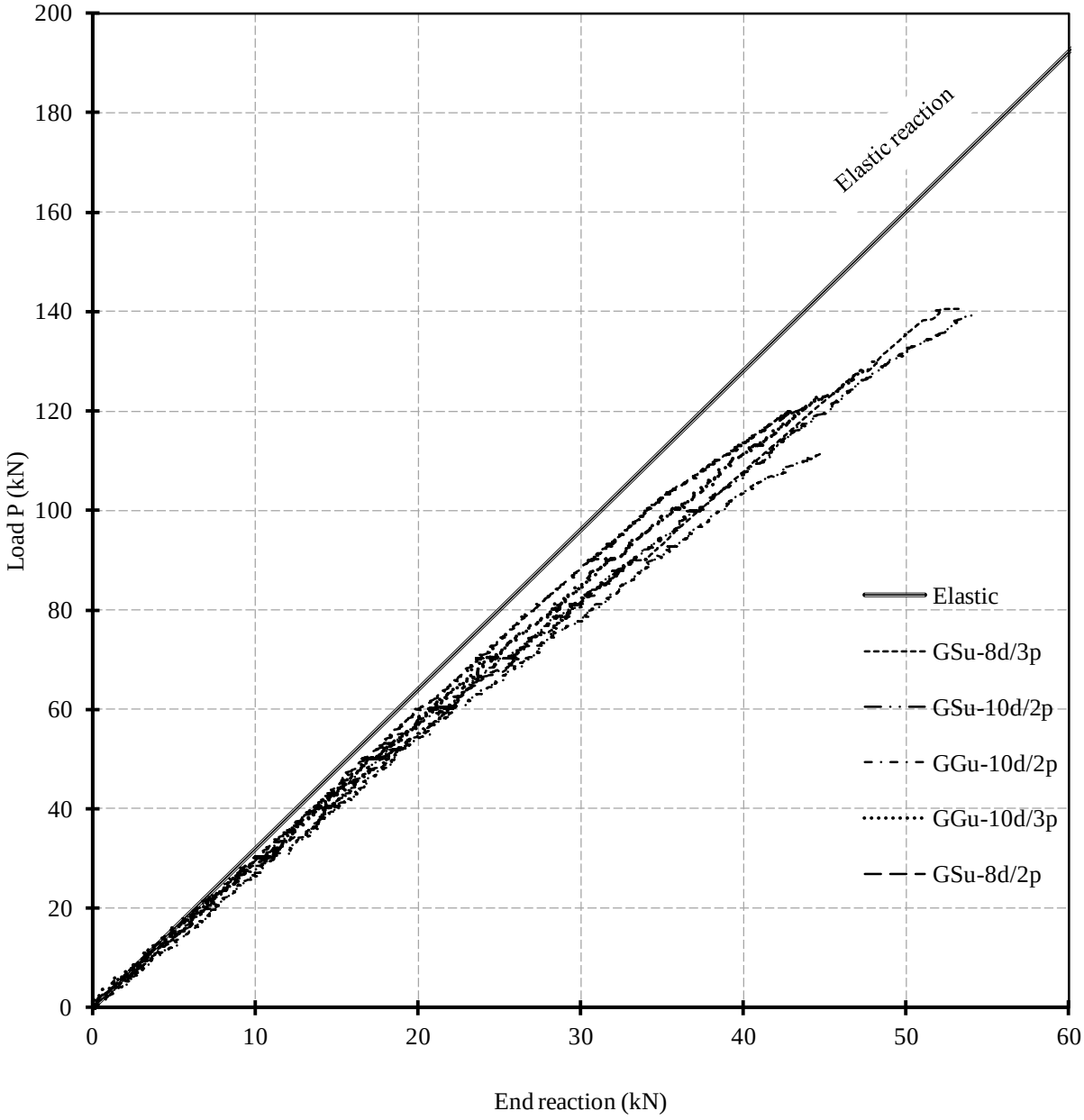

Figure (4.25): Load versus end support reactions of the tested beams

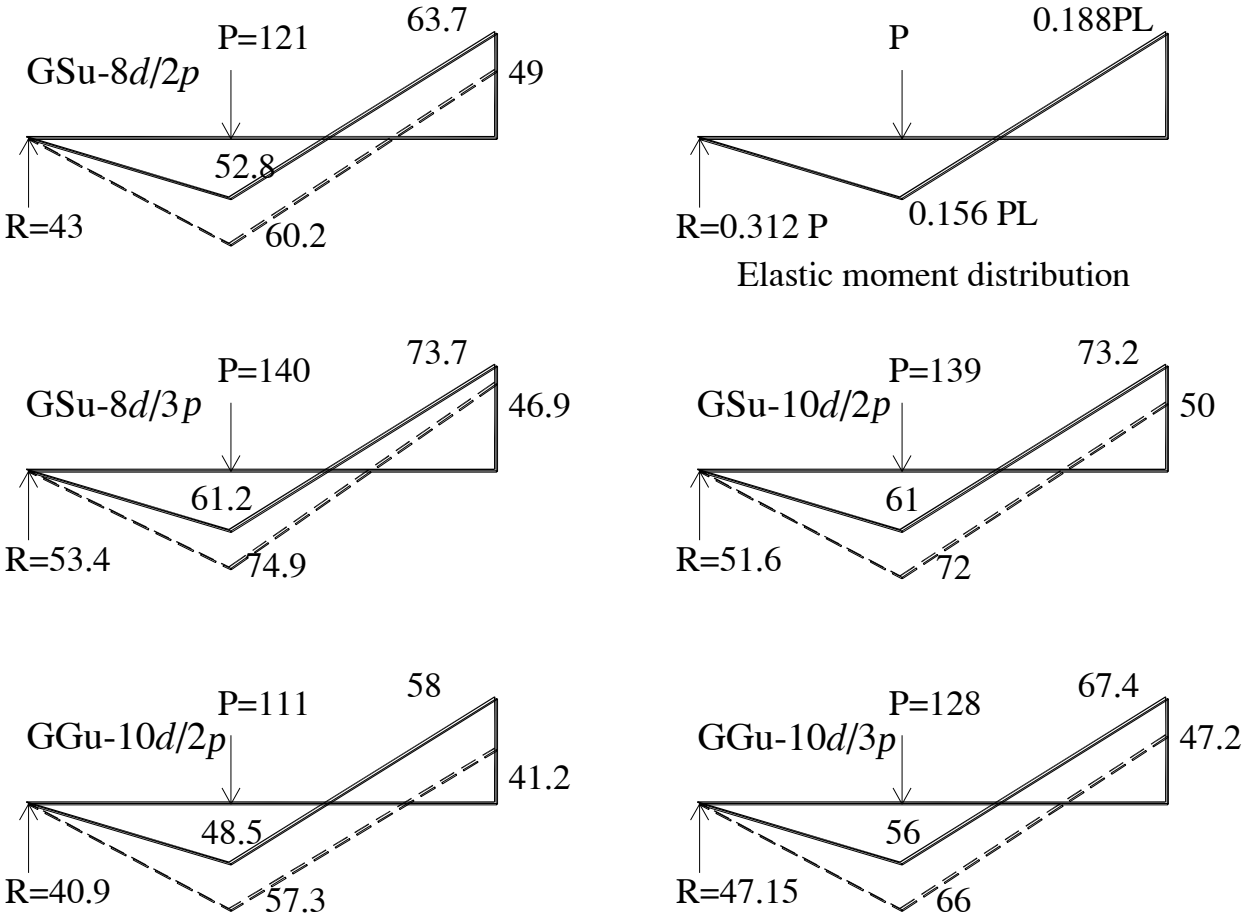

Figure (4.26): Actual versus elastic bending moment at failure

Moreover, Figure (4.27) shows the relationship between the applied load and the percentage of moment redistribution at middle support hogging moment. Beam GGu-10*d*/2*p* was designed assuming 20% redistribution of the elastic bending moment from middle support to mid-span. It was observed that this beams experienced an actual redistribution of bending moments at the service load level of about 13%, which represents 65% of the assumed design value. This is a similar behaviour compared to beam GSu-8*d*/2*p* which, again, supports the similar performance of GFRP stirrups compared to steel. It can also be seen that increasing the transverse reinforcement as in beams GSu-8*d*/3*p*, GSu-10*d*/2*p* and GGu-10*d*/3*p* had a positive effect on the achieved moment redistribution compared to beam GSu-8*d*/2*p*. The improvement was 30% for GSu-10*d*/2*p* and GGu-10*d*/3*p* and 60% for GSu-8*d*/3*p* compared to GSu-8*d*/2*p* at failure load level. Increasing the stirrups spacing while maintaining the same transverse reinforcement ratio had a significant positive impact on moment redistribution as can be seen from comparing beams GSu-8*d*/3*p* and GSu-10*d*/2*p*. Beam GSu-8*d*/3*p* had about 16% more moment redistribution than beam GSu-10*d*/2*p*.

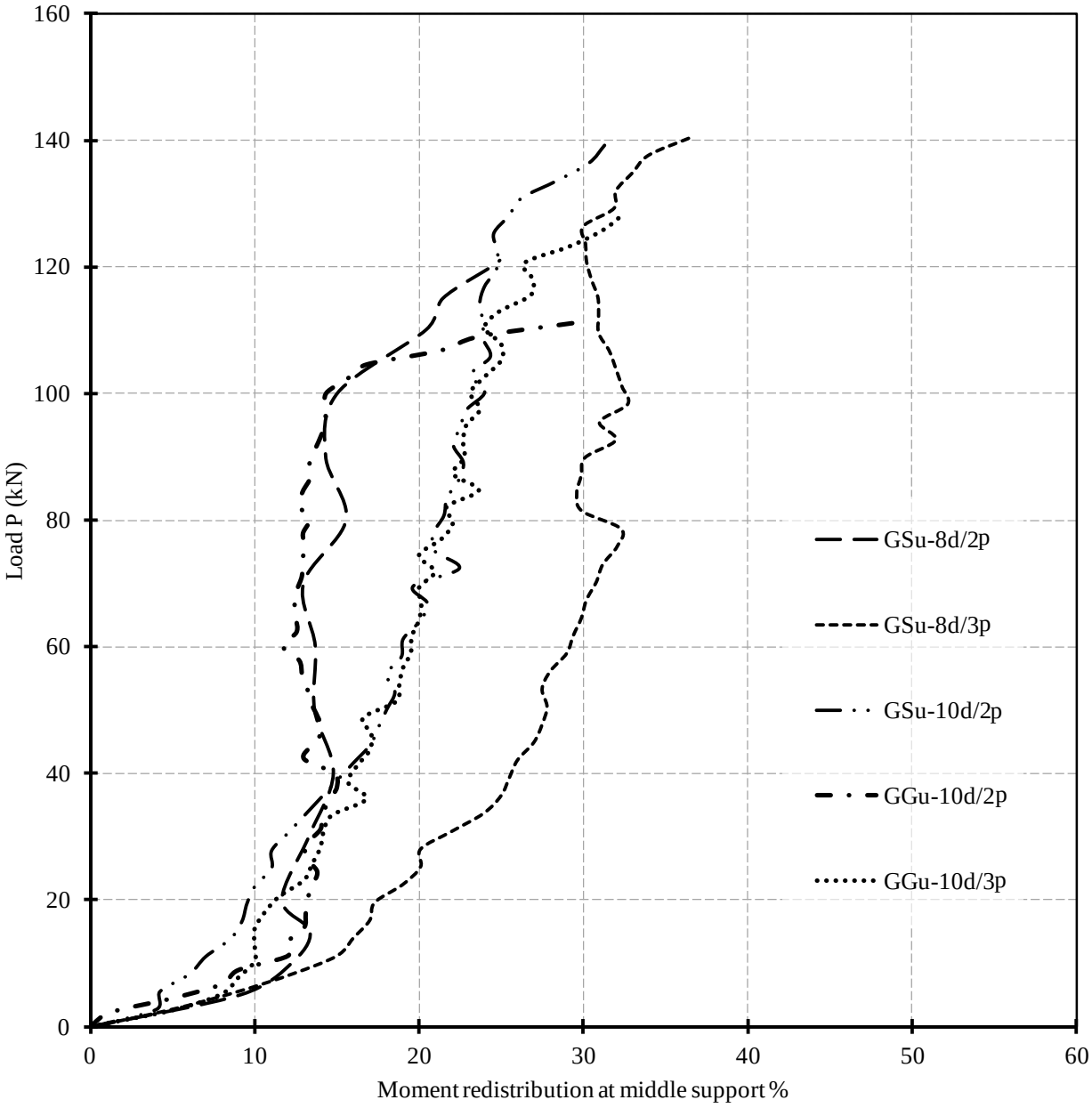

Figure (4.27): Load versus percentage of moment redistribution

4.4. Predicted Versus Actual Load Capacity

As previously mentioned, all tested beams, except for beam GSs-10*d*/2*p*, were designed to have similar ultimate load capacity of about 125 kN, however, the actual experimental failure loads where different due to difference between actual material properties, obtained in the laboratory, and those assumed in design (provided by manufacturer). The steel-reinforced beam was designed according to the CSA-A23.3-04 (CSA 2004), which allows for 20% moment redistribution. Table (4.1) shows the experimental load capacity along with the calculated failure load according to the applicable design standard. The calculated failure load is considered to be the load at which one of the critical sections develops the maximum flexural capacity. The predicted failure loads were calculated by equating the code-predicted flexural capacity of critical section with the corresponding distribution of bending moment allowed by the code as a function of the applied load (*P*). The lower value of the predicted failure load at middle support and mid-span was considered.

It can be seen that the applicable design standard successfully predicted the failure load of beam SSc-8*d*/2*p*, GSu-8*d*/2*p* and GSu-8*d*/2*e*, however failed to predict the failure location of beam CSu-8*d*/2*p*. The code predicted the failure to be at middle support of beam CSu-8*d*/2*p*, however, the failure was initiated due to concrete crushing at both middle support and mid-span sections. Also, the design code underestimated the failure load of GSu-8*d*/2*p*. This is due to significant moment redistribution from middle support section to mid-span, which enabled the higher flexural capacity at mid-span to be developed. Moreover, it can be seen from Table (4.1) that, in general, all critical sections reasonably achieved the predicted design flexural strength. However, the middle support section of beam CSu-8*d*/2*p* achieved only 61% of the expected flexural capacity. The explanation of this might be the fact that the assumed condition of perfect bond

between reinforcement and the surrounding concrete was no longer satisfied due to slippage and bond failure at this section, as previously discussed.

Beams GSu-8*d*/3*p*, GSu-10*d*/2*p*, GGu-10*d*/2*p* and GGu-10*d*/3*p* were designed in flexure to have similar target load capacity as beam GSu-8*d*/2*p* (125 kN), however each beam had a different combination of stirrups material, spacing and diameter to study the effect of transverse reinforcement on the flexural behaviour. Nonetheless, the expected failure load for each beam was different due to slight difference in the actual compressive strength of the concrete in each beam. Table (4.1) shows the experimental failure load recorded during testing (P_{exp}) and the predicted failure load (P_{cal}) calculated based on the expected flexural capacity of critical sections according to the CSA code. The calculated failure load is considered to be the load at which one of the critical sections develops the maximum flexural capacity. A 20% redistribution of the connecting bending moment from the middle support to the mid-span section was assumed in calculating the failure load. In addition, Table (4.1) shows both the experimental and predicted bending moments at critical sections. It can be seen that all tested beams, except GGu-10*d*/2*p*, achieved the expected failure load predicted based on the cross-section flexural capacity. This indicates that these beams were adequately reinforced in shear to develop the expected flexure strength. This observation is in good agreement with the recorded concrete compressive strains exceeding crushing strain at critical section. Beam GGu-10*d*/2*p* developed only 90% of the expected flexural capacity. This observation is also supported with the measured compressive strain in concrete at the middle support section of this beam which did not reach crushing strain. This can be attributed to the significant rotation exhibited by beam GGu-10*d*/2*p* at the middle support section to redistribute the bending moment (33% redistribution). This rotation caused relatively wide cracks, as in Figure (4.21), which dramatically reduced the concrete interlocking

portion of the concrete shear resistance of the cross-section. The fact that this rotation was higher in beam GGu-10*d*/2*p* compared to GSu-8*d*/2*p* (with steel stirrups and the same spacing) might be attributed to the lower modulus of elasticity of the GFRP stirrups.

The failure of the tested beams was accompanied with longitudinal bars rupture in dowel effect except for beam GSs-10*d*/2, as discussed previously.

Comparing the experimental and calculated bending moments at critical sections, it can be seen that the experimental bending moments are typically higher than the expected flexural capacity at mid-span with a ratio up to 25%. On the other hand, sections at middle support experienced bending moments up to 15% less than the expected flexural capacity at those sections. This might be attributed to the tendency of the tested beams to redistribute bending moments towards the stiffer mid-span sections which had higher reinforcement ratio than middle support sections.

Table (4.1): Experimental and calculated failure loads and bending moments

Beam	Experimental failure load P_{exp} (kN)	Calculated failure load P_{cal} (kN)[a]	P_{exp}/P_{cal}	Experimental bending moment (kN.m)		Predicted bending moment (kN.m)[a]		Experimental/predicted bending moment		Achieved Moment redistribution at failure
				- ve	+ve	-ve	+ve	-ve	+ve	
SSc-8*d*/2*p*	163	152	1.1	68.9	79.6	64.0	81.2	1.1	1.0	20%
GSu-8*d*/2*p*	121	122	1.0	49.0	60.2	51.3	59.8	1.0	1.0	23%
CSu-8*d*/2*p*	95	112	0.9	29.0	51.8	47.4[b]	56.4	0.6	0.9	42%
GSu-8*d*/2*e*	111	109	1.0	63.4	46.3	57.4	49.3	1.1	0.9	8%[c]
CSu-8*d*/2*e*	117	121	1.0	60.2	51.8	64.0	57.7	0.9	0.9	2%
GSu-8*d*/3*p*	140	131	1.1	46.9	74.9	55.0	64.0	0.9	1.2	36%
GSu-10*d*/2*p*	139	133	1.0	50.0	72.0	56.0	65.0	0.9	1.1	32%
GGu-10*d*/2*p*	111	119	0.9	41.2	57.3	50.0	59.0	0.8	1.0	29%
GGu-10*d*/3*p*	128	131	1.0	47.2	66.0	55.0	64.0	0.9	1.0	30%
GSs-10*d*/2*p*	201	172	1.2	70.8	105	73.0	84.0	1.0	1.3	33%

[a] Based on the actual material properties
[b] Calculated using ISIS (2007) as tension-failure section
[c] Moment redistribution from mid-span to middle support

4.5. Prediction of Load-deflection Response

As discussed earlier in the literature review chapter, extensive studies were dedicated to provide formulas to predict the load-deflection response of FRP-reinforced concrete beams. Most of the available formulas were based on Branson's equation to calculate the effective moment of inertia (I_e). As this equation was developed for steel-reinforced beams, modification factors were applied for the equation to be applicable with FRP-reinforced beams. These formulas were introduced earlier in Chapter 2 (Equations 2.1 to 2.5).

For continuous members, the CSA-A23.3-04 (CSA 2004) states that effective moment of inertia should be calculated at both critical sections and a ratio between them should be used as follows: I_e =0.85 I_{em} + 0.15 I_{ec}, where I_{em} and I_{ec} are effective moment of inertia at mid-span and middle support, respectively. The ACI 318-08 (ACI Committee 318 2008) states that the use of the effective moment of inertia at mid-span section is considered satisfactory as it has the dominant effect on deflection. The approach proposed by the ACI 318-08 code was used in this study to calculate deflection at mid-span using Equation (4.1).

$$\Delta = {}^{7}/_{768} * Pl^3/(E_c * I_e) \quad (4.1)$$

The deflection calculated based on theoretical models mentioned above were compared with the experimental results as shown in Figure (4.28), Figure (4.29) and Figure (4.30) for beams GSu-8*d*/2*p*, GSu-8*d*/2*e* and CSu-8*d*/2*p*, respectively. It can be seen that the modifications factor proposed by Habeeb and Ashour (2008) gives a reasonable prediction to the experimental results especially at high loading stage. Further experimental results would better confirm this observation.

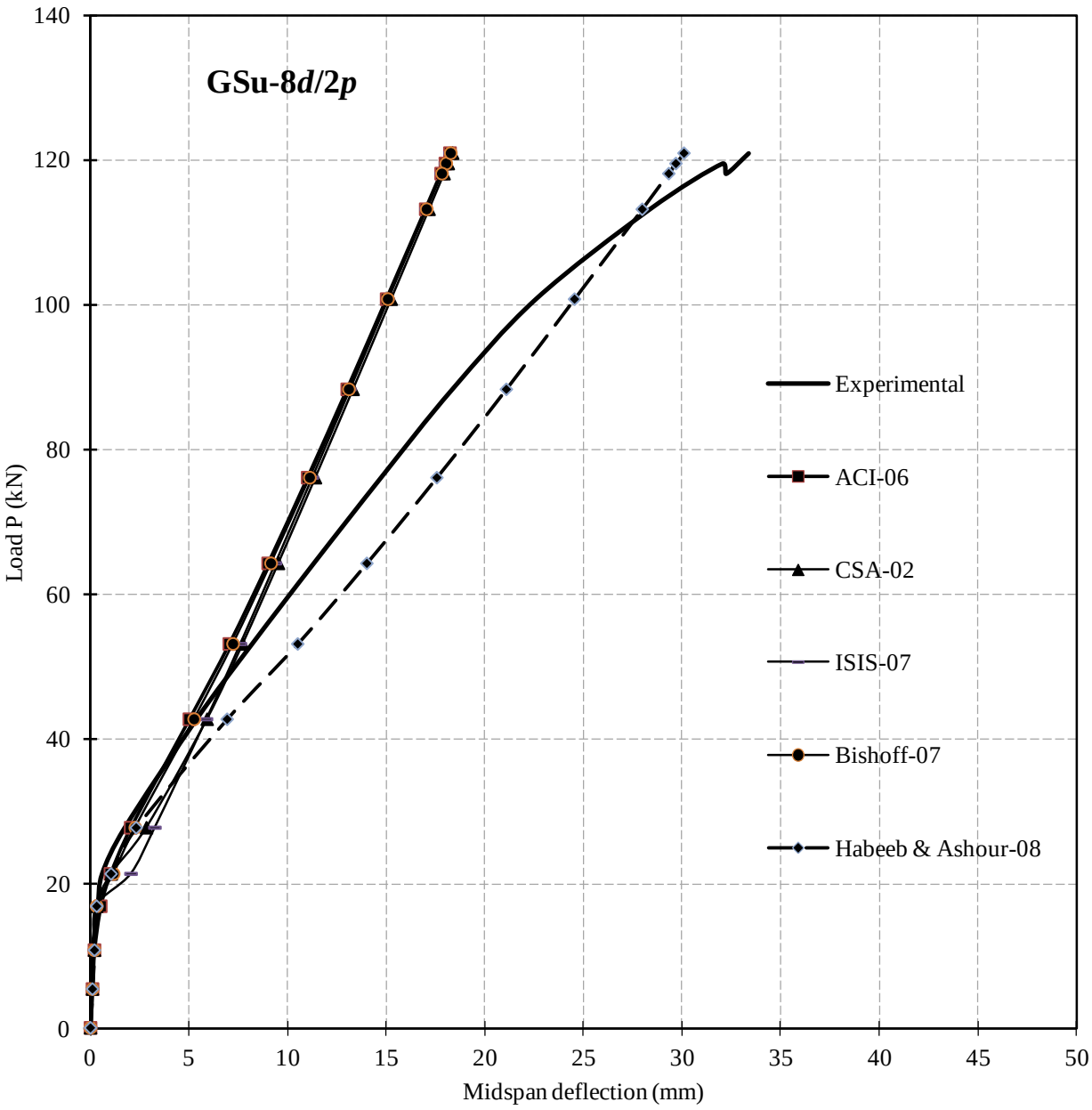

Figure (4.28): Experimental and predicted deflection for beam GSu-8*d*/2*p*

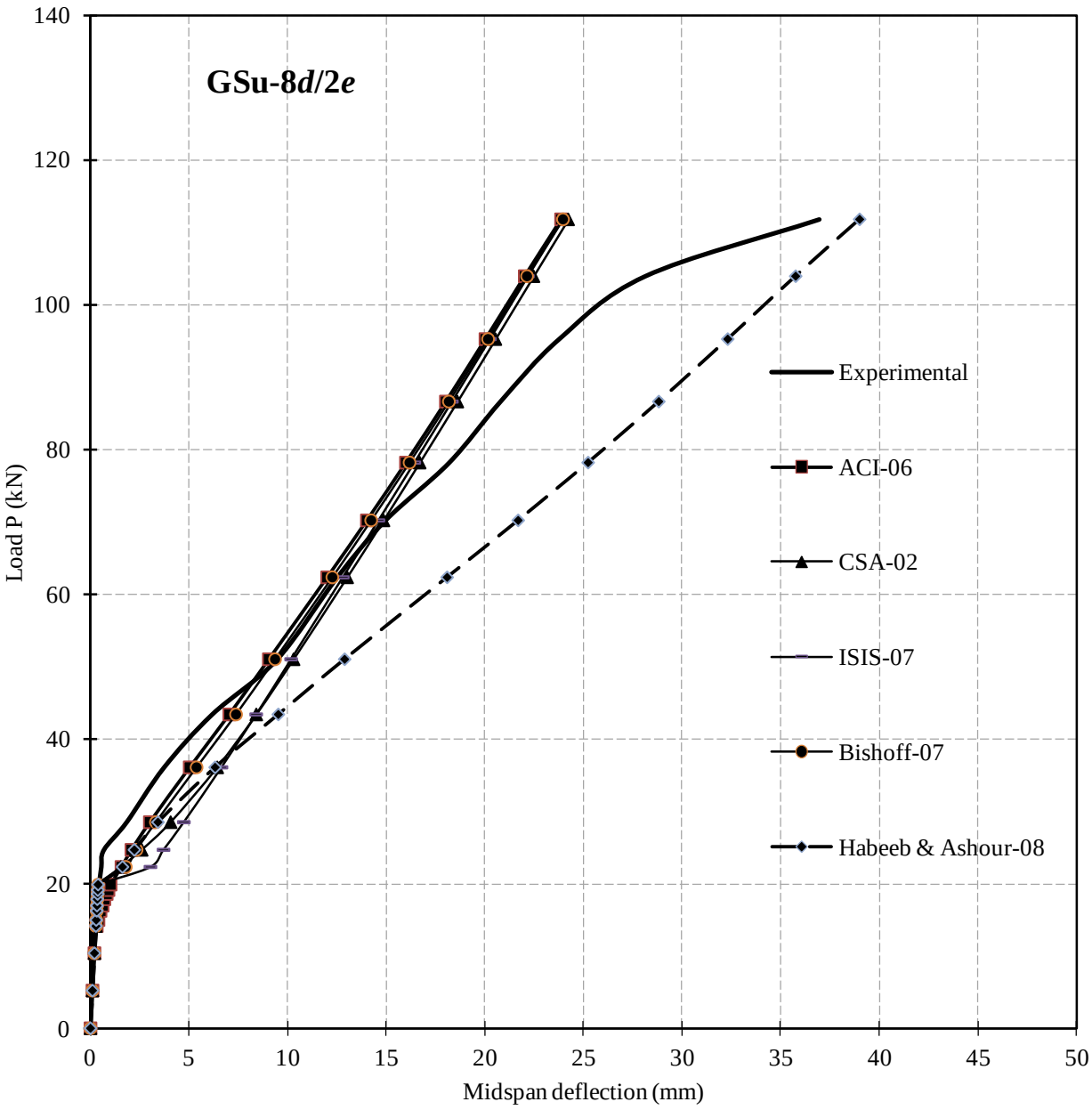

Figure (4.29): Experimental and predicted deflection for beam GSu-8*d*/2*e*

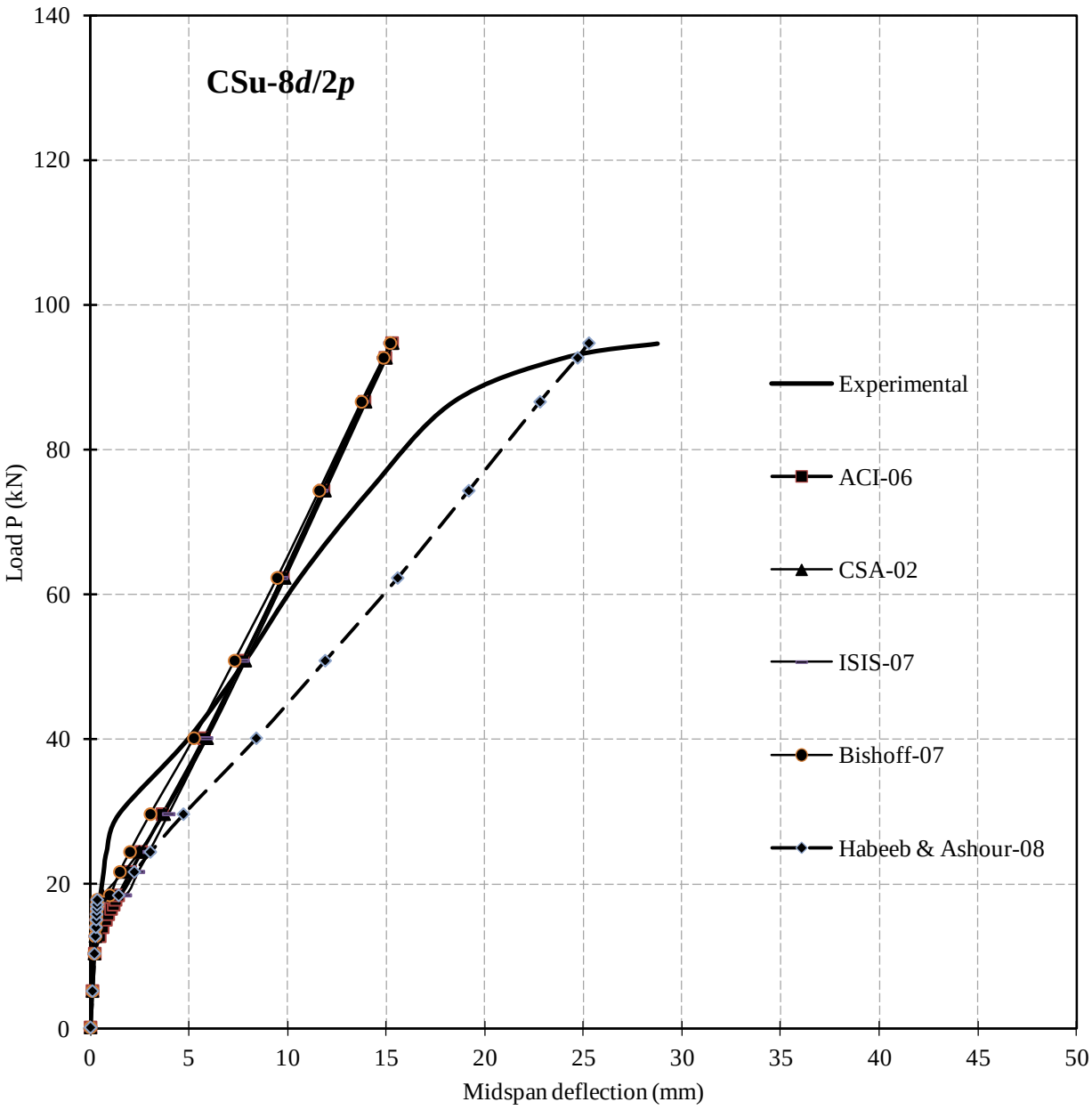

Figure (4.30): Experimental and predicted deflection for beam CSu-8*d*/2*p*

CHAPTER 5: FINITE ELEMENT MODELING

5.1. General

This chapter describes the numerical analysis study in this research. A non-linear finite element model (FEM) was constructed to simulate the flexural behaviour of continuous concrete beams reinforced with FRP bars. The commercially available finite element analysis software package, ANSYS (ANSYS 2010), was used in this process. The experimental results presented in the previous chapter were used to verify the accuracy of the constructed FEM. As the majority of tested beams in the experimental study were GFRP-reinforced, the main focus in this chapter is on GFRP bars.

In this chapter, the steps to construct the FEM including the elements used in modeling, material types and boundary conditions are explained in details. In addition, the different assumptions made in the finite element modeling process including meshing, constitutive models for concrete and the used solution method are also discussed.

The FEM was able to simulate the behaviour of the tested continuous concrete beams with reasonable accuracy. However, it was not able to predict the post-failure behaviour of concrete due to difficulties in convergence in the program solution once failure started.

The constructed FEM described in this chapter was used to conduct a parametric study to investigate the influence of key parameters on the behaviour of FRP-reinforced continuous concrete beams. The results of this study are presented in the next chapter.

5.2. Material Properties and Elements Types

5.2.1. Concrete material

In this study, concrete was modeled using three-dimensional eight-node solid elements. The solid element, SOLID65, was used for modeling of concrete. The main feature of this element is the ability to account for material nonlinearity. This element is capable of considering cracking in three perpendicular directions, plastic deformation and crushing. The element is defined by eight nodes having three translation degrees of freedom at each nod in the x, y and z directions as shown in Figure (5.1).

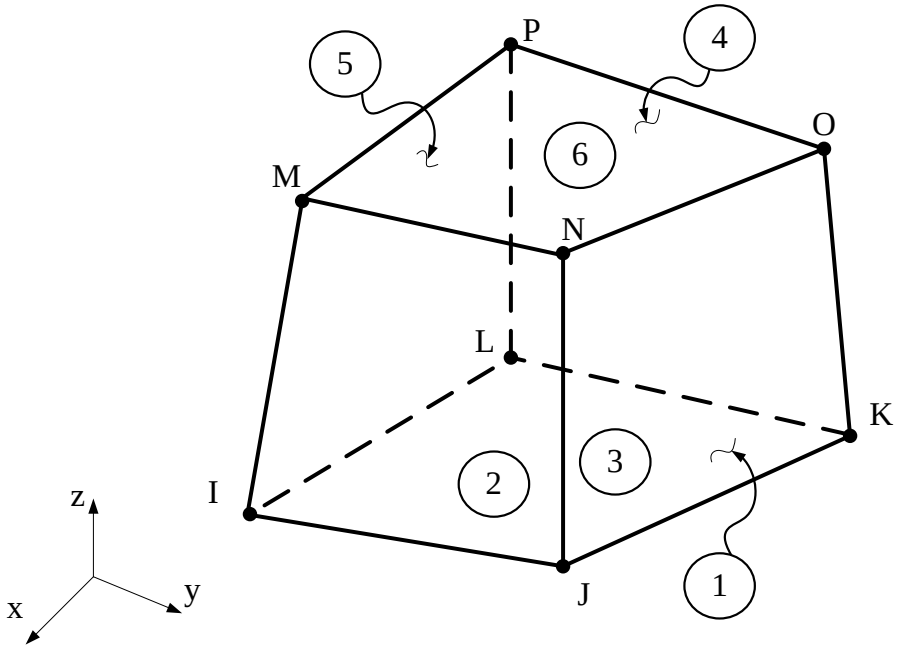

Figure (5.1): Element SOLID 65 (reproduced from user manual ANSYS 2010)

SOLID 65 elements require linear isotropic and multi-linear isotropic material properties in order to model concrete properly. The used multi-linear isotropic material uses Von-Mises failure

criterion in addition to the Willam and Warnke (1974) model to define the failure of the concrete (ANSYS 2010).

To define the concrete material, the modulus of elasticity (E_c) and the Poisson's ratio have to be identified. In this study, the Poisson's ratio was assumed to be 0.2 and the modulus of elasticity was calculated based on the following equation.

$$E_c = 4500\sqrt{f_c'} \tag{5.1}$$

The stress-strain relationship of normal strength concrete in compression typically consists of two parts; an ascending branch and a descending branch. In ANSYS software, however, the use of ideal stress-strain curve with the descending branch leads to convergence problems. Therefore, in this study, the descending branch of the concrete material model in ANSYS was ignored as recommended in previous studies (kachlakev et al. 2001; Wolanski 2004; Gorji 2009; Büyükkaragöz 2010).

To compute the ascending branch of the multi-linear isotropic stress-strain curve for the concrete, the following equations were used (MacGregor 1992).

$$f = \frac{E_c\,\varepsilon}{1 + \left(\frac{\varepsilon}{\varepsilon_o}\right)^2} \tag{5.2}$$

$$\varepsilon_o = \frac{2\,f_c^{`}}{E_c} \tag{5.3}$$

Where:

f = stress (in MPa) at any strain;

ε = strain at stress *f*;

ε_o = strain at the maximum compressive strength $f_c^{`}$.

Five points were used to define the curve as shown in Figure (5.2). The stress-strain relationship shown in Figure (5.2) is based on work done by Kachlakev, et al. (2001). The first point is defined to be at stress equals to 30% of the ultimate compressive strength of the concrete, considering the pre-defined Young's Modulus and satisfying Hooke's Law;

$$E = \frac{\sigma}{\varepsilon} \tag{5.3}$$

Points 2, 3 and 4 are calculated from Equations (5.2) and (5.3) by selecting a stress and calculating the corresponding strain. Point 5 is defined at the ultimate compressive strength of concrete ($f_c^{`}$) and strain equals to 0.0035 indicating traditional crushing of unconfined concrete as specified by the Canadian standards (CSA 2004).

In order to define the Willam and Warnke (1974) material model in ANSYS, there are nine different constants that should be defined (ANSYS 2010).

1. Shear transfer coefficients for an open crack;
2. Shear transfer coefficients for a closed crack;
3. Uniaxial tensile cracking stress;
4. Uniaxial crushing stress (positive)
5. Biaxial crushing stress (positive);
6. Ambient hydrostatic stress state;
7. Biaxial crushing stress under the ambient hydrostatic stress state;
8. Uniaxial crushing stress under the ambient hydrostatic stress state;

9. Stiffness multiplier for cracked tensile condition.

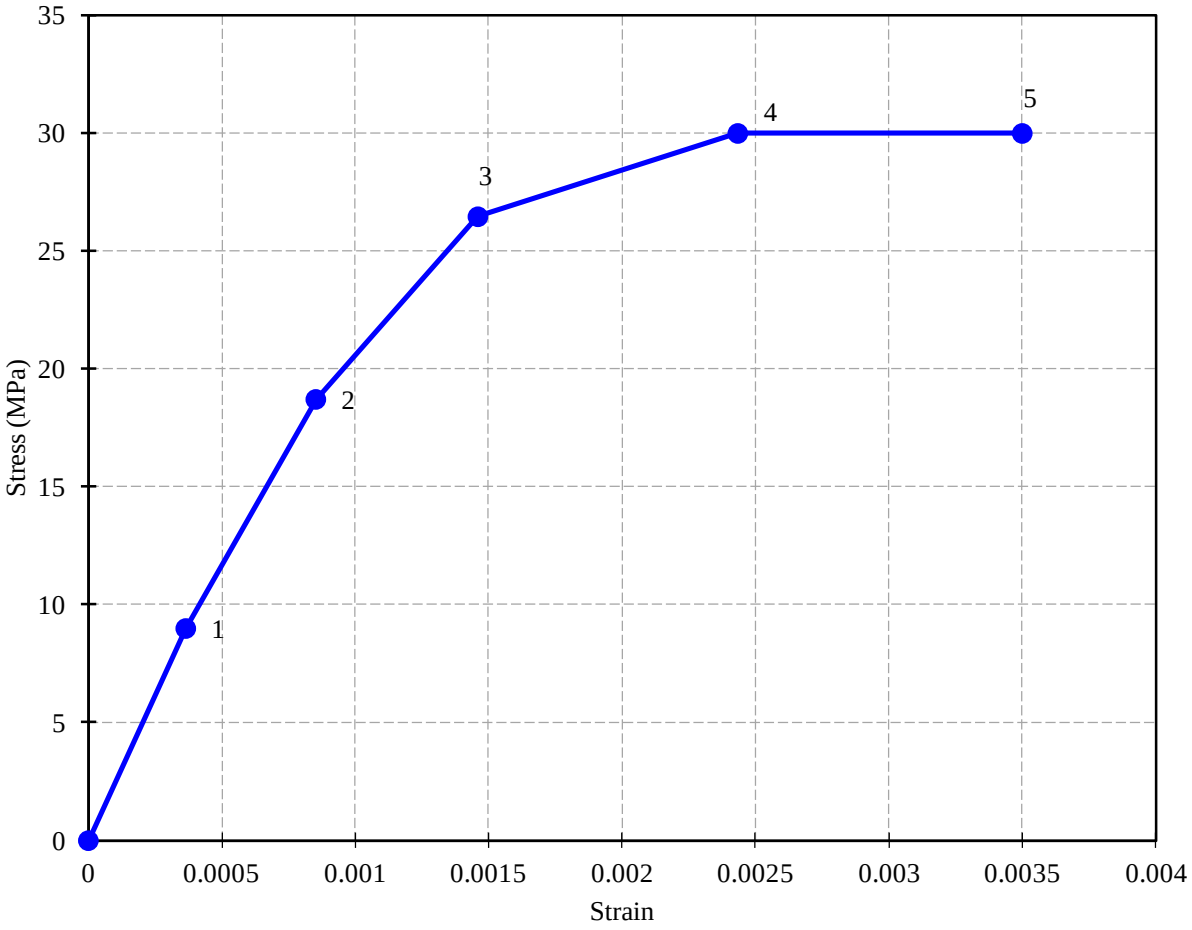

Figure (5.2): Simplified uniaxial stress-strain concrete curve

Typical shear transfer coefficients range from 0.0 to 1.0, with 0.0 representing a smooth crack (complete loss of shear transfer) and 1.0 representing a rough crack (no loss of shear transfer). The shear transfer coefficients for open and closed crakes were taken as 0.2 and 0.8 based on the work of previous researches (kachlakev et al. 2001; Wolanski 2004). The uniaxial cracking stress was based on the modulus of rupture and was calculated using the following equation.

$$f_r = 0.6\sqrt{f_c`} \tag{5.3}$$

In this study, stress concentrations at the loading zone and support locations resulted in conversions problems and sometimes premature failure. Therefore, the uniaxial crushing was entered as -1 to turn off the crushing capability of the concrete element to avoid such problems as suggested by many researchers (Kachlakev,et al. 2001, Wolanski 2004; Mostofinejad and Talaeitaba 2006; Gorji 2009; Büyükkaragöz 2010).

The remainder of the variables in the concrete model are basically parameters to define the biaxial compressive strength of concrete. As the failure surface can be defined by ANSYS program with a minimum of two constants, f_r and $f_c^{`}$, these variables were left to default.

5.2.2. Reinforcement materials

The reinforcement materials in this research (longitudinal bars and stirrups) were modeled as truss elements with one node at each end. The finite element LINK180 was used for that purpose. End nodes of this element have three degrees of freedom, translation in the nodal directions x, y and z. The behaviour of this element is capable of simulating nonlinearity and plastic deformations. The geometry and nodes of this element are shown in Figure (5.3).

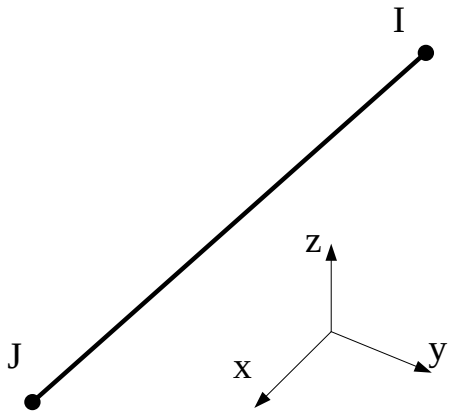

Figure (5.3): LINK180 finite element (reproduced from user manual ANSYS 2010)

To properly model steel reinforcement, LINK180 element requires linear isotropic and bi-linear isotropic material properties to be defined. To model FRP reinforcement, the same element was defined with linear-elastic material properties instead. The Poisson's ration was assumed to be 0.3 for steel reinforcement and 0.2 for FRP. The modulus of elasticity for reinforcement materials was obtained experimentally as described earlier in Chapter 3. Figure (5.4) shows the stress-strain relationship for the reinforcement material used in this study.

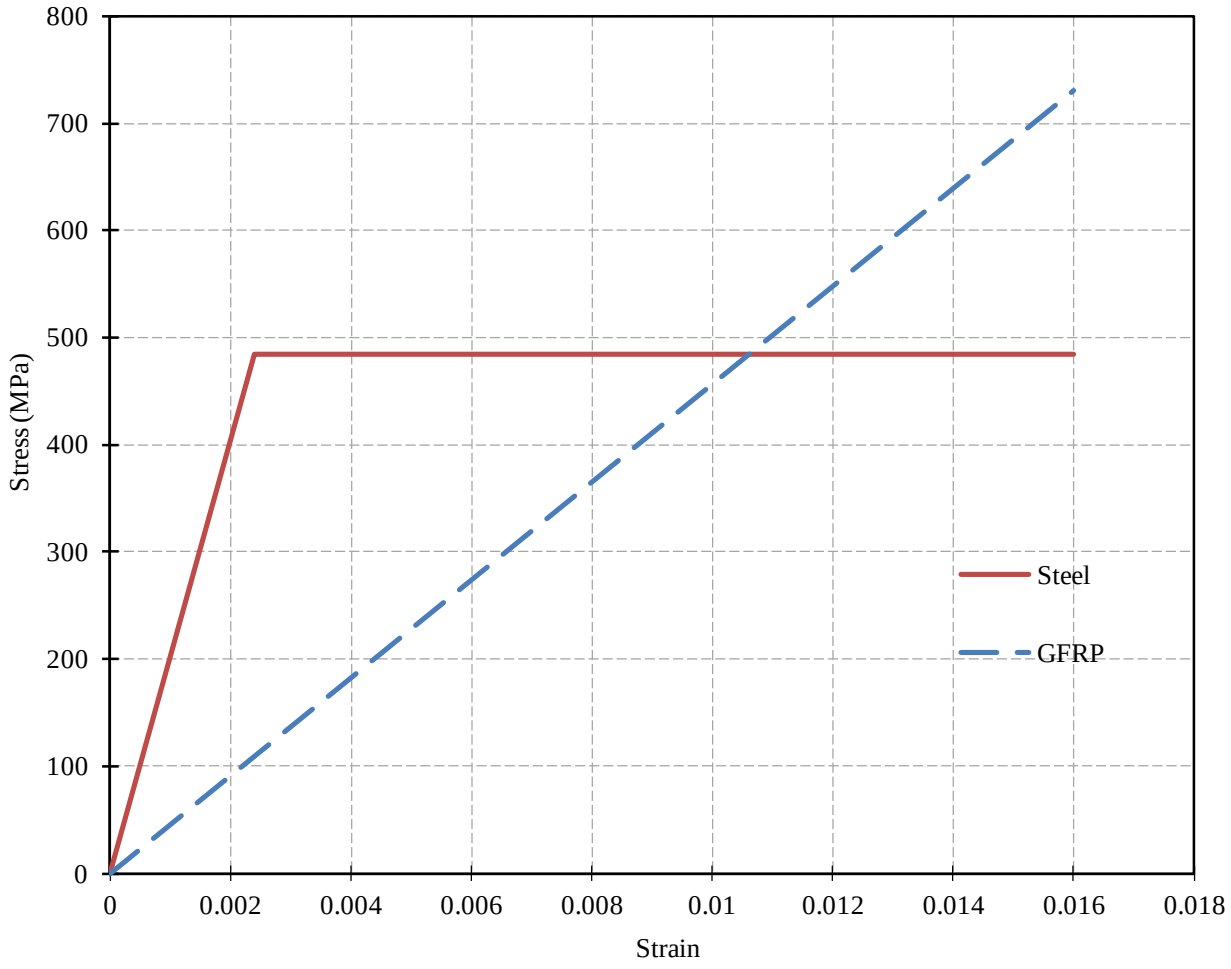

Figure (5.4): Stress-strain relationship of reinforcement materials used in finite element modeling

5.2.3. Bearing plates

The steel bearing plates used at supports and loading points to distribute concentrated stresses were also modeled. The finite element SOLID45 was used for this purpose. This element has eight nodes, each with three degrees of freedom as translations in x, y and z directions. The geometry and nodes of element SOLID45 are shown in Figure (5.5). The steel bearing plates were modeled as linear-elastic material with elasticity modulus of 200 GPa and 0.3 Poisson's ratio.

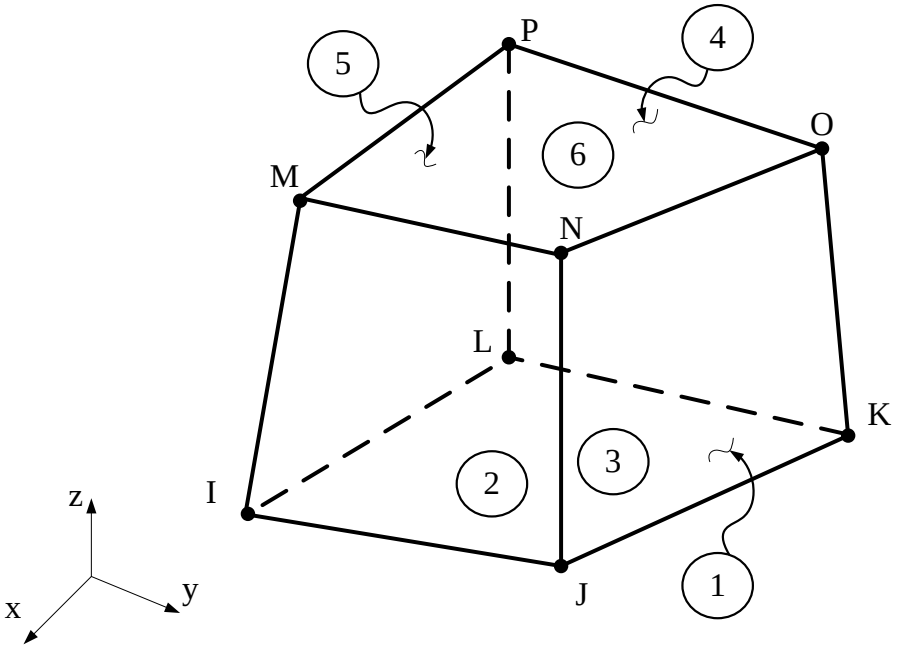

Figure (5.5): Element SOLID45 (reproduced from user manual ANSYS 2010)

5.3. Reinforcement-Concrete Interface

There are a number of techniques to model reinforcement in a concrete element. The two most common methods are discrete modelling and smeared modelling. The smeared modeling method assumes the reinforcement is uniformly distributed throughout concrete elements in a defined region of finite element mesh as shown in Figure (5.6) (Mady 2011). This approach is more suitable for cases where reinforcement location does not significantly affect the overall behaviour of the structure. In the discrete method, the reinforcement elements are connected to the same concrete mesh nodes locations, resulting in both elements sharing the same nodes as shown in Figure (5.6). The discrete modeling concept was used in this study.

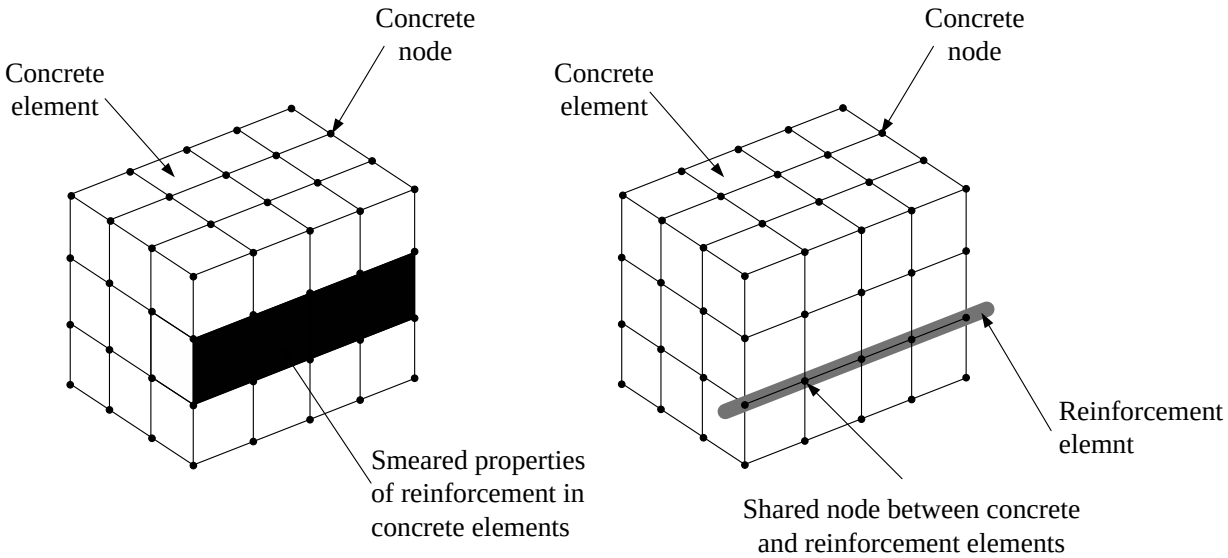

a) Smeared model b) Discrete model

Figure (5.6): Modeling reinforcement in concrete element (reproduced from Mady 2011)

According to previous studies reported earlier in Chapter 2 as well as observations from the experimental results of this study, the bond-slip relationship between FRP bars and the surrounding concrete has a significant effect of the overall behaviour of continuous beams. Therefore, instead of assuming a full contact between the nodes of concrete and reinforcement elements, the bond-slip relationship was taken into consideration. This was achieved by modeling the reinforcement nodes to share the same locations as concrete nodes while having different numbering. In other words, two different nodes with two different numbers are created at the same location with one for reinforcement elements and the other for concrete. This will allow the reinforcement elements to behave independently away from concrete elements. To connect them together, non-linear spring elements were used to connect the reinforcement and concrete elements nodes. Three different springs were used between each two connecting nodes. One spring element in the reinforcement direction to represent the longitudinal slip between the bar and surrounding concrete and two in perpendicular directions representing the shear strength or dowel action resistance of the bar. The most common spring element used for this purpose is COMBIN39 element (ANSYS 2010). This is a unidirectional element with nonlinear generalized force-displacement capability.

Two different bond-slip relationships were used to define the response of spring elements in the longitudinal direction of reinforcement; one for steel and one for GFRP bars. The adopted bond-slip model for steel bars in this study was the one introduced by the CEB-FIP Model Code (CEB-FIP 1990) for unconfined concrete with good bond conditions. The model consists of ascending curve followed by a descending branch with a steady-constant line at the end of the relationship as shown in Figure (5.7). The ascending branch of the model follows the formula given in Equation (5.4) (CEB-FIP 1990).

$$\tau = \tau_{max} \left(\frac{s_l}{0.6}\right)^{0.4} \tag{5.4}$$

Where τ and s_l are the bond stress and the corresponding slippage, respectively, and τ_{max} is the maximum bond strength of the steel bar embedded in concrete calculated from Equation (5.5). The relationship was defined by six points on the ascending branch. The descending branch of the model is linear all the way to bond stress of 0.15 τ_{max} followed by a constant stress values slip more than 1 mm as shown in Figure (5.7).

$$\tau_{max} = 2\sqrt{f_c'} \tag{5.5}$$

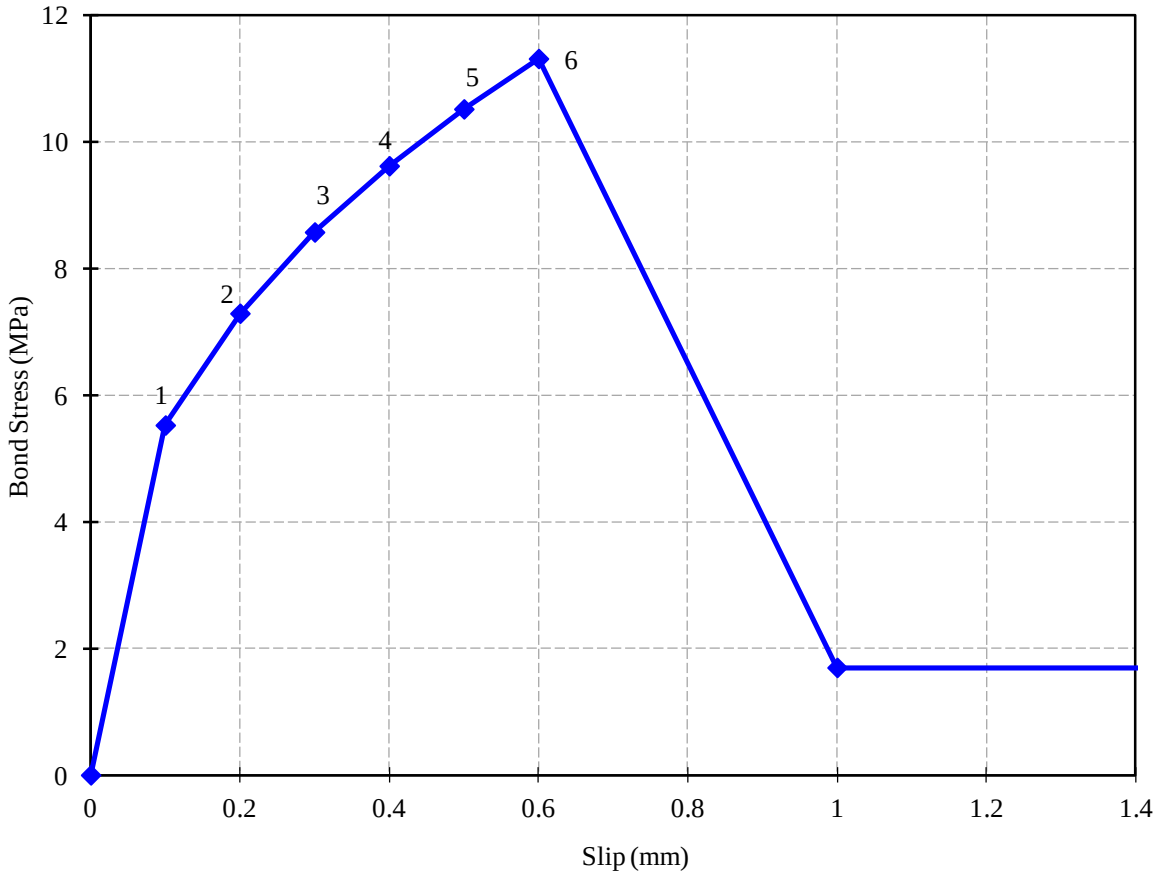

Figure (5.7): Bond-slip relationship for steel bars embedded in concrete (CEB-FIP 1990)

The used bond-slip relationship for GFRP bars was based on a recent study conducted at the University of Manitoba that evaluated the bond strength of GFRP bars similar to the ones used in this current study (Alves et al. 2011). The study proposed an average bond-slip relationship for sand-coated GFRP bars as shown in Figure (5.8).

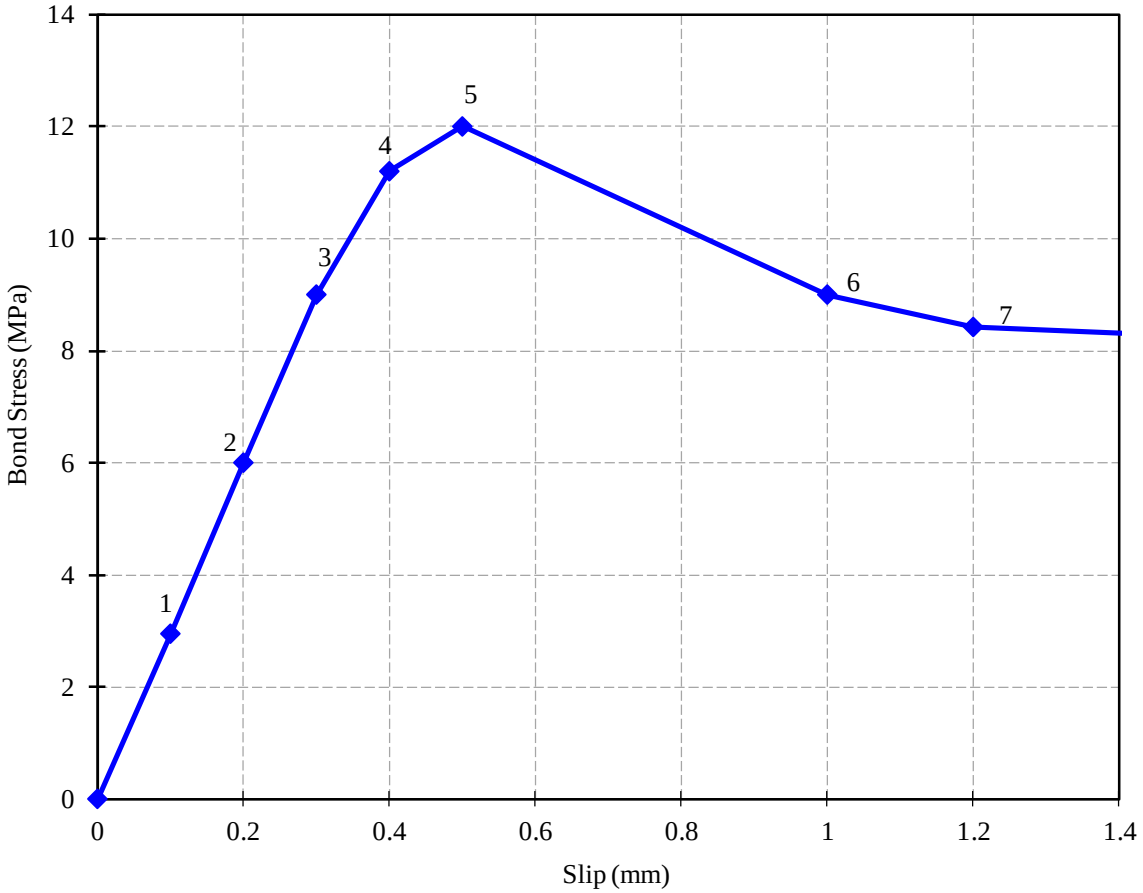

Figure (5.8): Bond-slip relationship for GFRP bars embedded in concrete (Alves et al. 2011)

The stress-displacement relationship for springs perpendicular to the reinforcement elements direction was assumed to be linear up to the shear strength of the bar. The corresponding displacement was calculated from the transverse strain (obtained from Poisson's ratio multiplied by the maximum longitudinal strain) multiplied by the bar diameter. The used GFRP bars had

shear strength of 195 MPa according to the manufacturer (Pultrall Inc. 2009) and the corresponding displacement was taken equal to 0.05 mm (0.016 × 0.2 × 15.9 mm). The shear strength of steel bars was assumed to be 400 MPa and the corresponding displacement equals to 0.0096 mm (0.002 × 0.3 × 16 mm).

5.4. ANSYS Model Geometry and Boundary Conditions

All tested beams are symmetric in geometry, loading and internal reinforcement in the longitudinal direction about the middle support location. The cross-section of the tested beams is also symmetric about the vertical axis passing through center of gravity of the cross-section. Only one-quarter of the beam was modeled in ANSYS taking advantage of symmetry about two axes. This approach significantly reduced the computational time and the required storage desk space, which facilitated using a finer mesh in modeling. The boundary conditions at the axes of symmetry were set to represent the effect of continuity. Figure (5.9) shows the considered axes of symmetry and boundary conditions of the model. The horizontal translation was restrained in the longitudinal direction at the middle support and in the transverse direction at the cross-section symmetry axis. The boundary conditions at the external supports were set to simulate a roller at the end support and a hinge at the middle support. This was achieved at the end support by restricting vertical translations only, while restricting both vertical and horizontal translations at the middle support. Moreover, translations at external supports were also prevented in the out-of-plan direction.

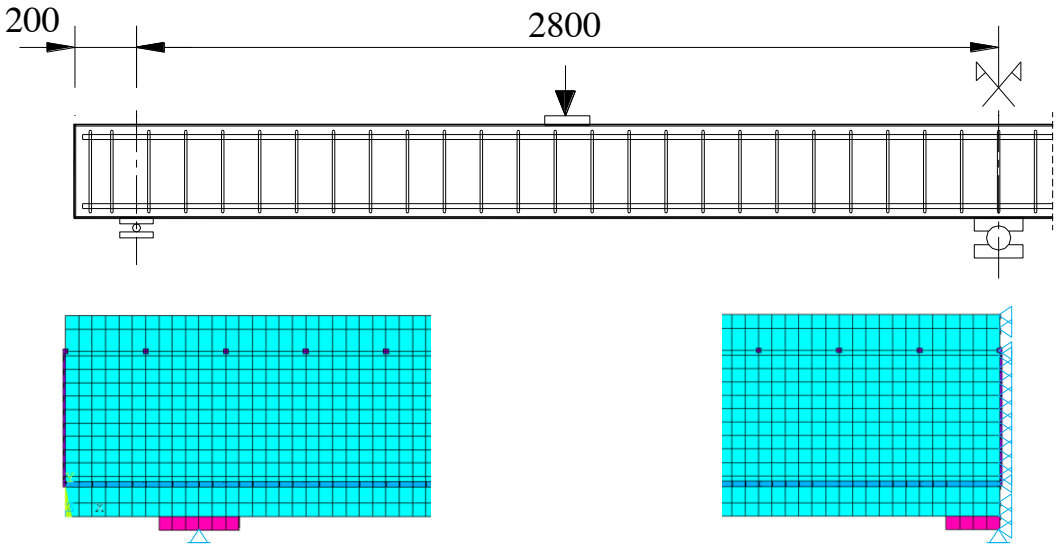

a) Beam longitudinal direction

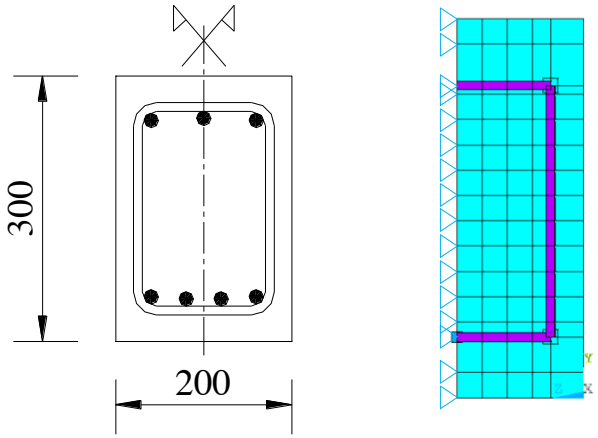

b) Cross-section

Figure (5.9): Symmetry axes and boundary conditions

The size of used mesh in the model was chosen carefully to have minimal effect on the results and simulate the behaviour of tested beams with the highest possible accuracy. To obtain the best results from Solid 65 element, square or rectangular mesh is recommended. The 3D dimensions of the used solid element were chosen to be within the ratio 2:1 as recommended by the program user's manual (ANSYS 2010) to avoid errors due to distortion effect. A preliminarily study was

conducted to evaluate the effect of mesh size on the finite element results. The main objective was to find suitable mesh size to achieve a reasonable balance between accuracy of the result and the number of nodes in the model which dramatically affects the required computer space and processing time to solve the model. A number of trials were conducted using different mesh size ranging from 75 mm to 10 mm. It was found the coarse mesh with bigger element size demonstrated unfavourable conversions problems which led to premature failure of the model, in addition to significant difference in the predicted results. This is because cracked elements in a coarse mesh cause problems when excluded from the global stiffness matrix. Using smaller mesh size improved the accuracy of the model and reduced the difference in results, however, required larger number of nodes. The accuracy of the finite element model converged using smaller mesh size with difference between size 20 mm and 10 mm as low as 0.05% (Figure 5.10). A 3D mesh size of 20 mm was adopted in the model to save on computation time.

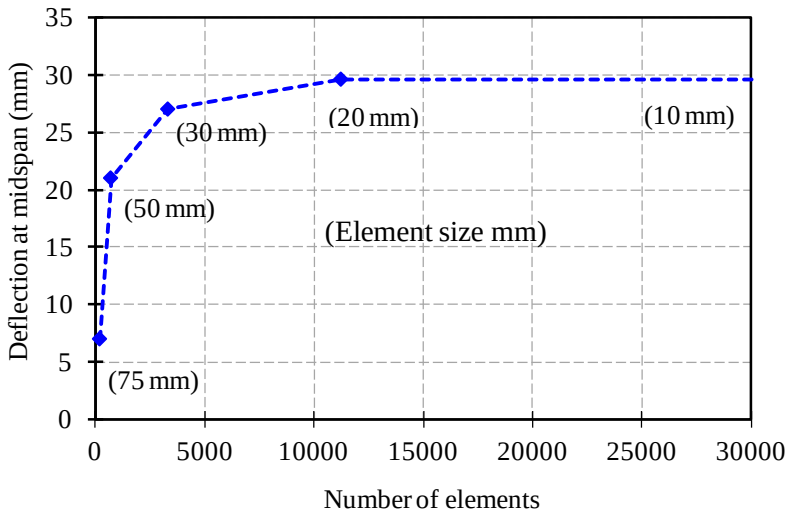

Figure (5.10): Mesh-size effect on accuracy

An isometric view of the geometry and dimensions of the 3-D model is shown in Figure (5.11). The longitudinal reinforcement and transverse shear stirrups are illustrated in Figure (5.12).

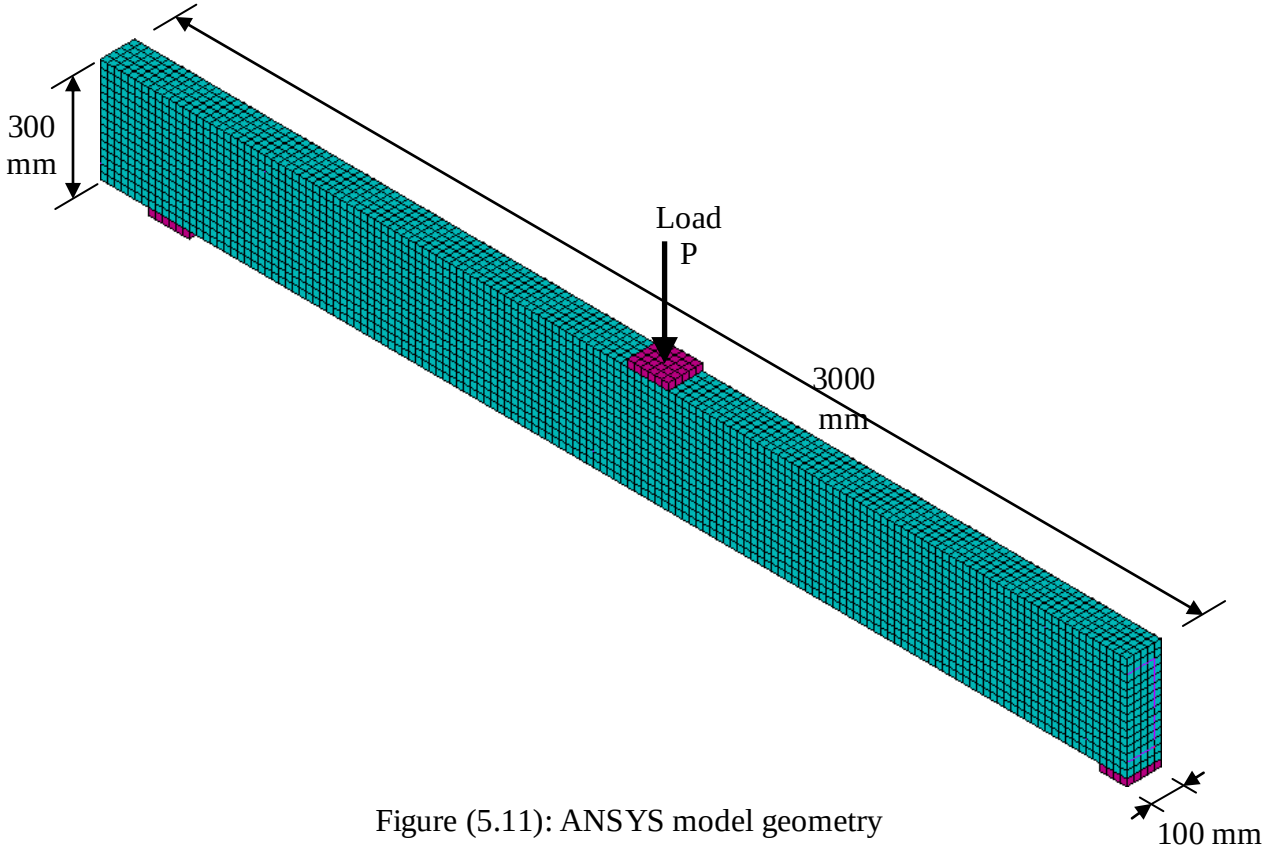

Figure (5.11): ANSYS model geometry

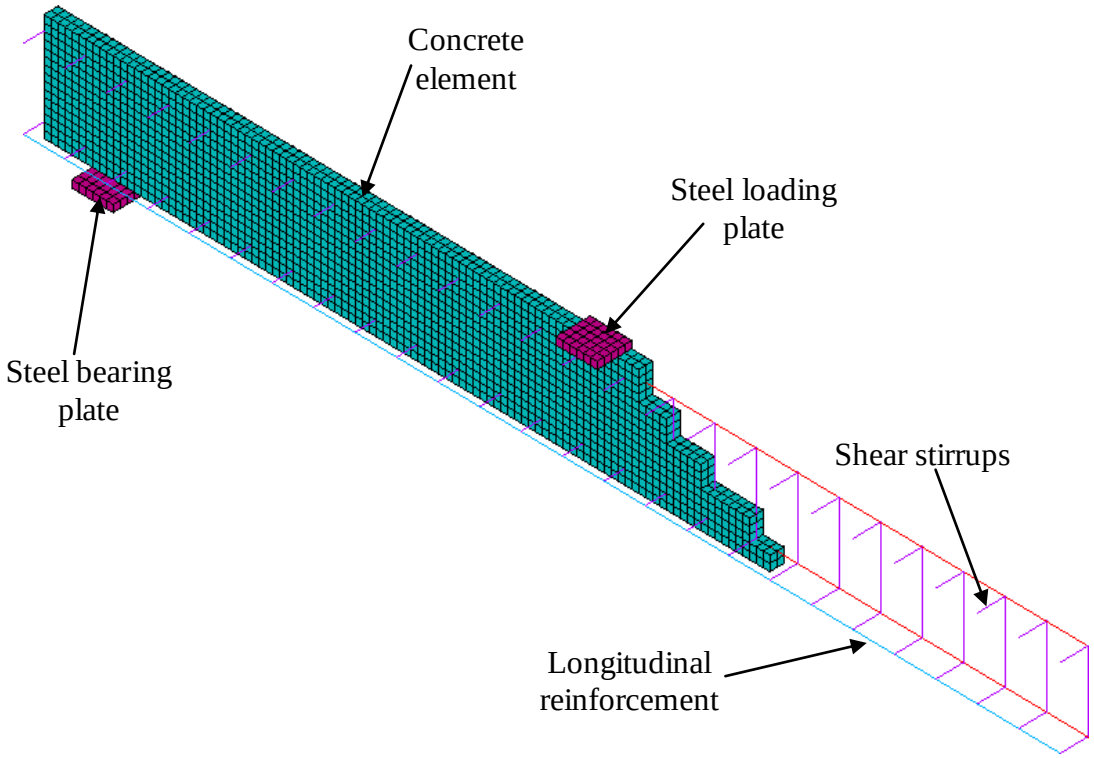

Figure (5.12): Reinforcement configuration

5.5. ANSYS Solution Control

In finite element analysis, the total applied load is divided into a series of load steps to take the effect of non-linearity into consideration. Each load step is assigned a specific load increment in a certain direction. The stiffness matrix of the model is adjusted at the end of each load step to include the non-linear changes to the stiffness before proceeding to the next step. Newton-Raphson equilibrium iterations technique was selected to update the model stiffness. This technique provides convergence at the end of each load step within a pre-defined tolerance limit. Prior to solving each load step, the out-of-balance load vector, which is the difference between forces corresponding to the element stresses and the applied load, is assessed. Convergence is achieved if the difference is within the tolerance limit. The out-of-balance load vector is re-evaluated, if the convergence criteria are not satisfied, and a new solution is attained. This process of iterations continues until the problem converges (ANSYS 2010).

5.6. Model Verification

The FEM described in this chapter was verified against the experimental results obtained from the specimens tested in this study. Three beams were selected for the verification process, beams SSc-8*d*/2*p*, GSu-8*d*/2*p* and GSs-10*d*/2*p*. The first beam was chosen with longitudinal steel reinforcement to verify the model against traditional steel-reinforced beams. The other two beams with GFRP reinforcement were chosen to verify the model against different longitudinal and transverse reinforcement ratios. The comparison was performed with respect to the load-deflection behaviour, tensile strains in reinforcement and end reactions.

5.6.1. Beam SSc-8*d*/2*p*

Figure (5.13) shows the load-deflection behaviour of the steel-reinforced beam SSc-8*d*/2*p* predicted by the FEM analysis against the experimental results. It can be seen that the FEM was able to demonstrate a similar response to the tested beam. The reduction of stiffness after cracking as well as the effect of steel yielding prior to failure was predicted by the model with a reasonable accuracy. The load-deflection diagram shows that the model predicted the failure load to be at 163 kN which is approximately 5% less than the experimental value.

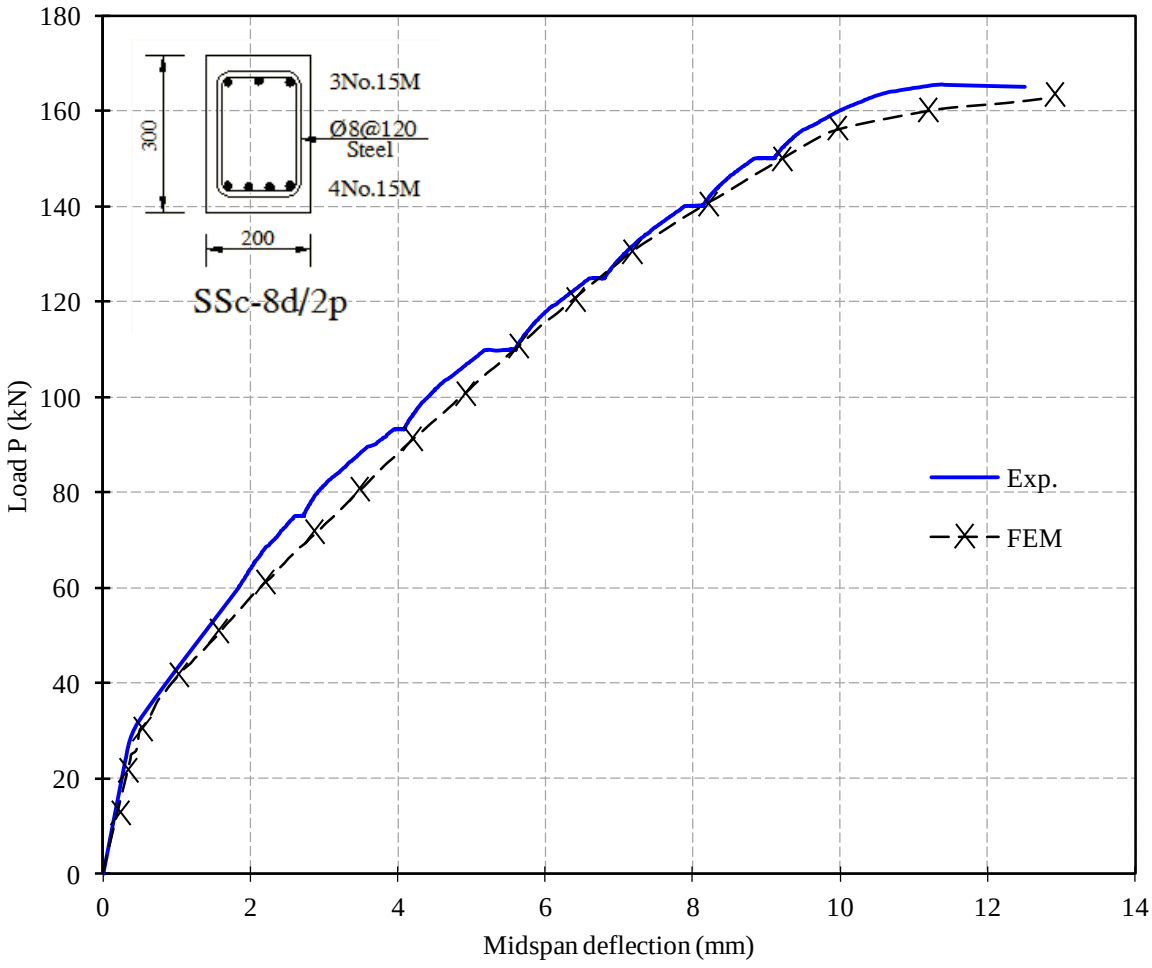

Figure (5.13): Load-deflection behaviour of beam SSc-8*d*/2*p*

Figure (5.14) and Figure (5.15) show the predicted and experimental tensile strains in reinforcement at middle support and mid-span sections, respectively. It can be seen that strains calculated by ANSYS are in good agreement with those measured experimentally. The model captured the effect of steel yielding on the tensile strain in reinforcement. The load at which the FEM predicted steel yielding was about 7% less than that observed experimentally. After steel yielding, the finite element model experienced significant rapid increase in deformations, which led the program to stop due to conversions difficulties. The good agreement between predicted and experimental strain measurements strengthen the confidence in the capability of the program to simulate the response of continuous concrete beams reinforced with traditional steel reinforcement.

Since the problem is statically indeterminate, the predicted and experimental end reactions were compared to evaluate the ability of the model to redistribute bending moments. Figure (5.16) shows the relationship between applied load and end reactions for both experimental and ANSYS results. Again a good agreement can be seen between the predicted and experimental results. These reaction results from ANSYS were used to calculate the bending moment at middle support section with different applied loads. The bending moments predicted by ANSYS are compared to the elastic bending moment at the same critical section ($0.188\ P\ell$, where P is the applied load and ℓ is the clear span) to calculate the moment redistribution percentage at middle support. The relationship between moment redistribution and applied load is then plotted and compared with the same relationship determined experimentally in Chapter 4 as shown in the following sections.

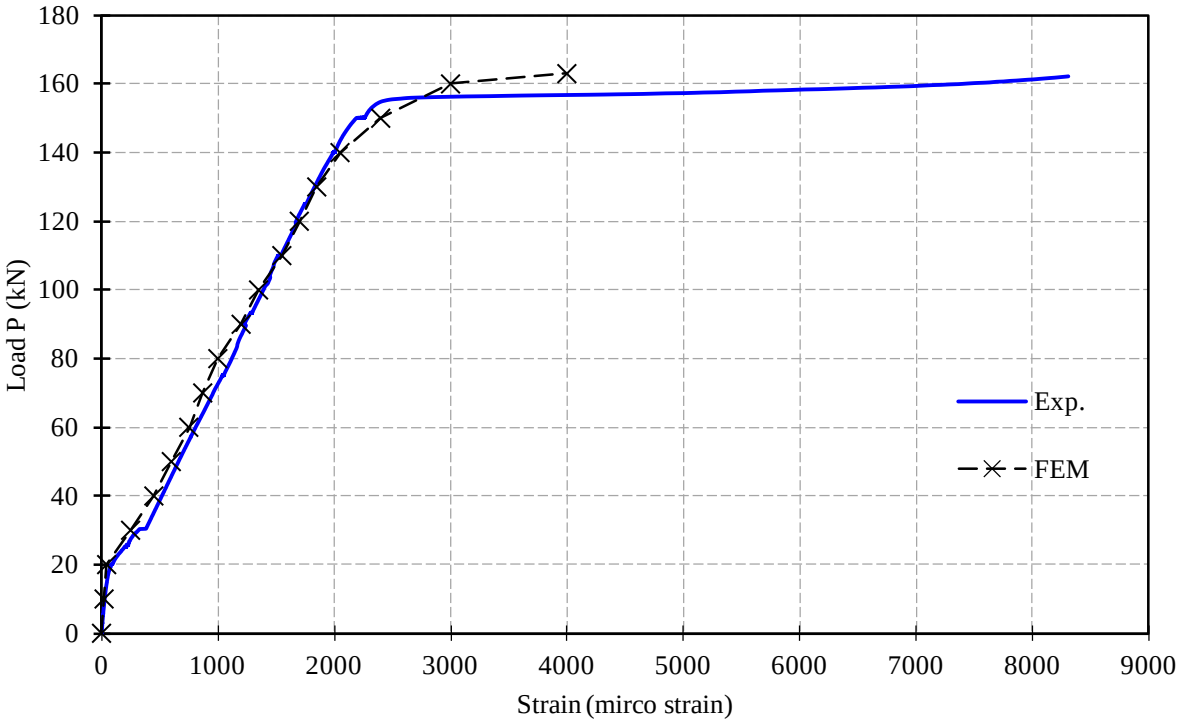

Figure (5.14): Tensile strains in reinforcement at the middle support section of beam SSc-8*d*/2*p*

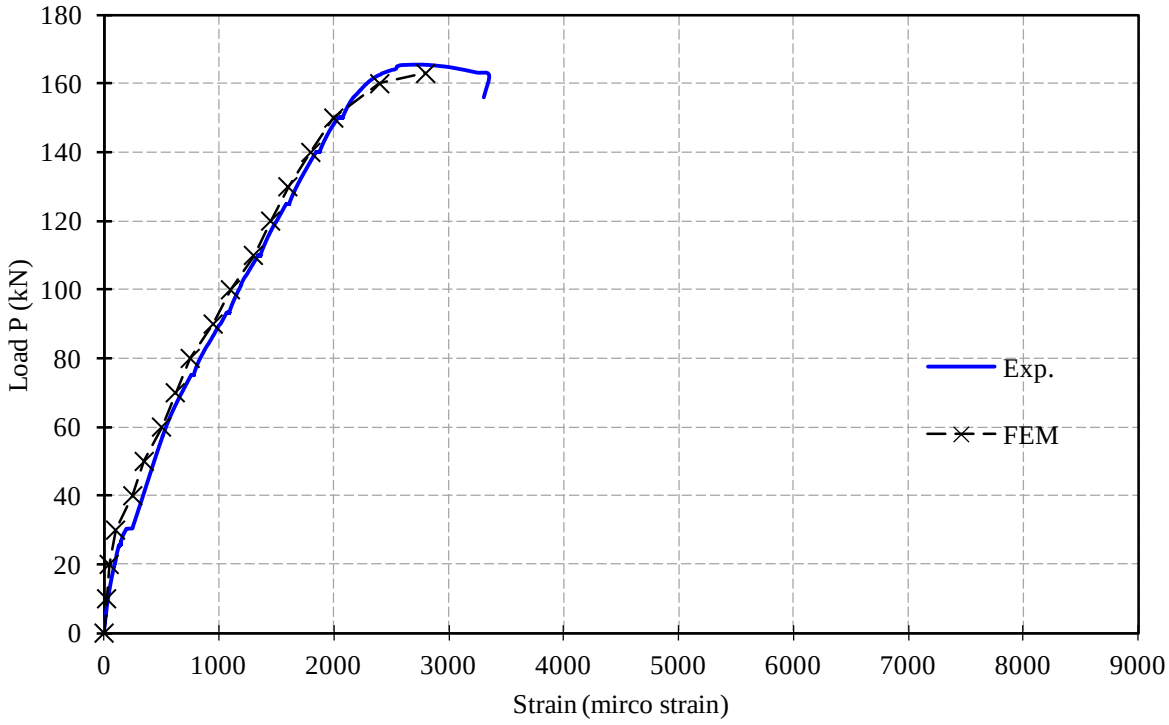

Figure (5.15): Tensile strains in reinforcement at the mid-span section of beam SSc-8*d*/2*p*

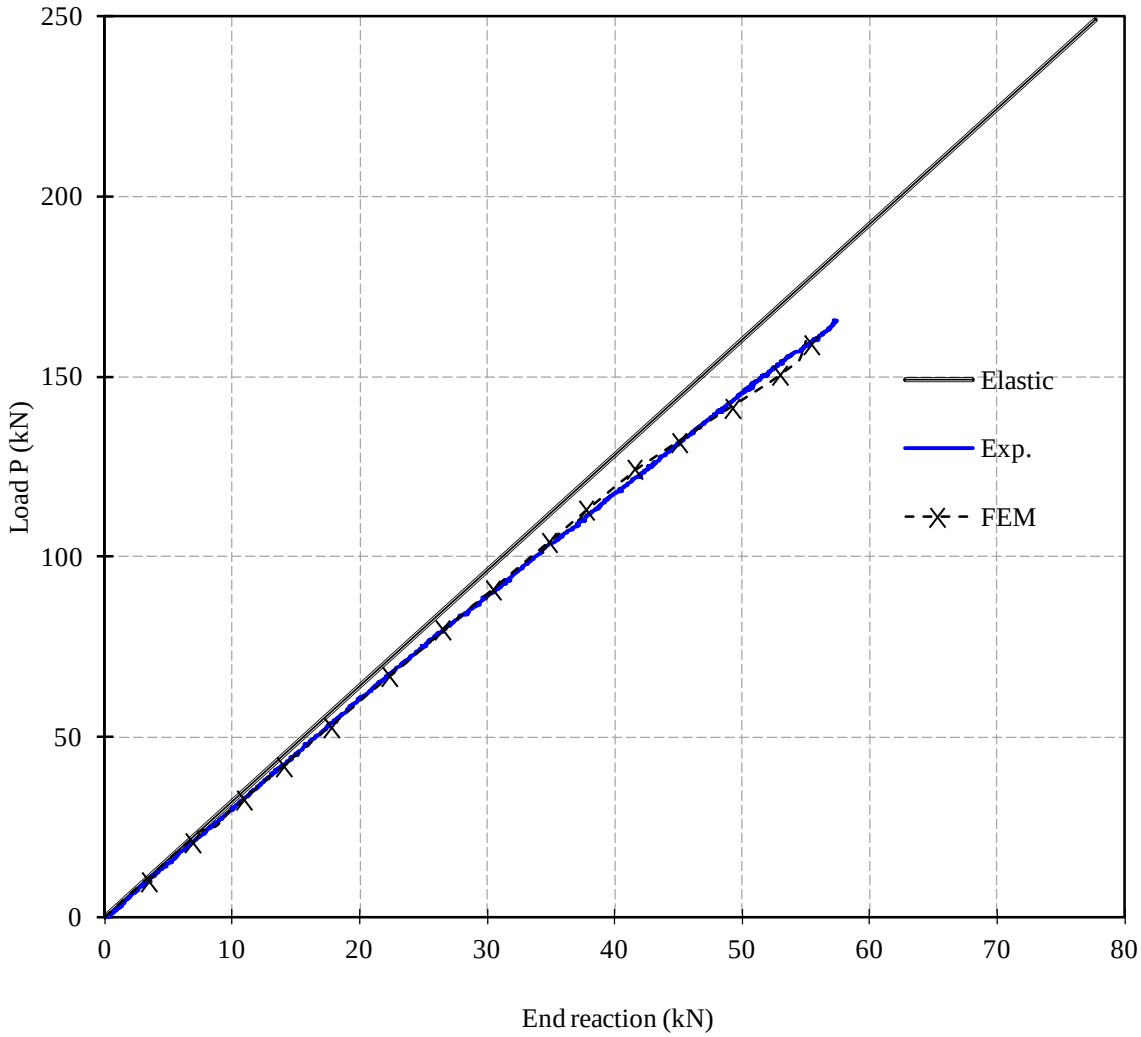

Figure (5.16): Load versus end reactions of beam SSc-8*d*/2*p*

The model was able to redistribute bending moments between critical sections since the predicted end reactions were higher than the elastic reaction at any load level. The relationship between the percentage of moment redistribution at the middle support section and the applied load is illustrated in Figure (5.16). It can be seen that the finite element model demonstrated significant moment redistribution right after cracking. This percentage increased as the load increased all the way up to failure. The predicted moment redistribution was within a range of 20% difference from experimental results.

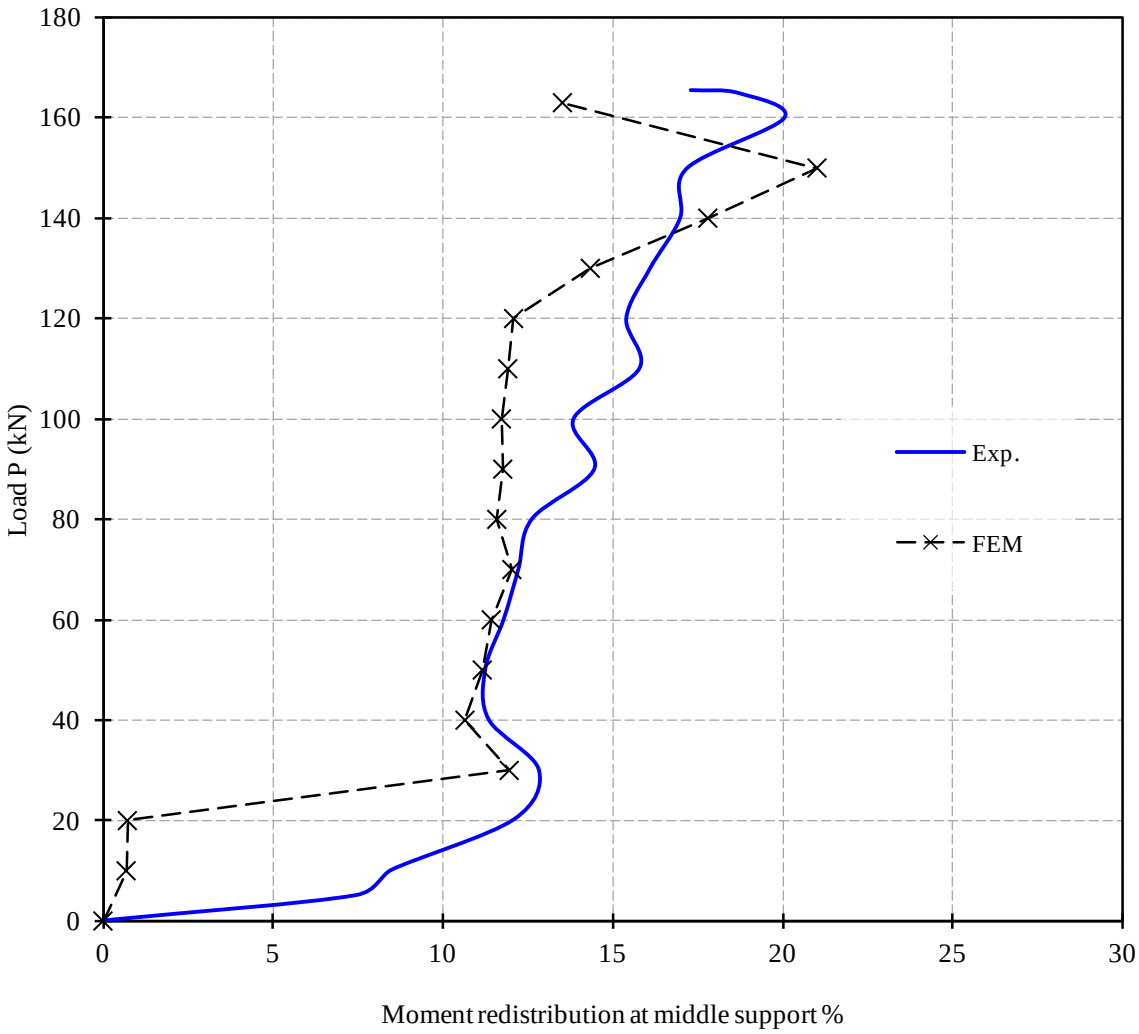

Figure (5.17): Load versus moment redistributions at middle support of beam SSc-8d/2*p*

5.6.2. Beam GSs-10*d*/2*p*

Figure (5.18) shows the load-deflection behaviour of beam GSs-10*d*/2*p*. It can be seen the model accurately predicted the response of the GFRP-reinforced beam after cracking and up to 90% of failure load. The tested beam experienced a sudden increase in mid-span deflection due to significantly wide cracks and signs of concrete crushing at critical sections. The model, however, could not simulate this behaviour and predicted a failure load about 5% less than the experimental.

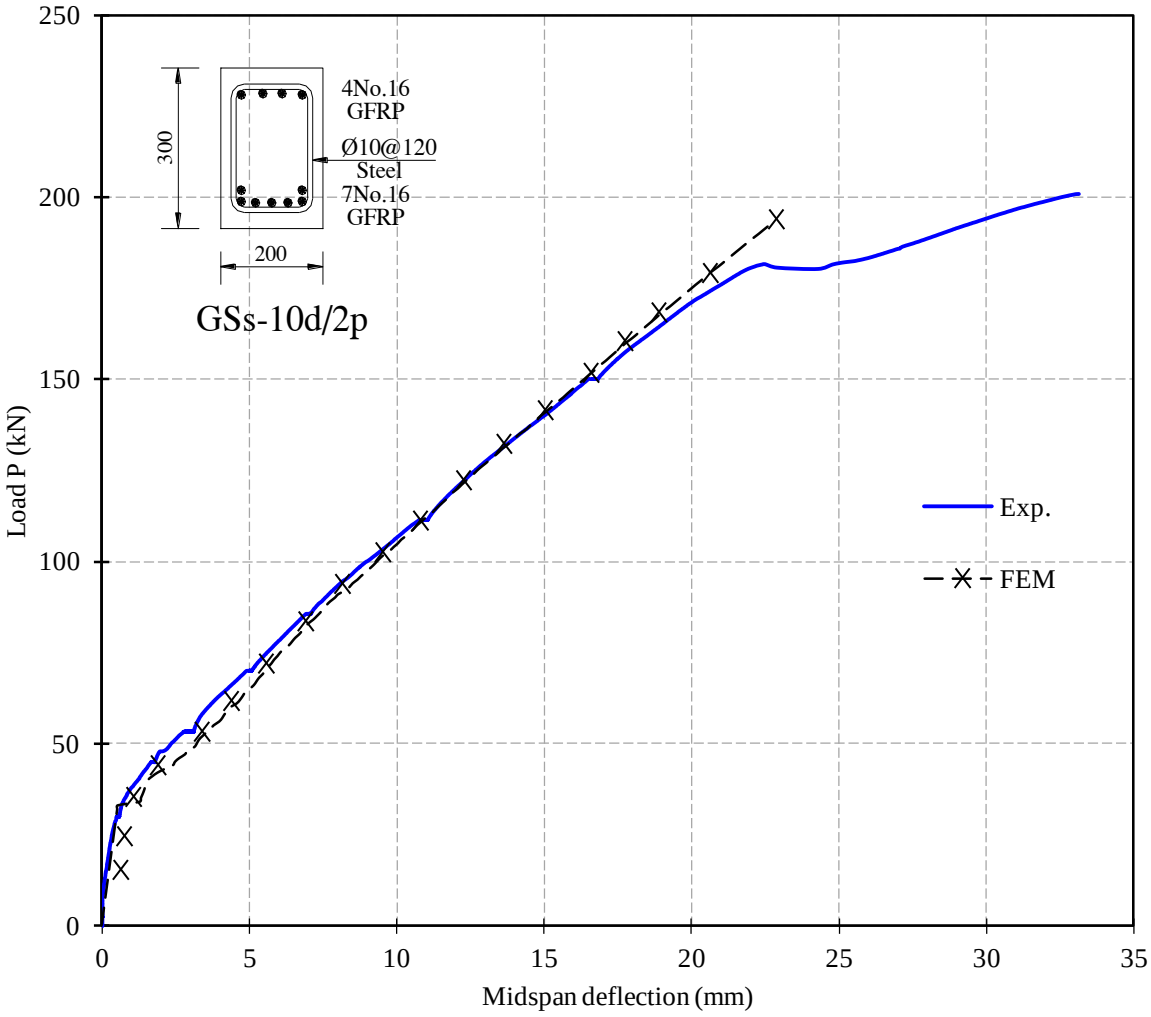

Figure (5.18): Load-deflection behaviour of beam GSs-10*d*/2*p*

Figure (5.19) and Figure (5.20) shows the tensile strain in reinforcement at critical sections. The FEM captures the tensile strains measure experimentally with a reasonable accuracy. The predicted strains by ANSYS were within 15% difference from experimental results. The model experienced sudden increase in tensile strains right after cracking which is expected due to the change in the stiffness of the cracked cross-section. The figures also show that the ultimate strain of the GFRP bars (16000 micro-strain) was not reached as expected as the beam was designed for compression failure with over-reinforced sections.

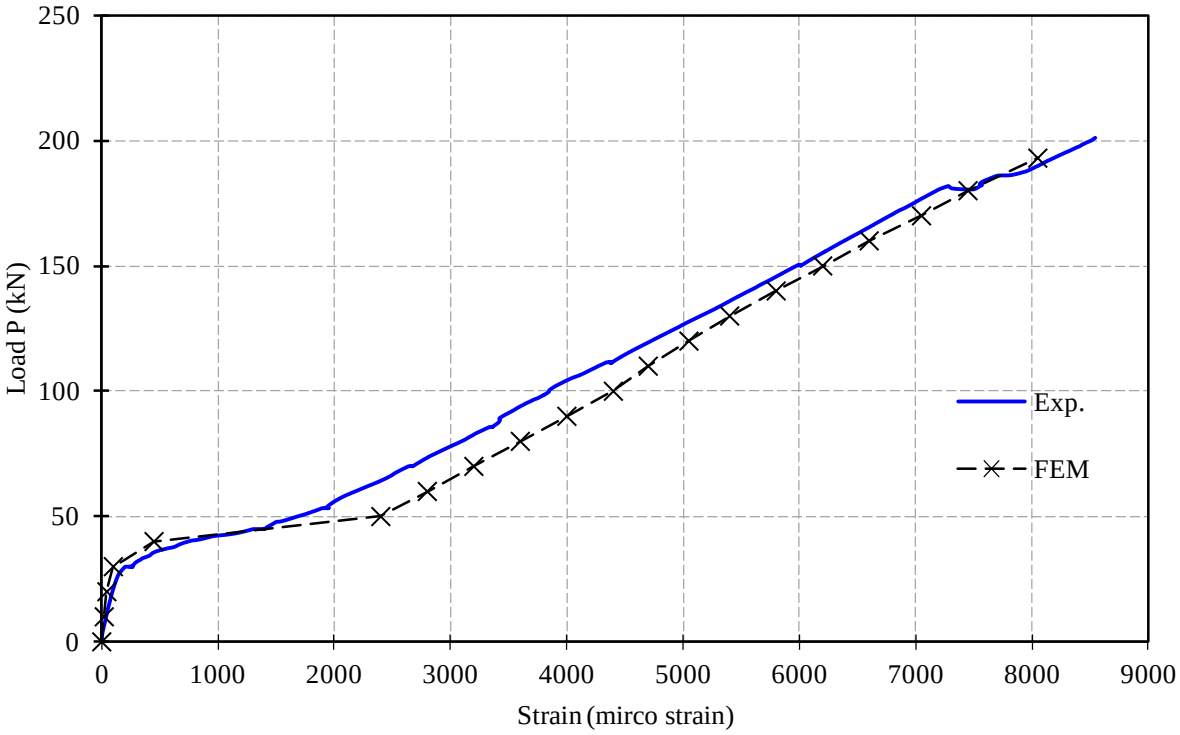

Figure (5.19): Tensile strains in reinforcement at the middle support section of beam GSs-10*d*/2*p*

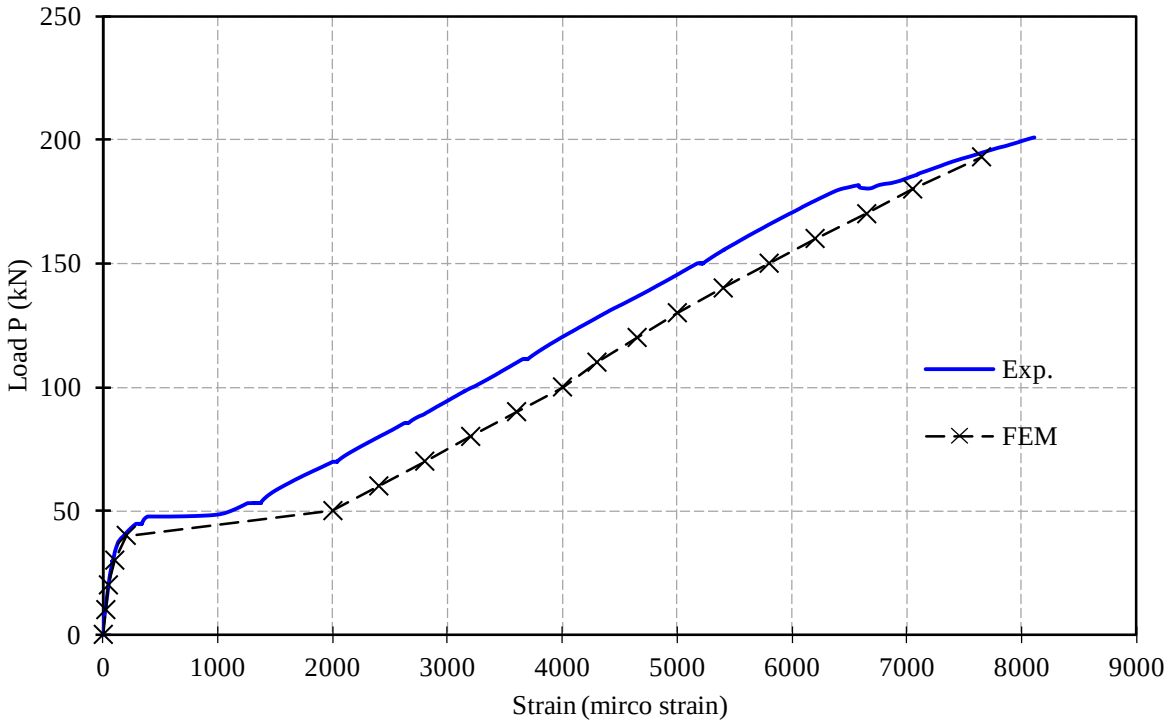

Figure (5.20): Tensile strains in reinforcement at the mid-span section of beam GSs-10*d*/2*p*

Figure (5.21) shows the measured and predicted end reactions for beam GSs-10*d*/2*p*. Again the model showed a correct prediction of the reactions with reasonable accuracy. The relationship between moment redistribution and applied load is presented in Figure (5.22). The model demonstrated significant moment redistribution right after cracking. This percentage increased as the load increased up to failure. This was in good agreement with the experimental response starting at 50% of ultimate load and up to failure. The predicted moment redistribution in this range was within 10% difference from experimental results.

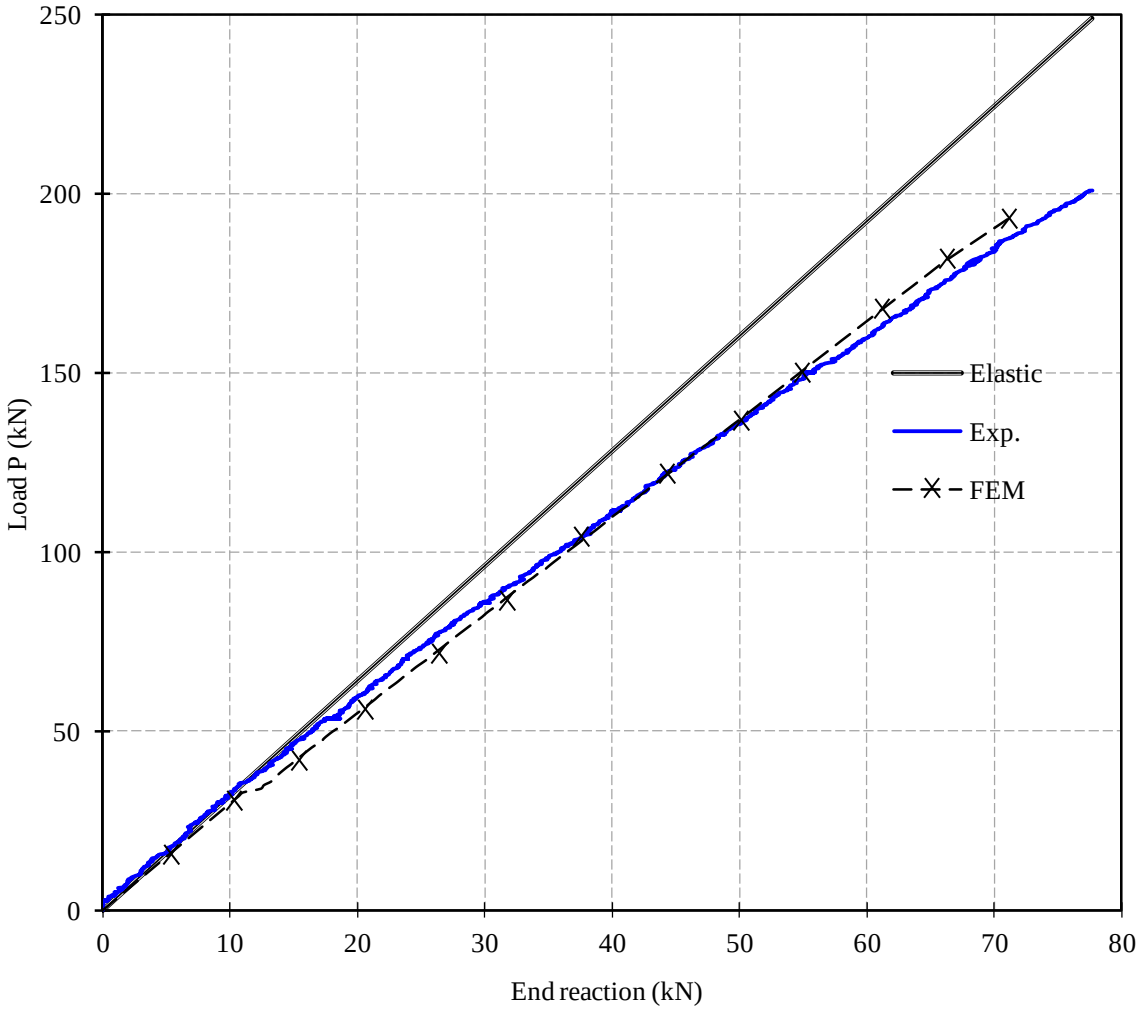

Figure (5.21): Load versus end reactions of beam GSs-10*d*/2*p*

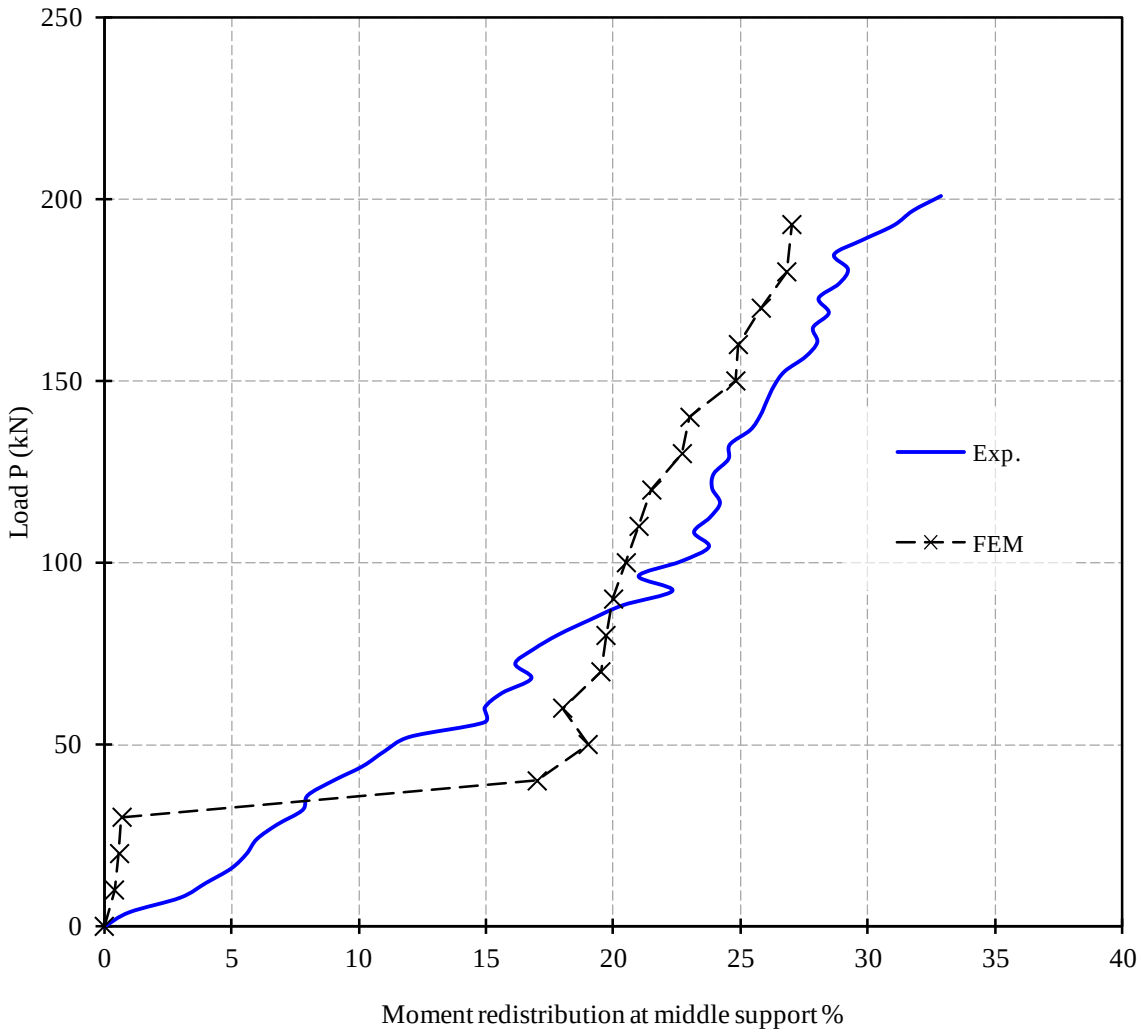

Figure (5.22): Load versus moment redistributions at middle support of beam GSs-10*d*/2*p*

5.6.3. Beam GSu-8*d*/2*p*

Figure (5.23) shows the load-deflection relationship of beam GSu-8*d*/2*p*. The model demonstrated a very accurate simulation to the load-deflection response at different loading stages. Close to failure, however, the experimental response of the tested beam showed a predominant increase in nonlinearity which could not be predicted by the finite element model. This had an impact on the achieved moment redistribution at high loading stage as discussed in the following sections.

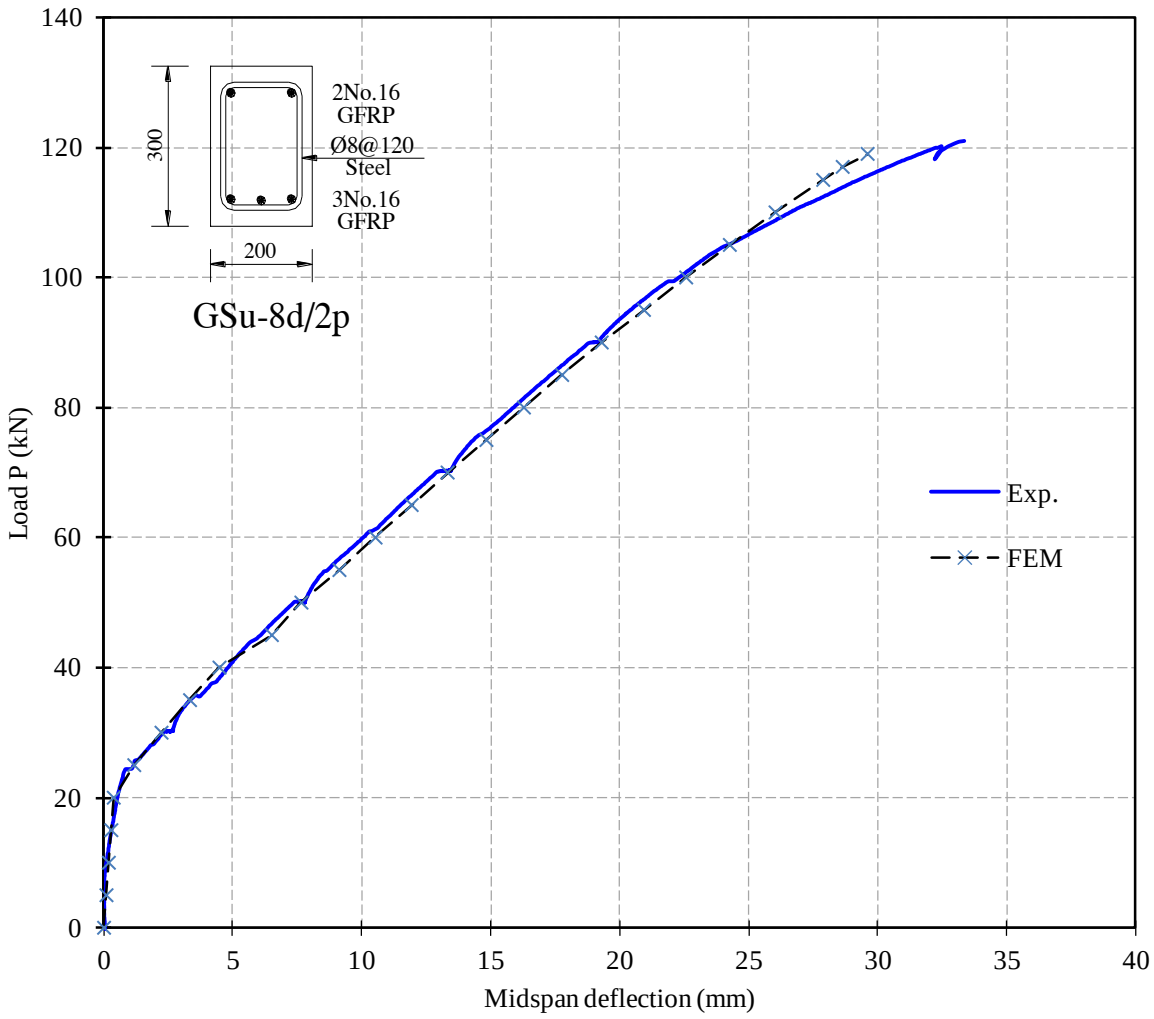

Figure (5.23): Load-deflection behaviour of beam GSu-8*d*/2*p*

Figure (5.24) and Figure (5.25) shows the tensile strain in reinforcement at critical sections. The FEM predicted the tensile strains measure experimentally with a very good accuracy. This good agreement in tensile strains between predicted and experimental results strengthens the confidence in the capability of the finite element model to predict the response of FRP-reinforced continuous beams. Again, the strains predicted by the model as shown in the figures did not reach the ultimate tensile strain values, which is in good agreement with the followed design concepts.

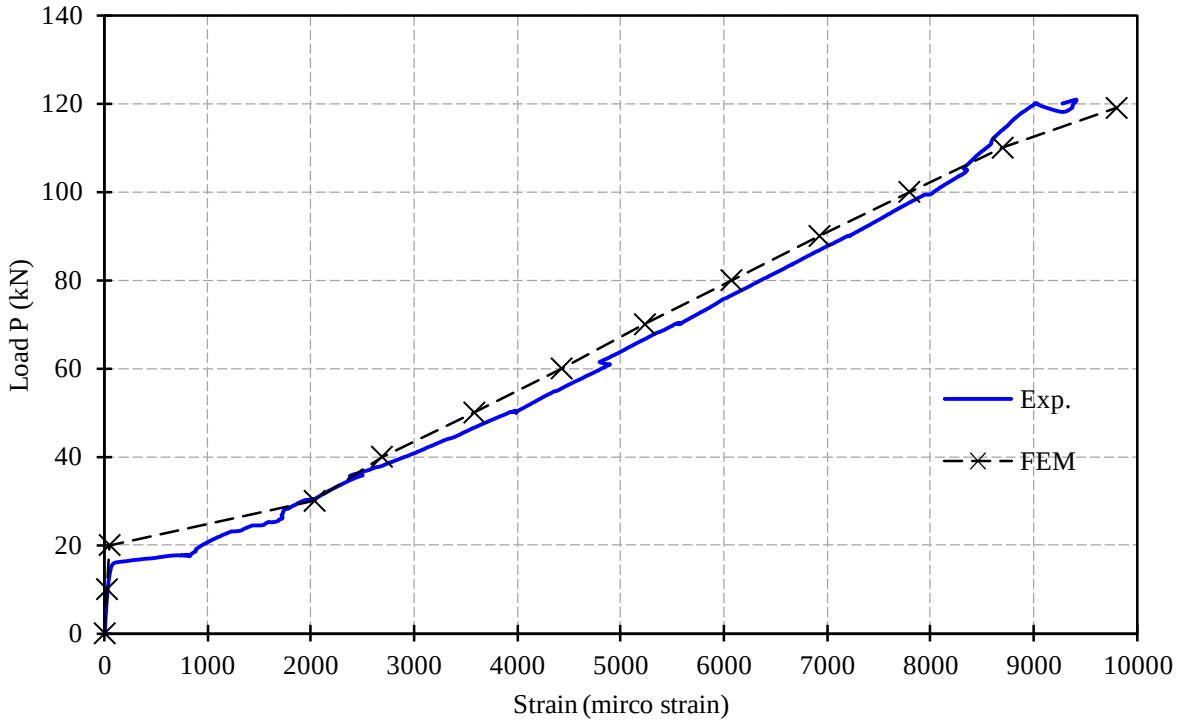

Figure (5.24): Tensile strains in reinforcement at the middle support section of beam GSu-8*d*/2*p*

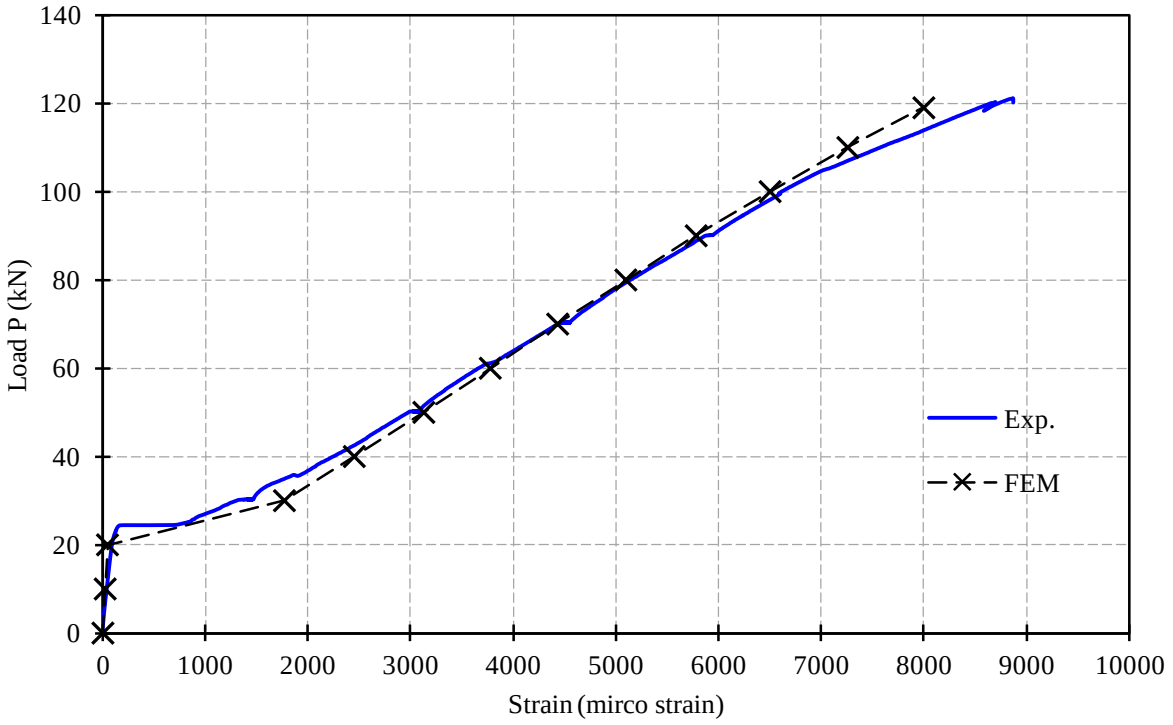

Figure (5.25): Tensile strains in reinforcement at the mid-span section of beam GSu-8*d*/2*p*

Figure (5.26) and Figure (5.27) show the end reactions and moment redistribution with applied load of beam GSu-8*d*/2*p*, respectively. The finite element model predicted the moment redistribution response of the tested beam accurately up to 80% of the ultimate load. In this loading range, the difference between predicted and experimental moment redistribution was within 20%. As load increased, the tested beam experienced significant increase in moment redistribution as a result of a combination of wide cracks, bar slippage and concrete crushing. The finite element model was not able to predict this increase.

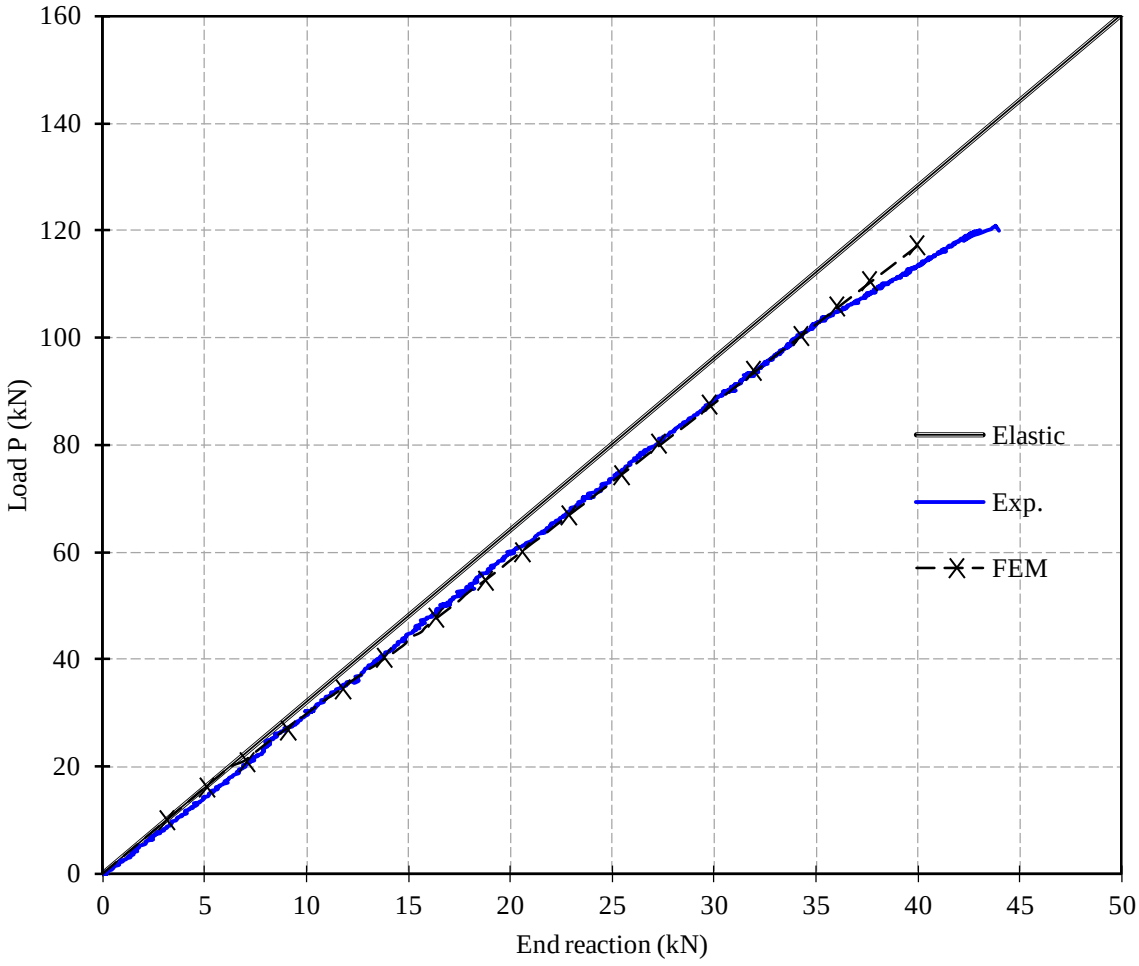

Figure (5.26): Load versus end reactions of beam GSu-8*d*/2*p*

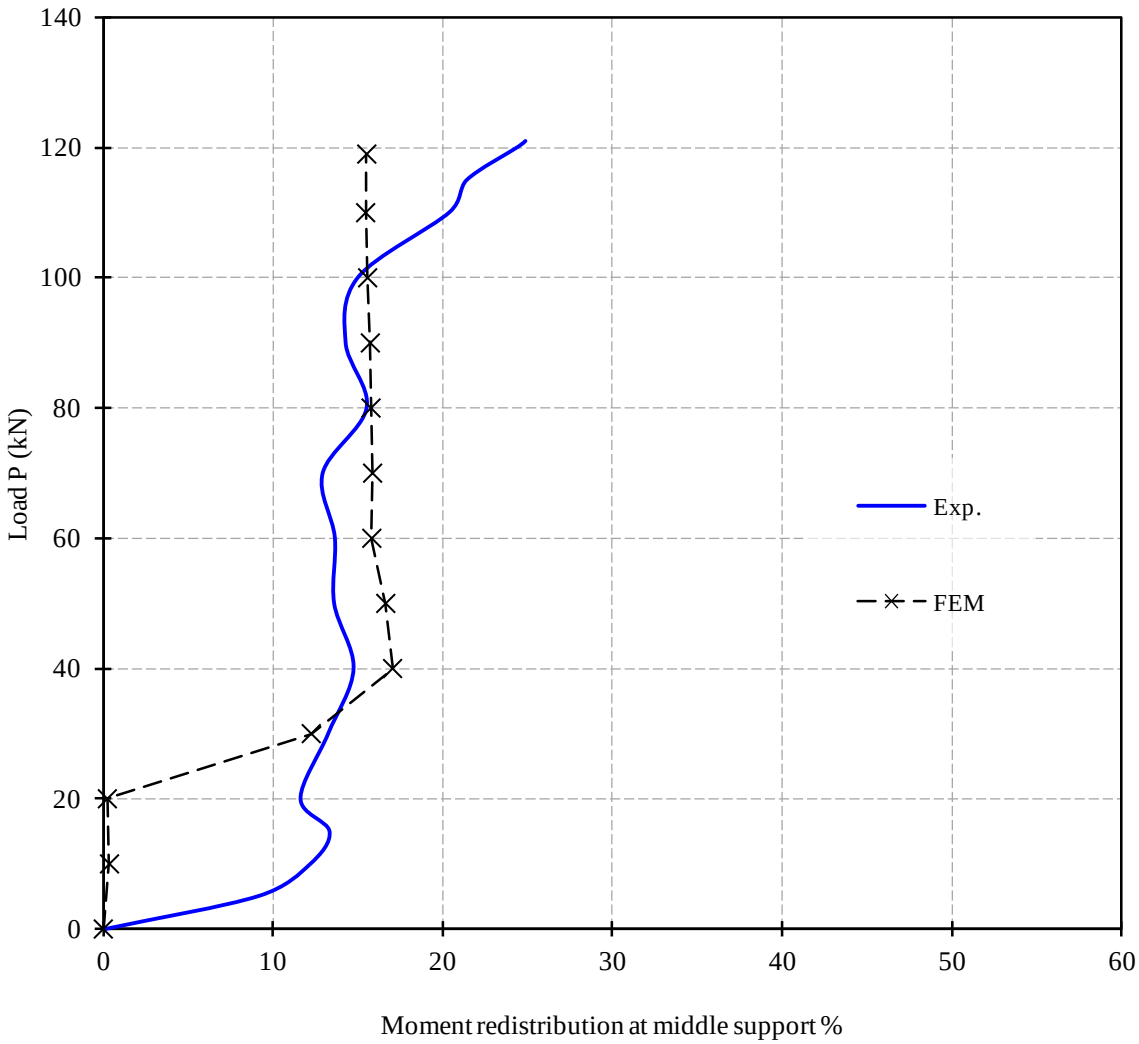

Figure (5.27): Load versus moment redistributions at middle support of beam GSu-8*d*/2*p*

5.7. Summary

The FEM described in this chapter was able to predict with reasonable accuracy the load-deflection behaviour and developed strains in the tensile reinforcement in addition to the available moment redistribution. However the model was not able to predict post-failure behaviour of concrete as the program experience difficulties in conversions once failure started.

Hence, the FEM can be used to conduct a parametric study to extend the range of the investigated parameters to better understand their influence on the behaviour of continuous beams reinforced with FRP. The results of this parametric study are presented in the following chapter.

CHAPTER 6: PARAMETRIC STUDY

6.1. General

This chapter presents results of the parametric study conducted using the finite element model (FEM) described and verified in Chapter 5. The study investigated the effect of four key parameters on the behaviour of FRP-reinforced continuous beams. The investigated parameters were compressive strength of used concrete, longitudinal reinforcement ratio, sagging / hogging longitudinal reinforcement ratio and transverse reinforcement ratio. The used FEM was based on the same geometry, material properties and assumptions used in modeling beam GSu-8*d*/2*p* in the verification section of the previous chapter. The reasons behind choosing this beam are the similarity in reinforcement configuration with most of the tested beams and the significantly close match between the experimental and predicted results from the finite element model. For each parameter, the studied variable was changed a number of times to cover a wide, but practical, range and ANSYS program was used to run the analysis and find the solution each time. The results were compared in terms of the load-deflection response and moment redistribution based on end reactions. The investigation resulted in a number of important conclusions regarding the effects of studied parameter on the behaviour of continuous concrete beams reinforced with FRP bars.

6.2. Concrete Compressive Strength

The current design codes and guidelines for reinforced-concrete structure recommend that the compressive strength of concrete in Civil Engineering applications should be between 25 and 70 MPa (CSA 2004). To evaluate the effect of this parameter considering the general behaviour and moment redistribution, the compressive strength of concrete in the selected FEM (based on beam GSu-8*d*/2*p*) was changed within 25-70 MPa with 5 MPa increment.

6.2.1. Load-deflection response

Figure (6.1) shows the change in the load-deflection relationship within the studied range of concrete compressive strength. The general behaviour of the model can be described as an approximately bilinear relationship. Deflection increases with the load in a linear relationship all the way up to the cracking load. The slope of this portion of the relationship represents the un-cracked stiffness of the beam. Nonlinearity in the model response starts as the tensile stresses in concrete elements in tension zones exceed the concrete rupture strength. These elements are considered cracked and deleted from the model stiffness matrix representing the reduction in inertia due to cracking. It can be seen from the figure that increasing the concrete compressive strength increased the cracking load due to the increase in concrete tensile strength. Increasing the concrete compressive strength from 25 to 70 MPa increased the cracking load by approximately 85%. After cracking, the slop of the curve is significantly reduced due to cracking which resulted in reduction of stiffness. The load-deflection relationship after cracking and up to ultimate load was found to be mainly linear, especially for low concrete strength (25 MPa). The model response showed considerable nonlinearity in the load-deflection behaviour as concrete strength was set to higher values. This was most notable at 70 MPa compressive strength. This might be attributed to the fact that concrete elements with higher strength require higher tensile strength in reinforcement to maintain equilibrium in the section. These high stresses in reinforcement bars emphasised the bond-slip effect in the model and consequently added to the nonlinearity of the problem. The same figure also shows that increasing the concrete compressive strength in the model increased the ultimate load capacity and increased the maximum deflection at mid-span. To get a closer insight to this observation, the relationship

between ultimate load capacity and the corresponding concrete compressive strength used in the model is plotted in Figure (6.2).

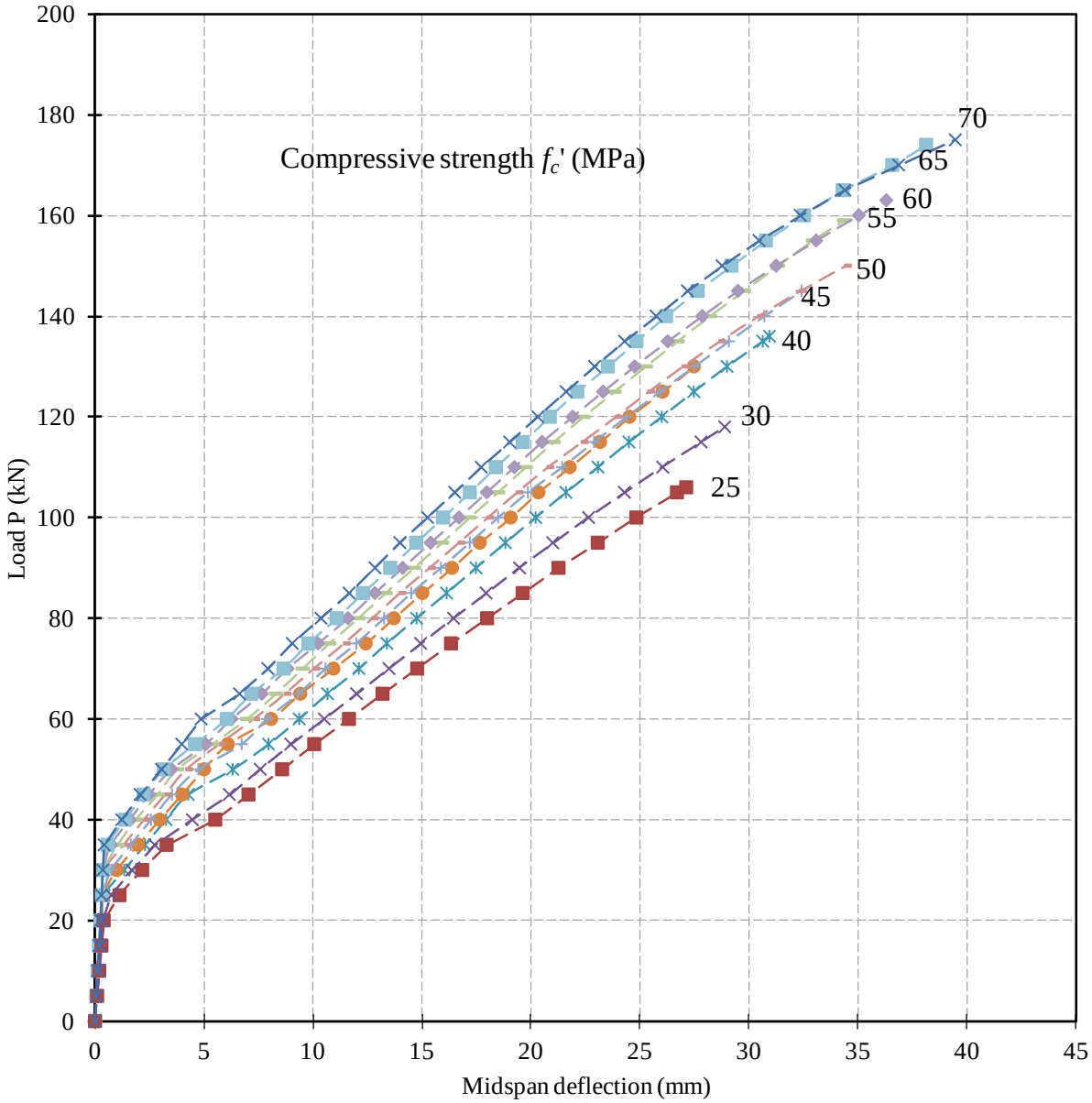

Figure (6.1): Variation in load-deflection relationship with concrete strength

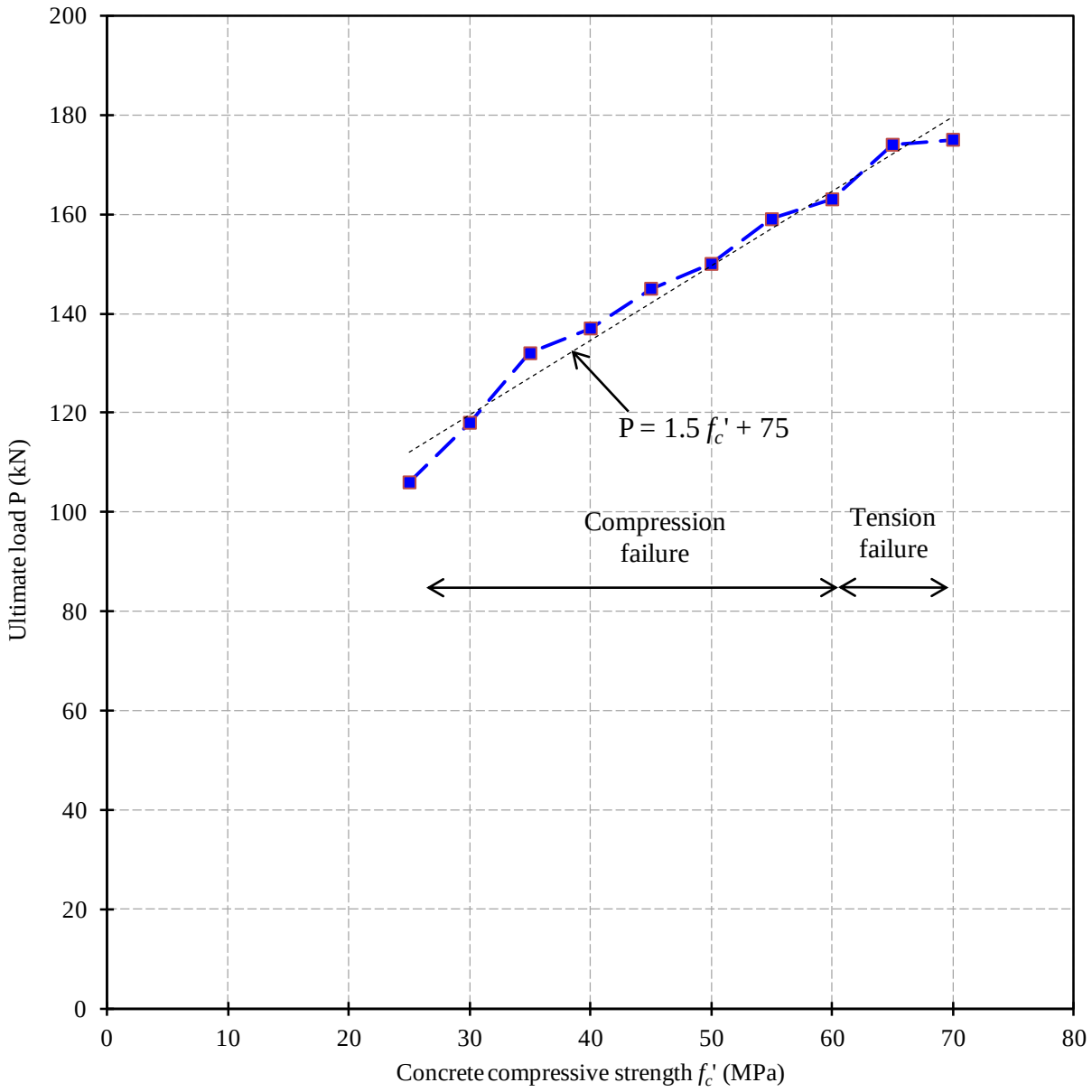

Figure (6.2): Effect of concrete strength on ultimate load capacity

The relationship between concrete strength and the ultimate load capacity was found to be approximately linear and could be described with a simple equation as shown on the figure. This relationship, however, would significantly change with any change in geometry, reinforcement or material properties. The same figure also shows the change in failure mode with different concrete strength in the model. The expected mode of failure of a cross-section is dependent on

the ratio between the longitudinal reinforcement ratio (ρ) and the balanced reinforcement ratio of the section (ρ_b). As shown in Equation (6.1), ρ_b is dependent on the concrete compressive strength (f_c'), modulus of elasticity (E_{frp}) and ultimate strain (ε_{frpu}) of used FRP bars. Since reinforcement configuration was constant and f_c' was the only variable, the ratio ρ/ρ_b decreased with increasing f_c'.

$$\rho_b = \frac{\alpha_1 \beta_1 f_c^{'}}{E_{frp}\varepsilon_{frpu}} \times \frac{0.0035}{\left(0.0035 + \varepsilon_{frpu}\right)} \tag{6.1}$$

The section at middle support becomes under-reinforced at concrete compressive strength of 50 MPa with $\rho/\rho_b < 1$ while the mid-span section remains over-reinforced at compressive strength of 70 MPa with ρ/ρ_b = 1.2 since more reinforcement was provided at this section. As expected, the FEM demonstrated compression failure mode at critical sections for low strength concrete. The tensile stress in reinforcement elements at middle support section exceeded the tensile strength of the used FRP bar, indicating tension-failure mode, at concrete strength of 65 MPa. The reason behind the delay in failure-mode change at the middle support section is believed to be the ability of the FEM to redistribute stresses from middle support to the mid-span as discussed in the following section.

6.2.2. Moment redistribution

Figure (6.3) shows the relationship between applied load and the end-reaction results of the FEM with different values of concrete strength. The variation of results was very small as the FEM end reactions were 9 to 11% higher than the theoretical elastic reaction at the same load level. The percentage of moment redistribution at the middle support section was calculated from the end reaction at ultimate load for each concrete strength values and presented in Figure (6.4). In

general, the effect of changing the concrete strength from 25 to 70 MPa resulted in a change within 25% in the achieved redistribution. Three main parameters affected the percentage of achieved moment redistribution in this study; concrete strength, bond-slip relationship and the mode of failure. At low concrete strength values, increasing the concrete strength slightly decreased the achieved moment redistribution. Increasing the concrete strength from 25 to 45 MPa decreased the moment redistribution by approximately 5%. This observation strengthens the thought that increasing concrete strength has a negative effect on the available rotation capacity, due to the increase in concrete stiffness, and consequently decreases moment redistribution. For concrete strength higher than 45 MPa, the middle support section approaches the balanced reinforcement ratio which results in significantly high tensile stresses in reinforcement. Consequently, the spring elements connecting the longitudinal bars with the surrounding concrete experience significant increase in slippage since the maximum bond stress is reached at this stress level. This reinforcement slippage at the middle support section provided additional rotation at this section and led to a rapid increase in moment redistribution to the mid-span section, which had no slippage at all. Increasing the concrete strength from 45 to 60 MPa improved the moment distribution by approximately 25%. The failure mode of the model changed for concrete strength higher than 60 MPa from compression failure to tension failure. This caused a dramatic reduction in the achieved moment redistribution leading to the conclusion that tension failure mode reduces the available moment redistribution.

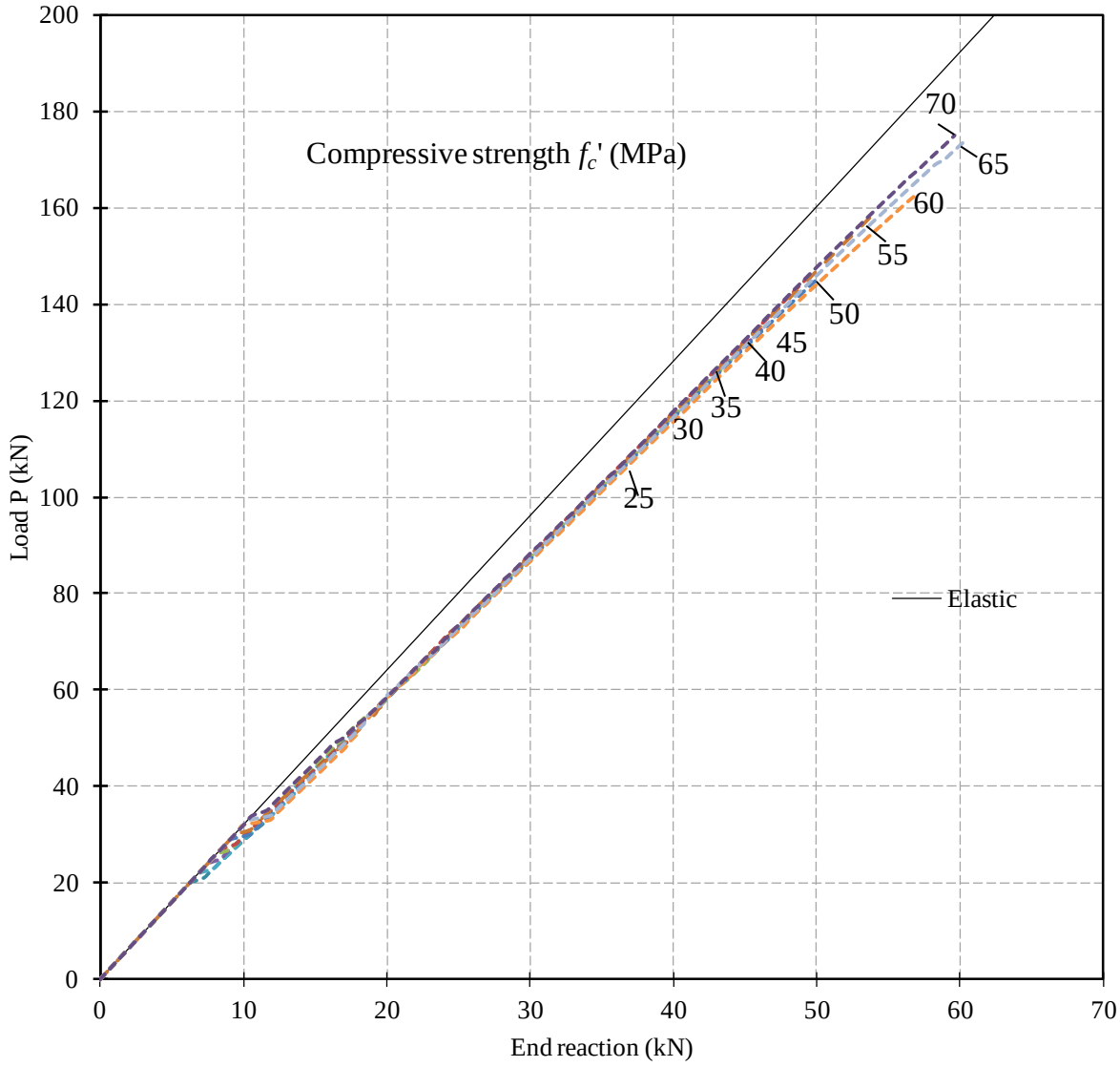

Figure (6.3): The relationship between end-reactions and applied load for different concrete strength values

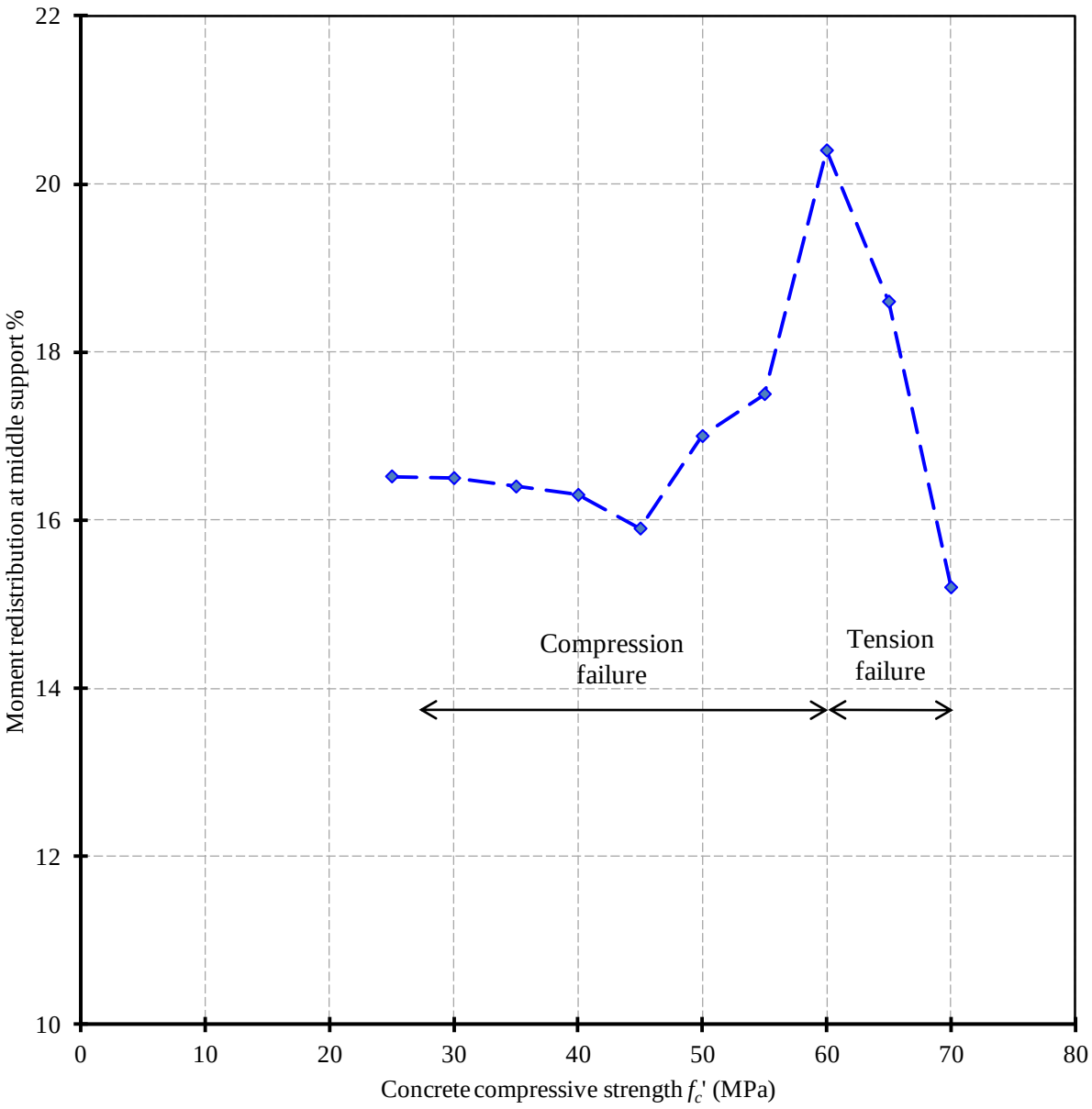

Figure (6.4): Effect of concrete strength on moment redistribution at middle support

6.3. Reinforcement Ratio at Critical Sections

As mentioned in previous chapters, the current available design codes and guidelines for the FRP-reinforced structures do not allow for moment redistribution in continuous beams reinforced with FRP bars. This means that critical cross-sections should be reinforced to satisfy the theoretical elastic moments of 0.188 $P\ell$ at the middle support and 0.156 $P\ell$ at mid-span. Since the reinforcement ratio (ρ) is directly proportionate to the moment capacity, the ratio between bottom reinforcement at mid-span (ρ_{bot}) to top reinforcement at middle support (ρ_{top}) should be approximately 0.83 (0.156/0.188). Previous literature as well as the experimental work of this study showed that increasing the bottom reinforcement at the mid-span to be greater than that at the middle support section is a key factor for moment redistribution. This is due to the fact that stiffness of a cross section after cracking is proportional to the amount of reinforcement, hence, stiffer mid-span section than middle support one will most probably result in moment redistribution. To investigate the effect of the ratio ρ_{bot} / ρ_{top}, the longitudinal reinforcement in the FEM was changed seven times and the analysis was run each time to determine the response of the model. Again, the model was based on the geometry, reinforcement and material properties of beam GSu-8*d*/2*p*. The top reinforcement at the middle support section was kept constant while the bottom reinforcement at mid-span was changed to produce ρ_{bot} / ρ_{top} ratios of 0.83, 1.0, 1.5, 1.75, 2, 2.5 and 3.0. This range was chosen such that the lowest ratio (0.83) satisfies the elastic moment distribution and the highest (3.0) represents the ratio that is expected to be equivalent to approximately 30% moment redistribution. It worth mentioning that, the effect of number of bars in cross-section and their diameter is out of the scope of the present study. Thus, the change in the bond-slip relationship from that defined in Chapter 5 due to changing bar diameter was neglected.

6.3.1. Load-deflection response

Figure (6.5) shows the variation in load-deflection relationship with different ρ_{bot} / ρ_{top} ratios. The general behaviour of the model is similar to that described earlier in the "Concrete Compressive Strength" section. It can be seen that the ρ_{bot} / ρ_{top} ratio of 0.83 demonstrated the lowest stiffness and ultimate load capacity. As the bottom reinforcement was increased, significant improvement in the flexural stiffness and ultimate load was observed up to ρ_{bot} / ρ_{top} ratio of 1.5. Increasing the ratio from 0.83 to 1.5 reduced the deflection at mid-span by 28% at the same load level. At higher ratios, the improvement in deflection and ultimate load continued with a lower rate. Increasing the ρ_{bot} / ρ_{top} ratio more than 1.5 considerably increased the slippage at middle support between reinforcement elements and the surrounding concrete. This was the reason behind the little-to-no increase in ultimate load at ρ_{bot} / ρ_{top} ratio equal to 3.0. It is obvious from the load-deflection results that increasing the bottom reinforcement at mid-span while maintaining the same amount of reinforcement at middle support section reduces the mid-span deflection and increases the ultimate load capacity. This observation was also confirmed by the experimental investigation conducted in this study.

The relationship between the ultimate load capacity and the increase in bottom reinforcement is illustrated in Figure (6.6). It can be seen that the gain in ultimate capacity rapidly declined starting at ρ_{bot} / ρ_{top} ratio of 1.5. The FEM experienced compression failure at critical sections at different values of reinforcement ratio. As indicated on the figure by curve fitting, the relationship can be described by a simple quadratic equation as a function of the ultimate load and ρ_{bot} / ρ_{top} ratio. Again, this formula would significantly change with any variation in geometry, reinforcement and material properties.

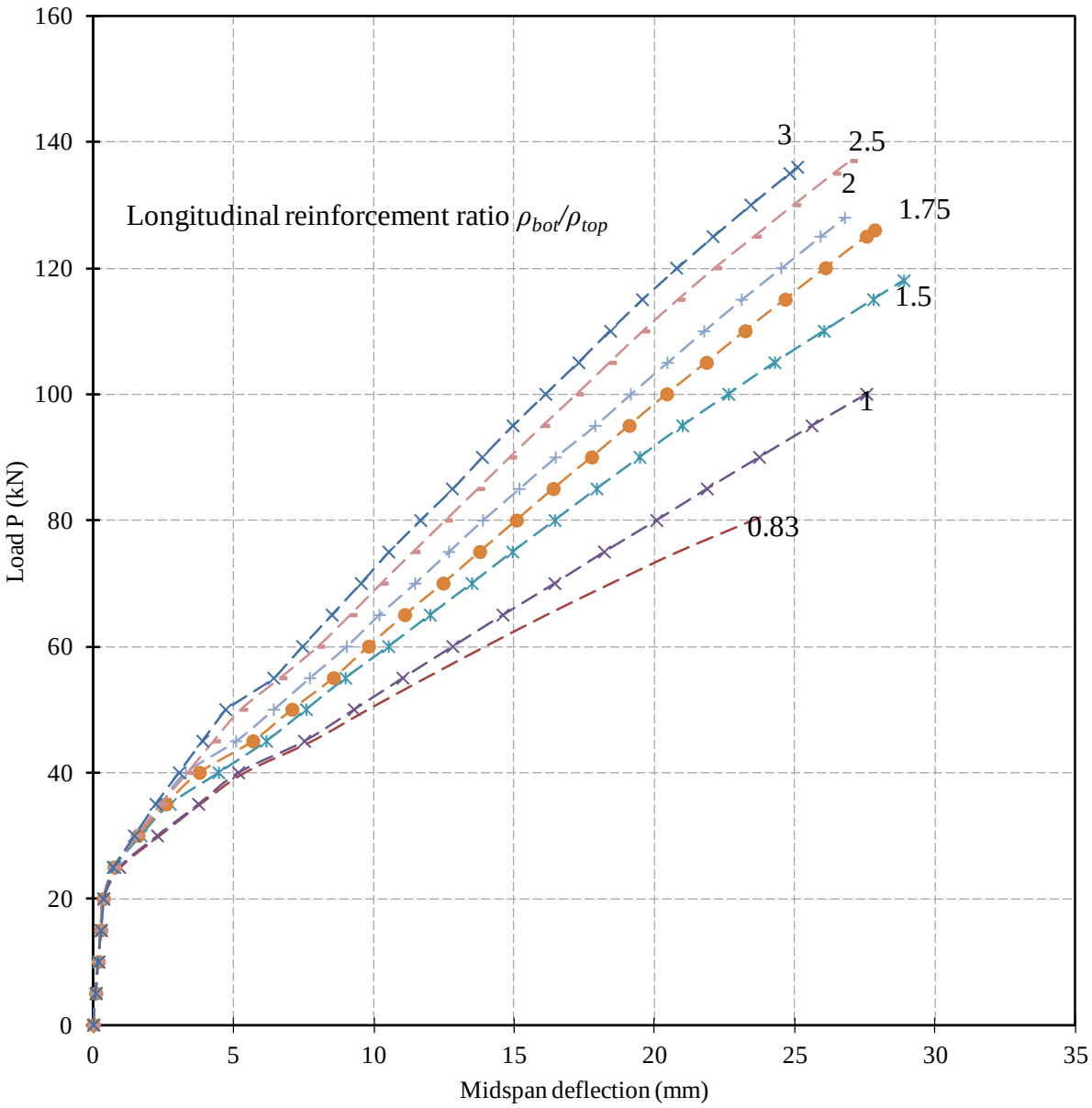

Figure (6.5): Variation in load-deflection relationship with ρ_{bot} / ρ_{top} ratio

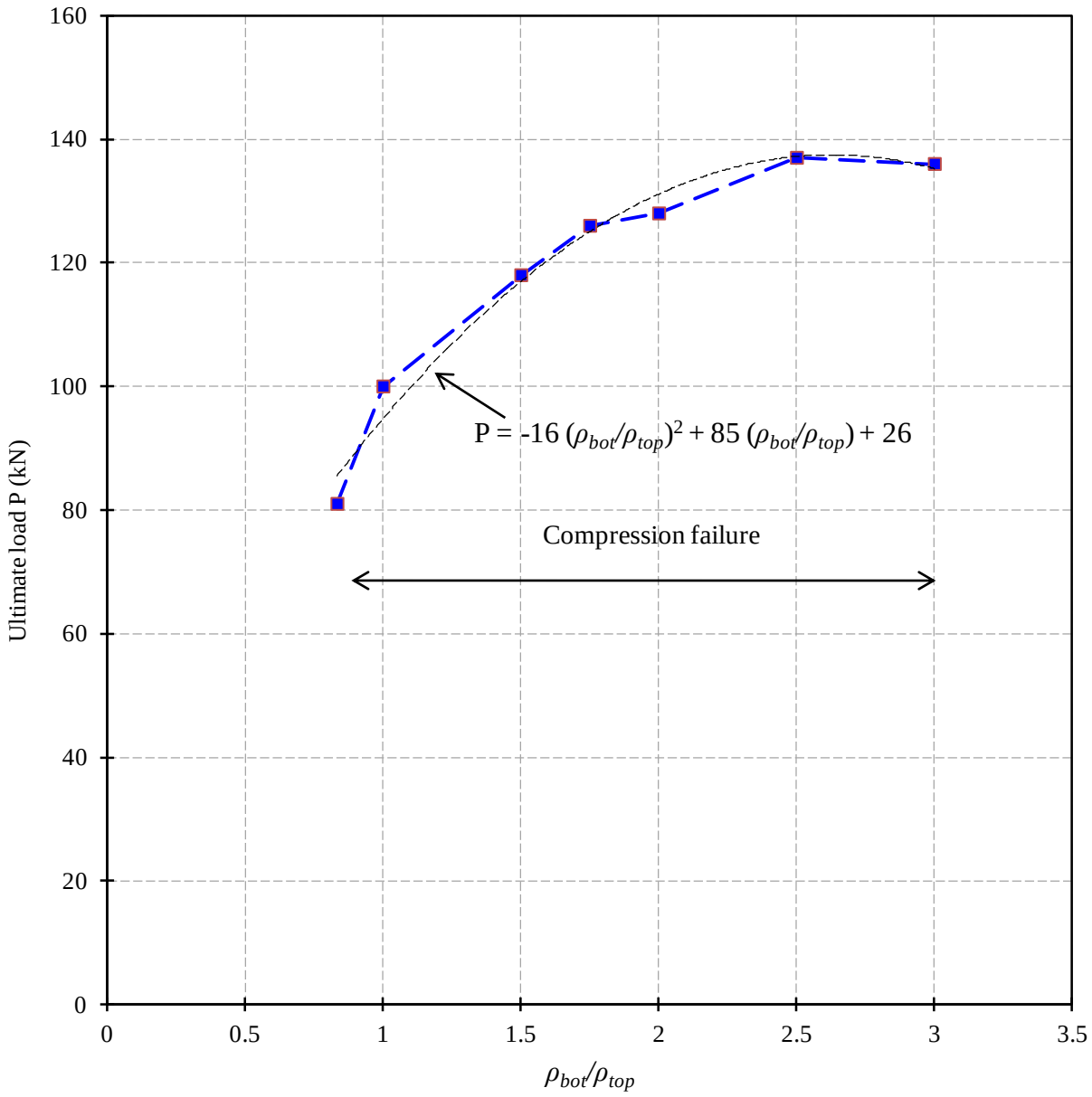

Figure (6.6): Effect of ρ_{bot} / ρ_{top} ratio on ultimate load capacity

6.3.2. Moment redistribution

Figure (6.7) shows the relationship between end reactions and applied load with different ρ_{bot} / ρ_{top} ratios. It can be seen that the amount of reinforcement ratio had a significant effect on the model response in terms of end reactions. The ρ_{bot} / ρ_{top} ratio of 0.83 resulted in end reactions approximately equable to the expected theoretical reactions. This supports the validity of the considered assumption of relating the ratio between reinforcement to the ratio between bending moments at critical sections. The figure also illustrates the remarkable increase in end-reactions values by increasing ρ_{bot} / ρ_{top} ratio. The increase of this ratio from 0.83 to 3.0 resulted in 19% increase in the end-reactions at the same load level. The percentage of moment redistribution at middle support was calculated using the end-reaction values at ultimate load for each reinforcement ratio. The relationship between achieved moment redistribution at failure and the ratio ρ_{bot} / ρ_{top} is shown in Figure (6.8). The achieved moment redistribution in the considered range varied between 0 and 30%. This strengthens the belief that moment redistribution after cracking mainly follows the ratio between the provided flexural reinforcement at critical sections.

The relationship between percentage of moment redistribution and the ratio between bottom and top reinforcement could be described as a third degree polynomial relationship obtained by curve fitting as demonstrated on the same figure. The proposed formula calculates the moment distribution as a function of ρ_{bot} / ρ_{top} ratio. This formula depends on the used geometry, reinforcement and material properties in this model and would significantly change with any change in these variables.

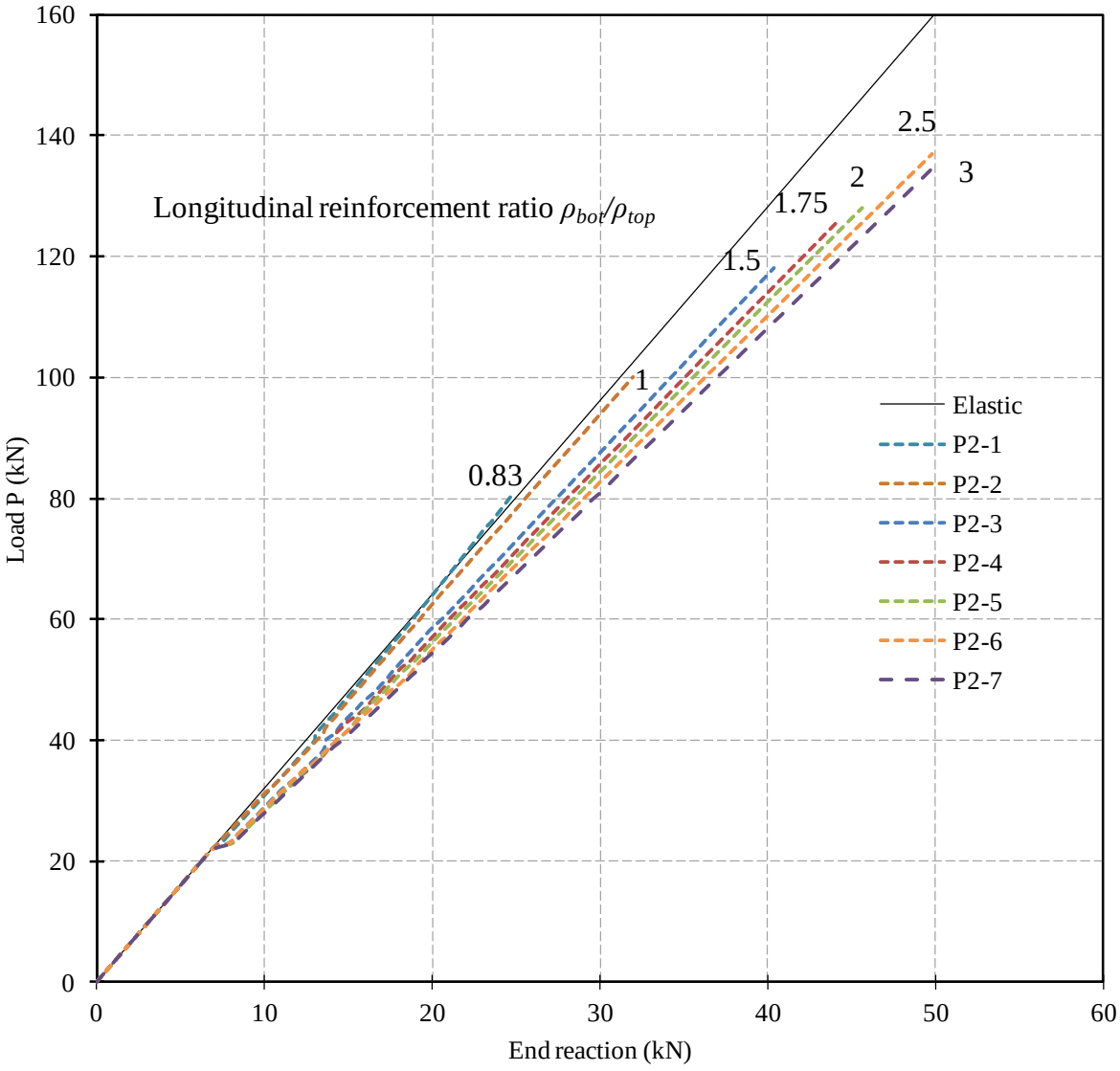

Figure (6.7): The relationship between end-reactions and applied load for different ρ_{bot} / ρ_{top} ratio

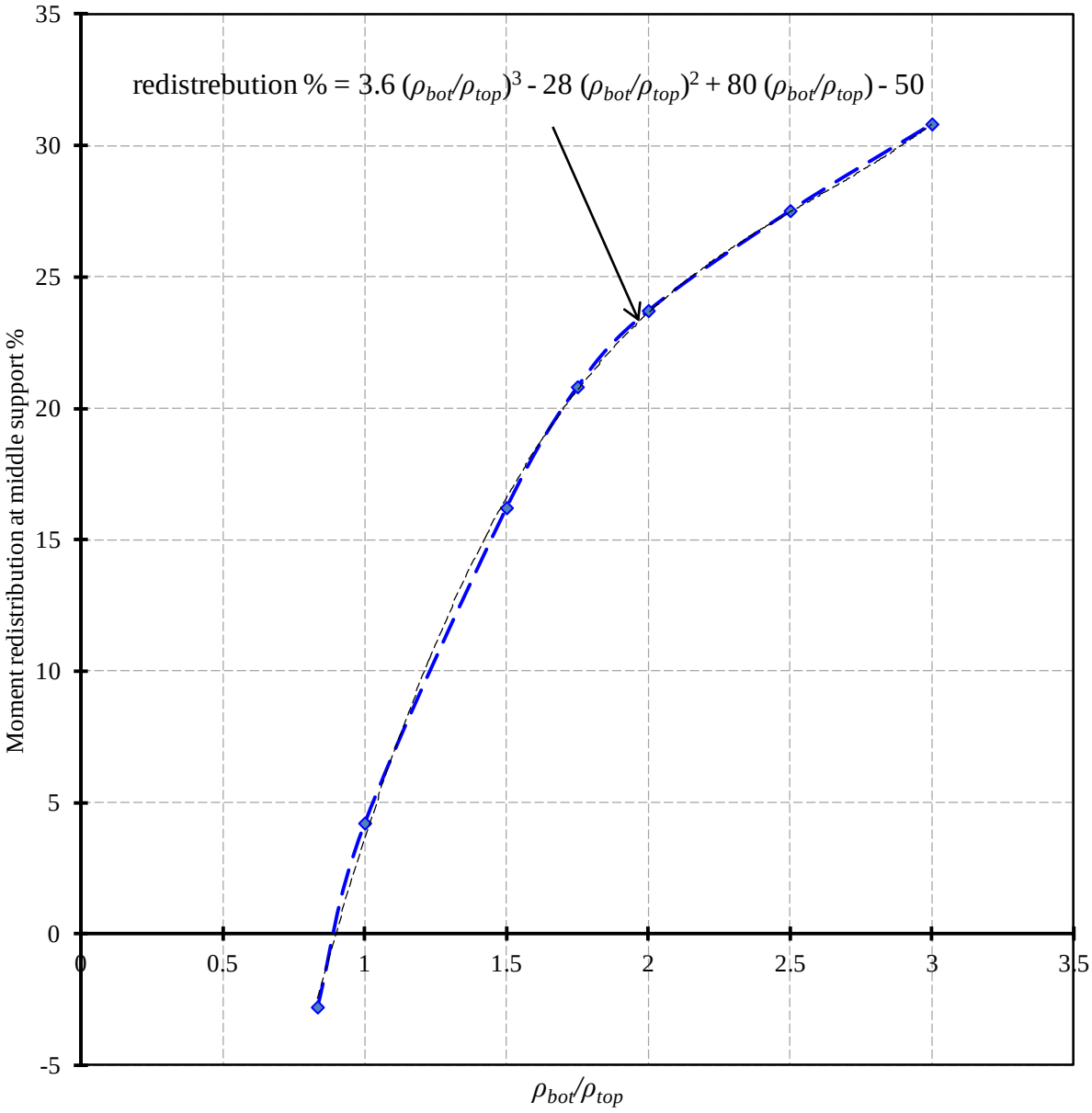

Figure (6.8): Effect of ρ_{bot} / ρ_{top} ratio on moment redistribution at middle support

6.4. Longitudinal Reinforcement Ratio

In this section, the effect of the longitudinal reinforcement ratio on the flexural behaviour of continuous FRP-reinforced beams is investigated. The current design codes and guidelines for FRP-reinforced structures recommend compression failure mode rather than tension failure. To achieve compression failure in any concrete section reinforced with FRP bars, the reinforcement ratio should not be less than the balanced reinforcement ratio (ρ_b). In a previous experimental study investigating moment-redistribution in FRP-reinforced continuous beams, Mostofinejad (1997) recommended that a reinforcement ratio between 2.0 to 3.0 ρ_b be selected for FRP reinforced flexural members. The author explained that this amount of reinforcement seems to provide adequate ductility to the member. In this current study, the finite element model based on specimen GSu-8*d*/2*p* was used to investigate the effect of longitudinal reinforcement ratio. The study investigated different reinforcement ratios at middle support section with a range from 1.0 ρ_b to 4.0 ρ_b. The ratio between reinforcement at mid-span and middle support was kept constant at a value of 1.5.

6.4.1. Load-deflection response

Figure (6.9) shows the variation in load-deflection relationship with different ρ/ρ_b ratios. It can be seen that the model with reinforcement ratio at middle support equal to ρ_b demonstrated the lowest stiffness and ultimate load capacity. As the reinforcement ratio at both critical sections was increased, significant improvement in the flexural stiffness and ultimate load was observed. Increasing the reinforcement ratio from 1.0 ρ_b to 4.0 ρ_b reduced the deflection at mid-span by approximately 50% at the same load level. However, the rate of deflection reduction was lower for reinforcement ratio greater than 3.0 ρ_b. The relationship between the ultimate load capacity and the increase in reinforcement ratio is illustrated in Figure (6.10). It can be seen that

increasing the reinforcement ratio had a positive impact on the ultimate load capacity. This might be attributed to the fact that increasing the reinforcement ratio increases the flexural capacity of the cross-section and consequently the ultimate failure load. Increasing the reinforcement ratio from 1.0 ρ_b to 4.0 ρ_b increased the ultimate load capacity by approximately 22%.

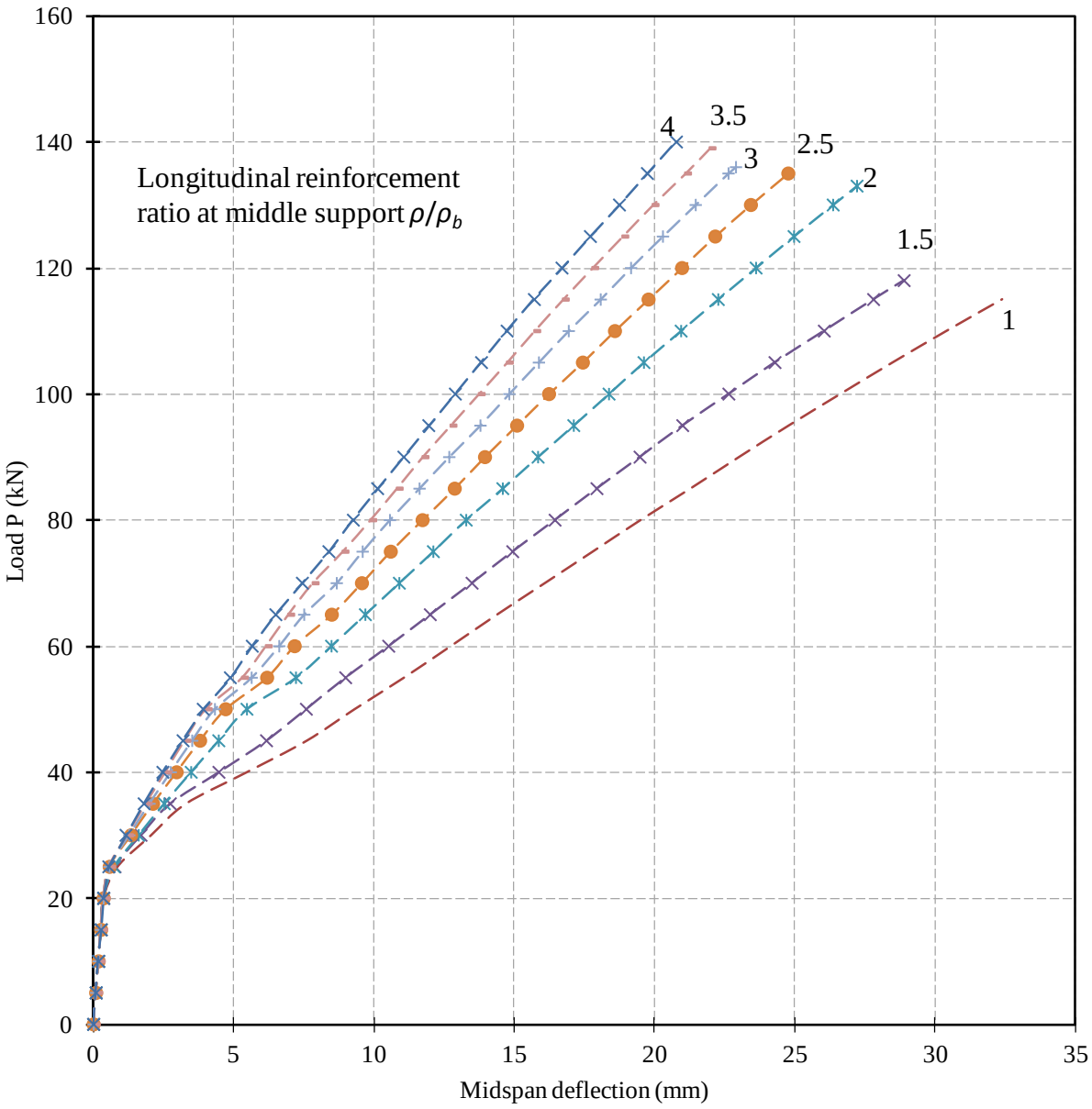

Figure (6.9): Variation in load-deflection relationship with flexural reinforcement ratio

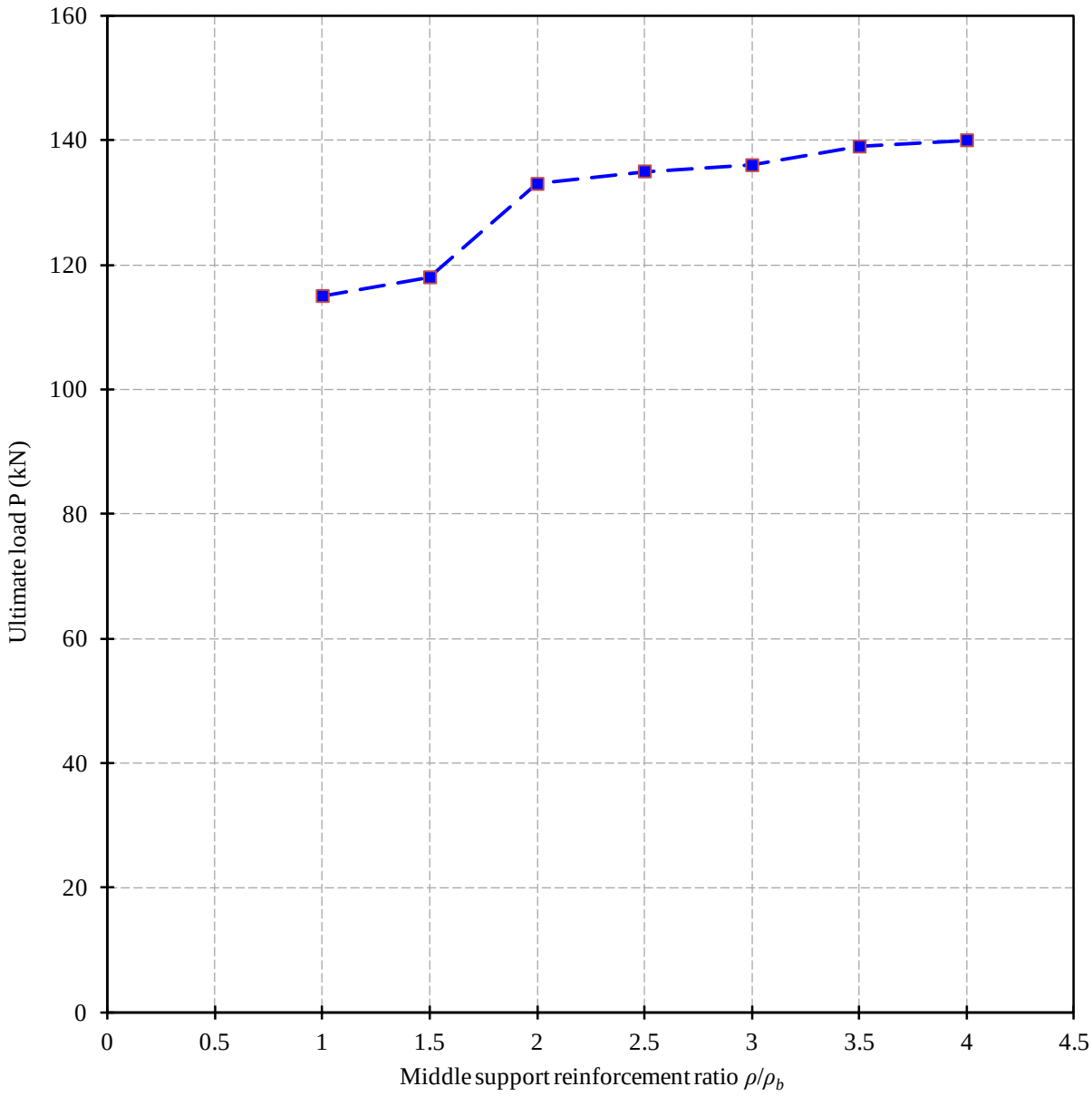

Figure (6.10): Effect of longitudinal reinforcement ratio on ultimate load capacity

6.4.2. Moment redistribution

The variation of end-reactions with different longitudinal reinforcement ratios is shown in Figure (6.11). It can be seen that increasing the reinforcement ratio had a slight increase in end-reactions. Increasing the reinforcement ratio from 1.0 ρ_b to 4.0 ρ_b increased the end reaction by 5%. The end-reactions were used to calculate the achieved moment redistribution at failure. Figure (6.12) shows the relationship between the longitudinal reinforcement and achieved moment redistribution at middle support. It can be seen that increasing the reinforcement ratio has a positive impact on the available moment redistribution. This might be attributed to the fact that increasing the flexural reinforcement increased the stiffness as well as flexural capacity which enabled the critical sections to tolerate higher stresses and provide more rotations. It can be seen that reinforcement ratio more than 2.5 ρ_b provided significant ductility of the beam and considerably improved the available moment redistribution. Increasing the reinforcement ratio from 1.0 ρ_b to 4.0 ρ_b increased the available moment redistribution by approximately 50%.

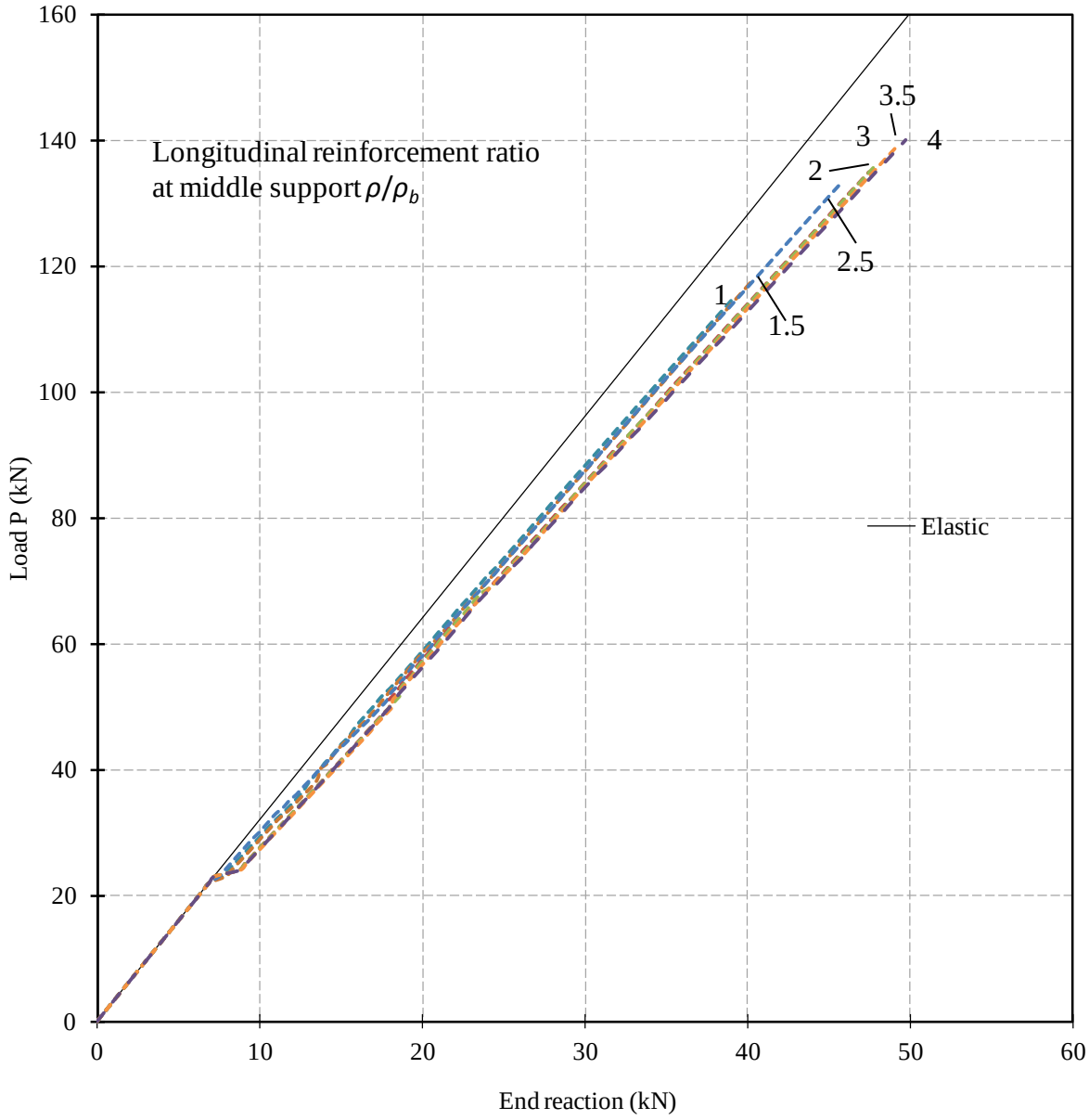

Figure (6.11): The relationship between end-reaction and applied load for different reinforcement ratios

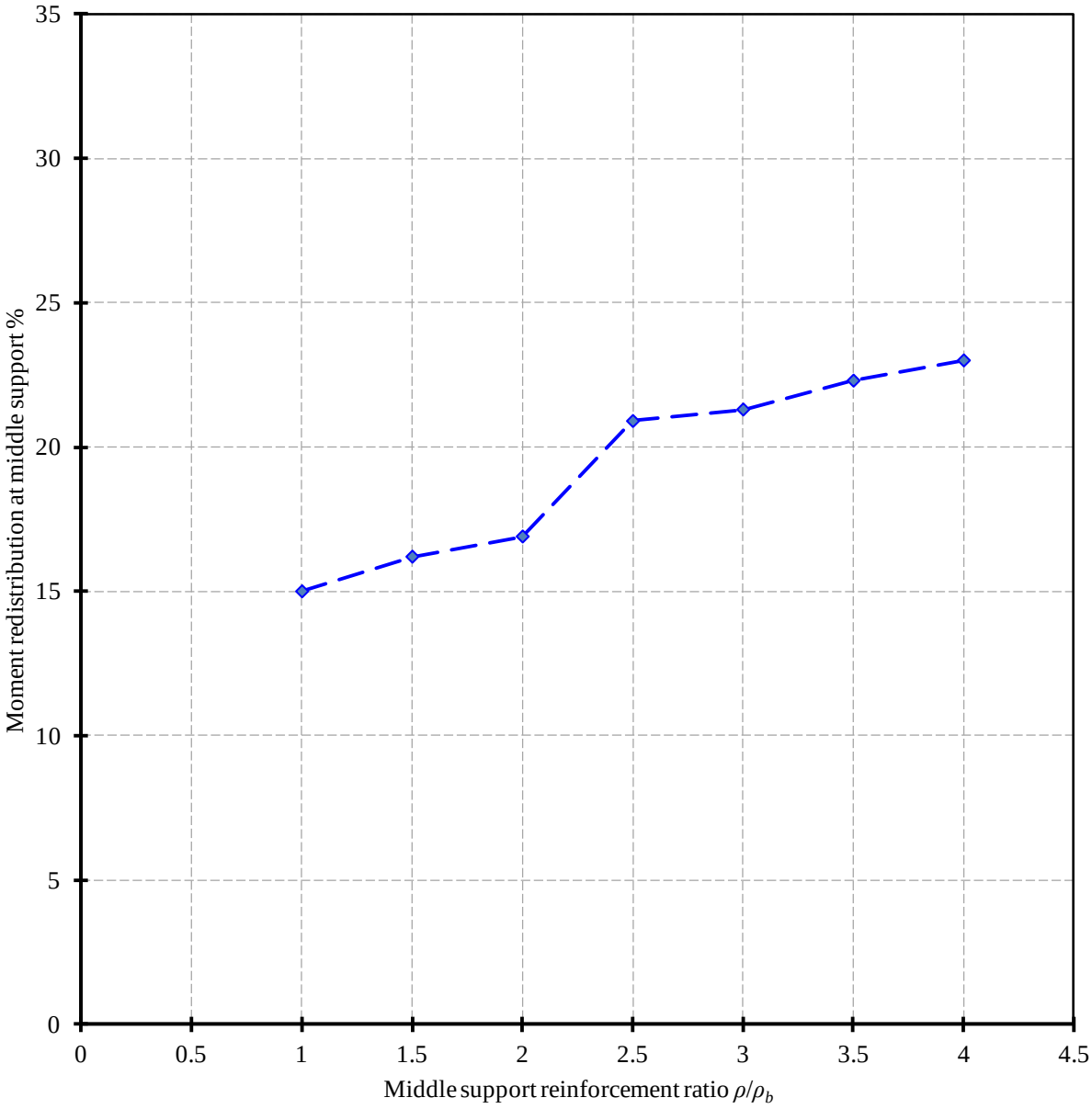

Figure (6.12): Effect of reinforcement ratio on moment redistribution at middle support

6.5. Transverse Reinforcement

The amount of transverse reinforcement usually determine the failure mode to be whether flexural failure or shear failure. Beams adequately reinforced for shear will allow the critical sections to develop their ultimate flexural capacity and consequently achieve the corresponding ultimate load. If the beam is provided with less transverse reinforcement than that required to achieve flexural capacity, this will result in a premature shear failure. The test beam GSu-8*d*/2*p* was provided with 8 mm @ 120 mm steel stirrups, which provided enough shear capacity to develop the flexural design load. A finite element model with similar geometry, reinforcement and material properties to this beam was used to evaluate the effect transverse reinforcement on continuous beams reinforced with FRP. The studied variable was the spacing of the transverse reinforcement. The required spacing for this reinforcement configuration to achieve flexural strength is 120 mm (*d*/2) as mentioned earlier. In the FEM, the minimum spacing considered was 40 mm (*d*/5), which is the minimum practical spacing to avoid honey-comb during concrete casting. Moreover, the Canadian code CSA-S806-02 (CSA 2002) specifies a maximum spacing of stirrups that should not be exceeded. The maximum spacing in this case was calculated to be 160 mm. The upper bound of the investigated spacing range was taken as 180 mm to investigate the effect of exceeding the maximum spacing on the behaviour of FRP-reinforced continuous beams.

6.5.1. Load-deflection response

Figure (6.13) shows the load-deflection relationship for different values of transverse reinforcement spacing. It can be seen that using spacing of 180 mm resulted in the lowest stiffness and ultimate failure load. As the spacing was reduced, the stiffness after cracking significantly improved up to spacing of 100 mm, below which, no significant impact was

observed on stiffness. The reason behind this behaviour is that reducing the spacing between the stirrups reduces the strains developed in the stirrups which limit the width of shear cracks and improve stiffness. Also, for lower values of stirrups spacing, the confinement around the concrete elements in compression is increased which increase the stiffness of the section and consequently reduce deflection. Figure (6.14) shows the effect of transverse stirrups spacing on the ultimate load capacity. It can be seen that very close stirrups spacing has insignificant effect on the failure load as the model becomes mainly dependent on the flexural capacity of the critical cross-sections. On the other hand, increasing the spacing beyond the maximum values allowed by the code (160 mm) significantly reduced the failure load. This is due to the fact that diagonal shear cracks start occurring in between the wide stirrup spacing which eliminate its contribution in the shear resistance and reduced it to that provided by the un-cracked portion of the concrete section. As a result the model fails due to premature shear failure at concrete elements close to the middle support.

It should be noted that the experimental results of beam GSu-8d/3p were not expected to be similar to the FEM result using 80 mm spacing due to the fact that there is 14% difference in the concrete compressive strength between both cases (32 MPa and 28 MPa respectively). By referring to (Figure 6.1), it could be seen that 14% increase in concrete strength is expected to result in approximately 8% and 7% increase in ultimate load and deflection respectively. This shows that the FEM predicts the ultimate load of beam GSu-8d/3p to be 138.7 kN, which is within 1% difference of the experimental results. Regarding the predicted deflections, the FEM results are approximately within 5% difference from the experimental results of beam GSu-8d/3p up to 90% of the ultimate load. At higher loads and prior to failure, beam GSu-8d/3p experienced sudden increase in mid-span deflection due to significantly wide cracks and signs of concrete

crushing at critical sections. The FEM, however, could not predict that increase in deflection prior to failure due to conversion problems in the program.

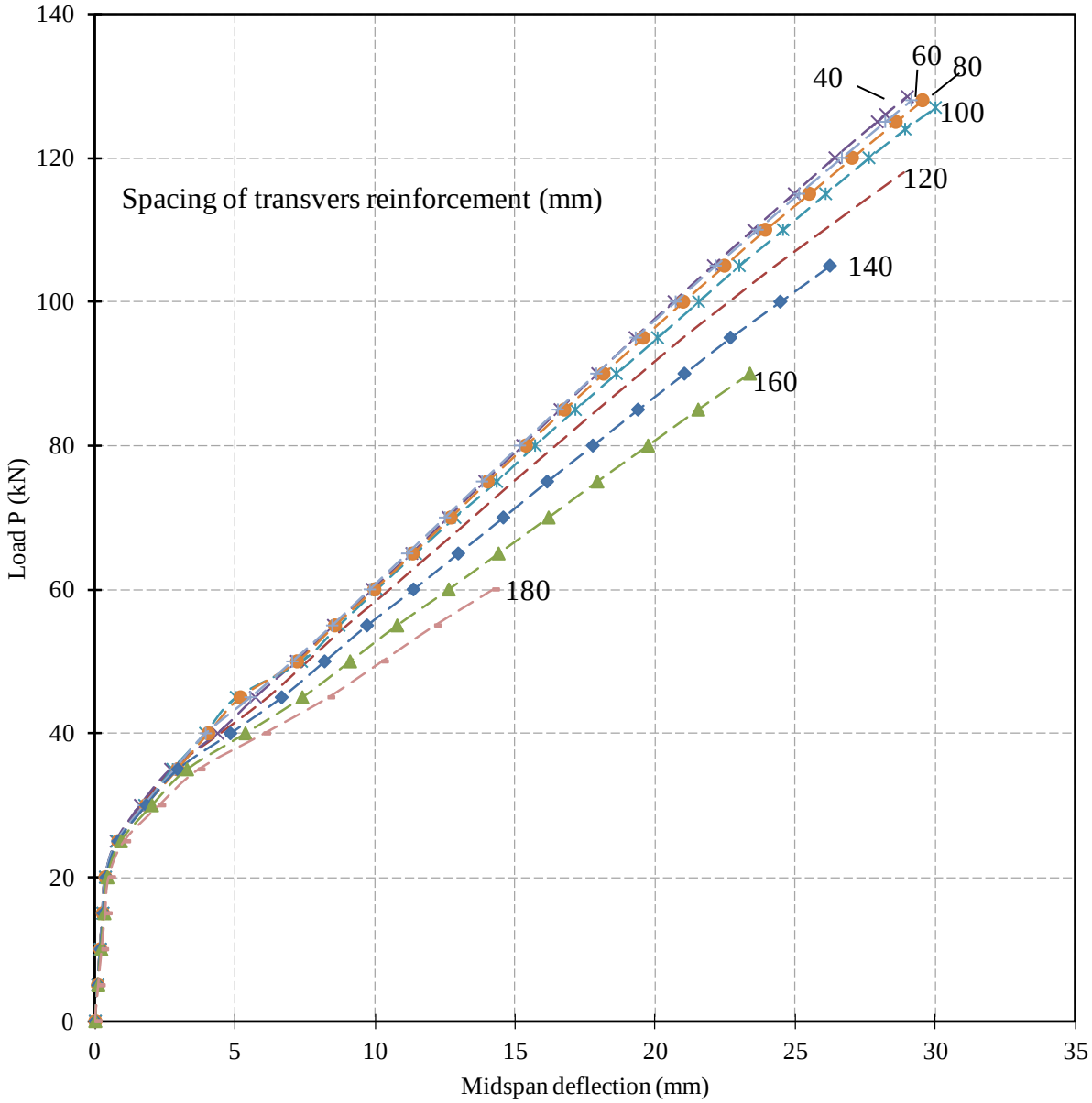

Figure (6.13): Variation in load-deflection relationship with transverse reinforcement spacing

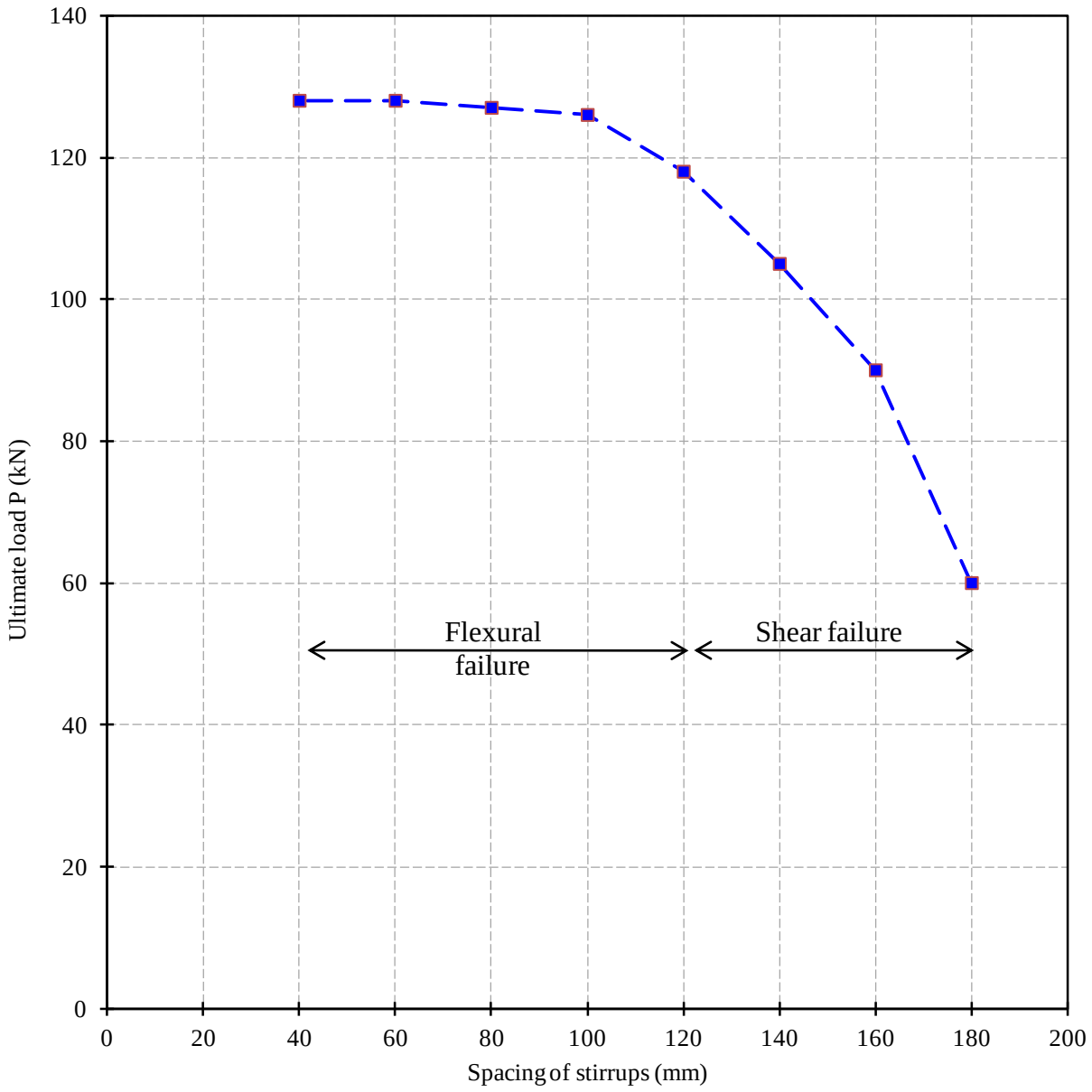

Figure (6.14): Effect of transverse reinforcement spacing on ultimate load capacity

6.5.2. Moment redistribution

Figure (6.15) shows the effect of transverse reinforcement on the available moment redistribution percentage. It can be seen that decreasing the spacing of stirrups has a positive effect on the available moment redistribution. This comes in good agreement with the experimental results presented earlier in Chapter 4. The reason behind this behaviour is believed

to be the improvement in confinement around the concrete element which increases the nonlinear effect in the concrete by taking its biaxial strength into consideration. Decreasing the spacing from 180 mm to 40 mm increased the moment redistribution percentage by 17%. However, it is worth mentioning that the rate of increase in moment redistribution for spacing smaller than 100 mm becomes insignificant.

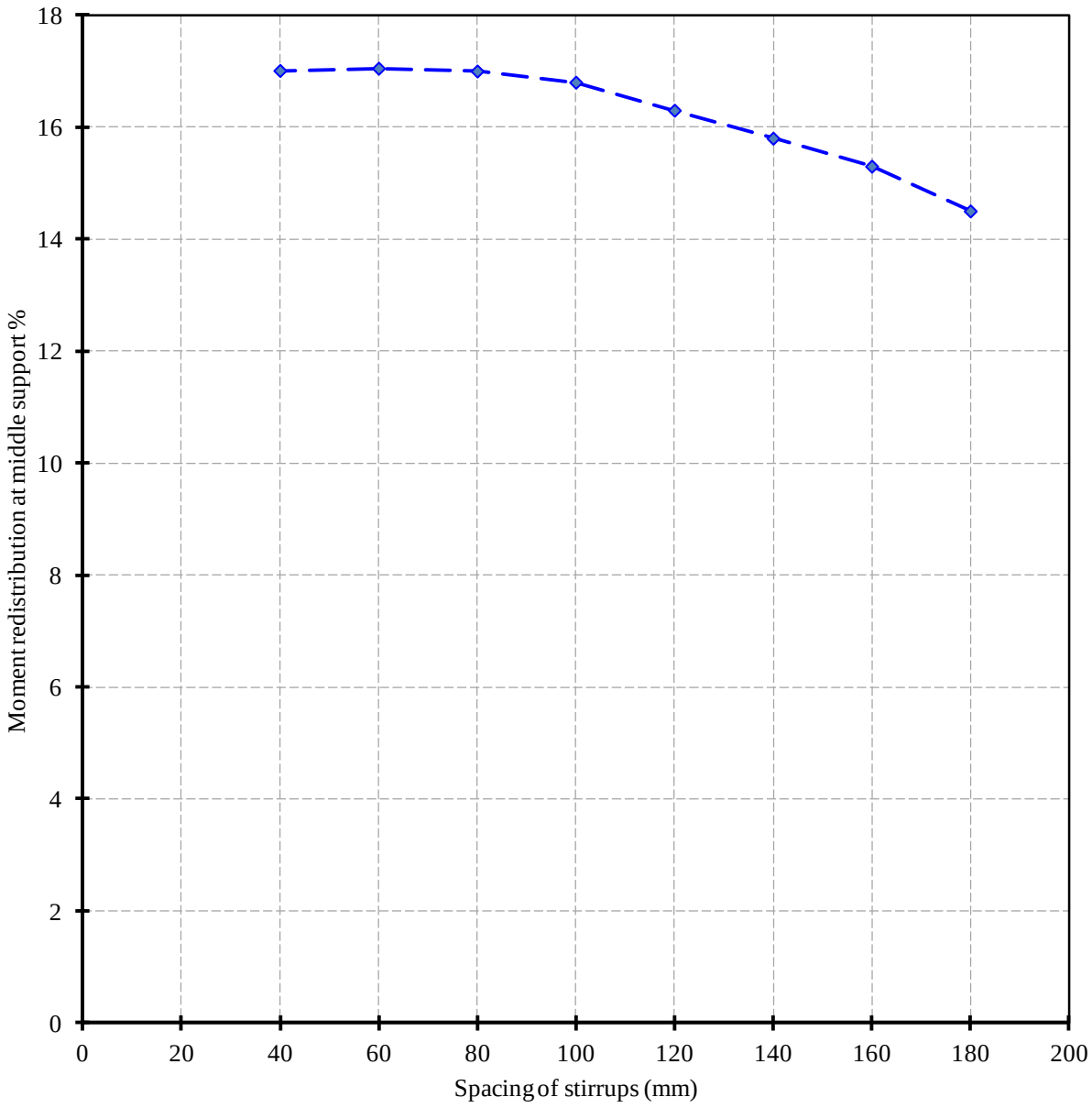

Figure (6.15): Effect of transverse reinforcement spacing on moment redistribution

6.6. Proposed Moment-Redistribution Limit

The definition and limitation of moment redistribution in continuous structures is a complex problem that depends on geometry and material properties of the structure in addition to other variables such as variations in slenderness and beam stiffness as illustrated by Scholz (1993). Nonetheless, the current design specifications for steel-reinforced structures define moment redistribution limit as function of the ratio *c/d*, where *c* is the depth of neutral axis and *d* is the effective depth of the section. The moment redistribution limit recommended by the Canadian code CSA-A23.3-04 (CSA 2004) is shown in Equation (6.2).

$$Moment\ redistribution\% = 30 - 50\ c/d \leq 20\% \qquad (6.2)$$

Based on the experimental results of GFRP-reinforced beams and analysis of the finite element model, the ratio *c/d* was calculated for the middle support section at failure to evaluate the validity of the formula in Equation (6.2) for FRP-reinforced beams. The depth of neutral axis , *c*, was calculated based on the strain compatibility assumption between compressive strain in concrete and tensile strain in flexural reinforcement as demonstrated in Figure (6.16) and Equation (6.3).

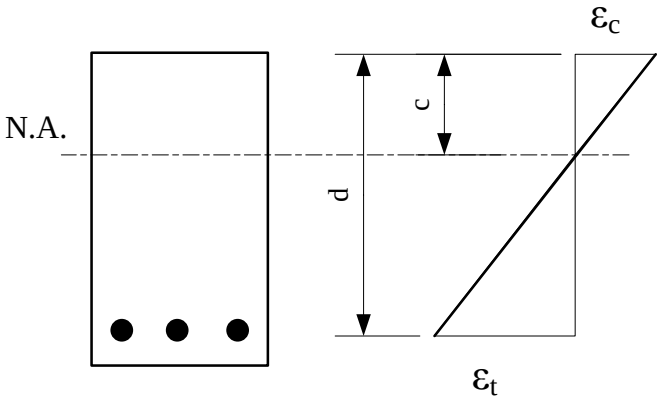

Figure (6.16): Strain compatibility and the depth of neutral axis

$$c/d = \left(\frac{\varepsilon_c}{\varepsilon_c+\varepsilon_t}\right) \quad (6.3)$$

Figure (6.17) shows the relationship between calculated *c/d* ratios at the middle support and the corresponding achieved moment redistribution at ultimate load. The moment redistribution limit proposed by the Canadian code is also shown on the same figure as well as results of steel-reinforced beams from literature. The values of *c/d* in this investigation ranged between 0.1 and 3.5. Within this range, the results seem to have the same trend as the code model but with un-conservative results in some cases. It is safe to say that within the considered *c/d* ratios in this investigation, all FRP-reinforced beams achieved at least 15% moment redistribution at the middle support prior to failure. Hence, it is suggested to allow for moment redistribution percentage in continuous beams reinforced with FRP according to the following equation as shown on the same figure.

$$Moment\ redistribution\% = 25 - 50\ c/d \leq 15\% \quad (6.4)$$

It can be seen that a number of experimental and numerical result demonstrated similar *c/d* ratios while experienced large difference in the achieved moment redistribution. This is due to the fact that the definition of moment redistribution in continuous beams is a complex problem that depends on a number of factors other than the ratio between the depth of neutral axis and the effective depth at one critical section. The moment redistribution was found to be mainly dependent on the relative stiffness between critical sections which could be affected by a range of variables such as formation of cracks, reinforcement ratio between critical sections, spacing of stirrups, material properties, and slippage of reinforcement. Different combination of these variables might result in similar *c/d* ratio at the middle support section with significantly different moment redistribution. In addition some of the FEM results experienced different

modes of failure (compression/tension and premature shear failure) which could also result in similar *c/d* ratio while experiencing different moment redistribution. Therefore, the approach proposed by the current design code was found to be rather conservative and could be improved to take other factor affecting moment redistribution into consideration.

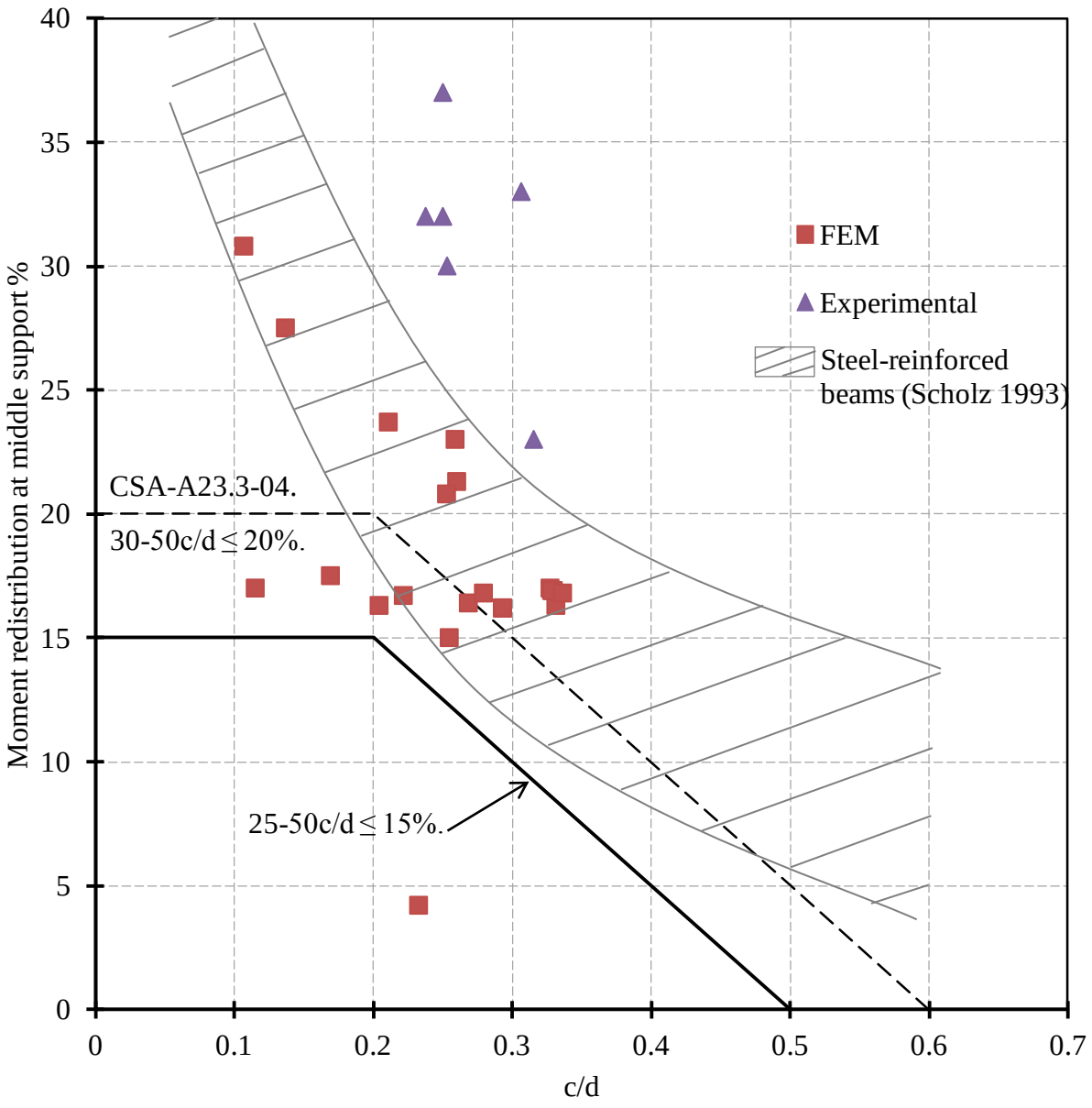

Figure (6.17): Relationship between moment redistribution and *c/d* ratio

CHAPTER 7: SUMMARY, CONCLUSIONS AND RECOMENDATIONS FOR FUTURE WORK

7.1. Summary

The structural behaviour of continuous concrete beams reinforced with FRP bars and stirrups was investigated in this study. The study consisted of two phases, experimental and finite element analysis investigations. The study resulted in a number of findings on the effect of different parameter on the behaviour of FRP-reinforced continuous beams. In addition, a number of recommendations and a proposed allowable limit for moment redistribution in such beams were also presented.

The experimental phase included the construction and testing of ten full-scale concrete beams continuous over two spans with rectangular cross-section. The tested beams were loaded up till failure under monotonic concentrated loads at midpoints of each span. The tested variables were flexural reinforcement ratio in both sagging and hogging bending moment sections, material of longitudinal reinforcement, transverse reinforcement material, spacing, and reinforcement ratio. The target design load was also an investigated parameter to evaluate the serviceability performance of continuous beams reinforced with FRP.

The analytical phase was commenced by creating a finite element model (FEM) to simulate the behaviour of continuous concrete beams. The FEM was validated against the results obtained from the experimental phase. Afterwards, a parametric study was conducted using the verified model to investigate a number of variables, such as concrete compressive strength, longitudinal reinforcement ratio, midspan-to-middle support reinforcement ratio and the amount of transverse reinforcement.

7.2. Conclusions

The findings of the present investigation support the following conclusions. It should be noted that conclusions regarding FRP materials concentrate on FRP types included in the scope of the present study (GFRP and CFRP).

7.2.1. Conclusions from the experimental investigation phase

1. Moment redistribution in FRP-reinforced continuous beams is possible albeit the linear-elastic nature of FRP materials. It was found that the extent of this redistribution depends on a number of key factors that play a significant role in this regard such as the in-elasticity of concrete, the capability of FRP materials to withstand large deformations and the bond-slip characteristics of FRP bars.
2. The tested GFRP-reinforced concrete beams designed assuming 20% moment redistribution successfully redistributed moments from the elastic hogging moment of middle support section into the mid-span without adversely affecting the ultimate load capacity.
3. Using a reinforcement configuration that allows for moment redistribution in GFRP-reinforced continuous beams had a positive effect on deflection reduction while maintaining the load carrying capacity similar to the case when the reinforcement configuration satisfies the elastic moment distribution.
4. For the tested continuous GFRP-reinforced concrete beams, redistribution of design bending moments by an amount of 20% does not appear to adversely affect the performance of the beam neither at service load nor at failure.
5. The tested FRP-reinforced continuous beams exhibited higher deflections and wider cracks compared to the steel-reinforced reference beam with similar flexural capacity;

6. Continuous beams reinforced with FRP bars in the longitudinal direction showed ample warning in the form of large deflections and wide cracks, prior to failure. When GFRP-stirrups were used the failure was accompanied by rupture of stirrups at the bent location.
7. The CFRP-reinforced concrete beam (CSu-8*d*/2*p*) demonstrated redistribution of the hogging bending moment from middle support to the mid-span section. However, this redistribution did not result in any increase in the failure load predicted by the CSA-S806-02 code (CSA 2002), which assumes no moment redistribution. That might be attributed to inadequate bond strength between tension reinforcement and the surrounding concrete at the middle support section.
8. The Canadian code CSA-S806-02 (CSA 2002) could reasonably predict the failure load for the tested beams reinforced with GFRP and CFRP bars to satisfy the elastic moment distribution. However, CFRP-reinforced beams failed to satisfy the serviceability requirements.
9. The correction factor proposed by Habeeb and Ashour (2008) to the ACI 440-06 (ACI 2006) equation to calculate effective moment of inertia for GFRP-reinforced continuous concrete beams shows a reasonable agreement with the experimental results especially at high loading stages.
10. Increasing the transverse reinforcement in GFRP-reinforced continuous beams without increasing the longitudinal reinforcement reduced deflection and improved moment redistribution.
11. Reducing the spacing of the stirrups, while maintaining the same transverse reinforcement ratio, $\rho_v = A_v / (b\ s)$, and longitudinal reinforcement ratio, increased the beam deformations and allowed for more moment redistribution.

12. The performance of the GFRP-reinforced beams provided with GFRP stirrups was similar to its counterpart reinforced with steel stirrups. This confirms the efficiency of GFRP stirrups used as transverse reinforcement. Moreover, the use of GFRP stirrups instead of steel had a positive impact on moment redistribution due to their ability to withstand higher elongations at low stress level which allowed for more rotations at critical sections.
13. The tested GFRP-reinforced concrete continuous beam (GSs-10*d*/2*p*) designed to carry a similar service load to the control beam (SSc-8*d*/2*p*), while meeting the FRP design code serviceability requirements, had a 23% higher failure capacity and achieved 65% more moment redistribution compared to those of the control beam.

7.2.2. Conclusions from the numerical investigation phase

14. The created finite element model using ANSYS program was able to analyse FRP-reinforced continuous concrete beams and predict the maximum load as well as the moment redistribution with a reasonable degree of accuracy. Nevertheless, the model was not able to predict the post-failure response of concrete, where the program experienced difficulty with the solution conversion once failure started.
15. The results of the analysis of the tested beams with the finite element model confirm the occurrence of moment redistribution in FRP-reinforced concrete beams.
16. Increasing the concrete compressive strength in the model appears to have undesirable effect on the available moment. Nonetheless, the increase in concrete strength enhanced the flexural strength and consequently increased the ultimate load capacity.

17. The ratio between sagging and hogging reinforcement amount was found to have the main influence on the available moment redistribution. This supports the hypothesis that stiffness and consequently distribution of moments follow the reinforcement configuration. The relationship between this ratio and the available moment redistribution can be described as a cubic polynomial equation.
18. It is recommended to provide the critical sections in FRP-reinforced continuous beams with reinforcement ratio equal to or greater than 2.5 ρ_b since this ratio appear to provide adequate deformability of the concrete member and achieve the expected load capacity.
19. The transverse reinforcement of FRP-reinforced continuous beams was found to play a significant role in determining the failure mode and the maximum load. However, closer spacing of transverse reinforcement less than 2d/5 (100 mm) which represents a reinforcement ratio, $\rho_v = A_v / (b\ s)$, greater than 0.5% had insignificant effect on the maximum load or the moment redistribution.
20. From the results obtained in this present study either experimentally or analytically, the ratio between the depth of neutral axis (c) and effective section depth (d) at failure was compared against the recommended moment redistribution limit in the Canadian code CSA-A23-04 (CSA2004). A modification was proposed to suit FRP-reinforced continuous beams that allow for moment redistribution percentage equals to 25-50 c/d but not more than 15%.

7.3. Recommendations for Future Work

1. Further experimental and analytical studies are required to investigate the behaviour of FRP-reinforced continuous beams with a wider range of reinforcement ratios and different cross-sections, such as T-shaped sections.

2. Since the current experimental work was carried out using only one loading configuration, a series of specimens should be tested under different loading configurations.
3. Experimental and analytical studies should be conducted to verify the proposed moment redistribution limit and drive guidelines for rotation demand and capacity in FRP-reinforced concrete beams.
4. As the present study was carried out using mainly GFRP reinforcement, more experiments should be conducted on beams reinforced with CFRP bars. In addition, similar tests should be performed on concrete beams reinforced with different types of fibres (such as aramid) and surface finishing (such as deformed or wrapped bars).
5. Using the proposed FEM model, more variables need to be investigated such as the number of spans and the effect of unequal spans.
6. It seems that there is an urgent need to study the influence of bond-slip relationship between FRP bars and surrounding concrete since the obtained results in this study was found to be particularly sensitive to this relation.

REFERENCES

ACI Committee 318. (2005). "Building code requirements for reinforced concrete." ACI 318-05, *American Concrete Institute*, Detroit, MI.

ACI Committee 440. (1996). "State-of-the-Art Report on Fiber Reinforced Plastic (FRP) Reinforcement for Concrete Structures." ACI 440R-96, *American Concrete Institute*, Detroit, MI.

ACI Committee 440. (2004). "Guide Test Methods for Fiber Reinforced Polymers (FRPs) for Reinforcing or Strengthening Concrete Structures." ACI 440.3R-04, *American Concrete Institute*, Farmington Hills, MI.

ACI Committee 440. (2006). "Guide for the Design and Construction of Structural Concrete Reinforced with FRP Bars." ACI 440.1R-06, *American Concrete Institute*, Detroit, MI.

ACI Committee 318. (2008). "Building code requirements for structural concrete and commentary," *ACI 318-08* and *ACI 318R-08*, respectively, *American Concrete Institute* (ACI), Farmington Hills, Mich.

Ahmed, E. A., El-Salakawy, E. and Benmokrane, B. (2010). " Performance Evaluation of Glass Fiber-Reinforced Polymer Shear Reinforcement for Concrete Beams." *ACI Structural Journal*, 107(1), 53-62.

Alves, J., El-Ragaby, A. and El-Salakawy, E. (2011). "Durability of GFRP Bars Bond to Concrete under Different Loading and Environmental Conditions," *Journal of Composites for Construction, ASCE*, 15(3), 249-262.

ANSYS (2010) *ANSYS Release 13.0 Finite Element Analysis System*, SAS IP, Inc.

Ashour, A. F. (2006). " Flexural and shear capacities of concrete beams reinforced with GFRP bars." *Construction and Building Materials*, 20(10), 1005-1015.

ASTM Standard A370. (2005), "Standard Test Methods and Definitions for Mechanical Testing of Steel Products," *ASTM International*, West Conshohocken, PA.

Baker, A. L. and Amarakone, A. M. (1965). "Inelastic Hyperstatic Frames Analysis." *Proceedings of the international symposium on Flexural Mechanics of Reinforced Concrete*, ASCE/ACI SP-12, 85-136.

Benmokrane, B., Chaallal, O. and Mamoudi, R. (1996). "Flexural Response of Concrete Beams Reinforced with FRP Reinforcing Bars." *ACI Structural Journal*, 93(1), 46-55.

Bischoff, P. H. (2007). "Deflection calculation of FRP reinforced concrete beams based on modifications to the existing Branson equation." *ASCE Journal of composites for construction*, 11(1), 4-14.

Büyükkaragöz, A. (2010). "Finite Element Analysis of the Beam Strengthened with Prefabricated Reinforced Concrete Plate," *Scientific Research and Essays*, 5(6), 533-544.

Carmo, R. N. F. and Lopes, S. M. (2006). "Required plastic rotation of RC beams." *Proceedings of the institution of civil engineers, structures and buildings*, 159(SB2), 77-86.

CEB-FIP. (1990). "Model code for concrète structures." comite Européen du béton, Paris France.

Cohn, M. Z. (1964). "Rotational compatibility in the limit design of reinforced concrete continuous beams." *Proceedings, International symposium on the flexure mechanics of reinforced concrete*, ASCE-ACI, Miami, 359-382.

Corley, W. G. (1966). "Rotational Capacity of Reinforced Concrete Beams." *ASCE Structural Division*, (92), 121-146.

CSA.(2002). "Code for the design and construction of building components with Fibre-Reinforced Polymers." CSA S806-02, *Canadian Standards Association*, Rexdale, Canada.

CSA. (2004). "Code for the design of concrete structures for buildings." CSA standard A23.3-04, *Canadian Standards Association*, Rexdale, Ont.

CSA. (2006). "Canadian Highway Bridge Design Code (CAN/CSA-S6-06)." *Canadian Standards Association*, Rexdale, Ontario.

CSA. (2009). "Canadian Highway Bridge design code," *CSA Standard S6-06 (addendum)*, Canadian Standards Association, Rexdale (Toronto), Ontario, Canada.

Eligehausen, R., Bertero, V. and Popov, E. (1983). "Local bond stress-slip relationships of deformed bars under generalised excitations." Report No. UBC/EFRC-83/23, University of California.

El-Mogy, M., El-Ragaby, A. and El-Salakawy, E. (2010). "Flexural Behaviour of FRP-Reinforced Continuous Concrete Beams." *ASCE Journal of Composites for Construction*, 14(6), 486-497.

El-Salakawy, E. and Benmokrane, B. (2004). "Serviceability of Concrete Bridge deck Slabs Reinforced with FRP Composite Bars." *ACI Structural Journal*, 101(5), 727-736.

El-Sayed, A. K., El-Salakawy, E. and Benmokrane, B. (2006). "Shear Strength of FRP-Reinforced Concrete Beams without Transverse Reinforcement." *ACI Structural Journal*, 103(2), 235-243.

Ernst, G. C. (1957). "Plastic Hinging at Intersection of Beam and Columns." *ACI Structural Journal*, 28(2), 1119-1144.

Ernst, G. C. (1958). Moment and Shear Redistribution in Two-Span Continuous Reinforced Concrete Beams. *ACI Structural Journal*, 30(55), 573-589.

GangaRao,V. S. and Vijay, P. V. (2007). "Reinforced Concrete Design with FRP Composites," *CRC press*, Boca Raton, FL.

Grace, N. F., Soliman, A. K., Abdel-Sayed, G. and Saleh, K. R. (1998). "Behavior and Ductility of Simple and Continuous FRP Reinforced Beams." *ASCE Journal of composites for construction*, 2(4), 186-194.

Gorji, M. S. (2009). "Analysis of FRP Strengthened Reinforced Concrete Beams using Energy Variation Method," *World Applied Sciences Journal*, 6(1), 105-111.

Gravina, R.J. and Smith, S. T. (2008). "Flexural behaviour of indeterminate concrete beams reinforced with FRP bars." *Journal of Engineering Structures*, 30(9), 2370-2380.

Gravina, R. J. and Warner, R. F. (2003). "Local deformation model for reinforced concrete members in flexure." *Australian Journal of structural engineering*, 5(1), 29-36.

Habeeb, M. N. and Ashour, A. F. (2008). "Flexural Behavior of Continuous GFRP Reinforced Concrete Beams." *ASCE journal of composites for construction*, 12(2), 115-124.

ISIS Canada. (2007). "Design Manual 3, Reinforcing concrete structures with fibre reinforced polymers (FRPs)." *ISIS Canada Corporation*, The Canadian Network of Centers of Excellence on Intelligent Sensing for Innovative Structures, Winnipeg, Manitoba, Canada.

Jaeger, L. G., Tadros, G. and Mufti, A. (1995). "Balanced section, ductility and deformability in concrete with FRP reinforcement." *Res. Rep*. 2-1995, Industry's Centre for Computer-Aided Engineering, CAS CAM, Tech. Univ. Of Nova Scotia, Halifax, Nova Scotia.

Kodur, V. K. and Campbell, T. I. (1996). "Evaluation of Moment redistribution in two-span continuous prestressed concrete beam." *ACI structural journal*, 93(6), 721-728.

Kachlakev, D., Miller, T., Yim, S., Chansawat, K. and Potisuk, T. (2001). "Finite Element Modeling of Reinforced Concrete Structures strengthened with FRP Laminates." *Final Report SPR-316*, Oregon Department of Transportation, Salem, Oregon.

Lin, C. H. and Chien, Y. M. (2000). "Effect of Section Ductility on Moment Redistribution of Continuous Concrete Beams." *Journal of the Chinese Institute of Engineers*, 23(2), 131-141.

Lopes, S. M. R. and Bernardo, L. F. A. (2003). "Plastic rotation capacity of high-strength concrete beams." *Journal of materials and structures*, 36(1), 22-31.

Macchi, G. (1965). "Elastic Distribution of moments on continuous beams." *Proceedings of the international symposium on the flexural mechanics of reinforced concrete.* , ASCE/ACI SP-12, 237-256

MacGregor, J. G. (1992), *Reinforced Concrete Mechanics and Design*, Prentice-Hall, Inc., Englewood Cliffs, NJ.

Mady, M. H. A. (2011). "Seismic Behaviour of Exterior Beam-Column Joints Reinforced with FRP bars and Stirrups," Ph.D. Thesis, Department of Civil Engineering, University of Manitoba, Winnipeg, Manitoba.

Mattock, A. H. (1959). "Redistribution of Design Bending Moments in Reinforced Concrete Continuous Beams." *The Institution of Civil Engineers*, V.13, 35-46.

Mattock, A. H. (1965). "Rotational Capacity of Hinging Regions in Reinforced Concrete Beams." *Proceedings of the International Symposium on Flexural Mechanics of Reinforced Concrete,* ASCE-ACI, Miami, 143-181.

Mostofinejad, D. (1997). "Ductility and Moment Redistribution in Continuous FRP Reinforced Concrete Beams," PhD thesis, Department of Civil and Environmental Engineering, Carleton University, Ottawa, Ontario, Canada.

Mostofinejad, D. and Talaeitaba, S. B. (2006). "Finite Element Modeling of RC Connections Strengthened with FRP Laminates," *Iranian Journal of Science & Technology*, 30(B1), 21-30.

Mota, C., Alminar, S. and Svecova, D. (2006). "Critical Review of deflection formulas for FRP reinforced concrete." ASCE *Journal of Composites for construction*,10(3), 183-194.

Mufti, A. A., Newhook, J. P. and Tadros, G. (1996). "Deformability versus ductility in concrete beams with FRP reinforcement." *Proc., 2nd Int. Conf. Adv. Composite Mat. In Bridges and Struct*., El-Badry. Ed., Can. Soc. For Civ. Engrg., Montreal, Canada, 189-199.

Newhook, J., Ghali, A. and Tadros, G. (2002). "Concrete flexural members reinforced with fiber reinforced polymer: design for cracking and deformability." *Canadian Journal of Civil Engineering*, 29(1), 125-134.

Park, R. and Paulay, T. (1975). *Reinforced Concrete Structures*. John Wiley and Sons, New York, NY.

Pultrall Inc. (2009). "V-ROD™ – Technical Data Sheet." ADS Composites Group Inc., Thetford Mines, Quebec, Canada, <http://www.pultrall.com> (Jan. 1, 2010).

Razaqpur, A. G. and Mostofinejad, D. (1999). "Experimental Study for Shear Behavior of Continuous Beams Reinforced with Carbon Fiber Reinforced Polymer for Reinforced Concrete Structures." *Proceedings of the Fourth International Symposium,* 169-178.

Rizkalla, S., Hwang, L. S. and El Shahawai, M. (1983). "Transverse reinforcement effect on cracking behavior of RC members." *Canadian Journal of Civil Engineering*, 10(4), 566-581.

Rodriguez, J. J., Bianchini, A. C., Viest, I. M. and Kesler, C. E. (1959). "Shear Strength of Two-Span Continuous Reinforced Concrete Beams." *ACI Structural Journal*, 55(4), 1089-1130.

Scholz, H. (1993). "Contribution to redistribution of moments in continuous reinforced concrete beams." *ACI structural journal*, 90(2), 150-155.

Shehata, E. F. G. (1999). "Fibre-Reinforced Polymer (FRP) for Shear Reinforcement in Concrete Prisms." Ph.D. Thesis, Department of Civil and Geological Engineering, University of Manitoba, Winnipeg, Manitoba.

Tezuka, M., Ochiai, M., Tottori, S. and Sato, R. (1995). "Experimental study on moment redistribution of continuous beams reinforced or pretensioned with fibre reinforced plastic." Non-Metallic (FRP) Reinforcement for Concrete Structures: *Proceedings of the Second International RILEM Symposium*, 287-394.

Theriault, M. and Benmokrane, B. (1998). "Effects of FRP reinforcement ratio and concrete strength on flexure behavior of concrete beams." *ASCE journal of composites for construction*, 2(1), 7-16.

Toutanji, H. A. and Saafi, M. (2000). "Flexural Behaviour of Concrete Beams Reinforced with Glass Fiber-Reinforced Polymer (GFRP) Bars." *ACI structural journal*, 97(5), 712-719.

Vijay, P. V., Kumar, S. V. and GangaRao, H. V. S. (1996). "Shear and ductility behaviour of concrete beams reinforced with GFRP rebars." *Proc., 2nd Int. Conf. Adv. Composite Mat. In Bridges and Struct.*, El-Badry. Ed., Can. Soc. For Civ. Engrg., Montreal, Canada, 217-226.

Vijay, P. V. and GangaRao, H. V. (2001). "Bending Behaviour and Deformability of Glass Fiber-Reinforced Polymer Reinforced Concrete Members." *ACI structural journal*, 98(6), 834-842.

Willam, K.J. and Warnke, E.P. (1974), "Constitutive Model for Triaxial Behaviour of Concrete," Seminar on Concrete Structures Subjected to Triaxial Stresses, *International Association of Bridge and Structural Engineering Conference*, Bergamo, Italy, 174.

Wolanski, A. J. (2004). "Flexural Behavior of Reinforced and Prestressed Concrete Beams using Finite Element Analysis," M.Sc. Thesis, Marquette University, Milwaukee, Wisconsin.

Wu, Y. F. (2006). "New avenue of achieving ductility for reinforced concrete members." *ASCE journal of structural engineering*, 132(9), 1502-1506.

Yost, J. R., Gross, S. P. and Dinehart, D. W. (2003). "Effective Moment of Inertia for Glass Fiber-Reinforced Polymer-Reinforced Concrete Beams." *ACI structural journal*, 100(6) , 732-739.

Zakaria, M., Ueda, T., Wu, Z. and Meng, L. (2009). "Experimental Investigation on Shear Cracking Behavior in Reinforced Concrete Beams with Shear Reinforcement." *Japan Concrete Institute, Journal of Advanced Concrete Technology*, 7(1), 79-96.

NOTATIONS

A = Area of reinforcement, mm^2

A_{frp} = Area of longitudinal FRP reinforcement, mm^2

A_{steel} = Area of longitudinal steel reinforcement, mm^2

A_v = Area of transverse reinforcement,mm^2

b = Beam width, *mm*

c = Depth of the neutral axis, *mm*

d = Effective depth of the cross-section, *mm*

d_c = Distance from extreme tension fibres to the centroid of outer reinforcement layer, *mm*

d_b = Bar diameter, *mm*

E = Modulus of elasticity, *GPa*

E_{frp} = Modulus of elasticity of the FRP bars, *MPa*

E_c = Concrete modulus of elasticity, *GPa*

f = Stress at any strain, *MPa*

f_c' = Concrete compressive strength, *MPa*

f_r = Concrete modulus of rupture, *MPa*

f_y = Yielding stress of steel, *MPa*

h = Height of beam, *mm*

h_1 = Distance from centroid of outer layer of reinforcement to neutral axis, *mm*

h_2 = Distance from extreme tension fibres to neutral axis, *mm*

I_{cr} = Cracked moment of inertia, mm^4

I_e = Effective moment of inertia, mm^4

I_{ec} = Effective moment of inertia at middle support, mm^4

I_{em} = Effective moment of inertia at mid-span, mm^4

I_g = Gross (un-cracked) moment of inertia, mm^4

L_p = Plastic hinge length, *mm*

ℓ = *Clear span, m*

M_a = Applied service load moment, *kN.m*

M_{cr} = Cracking moment, *kN.m*

M_{sp} = Moment in the span, *kN.m*

M_{sup} = Moment at middle support, *kN.m*

P = Applied load at mid-point of each span, *kN*

P_{cal} = Calculated failure load, *kN*

P_{cr} = Cracking load, *kN*

P_{exp} = Experimental failure load, *kN*

R = Reaction of end support, *kN*

s = Spacing of transverse reinforcement, *mm*

s_l = Slippage corresponding to bond stress, *mm*

α_1 = $0.85 - 0.0015\, f_c' \geq 0.67$

β = Moment redistribution ration

β_1 = $0.97 - 0.0025\, f_c' \geq 0.67$

β_d = Correction factor

γ_G = Modification factor for GFRP-reinforced continuous concrete beams

Δ = Deflection at mid-span, *mm*

ε = Strain at stress *f*

ε_{avg} = The average strain between cracks in reinforcement

ε_c = Concrete crushing strain

ε_{peak} = Peak tensile strain in reinforcement at the crack location

ε_t = Net tensile strain in reinforcement

ε_{frpu} = Ultimate strain of FRP bars

ε_o = Strain at maximum concrete compressive strength

ε_y = Yielding strain of steel

η = $1 - (I_{cr}/I_g)$

ρ = Reinforcement ratio

ρ_b = Balancing reinforcement ratio

ρ_{bot} = Bottom reinforcement ratio at mid-span

ρ_{top} = Top reinforcement ratio at middle support

ρ_v = Transverse reinforcement ratio

σ = Applied stress, *MPa*

τ = Bond stress between reinforcement bar and the surrounding concrete, *MPa*

τ_{max} = Maximum bond strength, *MPa*

APPENDIX A:

DESIGN OF TEST SPECIMENS

A.1. Design Criteria:

- b = 200 mm, h = 300 mm, clear cover = 40 mm, L = 2.8m
- concrete strain before crushing = 0.0035, f_c' = 30 MPa
- used longitudinal steel and stirrups properties: f_y = 400 MPa, E = 200 GPa
- used GFRP bar properties:
    - Size No.16, bar diameter = 15.9 mm, area = 198 mm^2, maximum tensile strength f_{frpu} = 731 MPa, E_{frp} = 46 GPa, ε_{frpu} = 1.6 %
- Used CFRP bar properties:
    - Size No.3, bar diameter = 9.5 mm, area = 71 mm, guaranteed tensile strength f_{frpu} = 1596 MPa, E_{frp} = 124 GPa, ε_{frpu} = 1.4 %

As the nominal section capacity is the target, all material safety factors shall be taken equal to unity.

A.2. Design of Specimen SSc-8*d*/2*p*

A.2.1. Design for flexure according to CSA A23.3-04.

Design of section at middle support:

$\alpha_1 = 0.85 - 0.0015 \times 30 = 0.8$

$\beta_1 = 0.97 - 0.0025 \times 30 = 0.895$

The tension reinforcement can be assumed to reach yield if $c/d \leq \frac{700}{700+f_y}$, (clause 10.5.2).

$\frac{c_b}{d} = \frac{700}{700+f_y} = 0.64$, using bars No.15M. d = (300-40-16/2) = 252 mm

$c_b = 0.64 \times 252 = 161.3$ mm

From equilibrium of internal forces (C = T):

$$\alpha_1 f_c' a\, b = A_s f_y \quad \Rightarrow \quad a = \beta_1 c = \frac{A_s f_y}{\alpha_1 f_c' b}$$

Using 3 No.15M, A_s = 3 x 200 = 600 mm^2

A minimum reinforcement should be provided in beams calculated as in clause 10.5.1.2 as follows: $A_{s,min} = \frac{0.2\sqrt{f_c'}}{f_y} b_t h = \frac{0.2\sqrt{30}}{400}\ 200\ x\ 300$ = 164.3 mm^2 < 600 mm^2

$$a = \beta_1 c = \frac{A_s f_y}{\alpha_1 f_c' b}$$

a = (600*400)/(0.80*35*200) = 50 mm

c = 50/ 0.895= 55.9 mm

Allowable moment redistribution (Clause 9.2.4) = (30-50 c/d)% ≈ 20%

Design load P=125 kN

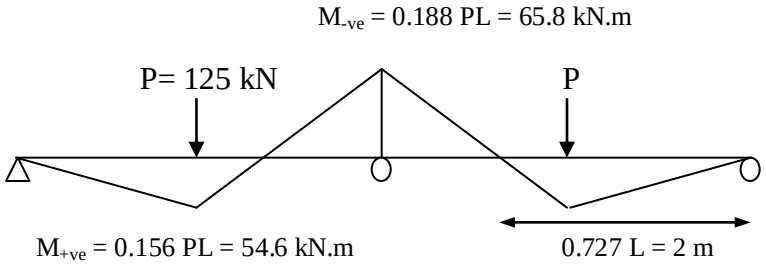

Using 20% redistribution:

M-ve = 0.8 x 65.8= 52.64 kN.m

M+ve = (125*2.8/4) – (52.64/2) = 61.2 kN.m

Section at middle support:

Use 3 No.15M, A_s = 3*200 = 600 mm^2, d = 300-40-16/2 = 252 mm

$M_{u\text{-}ve} = A_s f_y (d - a/2)$ = 600*400*(252-50/2) = **54.5** kN.m

Section at mid span:

Use 4 No.15M, A_s = 4*200 = 800 mm^2, d = (300-40-16/2) = 252 mm

$$a = \beta_1 \, c = \frac{A_s f_y}{\alpha_1 f_c' b}$$

a = 800*400/(0.8*30*200) = 66.7 mm

$Mu_{+ve} = A_s f_y (d - a/2)$ = 800*400*(252-66.7/2) = **70** kN.m

A.2.2. Design for shear

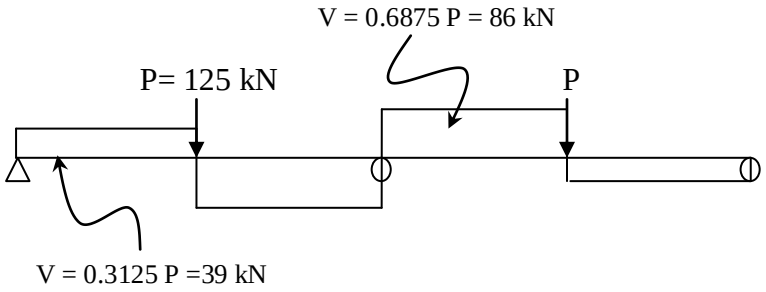

$V_r = V_c + V_s$, and V_r shall not be taken more than $0.25 \, \phi_c \, f_c' \, b_w \, d_v$

$V_r = V_c + V_s < 0.25 \, f_c' \, b_w \, d_v$

d_v = the greater of 0.9 d or 0.72h

= 0.9*252= 226.8 mm or = 0.72*300 = 216 mm

d_v = 226.8 mm

0.25 f_c ' b_w d_v = 0.25*30*200*226.8 = 340.2 kN

According to CSA (2004) clause 11.3.8.1 and clause 11.3.8.3, the maximum transverse spacing should not exceed 600 mm or $0.7d_v$. If the applied shear force exceeds $0.125\ \phi_c\ \lambda\ f_c'\ b_w\ d_v$, the maximum spacing should not exceed 300 mm or $0.35d_v$.

$0.125\ \phi_c\ \lambda\ f_c'\ b_w\ d_v$ = 0.125*1*30*200*226.8 = 170.1 kN > **86** kN (shear force corresponding to section flexural capacity)

Max spacing of stirrups = the less of $0.7d_v$ or 600mm = 0.7*226.8 = 150 mm

According to clause 11.2.8.2, a minimum area of shear reinforcement should be provided if the applied shear force exceeds concrete shear resistance or overall section depth is greater than 750 mm. The minimum shear reinforcement is calculated as follows:

$$A_v = 0.06\ \sqrt{f_c'}\ \frac{b_w\ s}{f_y}$$

$A_{vmin} =\ 0.06\ \sqrt{f_c'}\ \frac{b_w\ s}{f_y}$ = 0.06*$\sqrt{30}$*200*120/330 = 24 mm^2

In lieu of more accurate calculations, and provided that used yield strength of longitudinal steel does not exceed 400 MPa and concrete compressive strength is less than 60 MPa, θ can be taken as 35°. If the section contains the minimum transverse, the factor β can be taken as 0.18, (clause 11.3.6.3).

Clause 11.3.6.3, $\theta = 35°,\ \beta = 0.18$

According to clause 11.3.4 and clause 11.3.5, V_c and V_s can be calculated as follows:

$$V_c = \phi_c \lambda \beta \sqrt{f_c'}\, b_w\, d_v \quad and \quad V_s = \frac{\phi_c\, A_v\, f_y\, d_v\, \cot\theta}{s}$$

$V_c = \lambda \beta \sqrt{f_c'}\, b_w\, d_v$ = 1*0.18*$\sqrt{30}$*200*226.8 = 44.3 7kN

$V_s = \frac{A_v f_y d_v \cot\theta}{s}$, using Ø8 with 120 mm spacing

V_s = 2*50.26*330*226.8*1.43/120= 89.7 kN

V_r = 44.3 + 89.7 = **134.4** kN > 86 kN (shear force corresponding to flexural capacity)

$V_r < V_{r,max}$ =509.625 kN

Adequate shear reinforcement of Ø8 @120 will be provided to avoid shear failure.

A.2.3. Development length:

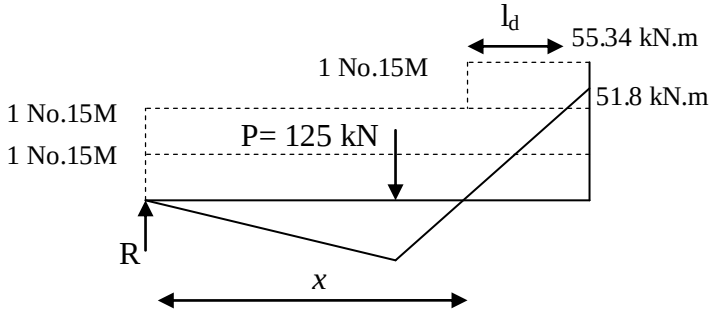

51.8= P*L/2 – R*L → R= 43 kN

∑M = 0 at distance *x* from external support:

R**x* = P (*x*-L/2), → $x = \frac{123*L}{2(123-43)} = 2.15\ m$

Point of zero moment = 2800-2150 = **650** mm from middle support

Point of zero moment for one bar = $650 * \frac{(51.8 - \frac{2}{3}55.34)}{51.8} = 187\ mm$

$$l_d = 0.45 k_1\ k_2\ k_3\ k_4\ \frac{f_y}{\sqrt{f_c'}} d_b \quad \text{(Clause 12.2.3)}$$

$$l_d = 0.45 * 1 * 1 * 1 * 0.8 * \frac{400}{\sqrt{35}} * 16 = 400\ mm$$

Negative reinforcement cut-off length = 400+187= 600 mm (measured form internal support), take = **1000** mm to avoid any bond slippage.

A.3. Design of Specimen GSu-8*d*/2*e*

A.3.1. Design for flexure according to CSA S806-02

According to Clause 8.6.5.1 and 8.6.6.2, design of continuous beams should satisfy the maximum elastic load distribution at critical section and no load redistribution is to be allowed.

As no load redistribution is allowed by code, this specimen will be design using elastic load distribution.

Mu-ve = 65.8 kN.m

Mu+ve= 54.6 kN.m

According to Clause 8.2.1 the failure of flexural element has to be due to concrete crushing rather than rupture of FRP bars.

Failure of section in bending should be due to concrete crunching (Clause 8.2.1).

Section at middle support: M_{design} = 65.8 kN.m

The concrete stress distribution is defined according to Clause 8.4.1.5. A uniform equivalent compressive strength of $\alpha_1 \varphi_c f_c'$ is assumed to be distributed over distance $a = \beta_1 c$.

Where:

$\alpha_1 = 0.85 - 0.0015 \times 30 = 0.8$

$\beta_1 = 0.97 - 0.0025 \times 30 = 0.895$

Using GFRP bars No.16, area = 198 mm^2, maximum tensile strength f_{frpu} = 731 MPa, E_{frp} = 46 GPa, ε_{frpu} = 1.6 %

d = 300-(40+ 15.9/2) = 252 mm

Using 3 No.16 GFRP bars A_{frp} = 594 mm^2:

$\rho = A_s/(b\ d) = (594)/(200*252) = 0.01178$

$$A_f\ E_{frp}\ \varepsilon_{frp} = \alpha_1 f_c' \beta_1\ b\ c \ \ and\ \frac{c}{d} = 0.0035/(0.0035 + \ \varepsilon_{frp})$$

$$f_{frp} = 0.5\ E_{frp}\ \varepsilon_{cu} \left[\left(1 + \frac{4\ \alpha_1\ \beta_1\ f_c'}{\rho_{frp}\ E_{frp}\ \varepsilon_{cu}} \right)^{1/2} - 1 \right]$$

$$= 0.5 * 46000 * 0.0035 \left[\left(1 + \frac{4*0.8*.895*30}{0.01178*46000*0.0035} \right)^{0.5} - 1 \right] = 468.9\ MPa$$

$a = (A_{sfrp}\ f_{frp}) / (\alpha_1\ f_c'\ b) = 594*\ 468.9/\ (0.8*30*200) = 57.66$ mm

$c = a / \beta_1 = 57.66/0.895 = 64.4$ mm

Check concrete strain:

Concrete stain at extreme fibres in compression shall be assumed to reach 0.0035 provided that the ratio $^{c}/_{d}$ satisfies Clause 8.4.1.4 as follows:

$$^{c}/_{d} \geq \frac{7}{7 + 2000\ \epsilon_{Fu}}$$

$$^{c}/_{d} = \frac{64.4}{252} = 0.256\ > \frac{7}{7 + 2000 * 0.016} = 0.179$$

M_{ult} = T (d- a/2) = 594* 468.9 (252-57.66/2) = **62.2** kN.m

Check if minimum reinforcement is provided:

The minimum reinforcement provided in the section should satisfy Clause 8.4.2.1.

$$M_r\ > 1.5\ M_{cr}$$

The cracking moment M_{cr} should be calculate according to Clause 8.3.2.6 as follows:

$$M_{cr} = f_r\ \frac{I_g}{y_t}$$

Concrete modulus of rupture could be taken as stated in Clause 8.5.4.

$$f_r = 0.6\ \lambda\ \sqrt{f_c'}$$

Where λ equals 1 for normal weight concrete.

$$M_{cr} = \ 0.6 * \sqrt{30}\ \frac{200 * 300^3}{12 * 300/2} = 9.9\ kN.m$$

Mr=62.2 kN.m > 1.5*9.9=14.85 kN.m (minimum reinforcement satisfied)

Section at mid span: M_{design} = 54.6 kN.m

Using GFRP bars No.16, area = 198 mm^2, maximum tensile strength f_{frpu} = 731 MPa, E_{frp} = 46 GPa, ε_{frpu} = 1.6 %

d= 300-(40+15.9/2) = 252 mm

Using 2 No.16 A_{frp} = 396 mm^2:

ρ= As/(b d) = 396/(200*252) = 0.00786

$$f_{frp} = 0.5\, E_{frp}\, \varepsilon_{cu} \left[\left(1 + \frac{4\, \alpha_1\, \beta_1\, f_c'}{\rho_{frp}\, E_{frp}\, \varepsilon_{cu}} \right)^{1/2} - 1 \right]$$

$$= 0.5 * 46000 * 0.0035 \left[\left(1 + \frac{4*0.8*.895*30}{0.00786*46000*0.0035} \right)^{0.5} - 1 \right] = 589.9\ MPa$$

Note: f_{frp} = 81% maximum tensile strength f_{frpu}

a = (A_{sfrp} f_{frp}) / (α_1 f_c' b) = 396 * 589.9/ (0.8*30*200) = 48.4 mm

M_{ult} = T (d- (a)/2) = 396 * 589.9*(252 – 48.4/2) = **53.23** kN.m

Check concrete strain:

$$c/d \geq \frac{7}{7 + 2000\, \epsilon_{Fu}}$$

$$c/d = \frac{54}{252} = 0.214 > \frac{7}{7 + 2000 * 0.016} = 0.179$$

Check if minimum reinforcement is provided:

The minimum reinforcement provided in the section should satisfy Clause 8.4.2.1.

$$M_r > 1.5\, M_{cr}$$

$$M_{cr} = 0.6 * \sqrt{30}\ \frac{200 * 300^3}{12 * 300/2} = 9.9\ kN.m$$

Mr=53.23 kN.m > 1.5*9.9=14.48 kN.m (minimum reinforcement satisfied)

A.3.2. Design for shear

V_f = 86 kN (corresponding to section flexure capacity)

The ultimate shear resistance for section reinforced with either FRP or steel stirrups should be calculated according to Clause 8.4.4.4 as follows:

$$V_r = V_c + V_{ss} \quad \leq V_c + 0.8\ \lambda\ \phi_c\ \sqrt{f_c'}\ b_w\ d \qquad (For\ steel\ stirrups)$$

For beams provided with minimum shear reinforcement, shear resistance provided by concrete V_c should be calculated as follows:

$$V_c = 0.035\ \lambda\ \phi_c\ (\ f_c' \rho_w\ E_F\ \frac{V_f}{M_F}\ d\ )^{1/3}\ b_w\ d$$

Provided that V_c satisfies:

$$0.1\ \lambda\ \phi_c\ \sqrt{f_c'}\ b_w\ d\ \leq\ V_c\ \leq 0.2\ \lambda\ \phi_c\ \sqrt{f_c'}\ b_w\ d$$

The term $\frac{V_f}{M_f}\ d$ should not be taken more than 1.

$$V_c = 0.035\ (\ f_c' \rho_w\ E_F\ \frac{V_f}{M_F}\ d\ )^{1/3}\ b_w\ d$$

$\frac{V_f}{M_F} d$=(86/65.8)*0.252 = 0.33

= 0.035*(30*0.01178 *46000*0.33)$^{1/3}$ 200*252 = 30 kN

$0.1\sqrt{f_c'}\,b_w\,d$ = 0.1$\sqrt{30}$*200*252 = 27.6kN

$0.2\sqrt{f_c'}\,b_w\,d$ = 0.2$\sqrt{35}$*200*252 = 59.634 kN

Take V_c = 30 kN

The shear resistance of steel stirrups V_{ss} should be calculated according to Clause 8.4.4.6 as follows:

$$V_{ss} = \frac{\phi_s A_v f_y d}{s}$$

$V_{ss} = \frac{A_v f_y d}{s}$ = 2*50.26*330*252/120 = 69.66 kN < $0.8\sqrt{f_c'}\,b_w\,d$ ok

$0.8\sqrt{f_c'}\,b_w\,d$ = 0.8$\sqrt{30}$*200*252 = 220.8 kN

V_r = 30 + 69.66 = 99.66 > V_f

Use same steel stirrups as in SSc-8*d*/2*p* (Ø8 @120)

A.3.3. Development length

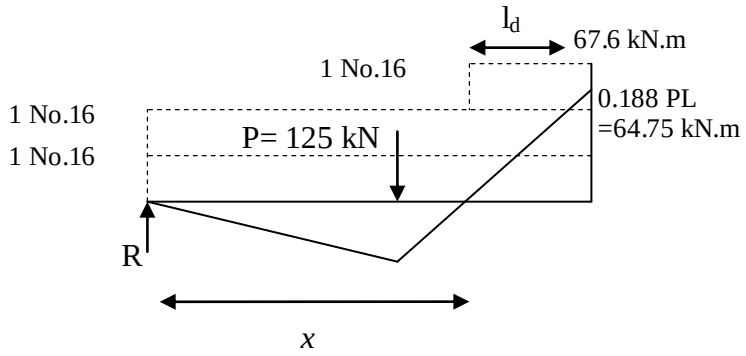

0.188PL= P*L/2 – R*L → R= 0.312 P

∑M = 0 at distance *x* from external support:

R**x* = P (*x*-L/2), $\rightarrow x = \frac{L}{2(1-0.312)} = 0.727\ L$

Point of zero moment = (1-0.727)*2800 = **800** mm from middle support

Point of zero moment for one bar = $800 * \frac{(64.75-\frac{2}{3}67.6)}{64.75} = 243.2\ mm$

$l_d = 1.15\ \frac{k_1\ k_2\ k_3\ k_4\ k_5}{d_{cs}}\ \frac{f_f}{\sqrt{f_c'}} A_b$ (clause 9.3.2)

$l_d = 1.15\ \frac{1*1*0.8*1*1}{35} * \frac{505.2}{\sqrt{35}} * 198 = 444.4\ mm$

Negative reinforcement cut-off length = 444.4+243. 2=700 mm (measured form internal support), take = **1000** mm to avoid bond slippage failure.

A.3.4. Service conditions

Due to the low modulus of elasticity of GFRP reinforcement compared to steel bars, the serviceability limitation usually govern the design. Thus it is importance to identify the status of the designed specimen under service load.

The beams will be tested up to ultimate capacity, however, for comparison purpose the service load acting on FRP-reinforced beams will be taken as the reference steel-reinforced beam. There is rational description for service loading level indicated in most design codes. The service load will be considered as the load developing 60% of yielding stress in longitudinal steel reinforcement at middle support of reference beam SSc-8*d*/2*p*.

Assuming that stress in concrete will not exceed 70% of f_c', triangulate stress distribution in concrete compression zone will be used:

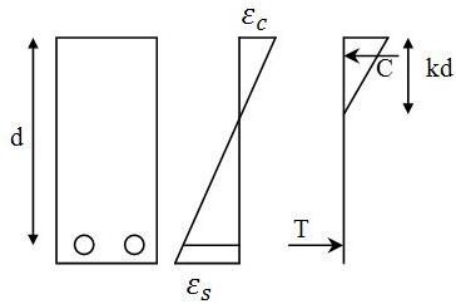

n= $\frac{E_s}{E_c} = \frac{200000}{4500\sqrt{30}} = 8.1$, ρ= 3*200/200/252= 0.0119

k= $\sqrt{2\rho\, n + (\rho n)^2} - \rho n = \sqrt{2 * 0.0119 * 8.1 + (0.0119 * 8.1)^2} - 0.0119 * 8.1 = 0.35$

kd = 0.35*252=89mm

$\varepsilon_c = \frac{kd}{d(1-k)} * \varepsilon_s = \frac{89}{252(1-0.35)} * \frac{400*0.6}{200000} = 0.000652$

$f_c = E_c * \varepsilon_c = 4500\sqrt{30} * 0.000652 = 16.1\ MPa\ \leq \quad 0.7f_c' = 21\ MPa$

$M_{ser} = A_s * 0.6\ f_y\ d\left(1 - \frac{k}{3}\right) = 600 * 0.6 * 400 * 252 * \left(1 - \frac{0.34}{3}\right) = 32.175\ kN.m$

$P_{ser} = \frac{M_{ser}}{0.188*L} = \frac{32.175}{0.188*2.8} = \mathbf{61.123}\ kN$

Check deflection at mid-span:

n= $\frac{E_{frp}}{E_c} = \frac{46000}{4500\sqrt{35}} = 1.728$, ρ= 2*198/(200*252)= 0.00786

k= $\sqrt{2\rho\, n + (\rho n)^2} - \rho n = \sqrt{2 * 0.0079 * 1.73 + (0.0079 * 1.73)^2} - 0.0079 * 1.73 = 0.15$

$I_{cr} = \frac{bd^3}{3}k^3 + n\,A_f d^2(1-k)^2 = \frac{200(252)^3}{3}0.15^3 + 1.73 * 396 * 252^2(1-0.15)^2$

= 35 033 270.73 mm^4

To calculate effective moment of inertia, I_e, reduction factor β_d will be used as follows:

$$I_e = \left(\frac{M_{cr}}{M_a}\right)^3 \beta\, I_g + \left[1 - \left(\frac{M_{cr}}{M_a}\right)^3\right] I_{cr} \quad and\ \ \beta = \alpha_d \left[\frac{E_{frp}}{E_s} + 1\right]$$

Using recommended value α_d=0.5

β=0.5 $\left[\frac{46000}{200000} + 1\right] = 0.62$

$$I_e = \left(\frac{10.65}{32.175}\right)^3 0.62 * \ 0.2 * \frac{0.3^3}{12} + \left[1 - \left(\frac{10.65}{32.175}\right)^3\right] * 3.5(10)^{-5} = 4.38(10)^{-5}\ m^4$$

For propped cantilever with point load at mid-span:

$$\Delta = \frac{7}{768}\frac{PL^3}{EI} = \frac{7}{768}\frac{61.123 * (2.8)^3}{EI_e} = 10.5\ mm \ > \frac{L}{360} = 7.78\ mm$$

Hence, the design is based on comparing ultimate load capacity with reference beam rather than satisfying serviceability.

A.4. Design of Specimen GSu-8*d*/2*p*

This beam is designed to study capability of GFRP-reinforced continuous beams to redistribute elastic bending moments. Using the same design load, P, of beams SSc-8*d*/2*p* and GSu-8*d*/2*p*, specimen GSu-8*d*/2*e* is designed assuming 20% redistribution of elastic moments.

A.4.1. Design for flexure

Assuming 20% redistribution:

M-ve = 0.8 x 65.8 = 52.64 kN.m

M+ve = (125*2.8/4) – (52.64/2) = 61.2 kN.m

Section at middle support: M_{design} = 52.64 kN.m

Using GFRP bars No.16, area = 198 mm^2, maximum tensile strength f_{frpu} = 731 MPa, E_{frp} = 46 GPa, ε_{frpu} = 1.6 %

d= 300-(40+15.9/2) = 252mm

Using 2 No.16, A_{frp}= 396 mm^2:

ρ= As/(b d) = 396/(200*252) = 0.00786

$$f_{frp} = 0.5\ E_{frp}\ \varepsilon_{cu} \left[\left(1 + \frac{4\ \alpha_1\ \beta_1\ f_c'}{\rho_{frp}\ E_{frp}\ \varepsilon_{cu}} \right)^{1/2} - 1 \right]$$

$$= 0.5 * 46000 * 0.0035 \left[\left(1 + \frac{4 * 0.8 * .895 * 30}{0.00786 * 46000 * 0.0035} \right)^{0.5} - 1 \right] = 589.9\ MPa$$

Note: f_{frp} = 81% maximum tensile strength f_{frpu}

a = (A_{sfrp} f_{frp}) / (α_1 f_c' b) = 396 * 589.9/ (0.8*30*200) = 48.4 mm

$\mathbf{M_{ult}}$ = T (d- (a)/2) = 396 * 589.9 *(252 – 48.4/2) = **53.23** kN.m

Check concrete strain:

$$c/d \geq \frac{7}{7 + 2000\ \epsilon_{Fu}}$$

$$c/d = \frac{54}{252} = 0.214 > \frac{7}{7 + 2000 * 0.016} = 0.179$$

Check if minimum reinforcement is provided:

The minimum reinforcement provided in the section should satisfy Clause 8.4.2.1.

$$M_r > 1.5\, M_{cr}$$

$$M_{cr} = 0.6 * \sqrt{30}\, \frac{200 * 300^3}{12 * 300/2} = 9.9\ kN.m$$

M_r=53.23 kN.m > 1.5*9.9=14.48 kN.m (minimum reinforcement satisfied)

Section at mid span: M_{design} = 61.2 kN.m

Using GFRP bars No.16, area = 198 mm^2, maximum tensile strength f_{frpu} = 731 MPa, E_{frp} = 46 GPa, ε_{frpu} = 1.6 %

d = 300-(40+15.9/2) = 252 mm

Using 3 No.16, A_{frp} = 594 mm^2:

ρ= As/(b d) = 3*198/(200*252) = 0.01178

$$f_{frp} = 0.5\, E_{frp}\, \varepsilon_{cu} \left[\left(1 + \frac{4\, \alpha_1\, \beta_1\, f_c'}{\rho_{frp}\, E_{frp}\, \varepsilon_{cu}} \right)^{1/2} - 1 \right]$$

$$= 0.5 * 46000 * 0.0035 \left[\left(1 + \frac{4 * 0.8 * .895 * 30}{0.01178 * 46000 * 0.0035} \right)^{0.5} - 1 \right] = 468.9\ MPa$$

a = (A_{sfrp} f_{frp}) / (α_1 f_c' b) = 3(198) * 468.9/ (0.8*30*200) = 57.66 mm

M_{ult} = T (d- (a)/2) = 3(198)*468.9*(252-57.66/2) = **62.2** kN.m

Check concrete strain:

$$c/d \geq \frac{7}{7 + 2000\ \epsilon_{Fu}}$$

$$c/d = \frac{60.9}{252} = 0.24\ > \frac{7}{7 + 2000 * 0.016} = 0.179$$

Check if minimum reinforcement is provided:

The minimum reinforcement provided in the section should satisfy Clause 8.4.2.1.

$$M_r\ > 1.5\ M_{cr}$$

$$M_{cr} = \ 0.6 * \sqrt{35}\ \frac{200 * 300^3}{12 * 300/2} = 10.65\ kN.m$$

Mr=**67.6** kN.m > 1.5*10.65=15.97 kN.m (minimum reinforcement satisfied)

A.4.2. Design for shear

V_f = 86 kN (corresponding to section flexure capacity)

Clause 8.4.4.4:

$$V_r = \ V_c + \ V_{ss} \quad \leq \ V_c + \ 0.8\ \lambda\ \phi_c\ \sqrt{f_c'}\ b_w\ d \qquad (For\ steel\ stirrups)$$

For beams provided with minimum shear reinforcement, shear resistance provided by concrete V_c should be calculated as follows:

$$V_c = 0.035\ \lambda\ \phi_c\ (\ f_c' \rho_w\ E_F\ \frac{V_f}{M_F}\ d\ )^{1/3}\ b_w\ d$$

Provided that V_c satisfies:

$$0.1\ \lambda\ \phi_c\ \sqrt{f_c'}\ b_w\ d\ \leq\ V_c\ \leq 0.2\ \lambda\ \phi_c\ \sqrt{f_c'}\ b_w\ d$$

The term $\frac{V_f}{M_f}\ d$ should not be taken more than 1.

$V_c = 0.035\ (\ f_c'\rho_w\ E_F\ \frac{V_f}{M_F}\ d\ )^{1/3}\ b_w\ d$

$\frac{V_f}{M_F}\ d$=(86/52.64)*0.252 = 0.41

= 0.035*(30*0.0078 *46000*0.41)$^{1/3}$ 200*252 = 29 kN

$0.1\ \sqrt{f_c'}\ b_w\ d$ = $0.1\sqrt{30}$*200*252 = 27.6 kN

$0.2\ \sqrt{f_c'}\ b_w\ d$ = $0.2\sqrt{30}$*200*252 = 55.2 kN

Take V_c = 29 kN

Clause 8.4.4.6:

$V_{ss} = \frac{A_v\ f_y\ d}{s}$ = 2*50.26*330*252/120 = 69.66 kN < $0.8\ \sqrt{f_c'}\ b_w\ d$ ok

$0.8\ \sqrt{f_c'}\ b_w\ d$ = $0.8\sqrt{30}$*200*252 = 220.8 kN

V_r = 29 + 69.66 = 98.66 > V_f

Use same steel stirrups as in GSu-8*d*/2*p* (Ø8 @120)

A.5. Design of Specimen CSu-8*d*/2*p*

This beam is reinforced with CFRP bars to study the effect of longitudinal reinforcing material. The beam is similarly designed as beams GSu-8*d*/2*e* assuming 20% redistribution of elastic moments.

A.5.1. Design for flexure

Assuming 20% redistribution:

M-ve = 0.8 x 65.8 = 52.64 kN.m

M+ve = (125*2.8/4) – (52.64/2) = 61.2 kN.m

Section at middle support: M_{design} = 52.64 kN.m

$\alpha_1 = 0.85 – 0.0015 \times 30 = 0.8$

$\beta_1 = 0.97 – 0.0025 \times 30 = 0.895$

Using CFRP bars No.3, area = 71 mm, guaranteed tensile strength f_{frpu} = 1596 MPa, E_{frp} = 124 GPa, ε_{frpu} = 1.4 %

d= 300-(40+9.5/2) = 255 mm

Using 3 No.3 CFRP bars, A_{frp} = 213 mm^2:

ρ= As/(b d) = 213.78/(200*255) = 0.0042

$$f_{frp} = 0.5\, E_{frp}\, \varepsilon_{cu} \left[\left(1 + \frac{4\, \alpha_1\, \beta_1\, f_c'}{\rho_{frp}\, E_{frp}\, \varepsilon_{cu}} \right)^{1/2} - 1 \right]$$

$$= 0.5 * 124000 * 0.0035 \left[\left(1 + \frac{4 * 0.8 * .88 * 35}{0.0042 * 124000 * 0.0035} \right)^{0.5} - 1 \right] = 1398.3\ MPa$$

Note: f_{frp} = 87% maximum tensile strength f_{frpu}

a = (A_{sfrp} f_{frp}) / (α_1 f_c' b) = 213 * 1398.3/ (0.8*35*200) = 53.35 mm

M_{ult} = T (d- (a)/2) = 213 * 1398.3*(255 – 53.35/2) = **68.1** kN.m

Check concrete strain:

$$c/d \geq \frac{7}{7 + 2000\ \epsilon_{Fu}}$$

$$c/d = \frac{60.45}{255} = 0.24 > \frac{7}{7 + 2000 * 0.014} = 0.2$$

Check if minimum reinforcement is provided:

The minimum reinforcement provided in the section should satisfy Clause 8.4.2.1.

$$M_r > 1.5\ M_{cr}$$

$$M_{cr} = 0.6 * \sqrt{35}\ \frac{200 * 300^3}{12 * 300/2} = 10.65\ kN.m$$

M_r = 68.1 kN.m > 1.5*10.65=15.98 kN.m (minimum reinforcement satisfied)

Section at mid span: M_{design} = 60.2 kN.m

Using CFRP bars No.3, area = 71 mm, guaranteed tensile strength f_{frpu} = 1596 MPa, E_{frp} = 124 GPa, ε_{frpu} = 1.4 %

d = 300-(40+ 12.7/2) = 255 mm

Using 3 No.3 CFRP bars A_{frp} = 213 mm^2:

ρ= A_s/(b d) = (213.78)/(200*255) = 0.0042

$$A_f\ E_{frp}\ \varepsilon_{frp} = \alpha_1 f_c' \beta_1\ b\ c\ \ and\ \frac{c}{d} = 0.0035/(0.0035 + \varepsilon_{frp})$$

$$f_{frp} = 0.5\, E_{frp}\, \varepsilon_{cu} \left[\left(1 + \frac{4\, \alpha_1\, \beta_1\, f_c'}{\rho_{frp}\, E_{frp}\, \varepsilon_{cu}} \right)^{1/2} - 1 \right]$$

$$= 0.5 * 124000 * 0.0035 \left[\left(1 + \frac{4 * 0.8\ * .88 * 35}{0.0042 * 124000 * 0.0035} \right)^{0.5} - 1 \right] = 1398.3\ MPa$$

a = (A_{sfrp} f_{frp}) / (α_1 f_c' b) = 213* 1398.3/ (0.8*35*200) = 53.35 mm

c = a / β_1 = 53.35/0.88 = 60.45 mm

Check concrete strain:

Concrete stain at extreme fibres in compression shall be assumed to reach 0.0035 provided that the ratio c/d satisfies Clause 8.4.1.4 as follows:

$$c/d \geq \frac{7}{7 + 2000\, \epsilon_{Fu}}$$

$$c/d = \frac{60.45}{255} = 0.24\ > \frac{7}{7 + 2000 * 0.014} = 0.2$$

M_{ult} = T (d- a/2) = 213* 1398.3 (255-53.35/2) = **68.1** kN.m

Check if minimum reinforcement is provided:

The minimum reinforcement provided in the section should satisfy Clause 8.4.2.1.

$$M_r\ > 1.5\, M_{cr}$$

The cracking moment M_{cr} should be calculate according to Clause 8.3.2.6 as follows:

$$M_{cr} = f_r\, \frac{I_g}{y_t}$$

Concrete modulus of rupture could be taken as stated in Clause 8.5.4.

$$f_r = 0.6\,\lambda\sqrt{f_c'}$$

Where λ equals 1 for normal weight concrete.

$$M_{cr} = 0.6 * \sqrt{35}\,\frac{200 * 300^3}{12 * 300/2} = 10.65\ kN.m$$

Mr=68.1 kN.m > 1.5*10.65=15.97 kN.m (minimum reinforcement satisfied)

A.5.2. Design for shear

Same amount of steel stirrups will be used as specimen GSu-8*d*/2*e*.

A.6. Design of specimen CSu-8*d*/2*e*

This beam is designed to study the effect of reinforcement configuration on CFRP-reinforced continuous beams. The design load is the same as previous tested four beams (P=125 kN). The reinforcement configuration in this beam (CSu-8*d*/2*e*) satisfies the elastic bending moment distribution to be compared with the tested beam CSu-8*d*/2*p* which was designed assuming 20% moment redistribution. To isolate the effect of reinforcement configuration, the same steel stirrups diameter and spacing will be used in this beam.

A.6.1. Design for flexure according to CSA S806-02

According to Clause 8.6.5.1 and 8.6.6.2, design of continuous beams should satisfy the maximum elastic load distribution at critical section and no load redistribution is to be allowed.

As no load redistribution is allowed by code, this specimen will be design using elastic load distribution.

Design load = 125 kN

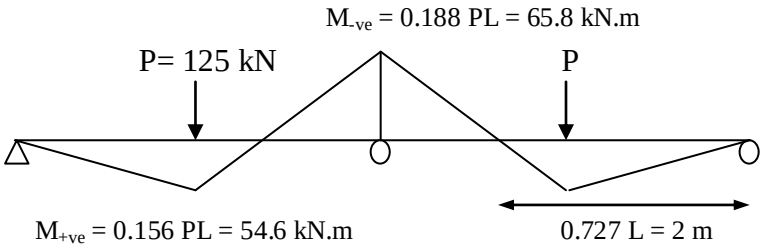

Mu_{-ve} = 65.8 kN.m

Mu_{+ve}= 54.6 kN.m

Failure of section in bending should be due to concrete crunching (Clause 8.2.1).

Section at middle support: M_{design} = 65.8 kN.m

The concrete stress distribution is defined according to Clause 8.4.1.5. A uniform equivalent compressive strength of $\alpha_1 \varphi_c f_c'$is assumed to be distributed over distance $a = \beta_1 c$.

Where:

α_1 = 0.85 – 0.0015 x 30 = 0.805

β_1 = 0.97 – 0.0025 x 30 = 0.895

Using CFRP bars No.3, bar diameter = 9.5 mm, area = 71 mm, guaranteed tensile strength f_{frpu} = 1388 MPa, E_{frp} = 116 GPa, ε_{frpu} = 1.2 %

d = 300-(40+ 9.5/2) = 255.25 mm

Using 4 No.3 CFRP bars A_{frp} = 284 mm^2:

ρ= A_s/(b d) = (284)/(200*255.25) = 0.00556

$$A_f\ E_{frp}\ \varepsilon_{frp}\ = \alpha_1 f_c' \beta_1\ b\ c\ \ and\ \frac{c}{d} = 0.0035/(0.0035 + \ \varepsilon_{frp})$$

$$f_{frp} = 0.5\ E_{frp}\ \varepsilon_{cu}\left[\left(1 + \frac{4\ \alpha_1\ \beta_1\ f_c'}{\rho_{frp}\ E_{frp}\ \varepsilon_{cu}}\right)^{1/2} - 1\right]$$

$$= 0.5 * 116000 * 0.0035\left[\left(1 + \frac{4*0.805*.895*30}{0.00556*116000*0.0035}\right)^{0.5} - 1\right] = 1069.25\ MPa$$

a = (A_{sfrp} f_{frp}) / (α_1 f_c' b) = 284* 1069.6/ (0.805*30*200) = 62.9 mm

c = a / β_1 = 62.9/0.895 = 70.3 mm

Check concrete strain:

Concrete stain at extreme fibres in compression shall be assumed to reach 0.0035 provided that the ratio c/d satisfies Clause 8.4.1.4 as follows:

$$c/d \geq \frac{7}{7 + 2000\ \epsilon_{Fu}}$$

$$c/d = \frac{70.3}{255.25} = 0.275\ > \frac{7}{7 + 2000 * 0.012} = 0.226$$

M_{ult} = T (d- a/2) = 284* 1069.25 (255.25-62.9/2) = **67.96** kN.m > 65.8 kN.m

Check if minimum reinforcement is provided:

The minimum reinforcement provided in the section should satisfy Clause 8.4.2.1.

$$M_r\ > 1.5\ M_{cr}$$

The cracking moment M_{cr} should be calculate according to Clause 8.3.2.6 as follows:

$$M_{cr} = f_r \frac{I_g}{y_t}$$

Concrete modulus of rupture could be taken as stated in Clause 8.5.4.

$$f_r = 0.6\,\lambda\sqrt{f_c'}$$

Where λ equals 1 for normal weight concrete.

$$M_{cr} = 0.6 * \sqrt{30}\ \frac{200 * 300^3}{12 * 300/2} = 9.86\ kN.m$$

Mr=67.6 kN.m > 1.5*9.86=14.8 kN.m (minimum reinforcement satisfied)

Section at mid span: M_{design} = 54.6 kN.m

Using CFRP bars No.3, bar diameter = 9.5 mm, area = 71 mm, guaranteed tensile strength f_{frpu} = 1388 MPa, E_{frp} = 116 GPa, ε_{frpu} = 1.2 %

d = 300-(40+ 9.5/2) = 255.25 mm

Using 3 No.3 CFRP bars A_{frp} = 213 mm^2:

ρ= As/(b d) = 213/(200*255.25) = 0.004172

$$f_{frp} = 0.5\,E_{frp}\,\varepsilon_{cu}\left[\left(1 + \frac{4\,\alpha_1\,\beta_1\,f_c'}{\rho_{frp}\,E_{frp}\,\varepsilon_{cu}}\right)^{1/2} - 1\right]$$

$$= 0.5 * 116000 * 0.0035\left[\left(1 + \frac{4 * 0.805 * .895 * 30}{0.004172 * 116000 * 0.0035}\right)^{0.5} - 1\right] = 1261.4\ MPa$$

Note: f_{frp} = 91% maximum tensile strength f_{frpu}

$a = (A_{sfrp}\ f_{frp}) / (\alpha_1\ f_c'\ b) = 213 * 1261.4/ (0.805*30*200) = 55.63$ mm

$\mathbf{M_{ult}} = T (d- (a)/2) = 213 * 1261.4*(255.25 – 55.63/2) =$ **61.1** kN.m > 54.6 kN.m

Check concrete strain: $c = a / \beta_1 = 55.63/0.895 = 62.156$ mm

$$^{c}/_{d} \geq \frac{7}{7 + 2000\ \epsilon_{Fu}}$$

$$^{c}/_{d} = \frac{62.156}{255.25} = 0.243\ > \frac{7}{7 + 2000 * 0.012} = 0.226$$

Check if minimum reinforcement is provided:

The minimum reinforcement provided in the section should satisfy Clause 8.4.2.1.

$$M_r\ > 1.5\ M_{cr}$$

$$M_{cr} =\ 0.6 * \sqrt{30}\ \frac{200 * 300^3}{12 * 300/2} = 9.86\ kN.m$$

Mr=61.1 kN.m > 1.5*9.86=14.8 kN.m (minimum reinforcement satisfied)

A.6.2. Design for shear

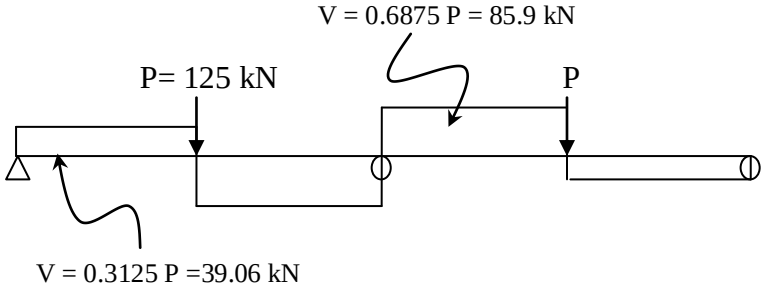

Expected failure load according to the provided reinforcement:

M_{+ve} = PL/4 – M_{-ve} /2 → 61.1= P*2.8/4 - 67.96/2

P= 135.8 kN

V_f = 93.4 kN (corresponding to section flexure capacity)

The ultimate shear resistance for section reinforced with either FRP or steel stirrups should be calculated according to Clause 8.4.4.4 as follows:

$$V_r = V_c + V_{ss} \leq V_c + 0.8\,\lambda\,\phi_c\,\sqrt{f_c'}\,b_w\,d \qquad (For\ steel\ stirrups)$$

For beams provided with minimum shear reinforcement, shear resistance provided by concrete V_c should be calculated as follows:

$$V_c = 0.035\,\lambda\,\phi_c\,(\,f_c'\rho_w\,E_F\,\frac{V_f}{M_F}\,d\,)^{1/3}\,b_w\,d$$

Provided that V_c satisfies:

$$0.1\,\lambda\,\phi_c\,\sqrt{f_c'}\,b_w\,d \leq V_c \leq 0.2\,\lambda\,\phi_c\,\sqrt{f_c'}\,b_w\,d$$

The term $\frac{V_f}{M_f}\,d$ should not be taken more than 1.

$$V_c = 0.035\,(\,f_c'\rho_w\,E_F\,\frac{V_f}{M_F}\,d\,)^{1/3}\,b_w\,d$$

$\frac{V_f}{M_F}d$=(93.4/67.96)*0.25525 = 0.35

= 0.035*(30*0.004172 *116000*0.35)$^{1/3}$ 200*255.25 = 30.7 kN

$0.1\sqrt{f_c'}\,b_w\,d$ = 0.1$\sqrt{30}$*200*255.25 = 27.96 kN

$0.2\sqrt{f_c'}\,b_w\,d$ = 0.2$\sqrt{30}$*200*255.25 = 55.92 kN

Take V_c = 30.7 kN

The shear resistance of steel stirrups V_{ss} should be calculated according to Clause 8.4.4.6 as follows:

$V_{ss} = \frac{A_v\,f_y\,d}{s}$ = 2*49.48*300*255.25/120 = 63.15 kN < $0.8\sqrt{f_c'}\,b_w\,d$ ok

$0.8\sqrt{f_c'}\,b_w\,d$ = 0.8$\sqrt{30}$*200*255.25 = 223.7 kN

V_r = 30.7 + 63.15 = 93.85 > V_f (93.4 kN)

Use same steel stirrups as in CSu-8*d*/2*p* (Ø8 @120)

A.6.3. Development length

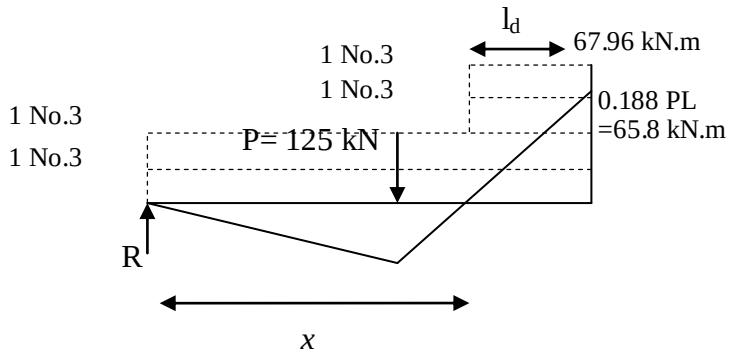

0.188PL= P*L/2 – R*L → R= 0.312 P

∑M = 0 at distance *x* from external support:

R**x* = P (*x*-L/2), $\rightarrow x = \frac{L}{2(1-0.312)} = 0.727\ L$

Point of zero moment = (1-0.727)*2800 = **800** mm from middle support

Point of zero moment for one bar = $800 * \frac{(65.8-\frac{1}{2}67.96)}{65.8} = 386.9\ mm$

$l_d = 1.15\ \frac{k_1\ k_2\ k_3\ k_4\ k_5}{d_{cs}}\ \frac{f_f}{\sqrt{f_c'}} A_b$ (clause 9.3.2)

$l_d = 1.15\ \frac{1*1*0.8*1*1}{\left(\frac{2}{3}\right)*38.17} * \frac{1069.25}{\sqrt{30}} * 71 = 501.1\ mm$

Negative reinforcement cut-off length = 501.1+386.9=888 mm (measured form internal support), take = **1300** mm to avoid bond slippage failure.

A.7. Design of Specimen GGu-10*d*/2*p*

This beam is designed to study the effect of shear reinforcement material. The same longitudinal reinforcement configuration will be used as the tested beam GSu-8*d*/2*p*. GFRP stirrups will be used to provide equivalent shear capacity as steel stirrups in beam GSu-8*d*/2*p*.

A.7.1. Design for flexure

Same as beam GSu-8*d*/2*p*

M-ve = 0.8 x 65.8 = 52.64 kN.m

M+ve = (125*2.8/4) – (52.64/2) = 61.18 kN.m

Section at middle support: M_{design} = 52.64 kN.m

Using GFRP bars No.16, area = 198 mm^2, maximum tensile strength f_{frpu} = 731 MPa, E_{frp} = 46 GPa, ε_{frpu} = 1.6 %

d= 300-(40+15.9/2) = 252mm

Using 2 No.16, A_{frp}= 396 mm^2:

ρ= As/(b d) = 396/(200*252) = 0.00786

$$f_{frp} = 0.5\ E_{frp}\ \varepsilon_{cu} \left[\left(1 + \frac{4\ \alpha_1\ \beta_1\ f_c'}{\rho_{frp}\ E_{frp}\ \varepsilon_{cu}} \right)^{1/2} - 1 \right]$$

$$= 0.5 * 46000 * 0.0035 \left[\left(1 + \frac{4 * 0.805 * .895 * 30}{0.00786 * 46000 * 0.0035} \right)^{0.5} - 1 \right] = 589.9\ MPa$$

Note: f_{frp} = 81% maximum tensile strength f_{frpu}

a = (A_{sfrp} f_{frp}) / (α_1 f_c' b) = 396 * 589.9/ (0.805*30*200) = 48.4 mm

M_{ult} = T (d- (a)/2) = 396 * 589.9*(252 – 48.4/2) = **53.2** kN.m

Check concrete strain:

$$c/d \geq \frac{7}{7 + 2000\ \epsilon_{Fu}}$$

$$c/d = \frac{54}{252} = 0.214 > \frac{7}{7 + 2000 * 0.016} = 0.179$$

Check if minimum reinforcement is provided:

The minimum reinforcement provided in the section should satisfy Clause 8.4.2.1.

$$M_r > 1.5\ M_{cr}$$

$$M_{cr} = 0.6 * \sqrt{30}\ \frac{200 * 300^3}{12 * 300/2} = 9.86\ kN.m$$

M_r=57.7 kN.m > 1.5*9.89=14.8 kN.m (minimum reinforcement satisfied)

Section at mid span: M_{design} = 61.18 kN.m

Using GFRP bars No.16, area = 198 mm^2, maximum tensile strength f_{frpu} = 731 MPa, E_{frp} = 46 GPa, ε_{frpu} = 1.6 %

d = 300-(40+15.9/2) = 252 mm

Using 3 No.16, A_{frp} = 594 mm^2:

ρ= As/(b d) = 3*198/(200*252) = 0.01178

$$f_{frp} = 0.5\ E_{frp}\ \varepsilon_{cu} \left[\left(1 + \frac{4\ \alpha_1\ \beta_1\ f_c'}{\rho_{frp}\ E_{frp}\ \varepsilon_{cu}} \right)^{1/2} - 1 \right]$$

$$= 0.5 * 46000 * 0.0035 \left[\left(1 + \frac{4 * 0.805 * .895 * 30}{0.01178 * 46000 * 0.0035} \right)^{0.5} - 1 \right] = 468.8\ MPa$$

a = (A_{sfrp} f_{frp}) / (α_1 f_c' b) = 3(198) * 468.8/ (0.805*30*200) = 57.66 mm

$\mathbf{M_{ult}}$ = T (d- (a)/2) = 3(198)*468.8*(252-57.66/2) = **62.2** kN.m

Check concrete strain:

$$c/d \geq \frac{7}{7 + 2000\ \epsilon_{Fu}}$$

$$c/d = \frac{64.4}{252} = 0.2556 > \frac{7}{7 + 2000 * 0.016} = 0.179$$

Check if minimum reinforcement is provided:

The minimum reinforcement provided in the section should satisfy Clause 8.4.2.1.

$$M_r > 1.5\, M_{cr}$$

$$M_{cr} = 0.6 * \sqrt{30}\, \frac{200 * 300^3}{12 * 300/2} = 9.86\ kN.m$$

Mr=**62.2** kN.m > 1.5*9.86=14.8 kN.m (minimum reinforcement satisfied)

A.7.2. Design for shear

Expected failure load according to the provided reinforcement:

M_{+ve} = PL/4 – M_{-ve} /2 → 62.2= P*2.8/4 – 53.2/2

P= 126.9 kN

V_f = 0.6875* 126.9 = 87.24 kN (corresponding to section flexure capacity)

Clause 8.4.4.4:

$$V_r = V_c + V_{ss} \leq V_c + 0.6\, \lambda\, \phi_c \sqrt{f_c'}\, b_w\, d \qquad (For\ FRP\ stirrups)$$

For beams provided with minimum shear reinforcement, shear resistance provided by concrete V_c should be calculated as follows:

$$V_c = 0.035\, \lambda\, \phi_c\, (\, f_c' \rho_w\, E_F\, \frac{V_f}{M_F}\, d\,)^{1/3}\, b_w\, d$$

Provided that V_c satisfies:

$$0.1\, \lambda\, \phi_c \sqrt{f_c'}\, b_w\, d \leq V_c \leq 0.2\, \lambda\, \phi_c \sqrt{f_c'}\, b_w\, d$$

The term $\frac{V_f}{M_f}\, d$ should not be taken more than 1.

$V_c = 0.035\ (\ f_c' \rho_w\ E_F\ \frac{V_f}{M_F}\ d\ )^{1/3}\ b_w\ d$

$\frac{V_f}{M_F} d$=(87.24/62.2)*0.252 = 0.35

= 0.035*(30*0.0078 *46000*0.41)$^{1/3}$ 200*252 = 28.7 kN

0.1 $\sqrt{f_c'}\ b_w\ d$ = 0.1$\sqrt{30}$*200*252 = 27.6 kN

0.2 $\sqrt{f_c'}\ b_w\ d$ = 0.2$\sqrt{30}$*200*252 = 55.2 kN

Take V_c = 28.7 kN

Clause 8.4.4.6: using No.10 GFRP @ 120, A= 71.3 mm^2, f_{fu}= 0.7*856 = 600 MPa

$V_{sf} = \frac{0.4\ A_v\ f_{fu}\ d}{s}$ = 0.4*2*71.3*600*252/120 = 71.87 kN < 0.8 $\sqrt{f_c'}\ b_w\ d$ ok

0.6 $\sqrt{f_c'}\ b_w\ d$ = 0.6$\sqrt{30}$*200*252 = 165.6 kN

V_r = 28.7 + 71.87 = **101.69** > V_f

A.8. Design of Specimens GSu-8*d*/3*p*, GSu-10*d*/2*p* and GGu-10*d*/3*p* According to CSA S806-02

A.8.1. Design for flexure

These beams are designed to study the effect of shear reinforcement spacing, diameter and material on GFRP-reinforced continuous beams. The design load is the same as previous tested beams (P=125 kN). The flexural reinforcement provided in these three beams is similar to beam GSu-8*d*/2*p* (already tested) which was designed assuming 20% moment redistribution. The same flexural reinforcement is used (2 No.16 and 3 No.16 GFRP bars at the top and bottom side respectively) in order to isolate the effect of shear reinforcement.

A.8.2. Design for shear

A.8.2.1. Beam GSu-8*d*/3*p*

This beam is designed to study the effect of steel stirrups spacing on GFRP-reinforced continuous beams. Beam GSu-8*d*/2*p* had ϕ8@120 steel stirrups. This beam will used the same steel stirrup diameter while using less spacing.

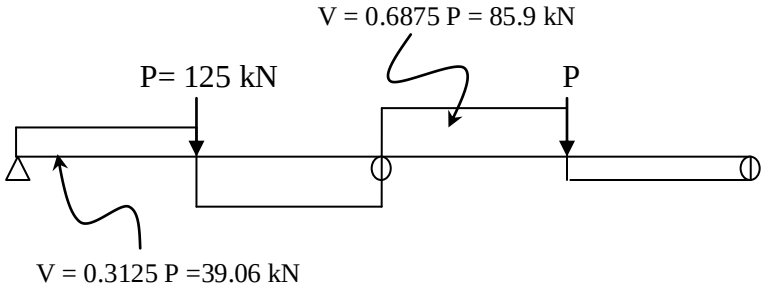

Expected failure load according to the provided reinforcement:

V_f = 85.9 kN

The ultimate shear resistance for section reinforced with either FRP or steel stirrups should be calculated according to Clause 8.4.4.4 as follows:

$$V_r = V_c + V_{ss} \leq V_c + 0.8\,\lambda\,\phi_c\,\sqrt{f_c'}\,b_w\,d \qquad (For\ steel\ stirrups)$$

For beams provided with minimum shear reinforcement, shear resistance provided by concrete V_c should be calculated as follows:

$$V_c = 0.035\,\lambda\,\phi_c\,(f_c'\rho_w\,E_F\,\frac{V_f}{M_F}\,d)^{1/3}\,b_w\,d$$

Provided that V_c satisfies:

$$0.1\ \lambda\ \phi_c\ \sqrt{f_c'}\ b_w\ d\ \leq\ V_c\ \leq 0.2\ \lambda\ \phi_c\ \sqrt{f_c'}\ b_w\ d$$

The term $\frac{V_f}{M_f}\ d$ should not be taken more than 1.

$$V_c = 0.035\ (\ f_c'\rho_w\ E_F\ \frac{V_f}{M_F}\ d\ )^{1/3}\ b_w\ d$$

$\frac{V_f}{M_F}\ d$=(85.9/52.5)*0.252 = 0.41

= 0.035*(30*0.00786 *46000*0.41)$^{1/3}$ 200*252 = 29 kN

$0.1\ \sqrt{f_c'}\ b_w\ d$ = $0.1\sqrt{30}$*200*252 = 27.6 kN

$0.2\ \sqrt{f_c'}\ b_w\ d$ = $0.2\sqrt{30}$*200*252 = 55.2 kN

Take V_c = 29 kN

The shear resistance of steel stirrups V_{ss} should be calculated according to Clause 8.4.4.6 as follows: **using ϕ8@80**

$V_{ss} = \frac{A_v\ f_y\ d}{s}$ = 2*49.48*300*252/80 = 93.51 kN < 0.8 $\sqrt{f_c'}\ b_w\ d$ ok

0.8 $\sqrt{f_c'}\ b_w\ d$ = $0.8\sqrt{30}$*200*252 = 220.8 kN

V_r = 29 + 99.75 = 122 kN > V_f (85.9 kN)

A.8.2.2. Beam GSu-10*d*/2*p*

This beam is designed to study the effect of steel stirrups bar diameter on GFRP-reinforced continuous beams. Beam GSu-8*d*/2*p* had ϕ8@120 steel stirrups. This beam will used the same steel stirrup spacing while using bigger bar diameter. The target shear capacity should be comparable to beam GSu-8*d*/3*p* (ϕ8@80, V_r = 122 kN).

The ultimate shear resistance for section reinforced with either FRP or steel stirrups should be calculated according to Clause 8.4.4.4 as follows:

$$V_r = V_c + V_{ss} \leq V_c + 0.8\,\lambda\,\phi_c\,\sqrt{f_c'}\,b_w\,d \qquad (For\ steel\ stirrups)$$

For beams provided with minimum shear reinforcement, shear resistance provided by concrete V_c should be calculated as follows:

$$V_c = 0.035\,\lambda\,\phi_c\,(\,f_c'\rho_w\,E_F\,\frac{V_f}{M_F}\,d\,)^{1/3}\,b_w\,d$$

Provided that V_c satisfies:

$$0.1\,\lambda\,\phi_c\,\sqrt{f_c'}\,b_w\,d \leq V_c \leq 0.2\,\lambda\,\phi_c\,\sqrt{f_c'}\,b_w\,d$$

The term $\frac{V_f}{M_f}\,d$ should not be taken more than 1.

$$V_c = 0.035\,(\,f_c'\rho_w\,E_F\,\frac{V_f}{M_F}\,d\,)^{1/3}\,b_w\,d$$

$\frac{V_f}{M_F}d$=(85.9/52.5)*0.252 = 0.41

= 0.035*(30*0.00786 *46000*0.41)$^{1/3}$ 200*252 = 29 kN

$0.1\sqrt{f_c'}\,b_w\,d$ = 0.1$\sqrt{30}$*200*252 = 27.6 kN

$0.2\sqrt{f_c'}\,b_w\,d$ = 0.2$\sqrt{30}$*200*252 = 55.2 kN

Take V_c = 29 kN

The shear resistance of steel stirrups V_{ss} should be calculated according to Clause 8.4.4.6 as follows: **using ϕ10@120**

$V_{ss} = \frac{A_v\,f_y\,d}{s}$ = 2*71.25*300*252/120 = 90 kN < $0.8\sqrt{f_c'}\,b_w\,d$ ok

$0.8\sqrt{f_c'}\,b_w\,d$ = 0.8$\sqrt{30}$*200*252 = 220.8 kN

V_r = 29 + 90 = 119 kN

A.8.2.3. Beam GGu-10*d*/3*p*

This beam is designed to study the effect of GFRP stirrup spacing on continuous concrete beams reinforced with GFRP bars. Beam GGu-10*d*/2*p* (casted already) had No.10 @ 120 GFRP stirrups. This beam, the same GFRP stirrup diameter will be used, however, with smaller spacing. The target design shear capacity should be close to beam GSu-10*d*/2*p* (ϕ8@80, V_r = 122 kN).

Clause 8.4.4.4:

$$V_r = V_c + V_{ss} \leq V_c + 0.6\,\lambda\,\phi_c\sqrt{f_c'}\,b_w\,d \qquad (For\ FRP\ stirrups)$$

For beams provided with minimum shear reinforcement, shear resistance provided by concrete V_c should be calculated as follows:

$$V_c = 0.035\ \lambda\ \phi_c\ (\ f_c'\rho_w\ E_F\ \frac{V_f}{M_F}\ d\ )^{1/3}\ b_w\ d$$

Provided that V_c satisfies:

$$0.1\ \lambda\ \phi_c\ \sqrt{f_c'}\ b_w\ d\ \leq\ V_c\ \leq 0.2\ \lambda\ \phi_c\ \sqrt{f_c'}\ b_w\ d$$

The term $\frac{V_f}{M_f}\ d$ should not be taken more than 1.

$$V_c = 0.035\ (\ f_c'\rho_w\ E_F\ \frac{V_f}{M_F}\ d\ )^{1/3}\ b_w\ d$$

$\frac{V_f}{M_F} d$=(85.9/52.5)*0.252 = 0.41

= 0.035*(30*0.0078 *46000*0.41)$^{1/3}$ 200*252 = 29kN

$0.1\ \sqrt{f_c'}\ b_w\ d$ = $0.1\sqrt{30}$*200*252 = 27.6 kN

$0.2\ \sqrt{f_c'}\ b_w\ d$ = $0.2\sqrt{30}$*200*252 = 55.2 kN

Take V_c = 29 kN

Clause 8.4.4.6: using **No.10 GFRP @ 80**, A= 71.3 mm^2, f_{fu}= 0.7*856 = 600 MPa

$V_{sf} = \frac{0.4\ A_v\ f_{fu}\ d}{s}$ = 0.4*2*71.3*600*252/80 = 108 kN < $0.6\ \sqrt{f_c'}\ b_w\ d$ ok

$0.6\ \sqrt{f_c'}\ b_w\ d$ = $0.6\sqrt{30}$*200*252 = 165.6 kN

V_r = 29 + 108 = **137 kN**

A.9. Design of Specimens GSs-10*d*/2*p* according to CSA S806-02

This beam was designed mainly to satisfy the serviceability requirements at the same service load (60 kN) as the control specimen reinforced with steel. The main design criteria was as follows

1. Limit the stress developed at service to 25% of ultimate tensile strength of the bar according to the CSA-S6-06 code (CSA 2006);
2. Calculated deflection and crack width at service load should satisfy the allowable limits permitted by the code;
3. Allow for 20% moment redistribution.

Section at middle support

$M = 0.15\ Pl = 0.15 \times 60 \times 2.8 = 25.2$ kN.m

While $M = A_s\ 0.25\ f_{frpu}\ (d\text{-}kd/3)$

Using 3No. 16 GFRP bars:

$\rho = 3\times198 / (200\times252) = 0.01178$ and $n = E_{frp}/E_c = 46000/(4500\times\sqrt{30})$

$k = \sqrt{2\rho n + (\rho n)^2} - \rho n = 0.1889$

$M = 3*198*0.25*731\ (252 - 0.1889*252 / 3) = 25.6$ kN

Section at mid span

Flexural capacity at middle support (3No. 16 GFRP bars) = 62 kN.

Corresponding bending moment at mid-span assuming 20% redistribution:

P = 62 / (0.15*2.8) =148 kN.m

M_{+ve}= 0.175 * 148 * 2.8 = **72.5** kN.m

Using 6 No.16, A_{frp}= 1188 mm^2:

d= 300-(48+15.9/2) = 244mm

ρ= As/(b d) = 1188/(200*244) = 0.024

$$f_{frp} = 0.5\, E_{frp}\, \varepsilon_{cu} \left[\left(1 + \frac{4\, \alpha_1\, \beta_1\, f_c'}{\rho_{frp}\, E_{frp}\, \varepsilon_{cu}} \right)^{1/2} - 1 \right]$$

$$= 0.5 * 46000 * 0.0035 \left[\left(1 + \frac{4 * 0.805 * .895 * 30}{0.024 * 46000 * 0.0035} \right)^{0.5} - 1 \right] = 306\ MPa$$

Note: f_{frp} = 42% maximum tensile strength f_{frpu}

a = (A_{sfrp} f_{frp}) / (α_1 f_c' b) = 1188 * 306/ (0.805*30*200) = 75 mm

M_{ult} = T (d- (a)/2) = 1188 * 306*(244 – 75/2) = **75** kN.m > 72.5 kN.m

Check concrete strain:

$$c/d \geq \frac{7}{7 + 2000\, \epsilon_{Fu}}$$

$$c/d = \frac{75}{244} = 0.3 > \frac{7}{7 + 2000 * 0.016} = 0.179$$

Check if minimum reinforcement is provided:

The minimum reinforcement provided in the section should satisfy Clause 8.4.2.1.

$$M_r > 1.5\, M_{cr}$$

$$M_{cr} = 0.6 * \sqrt{30}\, \frac{200 * 300^3}{12 * 300/2} = 9.86\ kN.m$$

M_r=75 kN.m > 1.5*9.89=14.8 kN.m (minimum reinforcement satisfied)

Check deflection at service load:

$\Delta \leq$ l/180 to l/480 (6mm to 15mm) according to CSA-S806-02

$$\Delta = \frac{7}{768} * \frac{Pl^3}{E_c I_e}$$

$I_e = \frac{I_{cr}}{1-\eta(\frac{M_{cr}}{M_a})}$ were $\eta = 1 - \frac{I_{cr}}{I_g}$ according to CSA-S806-02

M_{cr} = 9.86 kN.m, I_g = 450 000 000 mm^4

M_a = 0.175 * 60 * 2.8 = 29.4 kN.m, Icr = b (kd)3/3 + n Afrp (d-kd)2 = 82 545 352 mm4

Ie = 113 671 794 mm^4 , Δ= 7 / 768 * (60000 * 2800^3 / 4500$\sqrt{30}$ * 75 976 018) = 5mm (Safe)

Crack width:

a) ISIS Canada (2007)

$w = 2.2\, k_b\, f_{frp} / E_{frp} \times h_2/h_1\, (d_c A)^{1/3}$

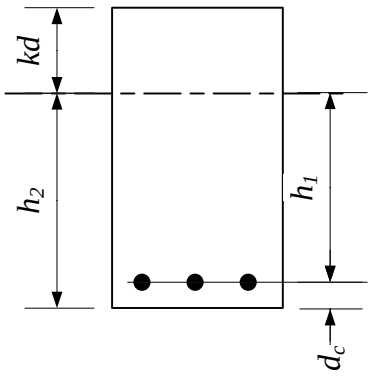

$h_2 = 300 - 0.189 * 252 = 252.4$ mm, $h_1 = 252.4 - 48 = 204.4$ mm

$A = 2\ d_c * b / n = 2 * 48 * 200 / 3 = 6400\ \text{mm}^2$

$w = 2.2 * 1 * 182.75 / 46000 * (252.4/204.4) * (48*6400)^{1/3} = 0.87\text{mm} > 0.5$ (CSA-S6-06) N.G

b) ACI-440.1R-06 (ACI 2006)

$w = 2\ k_b\ f_{frp} / E_{frp} \times h_2/h_1\ (d_c^2 + (s/2)^2)^{1/2}$ were $s = (b - 2\ d_c) / (n\text{-}1)$ and n is the number of bars

$s = (200\text{-}2*48) / (3\text{-}1) = 33.67$ mm

$w = 2 * 182.75/46000 * 252.4/204.4 * 1 * (48^2 + (33.67/2)^2) = 0.6 > 0.5$ N.G

c) CSA-S806-02 (CSA 2002)

$z = k_b\ E_s/E_{frp}\ f_{frp}\ (d_c\ A)^{1/3} \leq 38\ 000$ N/mm for external exposure

$z = 1 * 200\ 000/46000 * 182.75\ (48 * 6400)^{1/3} = 52700 > 0.5$ N.G.

Use 4No.16 at middle support and 7No.16 at mid-span to satisfy crack width criteria.

Design for shear:

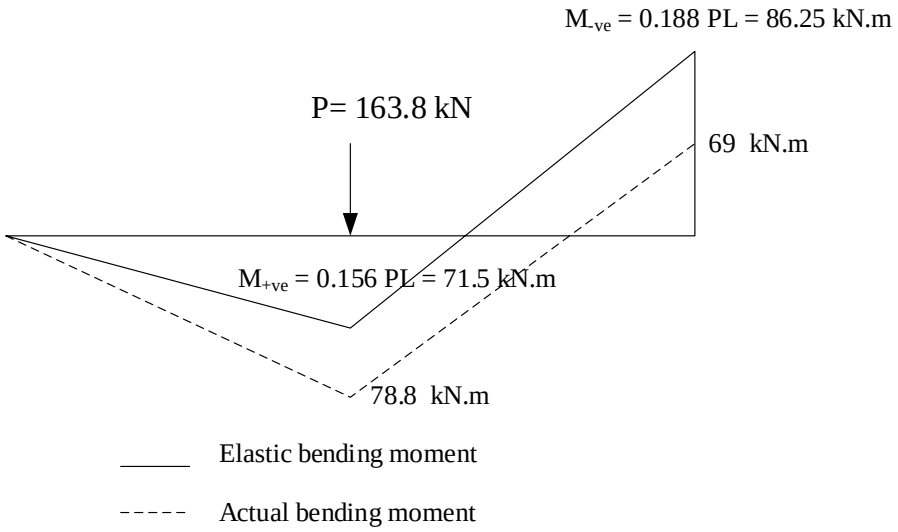

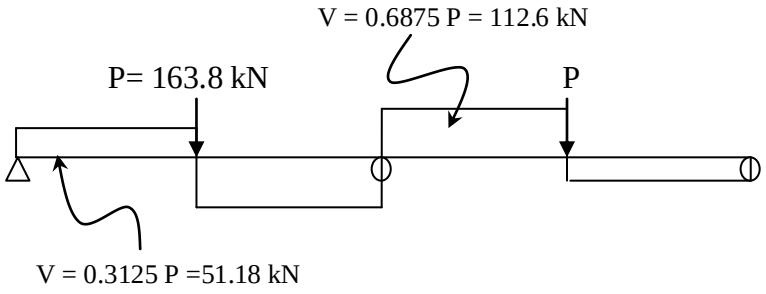

P= 164 kN ,V_f = 112.6 kN

The ultimate shear resistance for section reinforced with either FRP or steel stirrups should be calculated according to Clause 8.4.4.4 as follows:

$$V_r = V_c + V_{ss} \leq V_c + 0.8\,\lambda\,\phi_c\sqrt{f_c'}\,b_w\,d \qquad (For\ steel\ stirrups)$$

For beams provided with minimum shear reinforcement, shear resistance provided by concrete V_c should be calculated as follows:

$$V_c = 0.035\ \lambda\ \phi_c\ (\ f_c'\rho_w\ E_F\ \frac{V_f}{M_F}\ d\ )^{1/3}\ b_w\ d$$

Provided that V_c satisfies:

$$0.1\ \lambda\ \phi_c\ \sqrt{f_c'}\ b_w\ d\ \leq\ V_c\ \leq 0.2\ \lambda\ \phi_c\ \sqrt{f_c'}\ b_w\ d$$

The term $\frac{V_f}{M_f}\ d$ should not be taken more than 1.

$$V_c = 0.035\ (\ f_c'\rho_w\ E_F\ \frac{V_f}{M_F}\ d\ )^{1/3}\ b_w\ d$$

$\frac{V_f}{M_F}\ d$=(112.6/69)*0.252 = 0.44

= 0.035*(30*0.00786 *46000*0.44)$^{1/3}$ 200*252 = 29.7 kN

$0.1\ \sqrt{f_c'}\ b_w\ d$ = $0.1\sqrt{30}$*200*252 = 27.6 kN

$0.2\ \sqrt{f_c'}\ b_w\ d$ = $0.2\sqrt{30}$*200*252 = 55.2 kN

Take V_c = 29.7 kN

The shear resistance of steel stirrups V_{ss} should be calculated according to Clause 8.4.4.6 as follows: **using ϕ10@120**

$V_{ss} = \frac{A_v\ f_y\ d}{s}$ = 2*71.25*300*252/120 = 90 kN < $0.8\ \sqrt{f_c'}\ b_w\ d$ ok

$0.8\ \sqrt{f_c'}\ b_w\ d$ = $0.8\sqrt{30}$*200*252 = 220.8 kN

V_r = 29.7 + 90 = 119.7 kN > V_f (112.6 kN)

A.10. Predicted flexural capacity of tested beams based on actual material properties

Since the actual concrete compressive strength reported in Table (3.4) from Chapter 3 was slightly different from that assumed in the design criteria, the predicted bending moment capacity for all beams was updated and reported in Table (4.1) in Chapter 4.

APPENDIX B:

CODE PROVISIONS

B.1. Code Provisions for Steel-Reinforced Sections

The behaviour of steel-reinforced concrete beams is well established in the available design codes and guidelines. The following presents the provisions of the Canadian code (CSA 2004) and the American code (ACI 2008) regarding the design of steel-reinforced sections.

B.1.1 According to CAN/CSA-A23.3-04

B.1.1.1 **Flexural design:**

According to clause 8.6.1.1, used concrete compressive strength should not be less than 20 MPa or more than 80 MPa.

The modulus of elasticity of concrete can be determined according to clause 8.6.2.3 as follows:

$$E_c = 4500\sqrt{f_c'}$$

In lieu of the formula above, concrete modulus of elasticity can be taken as the secant modulus for a stress of 0.4 f_c', (clause 8.6.2.1).

Concrete modulus of rupture can be taken according to clause 8.6.4:

$$f_r = 0.6\lambda\sqrt{f_c'}$$

For continuous beams, the hogging moments at supports calculated by elastic analysis may be reduced by a percentage equals to (30-50 c/d) %, but not more than 20%, (clause 9.2.4).

According to clause 10.1.2, the strain in reinforcement and concrete shall be assumed to be directly proportional to the distance from neutral axis. In addition the maximum strain at the extreme concrete compression fibres can be assumed to be 0.0035, (clause 10.1.3).

The equivalent rectangular concrete stress distribution in compression is defined according to clause 10.1.7 as follows:

$$\alpha_1 = 0.85 - 0.0015\, f_c' \geq 0.67$$

$$\beta_1 = 0.97 - 0.0025\, f_c' \geq 0.67$$

A minimum reinforcement should be provided in beams calculated as in clause 10.5.1.2 as follows:

$$A_{s,min} = \frac{0.2\sqrt{f_c'}}{f_y}\, b_t h$$

Where:

f_c': concrete compressive strength;

f_y: reinforcement yielding strength;

b_t: width of tension zone of section;

h : overall section height.

The tension reinforcement can be assumed to reach yield if ${}^{c}/_{d} \leq \frac{700}{700+f_y}$, (clause 10.5.2).

B.1.1.2 **Shear Design:**

According to clause 11.2.8.2, a minimum area of shear reinforcement should be provided if the applied shear force exceeds concrete shear resistance or overall section depth is greater than 750 mm. The minimum shear reinforcement is calculated as follows:

$$A_v = 0.06\sqrt{f_c'}\,\frac{b_w\ s}{f_y}$$

Where:

b_w: beam web width

s : spacing of transverse reinforcement

The factored shear resistance for a reinforced section can be calculated according to clause 11.3.3 as follows:

$V_r = V_c + V_s$, and V_r shall not be taken more than $0.25\ \phi_c\ f_c'\ b_w\ d_v$

Where:

V_c : concrete shear resistance;

V_s : shear force resisted by stirrups;

d_v : effective shear depth taken as the greater of 0.9d or 0.72h

ϕ_c : factored concrete compressive strength = 0.65

According to clause 11.3.4 and clause 11.3.5, V_c and V_s can be calculated as follows:

$$V_c = \phi_c\ \lambda\ \beta\ \sqrt{f_c'}\ b_w\ d_v$$

$$V_s = \frac{\phi_c\ A_v\ f_y\ d_v\ \cot\theta}{s}$$

In lieu of more accurate calculations, and provided that used yield strength of longitudinal steel does not exceed 400 MPa and concrete compressive strength is less than 60 MPa, θ can be taken

as 35°. If the section contains the minimum transverse, the factor β can be taken as 0.18, (clause 11.3.6.3).

For members subjected to significant axial tension, a more accurate method can be used to determine the factors β and θ according to clause 11.3.6.4.

$$\beta = \frac{0.4}{(1 + 1500\ \varepsilon_x)}\ x\ \frac{1300}{(1000 + s_{ze})}$$

$$\theta = 29 + 7000\ \varepsilon_x$$

For sections containing the minimum shear reinforcement, the equivalent crack spacing parameter s_{ze} shall be taken as equal to 300 mm.

In lieu of more accurate calculations, the factor ε_x is the longitudinal strain at mid-depth of the member due to applied load can be calculated as follows:

$$\varepsilon_x = \frac{M_f/d_v + V_f + 0.5\ N_f}{2\ (E_s A_s)}$$

Where:

M_f : applied factored bending moment

V_f: factored shear force

N_f : applied factored axial force

d_v : effective shear depth taken as the greater of 0.9d or 0.72h

E_s : modulus of elasticity of reinforcement

A_s : area of longitudinal tension reinforcement

According to clause 11.3.8.1 and clause 11.3.8.3, the maximum transverse spacing should not exceed 600 mm or $0.7d_v$. If the applied shear force exceeds $0.125\ \phi_c\ \lambda\ f_c'\ b_w\ d_v$, the maximum spacing should not exceed 300 mm or $0.35d_v$.

B.1.2 According to ACI 318-08

B.1.2.1 **Flexural design:**

For continuous beams, the calculated bending moments calculated by elastic theory is permitted to be decreased by a percentage not more than the smallest of $1000\varepsilon_t$ or 20 percent, (clause 8.4.1). Redistribution is only permitted if ε_t equals to or greater than 0.0075, where ε_t is the net tensile strain in longitudinal reinforcement.

For normal weight concrete, modulus of elasticity for concrete shall be taken as $4700\sqrt{f_c'}$, (clause 8.5.1).

Concrete modulus of rupture can be calculated as follows: $f_r = 0.62\sqrt{f_c'}$

The maximum compressive strain in concrete is assumed to be 0.003 according to clause 10.2.3.

Equivalent rectangular concrete compressive stress is defined by uniform stress of $0.85f_c'$ distributed over an equivalent compression zone with depth a =$\beta_1 c$, (clause 10.2.7.1).

The factor β_1 shall be taken as 0.85 for f_c' between 17 and 28 MPa. β_1 shall be reduced linearly at a rate of 0.05 for each 7 MPa of strength in excess of 28 MPa, but β_1 should not be taken less than 0.65.

Sections are tension controlled if the net tensile strain in extreme tension steel equals to or greater than 0.005, (clause 10.3.4).

The minimum reinforcement of flexural member can be calculated according to clause 10.5.1 as follows:

$A_{s,min} = \frac{0.25\sqrt{f'_c}}{f_y} b_w d$, and not less than $1.4 b_w\, d/f_y$, where b_w is beam web width and d is the effective depth.

B.1.2.2 **Shear design:**

According to clause 11.1.1, the ultimate shear force resistance of a reinforced concrete section V_n can be calculated as follows:

$V_n = V_c + V_s$

Where:

V_c : concrete shear resistance;

V_s : shear forces resisted by transverse stirrups.

For members subjected to shear and flexure only, V_c can be calculated according to clause 11.3.1.1 as follows:

$$V_c = 0.17 \sqrt{f'_c}\, b_w\, d$$

Where:

f'_c: concrete compressive strength;

b_w: beam web width;

d: effective depth of section.

For members subjected to axial compression, V_c can be calculated according to clause 11.3.1.2 as follows:

$$V_c = 0.17\left(1 + \frac{N_u}{14A_g}\right)\sqrt{f_c'}\, b_w\, d$$

Where:

N_u: factored axial normal force acting simultaneously with V_u, positive for compression;

A_g: gross area of concrete section.

Concrete shear resistance can also be calculated by a more detailed calculation according to clause 11.3.2.1 as follows:

$$V_c = \left(0.16\sqrt{f_c'} + 17\,\rho_w \frac{V_u\, d}{M_u}\right)\, b_w\, d$$

However, V_c should not be taken greater than$0.29\sqrt{f_c'}\, b_w\, d$, and the term $V_u\, d/M_u$ should not be taken greater than 1.0.

Where:

ρ_w: ratio of reinforcement area to $b_w\, d$;

V_u: factored applied shear force;

M_u: factored applied bending moment.

According to clause 11.5.2, the yield strength used in design for shear reinforcement should not be more than 420 MPa.

The maximum spacing of shear reinforcement should not exceed d/2 or 600 mm, (clause 11.5.5.2). If the force resisted by stirrups V_s exceeds$0.33\sqrt{f_c'}\,b_w\,d$, maximum spacing should not be more than d/4 or 300 mm, (clause 11.5.5.3).

If applied factored shear force exceeds $0.5\,\phi V_c$, minimum shear reinforcement has to be provided according to clause 11.5.6.3 as follows:

$A_{v,min} = 0.062\sqrt{f_c'}\,b_w\,s/f_{yt}$, and should not be taken less than $0.35\,b_w\,s/f_{yt}$.

Where:

b_w: beam web width;

s : shear reinforcement spacing;

f_{yt}: yielding strength of shear reinforcement.

According to clause 11.5.7.2, shear force resisted by stirrups V_s can be calculated as follows:

$$V_s = \frac{A_v f_{yt} d}{s} \; and\; should\; not\; be\; more\; than\; 0.66\sqrt{f_c'}\,b_w\,d$$

Where:

A_v: the area of shear reinforcement within spacing **s**;

f_{yt}: yielding strength of shear reinforcement;

s : shear reinforcement spacing;

d : effective section depth.

B.2. Code Provisions for FRP-Reinforced Sections

B.2.1 According to CAN/CSA-S806-02

The Canadian code for design construction of building with fibre-reinforced polymers (CSA S806-02) gives guide line and recommendations as follows:

The concrete compressive strength used in design should not be less than 30 MPa and should not be more than 80 MPa, (Clause 8.5.1.1).

For normal weigh concrete with concrete compressive strength between 30 MPa and 40 MPa, concrete modulus of elasticity could be taken according to Clause 8.5.2.3 as follows:

$$E_c = 4500\sqrt{f_c'}$$

Concrete modulus of rupture could be taken as stated in Clause 8.5.4.

$$f_r = 0.6\,\lambda\sqrt{f_c'}$$

Where λ equals 1 for normal weight concrete.

FRP bars properties should be determined by testing according to Clause 7.1.1. Preshaped FRP bars such as ties and hoops should be tested for strength development, (Clause 7.1.5.3).

B.2.1.1 **Design for flexure:**

According to CSA S806-02 Clause 8.2.1 the failure of flexural element has to be due to concrete crushing rather than rupture of FRP bars.

The cracking moment M_{cr} should be calculate according to Clause 8.3.2.6 as follows:

$$M_{cr} = f_r \frac{I_g}{y_t}$$

Where:

f_r: Modulus of rupture of concrete,

I_g: Moment of inertia of gross concrete section, neglecting the reinforcement,

y_t: Distance from extreme fibres in tension to the centroidal axis of cross section.

The strain in concrete and reinforcement shall be assumed directly proportional in case of perfect bond, (Clause 8.4.1.1). The ultimate strain in concrete extreme compression fibres should be taken equal to 0.0035 according to Clause 8.4.1.2. Concrete tensile strength shall be neglected for the ultimate flexure strength calculation of the section, (Clause 8.4.1.3).

Concrete stain at extreme fibres in compression shall be assumed to reach 0.0035 provided that the ratio c/d satisfies Clause 8.4.1.4 as follows:

$$c/d \geq \frac{7}{7 + 2000\,\epsilon_{Fu}}$$

Where:

c: Distance from extreme compression fibres to neutral axis,

d: Distance from extreme compression fibres to the centroid of longitudinal tension force,

ϵ_{Fu}: Ultimate strain for FRP reinforcement.

The concrete stress distribution is defined according to Clause 8.4.1.5. A uniform equivalent compressive strength of $\alpha_1 \varphi_c f_c'$ is assumed to be distributed over distance $a = \beta_1 c$.

Where:

$$\alpha_1 = 0.85 - 0.0015 f_c' \quad \geq 0.67$$

$$\beta_1 = 0.97 - 0.0025 f_c' \quad \geq 0.67$$

As the design target is the nominal strength, the reduction factors will be taken equal to unity.

In the calculation of ultimate flexural resistance the compressive strength of FRP bars shall be neglected according to Clause 8.4.1.8.

The minimum reinforcement provided in the section should satisfy Clause 8.4.2.1.

$$M_r > 1.5 M_{cr}$$

B.2.1.2 **Design for shear:**

The maximum acting shearing force used for design could be taken at a distance d from the face of support, (Clause 8.4.4.2).

The ultimate shear resistance for section reinforced with either FRP or steel stirrups should be calculated according to Clause 8.4.4.4 as follows:

$$V_r = V_c + V_{sF} \leq V_c + 0.6 \lambda \phi_c \sqrt{f_c'} b_w d \qquad (For\ FRP\ stirrups)$$

$$V_r = V_c + V_{ss} \leq V_c + 0.8 \lambda \phi_c \sqrt{f_c'} b_w d \qquad (For\ steel\ stirrups)$$

Where:

V_r: Nominal shear resistance,

V_c: Concrete shear resistance,

V_{sF}: FRP stirrups shear resistance,

V_{ss}: Steel stirrups shear resistance.

For beams provided with minimum shear reinforcement, shear resistance provided by concrete V_c should be calculated as follows:

$$V_c = 0.035\ \lambda\ \phi_c\ (\ f_c' \rho_w\ E_F\ \frac{V_f}{M_F}\ d\ )^{1/3}\ b_w\ d$$

Provided that V_c satisfies:

$$0.1\ \lambda\ \phi_c\ \sqrt{f_c'}\ b_w\ d\ \leq\ V_c\ \leq 0.2\ \lambda\ \phi_c\ \sqrt{f_c'}\ b_w\ d$$

The term $\frac{V_f}{M_f}\ d$ should not be taken more than 1.

Where:

ρ_w: Longitudinal reinforcement ratio %

E_F: Modulus of elasticity of longitudinal FRP reinforcement

M_F: Ultimate bending moment at section under consideration

V_f: Corresponding ultimate shear force at section under consideration

For beams provided with shear reinforcement less than the minimum shear reinforcement, concrete shear resistance should be calculated as follows:

$$V_c = \left(\frac{130}{100 + d}\right) \lambda \, \phi_c \sqrt{f_c'} \, b_w \, d \quad \geq 0.08 \, \lambda \, \phi_c \sqrt{f_c'} \, b_w \, d$$

The shear resistance of FRP and steel stirrups V_{sF} and V_{ss} respectively should be calculated according to Clause 8.4.4.6 as follows:

$$V_{sF} = \frac{0.4 \, \phi_F \, A_v \, f_{Fu} \, d}{s} \quad , \quad V_{ss} = \frac{\phi_s \, A_v \, f_y \, d}{s}$$

Where:

A_v: Area of shear reinforcement,

f_{Fu}: Ultimate strength of FRP shear reinforcement,

f_y: Yield strength of reinforcement,

S: Spacing of shear reinforcement.

According to Clause 8.4.5.1 and Clause 8.4.5.2, minimum shear reinforcement should be provided whenever $V_f > 0.5 \, V_c$. The minimum are of shear reinforcement should be calculated as follows:

$$A_v = \frac{0.3 \sqrt{f_c'} \, b_w s}{f_{Fh}}$$

B.2.1.3 **Considering continuous beams:**

According to Clause 8.6.5.1 and 8.6.6.2, design of continuous beams should satisfy the maximum elastic load distribution at critical section and no load redistribution is to be allowed.

B.2.1.4 **Service conditions:**

According to clause 8.3.1.1, if the maximum strain in FRP tension reinforcement exceeds 0.0015 under service loads, cross-sections of maximum sagging and hogging moment should be proportioned as follows:

$$z = k_b \frac{E_s}{E_f} f_f \sqrt[3]{d_c A} \leq \begin{cases} 45\,000 \quad N/mm \quad for\ interior\ exposure \\ 38\,000 \quad N/mm \quad for\ exterior\ exposure \end{cases}$$

Where:

z: quantity limiting distribution of flexural FRP reinforcement bars;

k_b: coefficient dependent on the reinforcing bar bond characteristics;

E_s: modulus of elasticity of reinforcement;

E_f: modulus of elasticity of longitudinal FRP reinforcement;

f_f: stress in FRP reinforcement under specified loads;

d_c: distance from extreme tension fibre to the centre of the longitudinal bar;

A : effective tension area of concrete surrounding the flexural tension reinforcement and extending from the extreme tension fibre to the centroid of the flexural tension reinforcement and an equal distance past the centroid, divided by the number of bars.

In lieu of computing the stress in the steel reinforcement, f_f, it may be taken as 60% of the design ultimate stress of bars. The value k_b may be taken as 1.2 for deformed rods and taken as 0.8 for sand-coated FRP bars. In calculating d_c and A, the clear cover should not be taken more than 50 mm.

B.2.1.5 **Development length of bars in tension:**

According to clause 9.3.2, bars subjected to tension have to be embedded in concrete with development length, l_d, calculated as follows:

$$l_d = 1.15 \frac{k_1 k_2 k_3 k_4 k_5}{d_{cs}} \frac{f_f}{\sqrt{f_c'}} A_b$$

The factor d_{cs} should not be taken greater than 2.5 d_b. Provided that the clear cover and clear spacing of bars being developed are at least 1.5d_b and 1.8 d_b, l_d can be computed as follows:

$$l_d = 0.5 k_1 k_2 k_3 k_4 k_5 \frac{f_f}{\sqrt{f_c'}} d_b$$

Where:

l_d: the development length of bars in tension;

f_f: design stress in FRP tension reinforcement at ultimate limit state;

d_{cs}: the smaller of (a) the distance from the closest concrete surface to the centre of the bar being developed; or (b) two-thirds of the centre-to-centre spacing of the bars being developed;

A_b: area of an individual bar;

d_b: nominal diameter of a circular bar.

The factors k_1 , k_2 , k_3 , k_4 and k_5 can be taken as follows:

k_1 = 1.3 for horizontal reinforcement placed so that more than 300 mm of fresh concrete is cast in the member below development length

= 1.0 for other cases

k_2 = 1.3 for structural low-density concrete

= 1.2 for structural semi-low-density concrete

= 1.0 for normal density concrete

k_3 = 0.8 for $A_b \leq 300$ mm^2

= 1.0 for $A_b > 300$ mm^2

k_4 = 1.0 for CFRP and GFRP

= 1.25 for AFRP

k_5 = 1.0 for surface-roughened or sand-coated surfaces

= 1.05 for spiral pattern surfaces

= 1.0 for braided surfaces

= 1.05 for ribbed surfaces

= 1.80 for indented surfaces

B.2.2 According to CAN/CSA-S6-06

B.2.2.1 **Design for deformability:**

According to clause 16.8.2.1 the overall performance factor J for FRP-reinforced concrete beams or girders, should be at least 4.0 for rectangular sections and 6.0 for T-sections. The performance factor J can be calculated as follows:

$$J = \frac{M_{ult}\,\Psi_{ult}}{M_c\,\Psi_c}$$

Where:

M_{ult}: ultimate moment capacity of the section;

Ψ_{ult}: curvature at M_{ult}

M_c : moment corresponding to a maximum compressive concrete strain of 0.001 in the section;

Ψ_c : curvature at M_c.

B.2.2.2 **Minimum flexural resistance:**

The factored resistance M_r should be at least 50% greater than cracking moment M_{cr}. If the ultimate limit state design is governed by FRP rupture, M_r should be greater than 1.5 the factored applied moment M_f.

The maximum stress in GFRP bars at service load should not exceed 0.25 f_{FRPu}, where f_{FRPu} is the ultimate tensile strength of the bars.

B.2.2.3 **Design for shear:**

According to Clause 16.8.7, the nominal shear resistance should be calculated as follows:

$$V_r = V_c + V_{st} + V_{FRP}$$

Where:

V_r : ultimate shear resistance;

V_c : shear force resisted by concrete;

V_{st} : shear resistance provided by shear reinforcement V_s or V_{FRP};

V_s : shear resistance provided by steel stirrups;

V_{FRP}: shear resistance provided by FRP stirrups.

Shear force resisted by concrete V_c can be calculated as follows:

$$V_c = 2.5\ \beta\ \phi_c\ f_{cr}\ b_v\ d_{long}$$

Where:

β : the inclination angle of transverse reinforcement;

ϕ_c: resistance factor of concrete;

f_{cr}: cracking strength of concrete;

b_v: effective depth of beam web;

d_{long}: effective shear depth for longitudinal reinforcement;

E_{long}: modulus of elasticity of longitudinal reinforcement;

E_s : modulus of elasticity of steel.

$$\varepsilon_x = \frac{\frac{M_f}{d_{long}} + V_f + 0.5\ N_f}{2\ (E_s\ A_s + E_{FRP}\ A_{FRP})} \leq 0.003$$

Where:

ε_x: longitudinal strain at section mid height;

M_f: factored applied bending moment;

V_f: factored applied shear force;

N_f: factored applied normal force;

E_s: modulus of elasticity of steel;

A_s: cross-sectional area of steel or FRP;

E_{FRP}: modulus of elasticity of FRP bars;

A_{FRP}: cross-sectional area of FRP bars;

The factored shear resistance provided by FRP stirrups V_{FRP} can be calculated as follows:

$$V_{FRP} = \frac{\phi_{FRP}\, A_v\, \sigma_v\, d_{long} \cot\theta}{s}$$

Where $\sigma_v$is the smaller of $\begin{cases} \sigma_v = \frac{(0.05\, r/d_s + 0.3\,) f_{FRPbend}}{1.5} \\ \sigma_v = E_{vFRP}\ \varepsilon_v \end{cases}$

$$\varepsilon_v = 0.0001\ (\ f_c'\ \frac{\rho_s\ E_{FRP}}{\rho_{vFRP}\ E_{vFRPs}})^{0.5}\ \leq 0.0025$$

$$A_{v\,min} = 0.06\ \sqrt{f_c'}\ \frac{b_w\ s}{\sigma_v}$$

Where:

A_v: area of transverse shear reinforcement;

s : spacing of shear reinforcement;

r : radius of curvature of the bend or FRP stirrup;

d_s: diameter of FRP stirrup;

$f_{FRPbend}$: specified tensile strength of the straight portion of an FRP bent stirrup;

E_{vFRP}: modulus of elasticity of FRP stirrup;

ε_v: strain in FRP stirrup;

ρ_s : longitudinal FRP reinforcement ratio;

ρ_{vFRP}: FRP transverse reinforcement ratio;

$A_{v\,min}$: minimum required shear reinforcement;

b_w : beam web width.

B.2.3 According to ACI 440.1R-06

B.2.3.1 Design for flexure

The flexural capacity of FRP-reinforced member is dependent on the failure mode whether it is concrete-crushing failure or FRP-rupture failure. The mode of failure can be determined by comparing the FRP reinforcement ratio to the balanced reinforcement ratio ρ_{fb} as follows (clause 8.2.1):

$$\rho_{fb} = 0.85\,\beta_1\,\frac{f_c'}{f_{fu}}\,\frac{E_f\,\varepsilon_{cu}}{E_f\,\varepsilon_{cu} + \varepsilon_{fu}}$$

Where:

ρ_{fb}: FRP reinforcement ratio producing balanced strain conditions;

f_{fu}: design tensile strength of FRP, considering reductions for service environment;

E_f : modulus of elasticity of FRP;

ε_{cu}: ultimate strain in concrete;

ε_{fu}: design rupture strain of FRP reinforcement.

The nominal flexural strength of FRP-reinforced section when the failure is initiated by concrete crushing can be calculated as follows (clause 8.2.2):

$$M_n = A_f f_f \left(d - \frac{a}{2} \right)$$

$$a = \frac{A_f f_f}{0.85 f_c' b}$$

$$f_f = E_f \varepsilon_{cu} \frac{\beta_1 d - a}{a}$$

$$or \quad f_f = \left(\sqrt{\frac{(E_f \varepsilon_{cu})^2}{4} + \frac{0.85 \beta_1 f_c'}{\rho_f} E_f \varepsilon_{cu}} - 0.5 E_f \varepsilon_{cu} \right) \leq f_{fu}$$

Where:

M_n: nominal moment capacity;

A_f: area of FRP reinforcement;

f_f: stress in FRP reinforcement in tension;

d: distance from extreme compression fibre to centroid of tension reinforcement;

a: depth of equivalent rectangular stress block.

In case of tension failure of FRP bars the equivalent concrete stress block used at ultimate is no more valid. A simple and conservative calculation for nominal flexural strength in this case can be as follows:

$$M_n = A_f f_{fu} \left(d - \frac{\beta_1 c_b}{2} \right)$$

$$c_b = \left(\frac{\varepsilon_{cu}}{\varepsilon_{cu} + \varepsilon_{fu}} \right) d$$

According to clause 8.2.3, only if the failure of the member is controlled by FRP rupture, a minimum reinforcement should be provided to prevent failure upon cracking can be calculated as follows:

$$A_{f,min} = \frac{4.9\sqrt{f_c'}}{f_{fu}} b_w d \geq \frac{330}{f_{fu}} b_w d$$

B.2.3.2 **Design for shear**

According to clause 9.2, the nominal shear capacity of reinforced concrete cross-section can be calculated as follows:

$$V_r = V_c + V_F$$

V_r: ultimate shear strength;

V_c: nominal shear strength provided by concrete;

V_f: shear resistance provided by FRP stirrups.

The concrete shear capacity V_c of FRP-reinforced member can be calculated as follows:

$$V_c = \frac{2}{5}\sqrt{f_c'}bc$$

$$c = kd$$

$$k = \sqrt{2\rho_{frp}n_{frp} + \left(\rho_{frp}n_{frp}\right)^2} - \rho_{frp}n_{frp}$$

n_{frp}: ratio of modulus of elasticity of FRP bars to modulus of elasticity of concrete;

ρ_{frp}: FRP reinforcement ratio.

The shear resistance provided by FRP stirrups V_f can be calculated as follows:

$$V_f = \frac{A_v f_{fv} d}{s}$$

The stress level in the FRP shear reinforcement should be limited to control shear cracks. The stress level at ultimate used in design should be calculated as follows:

$$f_{fv} = 0.004\, E_{f,v} \leq f_{fb}$$

The required spacing and area of shear reinforcement can be computed as follows:

$$\frac{A_{fv}}{s} = \frac{V_u - \phi V_c}{\phi f_{fv}\, d}$$

According to clause 9.2.2 a minimum amount of shear reinforcement should be provided when V_u exceeds $\phi V_c/2$. The minimum area of shear reinforcement can be computed as follows:

$$A_{v,min} = 0.35\frac{bs}{f_{fv}}$$

Where:

$A_{v,min}$: minimum amount of FRP shear reinforcement within spacing s;

f_{fv}: tensile strength of FRP for shear design, taken as smallest of design tensile strengthf_{fu}v strength of bent portion of FRP stirrups f_{fb}, or stress corresponding to $0.004E_f$.

The effective stress level in FRP stirrups should be governed by the allowable stress in the stirrup at the location of the bend which is computed as follows:

$$f_{fb} = \left(0.3 + 0.05\frac{r_b}{d_b}\right) f_{fu}$$

Where:

f_{fb}: strength of bent portion of FRP bar;

f_{fu}: design tensile strength of FRP, considering reductions for service environment;

r_b: internal radius of bend in FRP reinforcement;

d_b: diameter of reinforcing bar.